MODELLING ENVIRONMENTAL EFFECTS ON FRACTURE DAMAGE OF NATURAL FIBRE - REINFORCED POLYMER COMPOSITES

by

Chizyuka Gungubwe Chizyuka

A thesis submitted in fulfilment of the requirements for the award of the degree of Doctor of Philosophy in Materials Engineering

The University of Zambia

2015

DECLARATION

I, **Chizyuka Gungubwe Chizyuka**, do hereby declare that this thesis is the result of my own investigation and research, except to the extent indicated in the Acknowledgments and References and by comments indicated in the body of the report, and that it has not been submitted in part or full for any degree to any other university.

Signature: .....

Date: .....

APPROVAL

This thesis of Chizyuka Gungubwe Chizyuka is approved as fulfilling the requirements for the award of the degree of Doctor of Philosophy in Materials Engineering by the University of Zambia.

NAME SIGNATURE

_____ _____

External Examiner

_____ _____

Internal Examiner

_____ _____

Internal Examiner

_____ _____

Chairperson

Abstract

The behaviour of sodium hydroxide treated sisal fibre-reinforced polyester composite subjected to environmental ageing conditions has been studied with the aim of modelling its effect on the composite fracture damage for the purpose of long-term performance prediction.

The composite was accelerated aged by hydrothermal ageing by immersing test specimens in distilled water at respective temperatures of 23^{o}C, 40^{o}C and 60^{o}C for a maximum period of 6 months. At regular intervals tests were conducted to assess the retention of the mechanical properties. Tests conducted included tensile tests on single sisal fibres, neat cured polyester resin, and sisal fibre reinforced polyester composite test specimens. Retention of fracture strength of the composite was further assessed both at macro and micro levels. The assessment of the fracture toughness properties was conducted on eccentrically loaded in tension single-edge-notch (ESE(T)) specimens; whereas fibre/matrix interfacial shear strength was assessed through the single fibre microbond method. Viscoelastic properties of matrix material which include storage modulus, loss modulus, and glass transition temperature were further determined and monitored using the Dynamic Mechanical Analysis (DMA) method. All tests conducted included test of non-hydrothermally treated test specimens for the purpose of setting a comparative baseline and determining the effect the ageing process poses on the composite properties.

Results from the single fibre microbond tests revealed significant reductions in the interfacial microbond strengths as the absorbed moisture levels intensified.

Results from fractographic differences in the Scanned Electron Microscopic (SEM) images of the fractured microbond test specimens indicate little to no traces of the residual matrix material present on the sisal fibre at the original location of the polyester resin droplet along the fibre. This brings out a possible conclusion that fibre debonding is an established fracture mechanism in hydrothermally aged sisal fibre reinforced composite systems. The presence of this residual matrix appears to be dependent on the duration of the applied hydrothermal ageing.

Dynamic mechanical analysis and tensile tests conducted on hydrothermally aged neat cured polyester test specimens revealed appreciations in both its glass transition temperature and elastic modulus, whereas deteriorations in the strength was recorded in both neat resin and composite specimens. An enhancement of the elastic modulus appears to have taken place in the hydrothermally aged composite test specimens during the early periods of moisture uptake probably as a result of hydrolysis of matrix material. Plasticisation of the same composite system appears to have taken into effect and more pronounced at higher ageing temperatures after prolonged continuous exposure to the ageing environments, subsequently resulting in the reduction in the mechanical property of the composite.

Isothermal water uptake studies were conducted alongside the hydrothermal ageing treatments for the determination of the relative rate of absorption of water by the sisal-polyester composite by immersing test specimens into distilled water at different pre-set temperatures.

Fracture toughness test results revealed that hydrothermal ageing yielded significant changes in the translaminar fracture toughness (K_{TL}), with more pronounced decrease in the property recorded with increase in ageing temperature. The resultant empirical model generated compares well with K_{TL} values obtained from both experiments and theoretical Arrhenius life-stress model.

To my Parents

ACKNOWLEDGMENTS

The success of this research required the help of various individuals. Without them, I might not have met the set objectives in doing this work. I would like to give gratitude to the following people for their invaluable help and support:

My deepest gratitude is to my local supervisors, Prof. Shamitiba B. Kanyanga and late Dr. C.K. Wamukwamba for their valuable guidance and support during the cause of this research.

To my University of Manchester supervisors, Professors Paul Hogg and Stephen Eichhorn for their thought-provoking insightful comments and constructive criticisms at the initial stages of this research.

Thanks to the University of Manchester, School of Material Science for providing me all the necessary research facilities without whom this research would have been possible.

To my wife and children for all their support.

TABLE OF CONTENTS

List of Appendices

List of Figures

List of Tables

NOMENCLATURE

The list contains only notations and symbols which are frequently used in the thesis, others are explained when they occur.

A	Factor which represents a frequency factor for the process
a_n	Notch length
ASTM	American Society for Testing and Materials
B	Specimen thickness
β_{Time}	Ageing time-based parameter
β_{μ}	Matrix swelling coefficient
C	One of the model parameters to be determined
D	Diffusion coefficient
D	Fibre diameter
d	Ageing duration
D_m	Matrix diffusion coefficient
DMA	Dynamic Mechanical Analysis
DSC	Differential Scanning Calorimeter
D_x	Edge diffusion correction factor
D_z	Diffusion coefficient of a material in the direction normal to the surface
E	Elastic modulus of the composite
E, E_a	Activation energy
$E^{/}$	Storage modulus
$E^{//}$	Loss modulus
E_f	Reinforcing fibre elastic modulus
E_m	Reinforced matrix elastic modulus
ϕ	Fibre angle with z direction
F_p	Pull-out force
G	Time – dependent dimensionless parameter related to diffusion coefficient of material
GFRP	Glass Fibre Reinforced Plastic
h	Thickness of material
ILSS	Interlaminar shear strength
K_{TL}	Translaminar fracture toughness
l	Fibre embedded length
$L(T)$	Quantifiable life measure as a function of a stress level

M	Moisture content of the composite specimen
MEKP	Methyl Ethyl Ketone Peroxide
M_i	Initial moisture concentration
M_m	Maximum moisture content of the composite specimen
M_t	Percentage moisture gain with time
NaOH	Sodium Hydroxide
NFRC	Natural Fibre Reinforced Composite
nmax	Maximum amount of iterations
P	Applied load
P	Load
PET	Polyethylene Terephthalate
P_{max}	Maximum load
PP	Polypropylene
R	Universal gas constant
r	Vector of time increment for which genfit calculates the percentage moisture gain
R(T)	Rate of reaction of the process
RH	Relative humidity
σ_{TSo}	Pre Ageing Tensile strength
σ_{TS}	Tensile strength
SEM	Scanning Electron Microscope
StdDev	Standard deviation
τ_{Int}	Interfacial shear strength
T	Ageing temperature
t	Time
T_g	Glass transition temperature
u_1	Diffusion coefficient
u_o	Maximum moisture content
UV	Ultra violet
W	Specimen width
w_f	Fibre Weight fraction
α	Dimensionless ratio (=a/W)
α_{Temp}	Ageing temperature-based parameter
ε_m	Volumetric strain of resin
ρ_m, ρ_w	Matrix and water density

CHAPTER 1 INTRODUCTION

1.1 Introduction

The advancement of composite materials and associated processing technologies stands out to be the most important developments in the evolution of engineering materials. Fibre-reinforced composite technology is built on taking advantage of both the high strength and stiffness of fibres, which are combined with matrix materials resulting in an inevitable interfacial bonding (U.S. Congress, 1998). In the formed reinforced composites, these two constituents retain their original physical and chemical characteristics, and yet in their combined form yield a composite which bears superior mechanical properties that in most cases cannot be achieved with either of the constituents acting independently, due to the existence of an interface created in between these two constituents (Kim, et al., 1998).

Composites have established themselves as important engineering materials that are now used extensively, not only in the high-performance aerospace applications, but also in a large and steadily increasing number of other commercial mechanical and civil engineering applications owing to their lower density nature (ibis). It is worthwhile to note that a good number of structural materials which exist in nature are in some form of composite. Good examples of naturally existing composites are wood, bamboo, bone, teeth, and shell. Furthermore, man-made composites have been in existence going back to the Biblical time where straw was used as a natural reinforcement in mad-bricks (Matsagar, 2014).

The issue of understanding the constitution and properties of interfaces in fibre-reinforced composite materials is still in its infancy regardless of the fact that there have been numerous publications devoted to research in this field (U.S. Congress, 1998). Part of the reason for this evolution is the interdisciplinary nature of the subject.

It is well known that the properties of an interface are controlled for the most part by the chemical/morphological make-up and physical/thermodynamic compatibility that exists between the two constituents (Zhang, 2010). This restricts the general

performance of the bulk composite. There is now a substantial amount of evidential data regarding the influences of interfaces on fracture toughness in both transverse and interlaminar fractures, and strength and stiffness of fibre reinforced composites in various failure modes and loading configurations (Kim, et al., 1998). Despite this understanding, the connection between documented material properties and the actual performances of composites is still in question. A more comprehensive understanding of the microstructure-property correlation at the interface region is an essential key to the successful design and application of composite materials.

This research therefore seeks to study the influence of the surrounding environment on the performance of natural fibre reinforced polymeric composite, considering the fact that that these materials are an emerging class of bio-degradable engineering composite material. This will eventually lead to the development of models for the prediction of the natural fibre reinforced composite's performance under the influence of specific environmental stress stimuli.

1.2 Problem Statement

Moisture is a critical environmental factor that can be destructive to natural fibre reinforced polymeric composite (NFRC) properties in general. Composite components can be constantly absorbing or desorbing moisture due to variability in service temperature and relative humidity levels resulting in lowering of the composite's mechanical properties. This apparent lowering of the mechanical properties of NFRC after continued exposure to ageing elements is of concern. Therefore, in order to utilise the full potential of these materials, their response to specific environmental conditions must be fully understood and is vital to their relevance as engineering materials.

As such, prediction of the composite's short and long term performance under specific environmental conditions is critical as these materials are an emerging class of engineering structural materials.

1.3 Research Objectives

The main objective of this research was to model the effect of the environmental effects on the fracture damage of treated sisal fibre-reinforced polyester composites.

The specific objectives were as follows:

1. Study the stability of sisal fibre-reinforced polyester composite when exposed to degradation by hydrothermal ageing with reference to fracture damage change.
2. Empirically model the observed environmental effects on fracture damage of the fibre-reinforced composite.
3. Theoretically model the environmental effects on fracture damage of these fibre-reinforced composite.
4. Compare and correlate the results in (2) with results obtained in (3).

1.4 Methodology

This section describes the design of experiments employed to investigate changes in the mechanical properties of the sisal fibre reinforced polyester composites, at both macro and micro composite levels, after being exposed to hydrothermal ageing. There are considerably many possible combinations of environmental conditions a composite can experience when in operation, and this necessitates carefully designed experimentation. Suitable ageing conditions have to be selected that provide a comprehensive idea about the quality of the composite and service life. Also, experiments carried out in the laboratory need to be pertinent to the problem at hand and should represent the actual field situation.

The observed property changes were further used to develop an empirical mathematical model for predicting fracture in sisal fibre reinforced composites when subjected to similar environmental operating conditions. The model developed was later compared with results obtained from theoretical models.

1.4.1 Accelerated Ageing Through Hydrothermal Induction

When polymeric composites are subjected to humid surrounding, moisture absorption by the composite is for the most part a diffusion process depending on the prevailing ambient conditions. As a result, time is an important factor in reproducing these effects. Since moisture absorption to saturation under typical field environmental conditions can take years, the ability to reproduce these effects in the laboratory in a more reasonable duration of days or weeks is essential.

The intent in this research was that after accelerated ageing conditioning process for a period of weeks in the case of macro composite specimens and days for micro composite specimens, the state of the test specimens would have approximated the condition that they would have been expected to be after years of service when exposed to moisture at different temperatures. This could be possible with the help of hydrothermal induced degradation of the composite.

This research required, first and foremost, hydrothermal conditioning before testing of the macro and micro composite specimens. Neat polyester specimen and loose sisal fibres were also required to be subjected to similar ageing condition for the purpose of assessing individual property changes in the constituents making up the composite. Hydrothermal conditioning was made possible with the help of three distilled water-filled 36 litre baths with water temperature set and maintained at 23^{o}C, 40^{o}C and 60^{o}C respectively. The exposure to these conditions was for a maximum period of 24 weeks, a period during which accelerated aging would have taken place and this was to be confirmed by the periodic mechanical property tests throughout this period.

Furthermore, scanned electron microscopic studies on the fractured specimens were performed to gain a closer view into the damage zone and establish its relationship to these hydrothermal loading conditioning environments.

1.4.2 Mechanical Property Testing

(a) Tests were carried out on conditioned neat polyester and sisal-polyester composite specimens to assess the retention of the composite's mechanical properties. Tests conducted included tensile and fracture toughness tests, in accordance with the ASTM Standards D5934-02, E132-04 and E1922-97 respectively, on laboratory test rigs modified to function as required in certain cases.

(b) Tensile tests on single conditioned and unconditioned randomly selected sisal fibres were conducted as described in accordance to ASTM D 3379-75 standard on an Instron 5564 testing machine. Property changes of the fibres were observed over 120 days.

1.4.3 Microbond Tests

The interfacial shear strength properties of the fibre-resin interface in sisal fibre reinforced polyester composite were determined by measuring the force needed to axially pull a single fibre out of a solid matrix bead with a very small embedded length with the fibre. These tests were conducted on an Instron 5564 testing machine.

1.5 Significance of the Research

The influence of environmental factors, such as elevated temperatures, high humidity, and subsequent ageing, just to mention a few, on the performance of polymer matrix composites is of concern in many applications. These environmental conditions may cause degradation in the mechanical and physical properties of a fibre-reinforced polymer. A lot of work has been done on fibre reinforced composites. However, a lot remains yet undone in the area of environmental effects on natural fibre reinforced composites as these materials are an emerging class of engineering materials. The results of this research will help in establishing the material's performance under the influence of environmental factors.

CHAPTER 2 LITERATURE REVIEW

2.1 Environmental Effects on Fibre Reinforced Composites

There is increasing attention in both civil and automotive industry to try and replace the expensive established fibreglass with natural fibre as reinforcing material in both thermosets and thermoplastic composites. One of the key drawbacks of using natural fibres as reinforcements in the production of automotive components is the low mechanical properties over time as a result of environmental degradation (Liang, et al., 2013). Environmental degradation is an important factor affecting the performance of natural fibre reinforced composites. It is the subsequent loss of resistance by a composite after it has been exposed to degradation agents such as, (Bagherpour, 2012)

- Thermal - static heat ageing, sub-zero exposure or thermal cycling;
- Humidity (including hot/wet) exposures;
- Complete immersion in water at ambient and elevated temperatures;
- Freeze/thaw and dry/wet cyclic conditions;
- Continuous or intermittent salt water immersion or spray;
- Weathering (including rain and sand erosion);
- Combined load (i.e. stress) and environmental exposures;
- Chemical (including water, fuel, acids, alkalis, solvents and oxygen);
- Ultraviolet and high-energy radiation;
- Electrical stress (e.g. lightning stress and galvanic reactions) and Micro-organisms (e.g. fungi).

In some circumstances, only a few hours of exposure may lead to catastrophic failure or seriously compromise structural integrity. In many applications, composite structures will be exposed to a combination of two or more factors, often resulting in complex synergistic degradation of the material. Accelerated degradation may be caused by the combined action of two or more vectors (e.g. temperature and humidity). (ibid)

2.1.1 Hydrothermal Effects

When polymeric composites are subjected to humid surrounding, a majority of these composites begin taking up moisture by diffusion through the matrix material. Research by Shen and Springer (1976a) and separately by Springer et al. (1980) on moisture absorption for epoxy and polyester matrix composites has shown that the moisture concentration increases steadily with time before reaching the material's point of saturation in a couple of days (Figure 2.1). The thickness of the laminate and the prevailing surrounding temperature influence the rate at which this equilibrium point is attained. In practice upon drying the composite, it has been observed that the rate of desorption tends to be higher than the absorption rate, but the two are equated however, for analytical purposes.

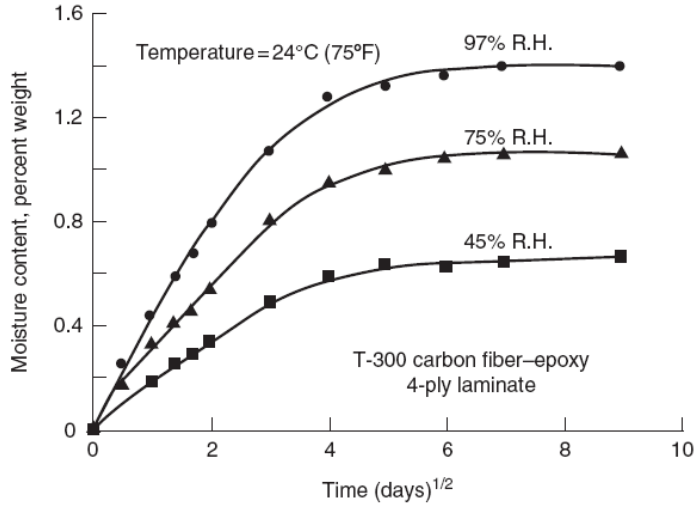

Figure 2.1: Moisture absorption in a carbon–epoxy composite at 24^{o}C. (Shen and Springer, 1976a)

Shen and Springer (1976a) showed that for any exposure duration to a humid environment at a given temperature, the moisture concentration *M,* averaged over composite thickness can be expressed as follows, where details are given in sub Section 2.1.1.1:

$$M = M_i + G(M_m - M_i)\ , \tag{2.1}$$

where

M_i - Initial moisture concentration, assumed to be equal to zero for completely dried materials

M_m- Maximum attained moisture content at saturation

G - Time-dependent dimensionless parameter related to the diffusion coefficient of the material

At constant environmental temperature, composite specimens subjected to a humid environment tend to experience increases in their equilibrium moisture concentration M_m with increase in relative humidity as opposed to specimens immersed in water whose equilibrium moisture concentration remain constant as seen in Figure 2.1 and Table 2.1.

Table 2.1: Equilibrium Moisture Content in Various Composite Laminates

Material	Laminate	RH(%)	Temperature (^{o}C)	M_m (%)
T-300 carbon-epoxy[a] (v_f = 68%)	Unidirectional (0^o) and quasi-isotropic	50	23	0.35
		75	23	0.7875
		100	23	1.4
		Fully submerged in water	23	1.8
E-glass-polyester[b] (w_f = 50%)	SMC-R50	50	23	0.10
		100	23	1.35
E-glass-vinyl ester[b] (w_f = 50%)	SMC-R50	50	23	0.13
		100	23	0.63

[a](Shen and Springer, 1976a)

[b](Springer et al., 1980)

Assuming a Fickian diffusion through the laminate thickness, the time dependent parameter G can be approximated as (ibid),

$$G \approx 1 - \frac{8}{\pi^2} exp\left(-\frac{\pi^2 D_z t}{c^2}\right), \quad (2.2)$$

Where

D_z- diffusion coefficient (mm ^{2}/s) of the material in the direction normal to the surface (moisture diffusion is in the thickness direction)

c - equivalent to the laminate thickness if both sides of the laminate are exposed to humid environment; it is 2*c*for exposure on one side.

t - time (s)

Equation (2.2) is valid for cases of large exposure times, *t*. But in the case of shorter exposure times, the average moisture concentration increases linearly with $t^{½}$, and the parameter *G* can be best expressed as

$$G = 4\left(\frac{D_Z t}{\pi c^2}\right)^{1/2} \tag{2.3}$$

The diffusion coefficient D_z is related to the matrix diffusion coefficient D_m by the following equation:

$$D_Z = D_{11}cos^2\phi + D_{22}sin^2\phi \tag{2.4}$$

Where

$D_{11} = D_m(1 - v_f)$

$D_{22} = D_m\left(1 - 2\sqrt{\frac{V_f}{\pi}}\right)$ - Assuming fibre diffusivity (D_f) ≪ matrix diffusivity (D_m)

ϕ = fibre angle with the *z* direction ($\phi = 90^o$ for fibres parallel to the laminate surface)

V_f= fibre volume fraction

Equations (2.1) through (2.4) can be used to estimate the moisture concentration in a polymer matrix composite. However, the presence of the following internal and external influences may cause shifts from the determined moisture concentrations, using the foregoing equations. (ibid)

1. Void content

Void content in composites tends to dramatically increase both the equilibrium moisture concentration and the resultant diffusion coefficient of the composite product. Enclosed voids provide water storage at much higher concentration than in the resin. (Thomason, 1995a, Thomason, 1995b)

2. Fibre type

Equation (2.4) is more applicable to glass, carbon, and boron fibres as it puts emphasis on the matrix diffusivity neglecting the effect of fibre diffusivity (Shen and Springer, 1976a). But in cases of Kevlar 49 and a number of natural fibres reinforced composites, the reinforcing fibres absorb a significant amount of moisture from the environment over a period of time. (ibid)

3. Resin type

To a certain extent, the resin chemical structural, makeup and consequent curing extent bears an effect on its moisture absorption properties (ibid). Wright (1981) in his research on epoxy/carbon fibre composite systems demonstrated that weight gain as a result of absorbed water may be at variance by a factor of 10 or more depending on the chemical structural composition of the resin. It may be by a factor of 3 or more for a similar resin that followed a different curing cycle. Many resin systems exhibit tendencies of prolonged absorption process over a long period and in some cases equilibrium fails to be reached even after being exposed to the humid environment for years.

4. Temperature

Temperature to a great extent affects the moisture diffusion coefficient of composites as the diffusion process is an energy activated process as shown in Table 2.2.

Table 2.2: Diffusion Coefficient for Absorption and Desorption in an Epoxy Resin at 100% Relative Humidity. (Wright, 1981)

Temperature (^{o}C)	Diffusion Coefficient (10^{-8}mm^2/s)	
	Absorption	Desorption
0.2	3	3
25	21	17
37	41	40
50	102	88
60	179	152
70	316	282
80	411	489
90	630	661

In general, the temperature dependence can be predicted from an Arrhenius-type equation (ibid):

$$D_z = D_{z0}\exp\left(-\frac{E}{RT}\right) \tag{2.5}$$

Where

E - activation energy (cal/g mol)

R - universal gas constant = 1.987 cal/(g mol K)

D_{z0} - a constant (mm^2/s)

5. Stress level

Gillat and Broutman (1978) showed that higher diffusion coefficients can be obtained by inducing an upward adjustment on the applied stress level on T-300 carbon-epoxy cross-ply laminate. This in turn has no effect on the laminate moisture content at equilibrium. Marom and Broutman (1981) have later established that the fibre orientation in the matrix has a bearing on the moisture absorption with maximum effect being at 90^{o}.

6. Microcracks

The existence of microcracks will tend to raise the moisture concentration beyond equilibrium concentration of laminates without microcracks owing to the capillary influence of microcrack in the matrix as well as the fact of exposed fibre-matrix interfaces along the edge of the laminate.

7. Reverse thermal effect

Adamson (1983) observed that cast-epoxy resins or epoxy-based laminates holding an equilibrium moisture concentration display increase in the rate of moisture absorption upon reduction of the exposure temperature. In his study on an AS carbon fibre reinforced epoxy composite laminate, its moisture concentration reached equilibrium at 2.3 wt% after 140 days of exposure to the environment at 74^{o}C. A reduction in the exposure temperature to 25^{o}C resulted in an increase in the equilibrium moisture content to about 2.6%. This phenomenon of inverse temperature dependency of moisture absorption is referred to as the reverse thermal effect.

Volumetric swelling as a result of absorbed moisture in the resin produces dimensional variations in the material. This amount of volumetric swelling can be expressed as follows, if it is assumed that the quantity of the absorbed moisture is equated to the resultant resin volume change (ibid):

$$\frac{\Delta V(t)}{V_0} = \frac{\rho_m}{\rho_w} M \tag{2.6}$$

Where

ρ_m - matrix density
ρ_w - water density ($\approx$1kg/mm^3)
M -moisture content at time t

The corresponding volumetric strain in the resin is (ibid):

$$\varepsilon_m = \frac{1}{3}\frac{\Delta V}{V_0} = \frac{1}{3}\frac{\rho_m}{\rho_w} M = \beta_m M \tag{2.7}$$

Where β_m is called the swelling coeficient.

$$\beta_m = \frac{1}{3}\frac{\rho_m}{\rho_w}$$

Moisture absorption has a detrimental effect on the resin's glass transition (T_g) as shown in Figure 2.2. Although performance of the resin subjected to moisture absorption at room temperature may not change with a reduction in T_g, its raised temperature properties are severely affected. For example, the modulus of an epoxy resin at 150°C (302°F) decreases from 2,070 MPa (300,000 psi) to 20.7 MPa (3,000 psi) as its T_g is reduced from 215°C (419°F) to 127°C (260°F). Equivalent effects may be anticipated for the matrix-dominated properties of a polymer matrix composite. (Shirrell et al., 1976).

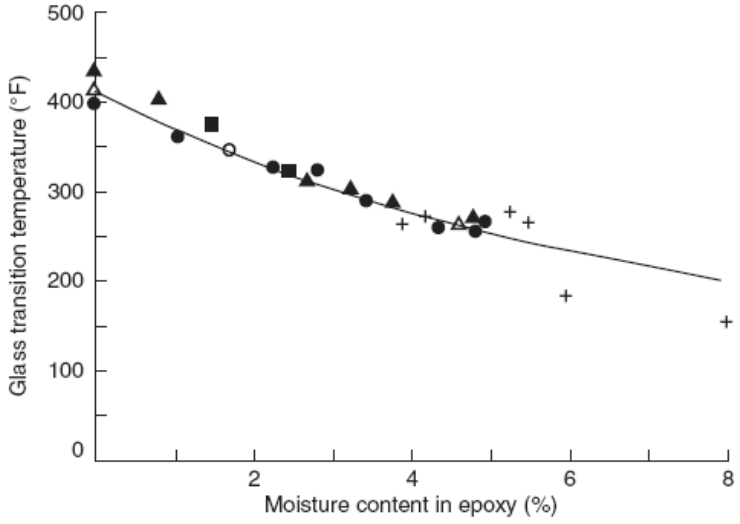

Figure 2.2: Variation of glass transition temperature of various epoxy matrices and their composites with moisture content (Shirrell et al., 1976).

The volumetric expansion of the matrix in the areas around reinforcing fibres reduces the residual compressive stresses at the fibre–matrix interface brought about by curing shrinkage. This result in the relaxation of both the chemical bonding and

mechanical interlocking that exists at the interfacial region between the fibre and surrounding matrix material.

8. Changes in Performance due to Moisture and Temperature

From the data presented by Shen and Springer (1977) based on studies conducted on the effects of temperature and the moisture content on the tensile strength and modulus of carbon and boron fibre-reinforced epoxy laminates, the following deductions can be made:

For 0^o and $[0/\pm45/90]_S$ quasi-isotropic laminates, changes in temperature of up to 107^oC (225^oF) have insignificant effects on the value of tensile property values in spite of the absorbed moisture in the material. Although the effect on modulus is insignificant below 177^oC (350^oF), there may be up to a 20% decrease in tensile strength as the temperature increases from 107^oC (225^oF) to 177^oC (350^oF).

For 0^o and $[0/\pm45/90]_S$ laminates, the tensile strength and modulus are not affected by moisture absorption below 1% moisture concentration. Although the modulus is not affected by even higher moisture concentration, the tensile strength may decrease by as much as 20% for moisture concentrations above 1%.

For 90^o laminates, increasing temperature and moisture concentration reduce both the tensile strength and the modulus by significant amounts. Depending on the temperature and moisture concentration, the reduction may range as high as 60%–90% of the room temperature properties under dry conditions.

Weathering is difficult to fully quantify because of the variation of the parameters according to the local conditions (Biron, 2003), such as:

- Hours of sun per annum
- Irradiation energy
- UV level
- Average and extreme temperatures
- Hygrometry, rain

The effect of laminate thickness on the rate of diffusion of oxygen in to the core of the polymer is illustrated in Figure 2.3.

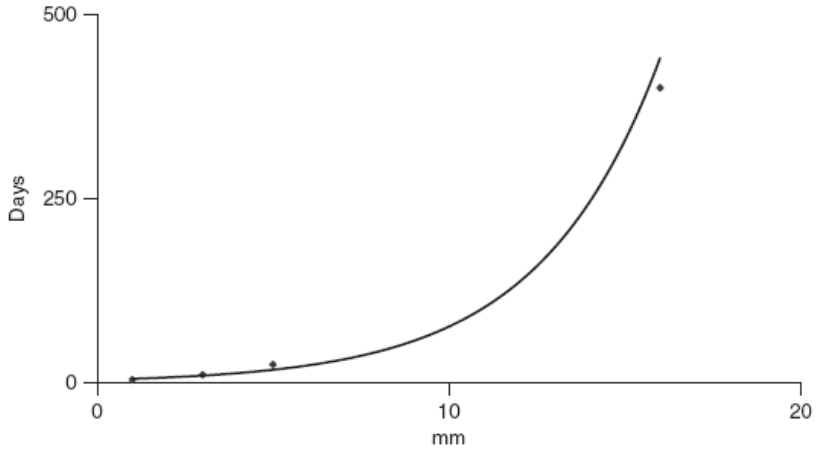

Figure 2.3: Ageing time (days) to reach the same degradation level versus sample thickness (mm). (Biron, 2003)

The consequences of weathering are similar to heat ageing with more pronounced surface degradation and notably:

- Discoloration, yellowing, gloss loss, decreased transparency for transparent polymers
- Chalking, crazing, hardening.

Chemical attack of polymeric composite matrix involves chemical reaction of the matrix with the absorbed fluids leading to the hydrolysis by water, acids and alkalis. Most particularly vulnerable are esters, amides, imides, and carbonate groups (Brown et al., 1995, Maxwell et al., 2005). A general hydrolysis representation can be portrayed as shown in Figure 2.4.

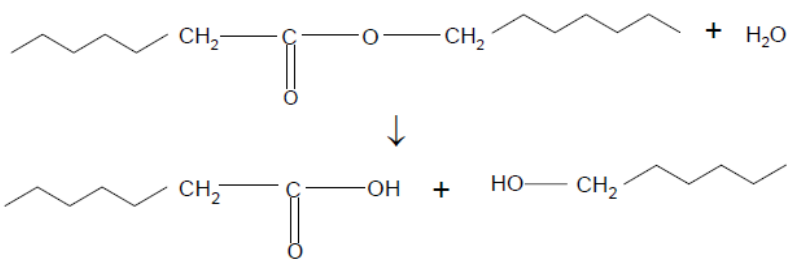

Figure 2.4: A general hydrolysis representation. Source: (Maxwell et al., 2005)

This results in the reduction in the molecular weight of the matrix, which eventually causes a reduction of fracture strain.

Stress is also known to also enhance the rate of fluid uptake (Maxwell et al., 2005), with the consequent effects of increasing the mechanical properties reduction at earlier stages (Wan et al., 2001). At later stages, a contrary trend is observed.

2.1.1.1 Fickian Diffusion Model

Assuming that initially the material is exposed to the environment on two sides with both sides being parallel, the initial temperature and moisture distribution inside the material are assumed to be uniform, the moisture content and temperature of the environment are assumed to be constant (Shen and Springer, 1976b, Surathi and Karbhari, 2006), Fickian diffusion theory describes the moisture content during absorption and desorption M_t as

$$M_t = G(M_m - M_i) + M_i \tag{2.8}$$

Where M_t – Percentage moisture gain with time.

M_i – Initial moisture content of the composite specimen.

M_m – Maximum moisture content in the composite specimen at saturation.

G – Time dependent parameter which is described as

$$G = 1 - \frac{8}{\pi^2}\sum_{n=0}^{\infty}\frac{exp\left[(2n+1)^2\pi^2\left(\frac{Dt}{h^2}\right)\right]}{(2n+1)^2} \tag{2.9}$$

Where

D – Diffusivity of the composite material normal to the surface. At times referred to as diffusion coefficient.

h – Thickness of the material.

It is assumed that the specimens used in moisture absorption study were initially dry and free of moisture, and M_i is taken to be equal to zero. Therefore the resultant

moisture content of the composite specimen after being exposed to the environment for time *t*, M_t is expressed as (ibid):

$$M_t = M_m \left[1 - \frac{8}{\pi^2} \sum_{n=0}^{\infty} \frac{exp\left[(2n+1)^2 \pi^2 \left(\frac{-Dt}{h^2} \right) \right]}{(2n+1)^2} \right] \tag{2.10}$$

For purpose of approximating both short and long term moisture contents, equation (2.10) can be reduced to equations (2.11) and (2.12) by defining a non-dimensional time parameter Dt/h^2 as follows.

For short term exposure, $Dt/h^2<0.04$:

$$M_t = M_m \left[\frac{4}{\pi} \sqrt{\frac{Dt}{h^2}} \right] \tag{2.11}$$

Whereas, for long term exposure, $Dt/h^2>0.04$, therefore:

$$M_t = M_m \left[1 - \frac{8}{\pi^2} exp\left(\frac{-Dt}{h^2} \pi^2 \right) \right] \tag{2.12}$$

2.1.1.2 Langmuir Diffusion Model

The Langmuir diffusion model assumes that absorbed moisture is made up of mobile and bound phases. Molecules of mobile phase diffuse with a concentration and stress-independent diffusion coefficient *D* and are absorbed (become bound) with probability per unit time α at certain sites whose nature is unspecified (Carter and Kibler, 1978, Surathi and Karbhari, 2006). Molecules are emitted from the bound phase, thereby becoming mobile, with a probability per unit time β. The moisture content in test specimens approaches an equilibrium value, M_m, when the number of mobile molecules per unit volume, *n*, and the number of bound molecules per unit volume, *N*, approach values such that

$$\beta n = \alpha N \tag{2.13}$$

Then the total moisture uptake in an initially dry single-dimensional specimen after being exposed for time *t*, is approximately represented by (Shen and Springer, 1976b, Surathi and Karbhari, 2006):

$$M_t = M_m \left[1 - \frac{\alpha}{\alpha + \beta} \exp(-\alpha t) - \frac{\alpha}{\alpha + \beta} \frac{8}{\pi^2} \sum_{n=0}^{\infty} \frac{\exp\left[(2n+1)^2 \pi^2 \left(\frac{-Dt}{h^2} \right) \right]}{(2n+1)^2} \right]$$

(2.14)

For short term exposure periods, that is the case where $Dt/h^2<0.04$, equation (2.14) can be reduced to (ibid):

$$M_t = M_m \left[\frac{\alpha}{\alpha + \beta} \frac{4}{\pi} \sqrt{\frac{Dt}{h^2}} \right]$$

(2.15)

And for long term exposure periods, that is the case where $Dt/h^2>0.04$, equation (2.14) can be reduced to (ibid):

$$M_t = M_m \left[1 - \frac{\alpha}{\alpha - \beta} \exp(-\alpha t) - \frac{\alpha}{\alpha + \beta} - \frac{8}{\pi^2} \exp\left(\frac{-Dt}{h^2} \pi^2 \right) \right]$$

(2.16)

2.1.1.3 Correction for Edge Effects

It is normally assumed that moisture enters the test composite specimen largely through the *nl* area surface of the specimen (see Figure 2.5). Due to the absence of an applied coating impermeable to moisture through the edges, a considerable amount of moisture finds its way through the edges into the specimen, and as such, edge correction has to be taken into account when studying moisture absorption (Surathi and Karghari, 2006, Shen and Springer, 1976b). Therefore, a correction factor has to be applied, taking into account for the edge diffusion, to the diffusion coefficient acquired for both Fickian and Langmuir diffusion models as follows,

$$D_x = D \left(1 + \frac{h}{l} + \frac{h}{n} \right)^{-2}$$

(2.17)

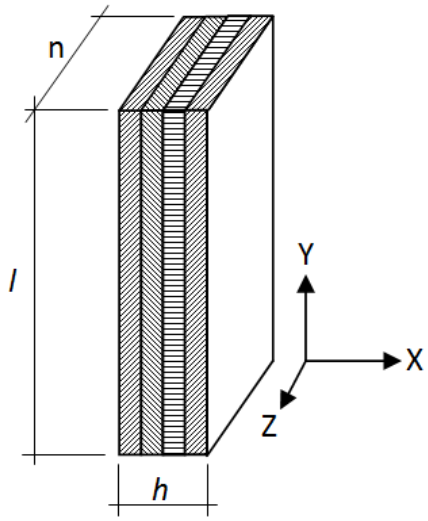

Figure 2.5: Schematic representation of a water absorption test specimen.

When this effect is neglected, the diffusion coefficient is then expressed as follows

$$D_x = D$$

2.1.2 Effect of Hydrothermal Ageing on Composites' Properties.

In order to test the long-term performance and durability of various composite systems, researchers have continued using aritificial hydrothermal ageing on various mechanical properties. Kotani et al., (2010) studied tensile strength degradation mechanism of plain woven glass fibre reinforced plastics by analysing the effects of absorbed moisture and immersion duration on the mechanical properties. This study was carried out by immersing the composite specimens in water at different temperatures of 40^{o}C, 80^{o}C, and 95^{o}C for a maximum duration of 4000 hours.

They concluded from the study that the strength and rupture strain had a propensity to decrease drastically in the early stages of the ageing process and to saturate towards certain strength values with long-term ageing as shown in Figure 2.6.

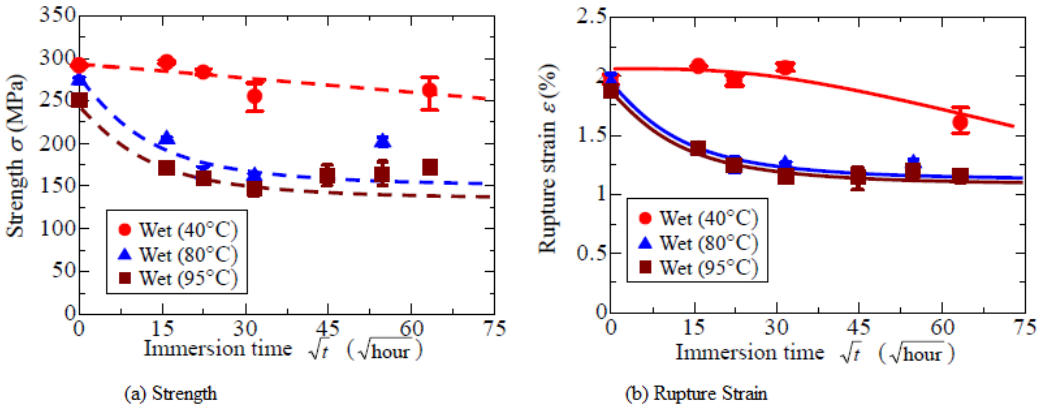

Figure 2.6: Tensile Strength and Rupture Strain variation respective plots.

Panigrahi and Mallick (2009) in their study characterised a hybrid FRP composite by exposing it to hydrothermal treatment under various ambient conditions. One group of carbon-glass fibre reinforced hybrid composite specimens was subjected to cryogenic conditions of -40^{o}C for duration of 2 hours whereas the other group was subjected to a water exposure condition at an ambient temperature of 50^{o}C for a similar duration. Conditioned samples were further subjected to 3 point bending test whose results were compared with baseline values of the unconditioned composite specimens. Differential Scanning Calorimetric (DSC) studies were also conducted to observe changes in the glass transition temperature (Tg). It was noted as seen in Figure 2.7 that the values of interlaminar shear strength (ILSS) increased initially and then later decreased with increase of absorbed moisture. This may be attributed to the relief of the stresses induced during curing. With subsequent moisture absorption, the ILSS decreased because the adhesion between the molecules was lowered. The role of moisture uptake swelling of the matrix on the residual stresses is considered to be important when considering effect of deterioration of interfacial shear properties (Cauich-Cupul et al., 2011). Both the combination of the radial stresses and the mechanical component of fibre-matrix are seen to decrease rapidly for higher moisture contents in the matrix and/or in the interface.

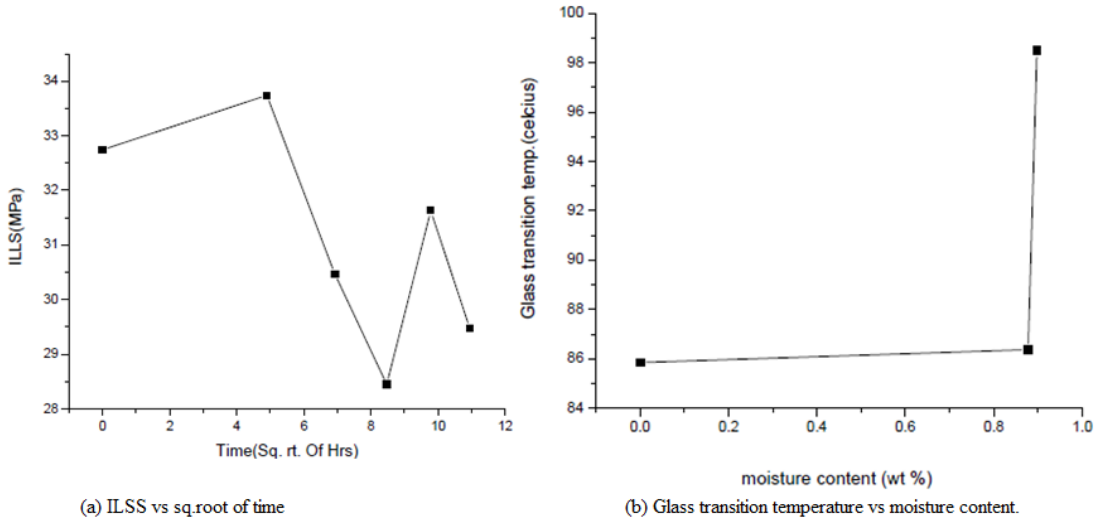

(a) ILSS vs sq.root of time (b) Glass transition temperature vs moisture content.

Figure 2.7: (a) ILSS variation Plot; (b) Glass transition temperature Plot.

Then a further increase was experienced in ILSS and this time around due to hydrolysis of polymer chains. In such a scenario, breakage of covalent bonds and the absorbed water molecules form strong hydrogen bonds with the hydrophilic groups of the epoxy network. Water with double hydrogen bonds acts as a physical crosslink. The formation of hydrogen bonds, in turn results in an increase in Tg and ILSS.

Mouzakis et al., (2007) conducted accelerated environmental ageing study of both polyester resin and polyester/glass fibre reinforced composites using alternating cycles of temperature, humidity and UV radiation on the neat polymers and reinforced composites in an environmental ageing chamber. Dynamic mechanical analysis (DMA), for a range of temperatures and frequencies under tensile and three-point bending loadings, revealed that the aged composite specimens gained in stiffness, whereas a small deterioration in strength was recorded as indicated in Table 2.3.

Table 2.3: Average tensile mechanical properties of the environmentally aged isophthalic polyester in virgin, humid, reinforced (ECH) and dried (ECD) specimens, respectively. (Mouzakis et al, 2007)

Polyester	σ_{ult} (MPa)	E (GPa)	ε_{ult}(%)
Virgin	47.27 ±3.3	2.37 ±0.04	2.52 ±0.25
ECH	47.08 ±4.94	2.59 ±0.04	2.18 ±0.28
ECD	45.01 ±5.50	2.67 ±0.07	1.99 ±0.35

Where

ECH – (E) E-glass of (C) continuous filaments of (H) 10 microns diameter.

ECD – (E) E-glass of (C) continuous filaments of (D) 5 microns diameter.

The effects of hydrothermal ageing on the bond strength of polymeric composites were studied by Gaur et al., (1994). For the fibres embedded in Epon 828 and polycarbonate resins, uniform and sizeable bond strength reductions (13- 50%) were achieved after refluxing in water at 88°C. However, the interfacial shear strengths for the same three fibres embedded in polyethylene resin were increased irreversibly by 36 to 46% upon exposure to the same ageing conditions for 24 hours.

Table 2.4 shows a summary of some previous research carried out on hydrothermal ageing of various polymeric composite materials.

Table 2.4: Summary of some previous research on hydrothermal ageing of various composite systems.

Author(s)	**Fibre**	**Matrix**	**Ageing Envirnt**	**Ageing Temp (^oC)**	**Ageing Duration**	**Findings**
Kotani et al. (2010)	Glass Fibre	Vinylester	Deionised water	40, 80, 95	4000hrs	Strength and rupture strain had a propensity to decrease drastically in the early stages of the ageing process and to saturate towards certain strength values with long-term ageing.
Panigrahi and Mallick (2009)	Carbon-Glass Hybrid	Epoxy	Water & Cryogenic	50, -40	2 hours	Breakage of covalent bonds and the absorbed water molecules form strong hydrogen bonds with the hydrophilic groups of the epoxy network. Water with double hydrogen bonds acts as a physical crosslink. The formation of hydrogen bonds, in turn results in an increase in Tg and ILSS.
Mouzakis et al. (2007)	Glass Fibre	Polyester	Humidity, UV	1) 23^{o}C (50% RH) 2) 98% RH (60^{o}C) 98% RH (50^{o}C) 98% RH (50^{o}C)	7 days 4 hrs (w/o condensation) 42 days (with condensation)	Dynamic mechanical analysis (DMA), for a range of temperatures and frequencies under tensile and three-point bending loadings, revealed that the aged composite specimens gained in stiffness, whereas a small deterioration in strength was recorded.

Author(s)	Fibre	Matrix	Ageing Envirnt	Ageing Temp (^oC)	Ageing Duration	Findings
Kennedy et al. (1998)	photo polymerised silicate glass fibre	Dimethacrylate - copolymer	Water	37^oC	90 days	Results showed a slight increase in the stiffness of S2-glass composites; however, higher reinforcement levels reduced the retention of strength in S2-glass composites.
Joseph et al. (1995)	Sisal (Treated & Untreated)	Low density polyethylene	Water Air	100^oC 70^oC	7 hours 7 days	• CTDIC-treated composites exhibited superior mechanical properties and better dimensional stability compared to untreated composites subjected to identical ageing conditions. • Greater resistance of the treated composites under different ageing conditions indicated the existence of an efficient interfacial area between the fibre and the polymer matrix.
Gaur et al. (1994)	Kevlar 49, AS4 Carbon, E-glass	Epon 828 (Thermoset); Polyethylene and Polycarbonate (both thermoplactics)	Water	88^oC	24 hours	The interfacial shear strengths for the same three fibres embedded in polyethylene resin were increased irreversibly by 36 to 46% upon exposure to the same ageing conditions for 24 hours.

Author(s)	Fibre	Matrix	Ageing Envirnt	Ageing Temp (^oC)	Ageing Duration	Findings
Ray (2006)	Glass Fibre	Epoxy, Polyester	Humidity	50^oC (60% RH) 50^oC (95% RH) 50^oC (60% RH) 70^oC (60% RH)	1 hour cycle 1 hour 1 hour cycle 1 hour	• It was concluded that moisture was absorbed in changing humidity cycle with a constant temperature environment. • The type of the matrix resin and the weight fraction of the constituents were found to have an influence on the nature of moisture absorption.
Gaur and Miller (1990)	Aramid (Kevlar), Glass fibre	Epoxy, Epon, Polycarbonate	Water	100^oC (Steam) 88^oC (Water)	72 hours	Significant reduction in both average shear strength and in shear strength distributions on exposing aramid (Kevlar)/epoxy and E-glass/epoxy microbond assemblies to steam (100^oC) or hot water (88^oC) were observed.For the fibres embedded in Epon 828 and polycarbonate resins, uniform and sizeable bond strength reductions (13- 50%) were achieved

Author(s)	**Fibre**	**Matrix**	**Ageing Envirnt**	**Ageing Temp (^{o}C)**	**Ageing Duration**	**Findings**
Yilmaz and Sinmazcelik (2010)	Glass fibre	Polyetherimide (PEI)	Water	0^{o}C – 100^{o}C Cycle	2 minutes/ Cycle (100 cycles total)	• The hydrothermally aged laminates saw an increase in the amount of moisture contained which consequently caused decrease in the glass transition temperature and further deterioration in mechanical properties, namely interlaminar shear strength, flexural modulus, bearing strength, et cetera. • Fractographic analysis showed interfacial debonding as the dominant failure mechanism, signifying a strong influence of water degradation on the results of fracture toughness.
Mula et al. 2006)	Glass fibre	Epoxy Polyester	Water Freezer	60^{o}C -20^{o}C (Later)	64 hours 1 hour	Samples which were subsequently frozen showed higher interlaminar shear strength (ILSS) initially, although this trend was reversed after a certain conditioning period.
Biro et al. (1993)	Carbon fibre	Epoxy	Water	21^{o}C, 80^{o}C	24 hours	The observed reduction in shear strength was attributed due to plasticisation of the resin by water as well as decrease in mechanical interlocking pressures arising from thermal expansion mismatching of the fibre and matrix.

Author(s)	Fibre	Matrix	Ageing Envirnt	Ageing Temp (^oC)	Ageing Duration	Findings
Roy et al. (2001)	Glass fibre (Treated & Untreated)	Vinylester	Water	100^oC	2, 4, 6, 8, 24 hours	The resultant mechanical properties were relatively inferior when treated with boiling water for longer hours which was attributed to access of moisture by capillary action through the interface between the fibre and the resin matrix. Scanned electron microscopic analysis of the fractured surfaces revealed heavy fibre pull-out in the tensile zone whilst shear fracture of the fibre bundles was predominant at the compressive zone of the samples tested for flexural strength properties.
Karbhari (2004)	Glass fibre	Vinylester	Water	5^oC – 60^oC	225 weeks	
Gopalan et al. (1989)	Polyester Epoxy	Hybrid fibres (glass-carbon, carbon-kevlar and Kevlar-glass)	Water	70^oC	20 days	Degradation in ultimate tensile strength and Young's modulus due to the moisture content were experimentally determined and found to be quite significant. Further scanning electron microscope (SEM) studies on failed hydrothermally conditioned and unconditioned specimens revealed resin leach out and fibre swelling.

- Hydrothermal dilapidation of matrix material owing to the absorbed moisture results in the reduction of major mechanical the composite.
- Notable appreciation in Tg, ILSS and E during early stages of hydrothermal ageing have been observed.
- Surface treatment of fibres prior to reinforcement offers resistance against hydrothermal attack of the fibre matrix interface.

2.1.2.1 Arrhenius Life-Stress Analysis

Design of engineering structural components requires a thorough understanding of its mechanical properties and how its constituent materials respond to the prevailing service environment. Over time, variability in the surrounding temperature and humidity levels results in composite components constantly absorbing and desorbing moisture causing material property degradation (Shen and Springer, 1976a). It is therefore vital to establish the mechanical performance of the composite material and its resultant life.

When polymeric composites are subjected to humid surrounding, moisture absorption by the composite is, for the most part a diffusion process depending on the prevailing ambient conditions. As such, it requires many years to reproduce desired effects hydrothermal ageing would pose on the material properties since moisture absorption to saturation by a composite takes years.

The Arrhenius Life-Stress Prediction model a useful model for gauging the lifetime of polymeric materials. It has been used adequately to predict combined effects of the applied stress over time (Phani and Bose, 1987; Maxwell et al., 2005). It has for most part been effectively used for the accelerated response testing of polymers as it allows the use of short-term tests conducted at elevated temperatures to assess long-term performance when exposed to lower temperatures. It is therefore for this reason that it is the theoretical model which has been adopted in this research.

The Arrhenius relationship is represented by the equation (ibid):

$$R(T) = Aexp\left[{-E_a}/{RT}\right] \tag{2.18}$$

Where $R(T)$– is the rate of reaction of the process.

E_a– is the activation energy, in J/mol K. This is the minimum amount of energy required by a molecule in order for it to take part in a reaction. It is a measure of the effect that temperature has on the reaction.

R – is the universal gas constant (R=8.3144J/mol K)

T – is the absolute temperature, in Kelvin.

A – is an unknown non-thermal constant.

The Arrhenius life-stress relationship is an expression which is based on the assumption that the life is proportional to the inverse reaction rate of a process and it is represented as follows (ibid):

$$L(T) = Cexp\left[{}^{B}/_{T}\right] \tag{2.19}$$

Where

L(T) - represents the quantifiable life measure as a function of a stress level

T - represents the stress level (temperature in Kelvin. Note that the temperature value is in absolute units).

C - is an unknown model parameters to be determined, (*C*> 0).

B - is another model parameter to be determined.

The Arrhenius relationship can be linearised and plotted on a life vs. Stress (which in this case is the temperature) plot which is often referred to as the Arrhenius plot. The Arrhenius life-stress relationship is linearised by taking natural logarithms of both sides of the equation 2.19,

$$ln[L(T)] = \ln(C) + {}^{B}/_{T} \tag{2.20}$$

Equation 2.20 represents a line in the slope-intercept form, where the constant *B* determines the gradient of that line, *ln(C)* is the y-intercept and the variable on the horizontal axis is the inverse of temperature. Comparing equations 2.18 and 2.19, it is apparent that the constant *B* possesses the same attributes as the activation energy (E_a), suggesting that *B* is a measure of the effect that the stressing or forcing, function has on the longevity of the material. The larger the value of *B*, the higher the dependency of the life on the stress (temperature).

2.2 Composite Fracture

2.2.1 Macro Fracture

Aveston et al.(1971) developed a fracture mechanics based model for the determination of the fracture resistance of composites founded on the assumption that only frictional stress plays a role of holding reinforcing fibres in the surrounding matrix. Buduansky et al.(1986) used some of Aveston's results in their study on matrix cracking stress for a composite with unbonded and initially bonded, debonded fibres. Buduansky et al.(1995) later used the link existing between cracks, bridging stress σ, and crack open displacement *u*, to describe the role fibres play in the overall propagation of a crack, assuming that the interfacial sliding stress τ remains constant, as:

$$u = \lambda\sigma^2 \tag{2.21}$$

where

$$\lambda = \frac{2r(1-V_f)^2 E_m^2}{4V_f^2 \tau E_f E^2}$$

E – Composite's modulus of elasticity

E_m *and* E_f – Matrix and fibre's moduli of elasticity

r – reinforcing fibre radius

V_f – Fibre volume fraction.

τ - Interfacial sliding stress

Marshall et al.(1985) and Marshall and Cox(1987) used the stress intensity approach to determine the matrix cracking stress in a composite with the fibre held by the matrix merely by friction. In this case, the bridging fibre was represented by the traction forces which connect the fibres through the crack. By equating the composite stress intensity factor to the matrix critical stress intensity factor, the matrix cracking stress was determined.

Pagano and Kim(1994) studied damage initiation and propagation in glass fibre reinforced ceramic composites when subjected to flexural loading. Assuming that a

crack surrounding a fibre only extends to the neighbouring fibre of the hexagonal array fibre set up, a damage model was developed and further related the energy release rate as a function of the composite fibre volume fraction.

The behaviour of carbon fibre reinforced epoxy composite under static and fatigue loading was studied by Kanyanga, (1988) using centre notched unidirectional and cross-ply laminate specimens. Under static loading conditions, the investigation involved determining the fracture strengths of research specimen type and monitoring damage initiation and growth from notch tips. Static strength results were analysed and compared with existing theories. Fracture stresses generally exhibited a dependence on notch size but showed limited dependence on notch type. The initiation of splitting under static loads was governed by a parameter dependent on split initiation stress and notch size. The cross-ply laminates were less resistant to splitting than unidirectional ones.

2.2.2 Micro Fracture

Figure 2.8, depicts a typical microbond single fibre pull-out test plot of interfacial shear stress as a function of relative displacement at the interface existing between the fibre and the matrix. Region I relates to a still intact interface, whereas Region II describes the linear stress reduction in the zone with ‘‘imperfect interface’’, and Region III (with constant stress, which depends on the consistency in the fibre diameter) describes a fully debonded interface which transfers friction load only (Zhandarov and Mader, 2005). In order to characterise interfacial strength in fibre reinforced composites using micromechanical methods, different approaches were taken by these researchers but more emphasis was paid on single fibre pull-out and microbond test procedures for both stress-based and energy-based approaches.

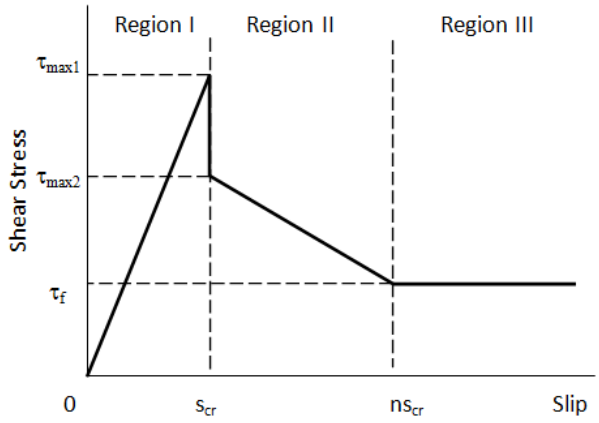

Figure 2.8: Typical microbond debonding plot with two-stage debonding (imperfect interface).

Biro et al.(1993) also applied the microbond technique to study the effects of hydrothermal exposure on carbon fibre/epoxy interfaces by immersion of the composites in water at a temperature of 80^{o}C for a maximum period of 24 hours. X-ray photoelectron spectroscopy analysis on the aged composites revealed little variation in the concentration of functional surface groups on the fibres after hydrothermal exposure. The reduction in shear strength was attributed to plasticisation of the resin by water as well as a decrease in mechanical interlocking pressures arising from thermal expansion mismatching of the fibre and matrix.

Miller et al.(1987) analysed and further used the approach which requires depositing a droplet of the epoxy resin on both silane treated and untreated fibres (Aramid and carbon fibres) and to support the cured droplet appropriately during single fibre pull-out analysis for the fibre/matrix interfacial bond strength fracture. From the results obtained it was observed that the microbond method makes it possible to investigate composite microbond failure under conditions where the resin is not available in a large quantity with success.

A round-robin programme was embarked on by Pitkethly et al.(1993) to evaluate the compatibility in a number of micromechanical practises used to assess the interfacial shear strength of the bond existing in between fibre /matrix in polymeric composite. Twelve laboratories were involved in this study each supplied with resin and fibres from the same suppliers. One of the methods put to test is the single fibre

pull-out test. The results from this study suggested that there is great potential for developing standard procedures for the evaluation of fibre/matrix interfacial shear strength and thus eliminating inter-laboratory scatter in results.

Thomason and Schoolenberg (1994) investigated interfacial strength existing between the reinforcing glass fibre and the polypropylene matrix composite system and it influence on the overall composite strength. This study compared the effect of fibre surface coating on the overall performance of polypropylene. The results showed that silane coupling agent by itself produces marginal effect on the interfacial strength of glass fibre/polypropylene system, which only significantly improved when combined with other components of coating.

Gaur and Miller(1990) used the microbond method in the direct determination of interfacial shear strengths in a bid to assess the influence of environmental conditions on the interfacial adhesive bond in aramid/epoxy and glass fibre/epoxy micro composite systems. Sizable drops in the average shear strength and changes in the shear strength distribution were observed after exposing the micro composite assemblies to steam or hot water for short periods of time, with glass fibre/epoxy system recording the most drastic changes. Full restoration of the shear strength upon vacuum drying in the aramid/epoxy micro-assembly was observed. The glass fibre/epoxy system recorded marginal recovery in its interfacial shear strength.

Microbond technique method was also applied by Biro et al.(1993) in studying the effects of hydrothermal exposure on carbon fibre/epoxy system interfaces. It was found that within the initial hour of exposure by immersing the micro composite (T300/Epon 828 or AS4/Epon 828) in water at a temperature of 80°C, the interfacial shear strengths lowered in both composite systems. After 6h of continuous exposure to the same aging environment, reductions of 41% for the T300/Epon 828 samples and 20% for the AS4/Epon 828 samples were observed. This resulted in doubling and tripling of the frictional component of the interface in the sheared droplet as it slid along the fibre length in the AS4/Epon 828 and T300/Epon 828 system respectively for the same exposure to hot/wet conditions.

Craven et al. (2000) similarly employed the microbond testing technique to evaluate the interface that exists in a silkworm silk fibres/epoxy composite system. The tests yielded average interfacial shear strength of about 15 ± 2 MPa owing to the high tensile strength of silk fibres, and its high extensibility when compared to that of synthetic polymer or even glass fibres, thus increasing its possible use in tough composites. Practical limitations observed in using this test method include the low load bearing capability of the silk fibres (due to their small average diameter), as well as the inherent variability in the cross-sectional geometry and tensile properties of natural silk.

Interface strength in glass fibre–polypropylene was determined by Yang and Thomason(2010)in which both the fibre pull-out and microbond test methods were employed. Outstanding correlation between the two methods was obtained. Data from microbond test could be divided into two groups according to whether or not there was constant interfacial friction after debonding. Microscopy observation on tested microbond samples which had exhibited decreasing interfacial friction after debonding revealed considerable residual resin around the debonded area of samples. Further investigation indicated that this unexpected difference was caused by the variation in mechanical properties of the matrix due to thermal degradation during sample fabrication.

A summary of studies previously conducted on the composite microbond interface is listed in Table 2.5.

Table 2.5: A summary of previous composite microbond interface studies.

Author(s)	Fibre	Matrix	Microbond Research Conducted	Conclusion
Miller et al. (1987)	Aramid and Carbon Fibre	Epoxy	A Microbond Method for Determination of the Shear Strength of a Fibre/Resin Interface	Interfacial bond strength results for an epoxy resin and several fiber types are adequately reproducible using this test method.
Pitkethly et al. (1993)	Carbon Fibre	Epoxy	A Round-robin Programme on Interfacial Test Methods	The results suggest that there is great potential for achieving standard procedures for these testing methods.
Thomason and Schoolenberg (1994)	Glass Fibre (Both silane coated and uncoated)	Polypropylene	An Investigation of Glass Fibre/Polypropylene Interface Strength and its Effect on Composite Properties	The flexural strength results correlated well with the level of interfacial shear strength as measured by the single fibre pull-out test.
Zhandarov and Mader (2005)	Glass Fibre (NaOH Treated/ Untreated); 3 different Aramid fibres	Epoxy; Cement matrix.	Characterization of fibre/matrix interface strength: applicability of different tests, approaches and parameters	The use of the debond force for determining adhesion parameters and both, debond and maximum force to estimate interfacial friction, gives the best results for both, polymeric and cementitious composites.

Author(s)	Fibre	Matrix	Microbond Research Conducted	Conclusion
Gaur and Miller (1990)	Aramid; Glass Fibre	Epoxy	Effects of Environmental Exposure on Fibre/Epoxy Interfacial Shear Strength	1) It has been shown that the microbond technique is effective in isolating and evaluating the effects of environmental exposure on interfacial shear strength in composites. 2) Due to the small amount of resin used and the resultant small embedment areas, moisture diffusion and capillary transport are not rate controlling processes.
Biro et al. (1993)	Carbon Fibre	Epoxy	Effects of Hydrothermal Exposure on Carbon Fibre/Epoxy Interfaces exposed to hot wet conditions	The diminution in shear strength is probably related to:1) plasticization of the resin bywater;2) reduction in mechanical interlocking pressures arising from thermal expansion mismatching of the fiber and matrix.
Craven et al. (2000)	Silk Fibres	Epoxy	Evaluating the silk/epoxy interface by means of the Microbond Test	Practical limitations of using the Microbond Test with natural silk fibres are: 1) limitations include the low load bearing capacity of the fibres (due to their small average diameter); 2) intrinsic variability in the cross-sectional geometry and tensile properties of natural silk.
Yang and Thomason (2010)	Glass Fibre	Polypropylene	Interface strength in glass fibre–polypropylene measured using the fibre pull-out and microbond methods	Interfacial shear strength is an adequate quantitative parameter which can characterise the mechanism of interfacial failure in glass fibre–thermoplastic composites.

2.3 Research Materials

2.3.1 Sisal Fibres

Sisal remains one of the most extensively used natural fibres and very easily cultivated. But its use over the years has steadily diminished with the introduction of polymeric yarns such as polypropylene, which are used for the same purpose. Amid the variety of natural fibres being exploited as reinforcement, sisal fibres have continued receiving notable attention in that they form high impact strength composites despite them having moderate flexural and tensile strengths(Baby et *al.*, 2016).

In 2009 the world production of sisal stood at nearly 300 000 tonnes, valued at $75 million with Brazil (120 000 tonnes), Tanzania (30 000) and Kenya (25 000) being the three notable producers (natural fibres, 2014).It is a hard fibre extracted from sisal leaves (*Agave sisalana*) through a process known as decortication. Normal length of sisal is between 1.0 to 1.5m and with diameter of 100 - 300μm (Li et al., 2000b). The fibres are actually made of bundle of hollow sub-fibres. Their cell walls are reinforced by spiral orientated cellulose in a hemicellulose/lignin matrix. So, the cell wall is a composite structure of lignocellulose material reinforced by helical microfibrillar bands of cellulose. The composition of the external surface of the cell wall is a layer of lignacceous material and waxy substances, which bond cells to its adjacent neighbours. Hence, this surface will not form a strong bond with a polymer matrix unless appropriate surface treatment is applied. Also, as mentioned above, cellulose, which comprises a large amount of hydroxyl groups, giving the fibre hydrophilic properties (Li et al., 1987), with subsequent poor interfacial bonding between sisal fibre and hydrophobic matrix and giving the composite very poor moisture absorption resistance. It is a well known fact that the interface that exist between the two composite constituents plays a major role in transfer of load within the composite, a good interface is indispensible in taking advantage of both composite components(Kim and Mai, 1998; Geo and Cotterell, 1988). As such, it is essential to surface treat the fibres with coupling agents to give them improved interfacial bond strength with the surrounding matrix and subsequent toughness. Figure 2.9 shows SEM views of improvement on the sisal fibre after surface treatment with permanganate.

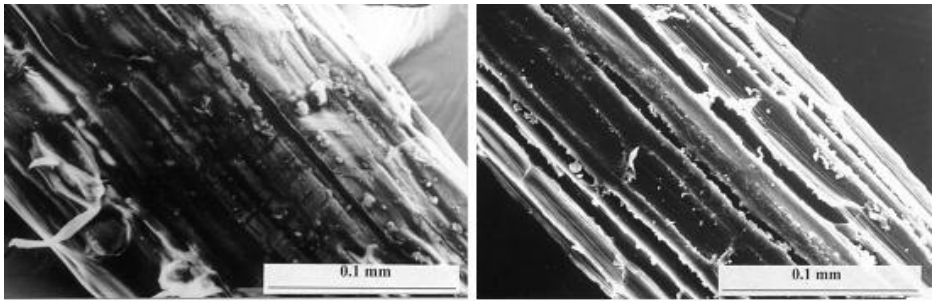

Figure 2.9: Sisal fibre surfaces (a) before surface treatment with permanganate and (b) after surface treatment with permanganate. (Source: Li et al., 2006).

The effects of suface treatments on the mechanical properties of natural fibre reinforced composites have been extensively studied by Valadez-Gonzalez et al.(1999); Sreekala and Thomas (2003); Thais et al.(2003); (Rong et al.(2001); andLuyt and Malunka(2005).

In Table 2.6 is a summary of previous studies done on sisal fibre reinforced polymeric composite

Table 2.6: Summary of various studies on sisal fibre reinforced polymeric composites.

Author (s)	Matrix	Fibre Orientation/ Nature	Studies Conducted	Study Conclusions
Paramasivam and Abdulkalam(1974)	Epoxy	Unidirectional	Feasibility of developing polymer based composites using sisal fibres due to the low cost of production of composites	1. Fabrication fairly easy and cost of production was quite low. 2. Tensile strength of the composite ranged between 250-300 MPa 4. Because of the low density of the sisalfibre, however, the specific strength of sisal composites was comparable with that of glass composites. 5. Unidirectional modulus of the composite system was found to be about 8.5 GPa
Satyanarayana et al.(1984)	Polyester	Chopped random	Mechanical Properties	1. Specific modulus of the composite was 1.90 compared with 2.71 for glass fibre reinforced plastics. 2. Specific strength was of the same order as that of polyester neat resins (34 - 41 MPa). 3. The impact strength was 30 J m^{-2}, 3 times more than that of polyester and 30% less than glass fibre

Author (s)	Matrix	Fibre Orientation/ Nature	Studies Conducted	Study Conclusions
				reinforced composite systems.
Pavithran et al.(1987)	Polyester	Unidirectional	Impact Strength of various natural fibre reinforced composites	Sisal composite systems have the highest work of fracture followed by pineapple fibre composite. Composites of banana and coir fibre exhibited moderately low work of fracture.
Pavithran et al.(1988)	Polyester	Unidirectional	Compared the impact properties with ultra high-density polyethylene/glass fibres composites.	1. Work of fracture identical with that of ultra high-modulus polyethylene composites 2. Toughness of sisal fibre composites is only 25% less than that of glass fibre composites when the density of the latter is taken into account
Bisanda and Ansell(1991)	Epoxy	(Not specified)	Effect of silane treatment and alkali treatment on the mechanical and physical properties.	1. The resulting composite yields stiff and strong composite materials. 2. Treatment of sisal fibres with silane improves wettability, mechanical properties and water resistance.
Joseph et al.(1996)	**Thermoset** (polyester, epoxy, phenol formaldehyde) **Thermoplastic** (low density	Short Fibres	Influence of interfacial adhesion on the mechanical and fracture behaviour with respect to the fibre length and fibre loading.	1. Composites showed a general trend of increasing properties with fibre loading. 2. The optimum length of the fibre required to obtain an increase in properties varied with the type of matrix 3. Observed that the fibre pull-out stress or

Author (s)	Matrix	Fibre Orientation/ Nature	Studies Conducted	Study Conclusions
	polyethylene)			debonding stress of sisal-polyester composites is only 166 MPa whereas, the debonding stress of sisal-epoxy matrix is about 226 MPa. 4. Observed that, among polyester, epoxy and phenol - formaldehyde composites of sisal fibre, a phenolic type resin performed as a better matrix than epoxy and polyester resins with respect to tensile and flexural properties.
Singh et al.(1996)	Polyester	Sisal	Effect of several chemical treatments, such as organotitanate, zirconate, silane, and N substituted methacrylamide, on the physical and mechanical Properties.	The strength retention of surface-treated composites (except silane) is high compared with untreated composites. It is observed that N substituted methacrylamide treated sisal composites exhibited better properties under dry as well as wet conditions.
Bai et al.(1999)	Epoxy	Continuous	Failure mechanisms	Reported that sisal fibre bundle-epoxy interface had a moderate high strength, but the adhesive strength between the micro-tubular fibre and the bonding material appeared to be small.

Author (s)	Matrix	Fibre Orientation/ Nature	Studies Conducted	Study Conclusions
Thermoplastics				
Joseph et al.(1992);Joseph et al.(1993);Joseph et al.(1994)	Low Density Polyethylene	Longitudinal Unidirectional; Short fibres; Random.	Mechanical properties as a function of processing method, fibre content, fibre length and orientation.	1. Fibre damage normally occurs during blending of fibre and the polymer by the melt mixing method and can be avoided by adopting a solution mixing procedure. 2. Unidirectional alignment of the short fibres achieved by an extrusion process enhanced the tensile strength and modulus of the composites along theaxis of the fibre alignment by more than two fold compared to randomly oriented fibre composites.
Kalaprasad et al.(1997)	Low Density Polyethylene	Short Fibres	Influence of short glass fibre addition on the mechanical properties of short sisal fibre reinforced LDPE composites	1. They observed that by the addition of a small volume fraction of (≅ 0.03) short glass fibre into the resin system enhanced the tensile strength of longitudinally oriented composites by more than 80%. 2. It was also observed that water absorption

Author (s)	Matrix	Fibre Orientation/ Nature	Studies Conducted	Study Conclusions
				tendency of the composite decreases with the process of hybridisation.
Joseph et al.(1994); Joseph et al.(1992); Joseph et al.(1993)	Low Density Polyethylene	Longitudinal Unidirectional	Viscoelastic and rheological properties as a function of processing method, fibre content, fibre length and orientation	1. Maximum storage moduli and a critical fibre length of 6 mm is necessary to obtain maximum dynamic moduli.
Carvalho(1997);Marcovich et al.(1997)	Polypropylene	*(Not Stated)*	Chemical modification of Lignocellulosic materials	1. Poor wettability and weak interfacial bonding with the polymer due to the inherently poor compatibility as well as dispersability of the hydrophilic cellulose fibres with the hydrophobic thermoplastics 2. Pre-treatment of the fibre surface or the incorporation of surface modifier during processing is required.

From Table 2.6, it can be established that gaps do exist in as far as research on the performance of the sisal-polyester composite systems when subjected to various hydrothermal conditions of operations. Furthermore, no work has been conducted in as far as subsequent prediction of its performance under these selected ageing conditions.

Table 2.7 lists some sisal fibre properties extracted from earlier studies conducted. It is worth noting that apart from the structure of the natural fibre, condition upon which the experiments were conducted, for example test speed, fibre gauge length, etc. all bear some influence on the resultant properties of the fibres(Satyanarayana et al., 1990; Hornsby et al., 1997).

Table 2.7: Properties of sisal fibres reported in literature.

Density (Kg/m^3)	**Moisture content (wt%)**	**Tensile Strength (MPa)**	**Tensile Modulus (GPa)**	**Maximum Strain (%)**	**Diameter (μm)**	**Source**
1450	11	604	9.4 – 15.8	-	50 – 200	(a)
1450	-	530 – 640	9.4 – 22	3 – 7	50 – 300	(b)
-	-	347	14	5	-	(c)
1030	-	500 – 600	16 – 21	3.6 – 5.1	-	(d)
1410	-	400 – 700	9 – 20	5 – 14	100 – 300	(e)
1400	-	450 – 700	7 – 13	4 – 9	-	(f)
-	-	530 – 630	17 – 22	3.64 – 5.12	100 – 300	(g)
1450	-	450 – 700	7 – 13	4 – 9	-	(h)

Sources:

(a) (Satyanarayana et al., 1990)
(b) (Chand et al., 1988)
(c) (Bessel and Mutuli, 1982)
(d) (Pavithran et al., 1987)
(e) (Kalaprasad et al., 1997)
(f) (Manikandan et al., 1996)
(g) (Mukherjee and Satyanarayana, 1984)
(h) (Kumar et al., 1995)

2.3.2 Polyester Resin

Polyester is a synthetic polymer which is made from purified terephthalic acid (PTA) or dimethyl ester dimethyl terephthalate (DMT) and monoethylene glycol (MEG). Despite it currently holding 18% of the world market share of all plastic materials produced, it ranges third after polyethylene (33.5%) and polypropylene (19.5%) (Pai and Chandra, 2013).Polyester is a category of polymers which contain the ester functional group in their main chain. Although there are many types of polyester, the term "polyester" as a specific material most commonly refers to polyethylene terephthalate (PET).

Depending on the chemical structure polyester can be a thermoplastic or thermoset, however the most common polyesters are thermoplastics (Rosato et al. 2004).Polyester resins can be formulated in a variety of properties ranging from hard and brittle to soft and flexible. Its advantages over other laminating resins include low viscosity, fast cure time, and low cost.

CHAPTER 3 MATERIALS AND TESTING PROCEDURES

3.1 Introduction

This section discuses first the method employed in making of composite test specimens, also highlighting the fibre surface treatment employed for the improvement of the interfacial bonding when forming both the microbond and macro composites test specimens. It further looks at the hydrothermal ageing process used to induce accelerated ageing of both the microbond and macro composite specimens. It further describes the procedure conducted in performing isothermal water uptake studies in order to determine moisture contents and rates of moisture diffusion for the sisal reinforced polyester composite as functions of both the exposure temperature and duration.

3.2 Materials

3.2.1 Composite

The composite selected to be used in this research was a sisal/polyester composite system with a volume fraction of 50-55%. Vacuum Assisted Resin Infusion process was used to make the composite specimens. Sisal fibre was selected as reinforcement material over other natural fibres because of its ready availability. There is also the desire of promoting sisal farming through its cultivation as Zambia is striving to diversify its agriculture away from traditional cash crops following the direction of countries like Tanzania and Kenya in the region. And the choice of polyester resin as matrix material was arrived at considering factors such as the cost of the resin when compared to resins such as epoxy which are many time higher than that of polyester. The curing aspect was also another important factor. Curing of cast polyester resin specimens do not require specific curing regimes to be followed since polyester cures under ambient temperature, cutting down on the need of the use of an available already over-stretched curing oven.

3.2.1.1 Sisal Fabric Mat

Essentially, the production of sisal fibre reinforcing fabric can be briefly broken down as follow: sisal plant cultivation in a field, harvesting and collection of the

green leaves, water retting for an optimum time period, fibre separation, repeated fibre hackling, and finally fabric weaving.

The sisal yarns used during this research were sourced from James Lever Ltd of Bolton, England. Table 3.1 lists some of its properties.

Table 3.1: Properties of Sisal Fibres

Properties	**Values (SI)**
Specific gravity	1.35
Young's modulus	≈29 GPa
Coefficient of thermal expansion	16.8μm/m^{o}C – Longitudinal 70.8μm/m^{o}C – Transverse
Operating Temperature	Up to 135^{o}C

The 2D plain sisal fibre fabric used as reinforcement in the composite panels was weaved on manually operated handloom weaving machine shown in Figure 3.1. A principle set up of the loom is illustrated in Figure 3.2.

This process basically consists of interlacing sisal yarn in the weft direction with threads of cotton yarn in the warp direction producing a 2D plane weave. The cotton warp thread used primarily in this case was sorely for the purpose of holding in place the unidirectional sisal yarn in the fabric. It was very difficult to use similar sisal yarns also in the warp direction as there existed a lot of friction as the yarn passed through the heddle of the loom which in turn resulted in build-up of sisal "wool" at the entry into the eye. This caused the thinning of the yarn which made it through the heddle, the result of which a decision was made to use cotton thread along the non-load bearing direction of the reinforcing fabric.

The woven sisal fibre fabric was further surface modified in order to improve its adhesion with the polyester resin. This was achieved by subjecting the fabric to a 5% sodium hydroxide (NaOH) solution treatment for 1 hour at laboratory room temperature. Afterwards the fabric was washed thoroughly with water to remove all

traces of the NaOH until the pH of the rinsing water was 7.0. The fabric was further dried under vacuum before it was used as reinforcement.

Figure 3.1: Composite reinforcing sisal fabric weaved on a manually operated handloom.

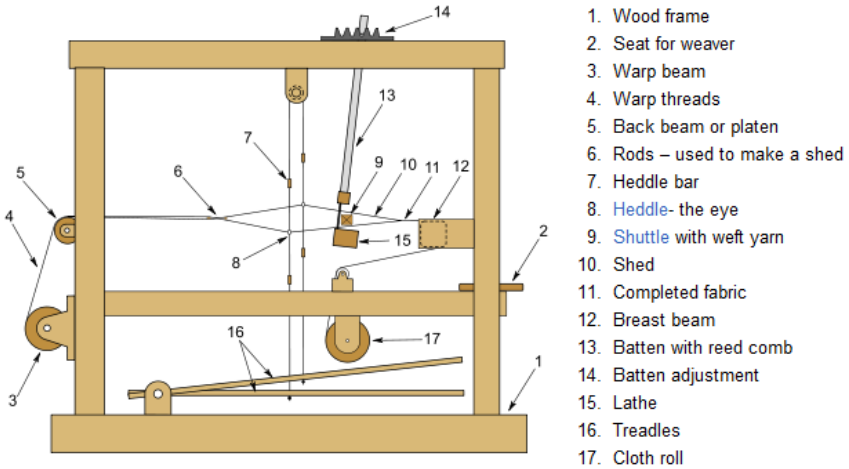

Figure 3.2: A typical Handloom Weaving Machine schematic diagram. (Source: https://classes.lt.unt.edu/Spring_2011/CECS_5420_020/cmv0046/assign5/floor.html)

3.2.1.2 Polyester Matrix

The matrix material selected for the sisal fibre reinforced composite was the General Purpose Polyester Laminating Resin supplied by ABL (Stevens) Resin and Glass Co. of Cheshire, England. Table 3.2 list some mechanical properties of cured unreinforced polyester resin material.

Table 3.2: Mechanical properties of clear-cast (unreinforced) polyester resins (Source: ABL (Stevens) Resin and Glass Co.)

Tensile Strength (MPa)	Tensile Modulus (GPa)	Elongation (%)	Flexural Strength (MPa)	Flexural Modulus (GPa)	Compressive Strength (MPa)	Heat Deflection Temperature (^{o}C)
75	3.38	3.3	130	3.59	120	90

3.2.1.3 Microbond Test Specimen Preparation

Generally mechanical properties of fibre-reinforced composites are evaluated based on a variety of standard tests performed on the bulk composite specimens. These tests do provide, to an extent, useful data about the general performance of the composite when loaded. Unfortunately, fibre-matrix interfacial properties within the composite cannot be established using these established standard testing methods, other than through known relationship between matrix yield strength and interfacial shear strength reported by Bagherpour (2012). Therefore, there is a great desire to be fully aware of the interaction that exists along the interface between the composite reinforcing fibre and the surrounding polymer matrix of various fibre reinforced composite systems. For this reason, microbond test method was selected in this research for the investigation of the fibre-matrix interfacial strength owing to the small dimensions involved in the method. This makes it possible for uniform exposure of the composite system to the ageing environmental conditions in a short period of exposure time.

Making of microbond test specimens basically requires the placement of a liquid polyester resin micro droplet concentrically around a portion of sodium hydroxide treated sisal fibre. The placement of the droplet is done with the help of tweezers. The fibres were initially subjected to a 5% diluted NaOH treatment for duration of one (1) hour in order to improve its surface in readiness for bonding. A small amount of resin was first prepared in an open polypropylene container by mixing the polyester resin with an organic peroxide catalyst (Methyl Ethyl Ketone Peroxide) in a quantity of 2% of the weight of the resin to be mixed with.

Once the resin droplets cured at room temperature, these micro composites were then placed onto three porous Petri dishes for further hydrothermal ageing conditioning in 36 litre water baths (later shown in Figure 3.7) at pre-set temperatures of 23^{o}C, 40^{o}C, and 60^{o}C respectively for a maximum of 8 days (192 hours). During this time, periodic pull-out tests were conducted at intervals of 24 hours on the specimens with the view of assessing the resultant effect of the hydrothermal ageing on the microbond interfacial shear strength. Each test sample consisted between 23 – 35 tests specimens, were dried under vacuum in an autoclave before preparation of coupon specimens. Specimen coupons were then prepared by gluing individual fibre onto cardboard paper coupons bearing an open gauge length of 10mm. The microbond test coupon specimen arrangement is shown in Figure 3.3. Measurements of droplet embedded lengths and fibre diameters were taken with the aid of an Olympus optical microscope and recorded for further use in the analysis.

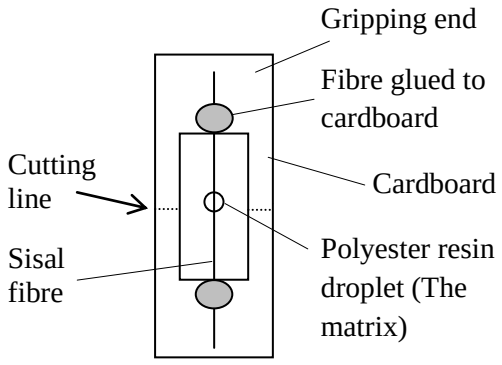

Figure 3.3: Microbond test specimen arrangement.

3.2.1.4 Composite Panel Fabrication

The sisal fibre reinforced composite panels from which test specimens were extracted were moulded using Vacuum Assisted Resin Infusion moulding process.

The first step involved in composite panel making required cleaning of the aluminium moulding plate with acetone. A film elevated temperature tolerant mould release liquid was then applied on the surface of the plate on the face on which moulding was to be done. The conventional mould release wax would have been ideal owing to the fact that curing the resin used in this research cures at room temperature.

The second step required the preparation of the dry sisal fabric mat and its accompanying moulding consumable materials which usually include release films, peel plies, flow media, sealing tape (sometimes referred to as Tacky tape) and vacuum bag. Measurements of the sisal fabric length, breadth, thickness and mass were carried out and recorded. The fabric and the accompanying moulding consumables were laid on surface of the moulding plate in an arrangement as described in Figure 3.4. A peel ply is the layered first covering the entire area of the size of the reinforcing sisal fabric on the moulding panel and it serves an important purpose for easy peeling off of the infused composite panel, leaving a comparatively even surface. The flow media allows the free and easy flow of resin under total vacuum from the infusion spiral through the reinforcing fabric, the breather and finally to vacuum hose. Placed in direct contact with both sides of the fabric are two release films which separate fabric from the other distribution medium. They also help, through its inherent perforations, in the removal of trapped air which might be present inside the fabric. Apart from allowing air to flow through, breathers and resin traps help in absorbing excess resin after complete impregnation of the sisal fabric has been achieved failure to which the excess resin would find its way into the vacuum pump and subsequently damaging it.

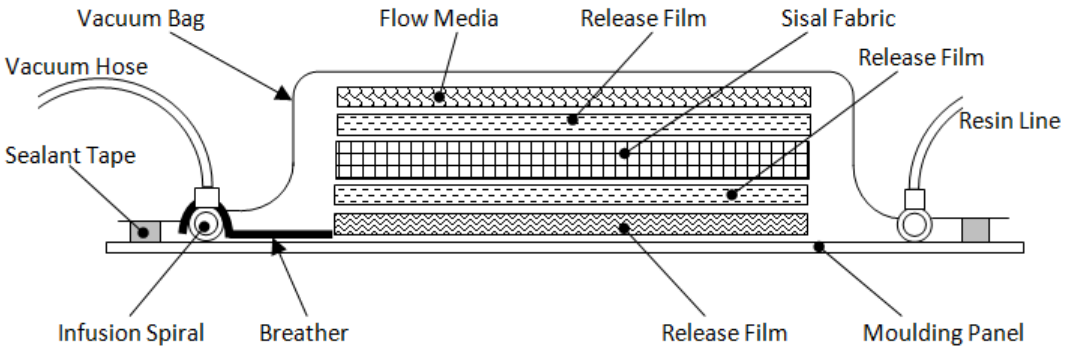

Figure 3.4: A schematic layout of the vacuum assisted resin infusion mould.

The entire arrangement was then placed inside a vacuum bag sealed with a double sided sealant tape creating a closed system. The trapped air was then extracted by the vacuum pump. The location of the vacuum spiral tube right on the flow media allows an excellent media for flow of both air and resin once the vacuum is induced. The final setup of the vacuum assisted resin infusion process is shown in Figure 3.5. Air leaks pose the biggest problem in vacuum bagging, and as such any indication of a drop in the vacuum (as indicated by the vacuum pump manometer) should be taken seriously otherwise it would impact negatively on the final product as it would contain a lot of voids.

The resin mixed with an organic peroxide catalyst Methyl Ethyl Ketone Peroxide (MEKP) in a quantity of 2% of the weight of the resin to be mixed with, was then prepared in a resin catch pot and then drawn by vacuum into the vacuum bag until complete impregnation of the fabric was achieved. Once the fabric was completely wet, the resin line was clamped off to prevent the suction of unwanted air from entering into the mould.

Curing process of polyester resin is an exothermic type and as such, had to be done under ambient temperature as was advised by resin suppliers ABL (Stevens) Resin and Glass of Cheshire, England. The entire mould arrangement was allowed to stay for 24 hours to ensure complete curing to take place though it normally takes a few hours for the polyester resin to harden. And finally, de-moulding process followed to extract the composite product and then the final mass, length and width of the product was measured and recorded. Figure 3.6 shows a composite panel produced using vacuum assisted resin infusion process.

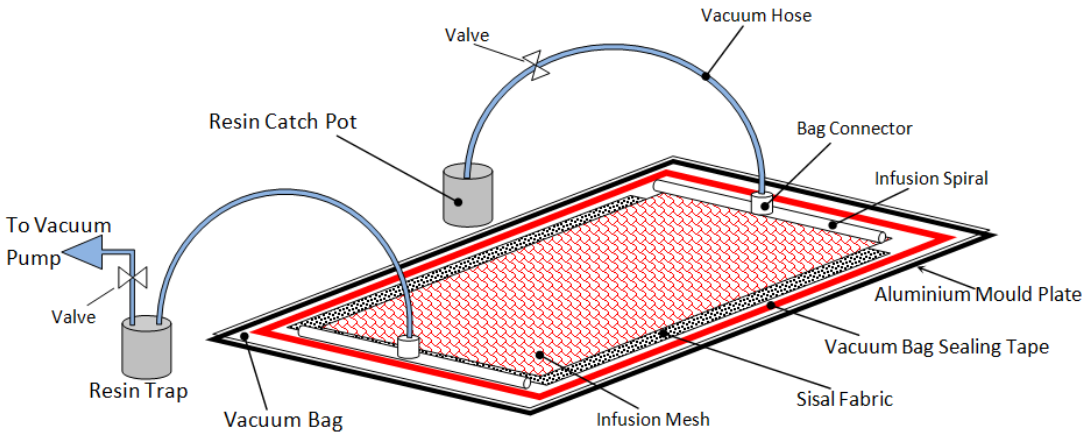

Figure 3.5: A pictorial layout of the vacuum-assisted resin infusion process mould.

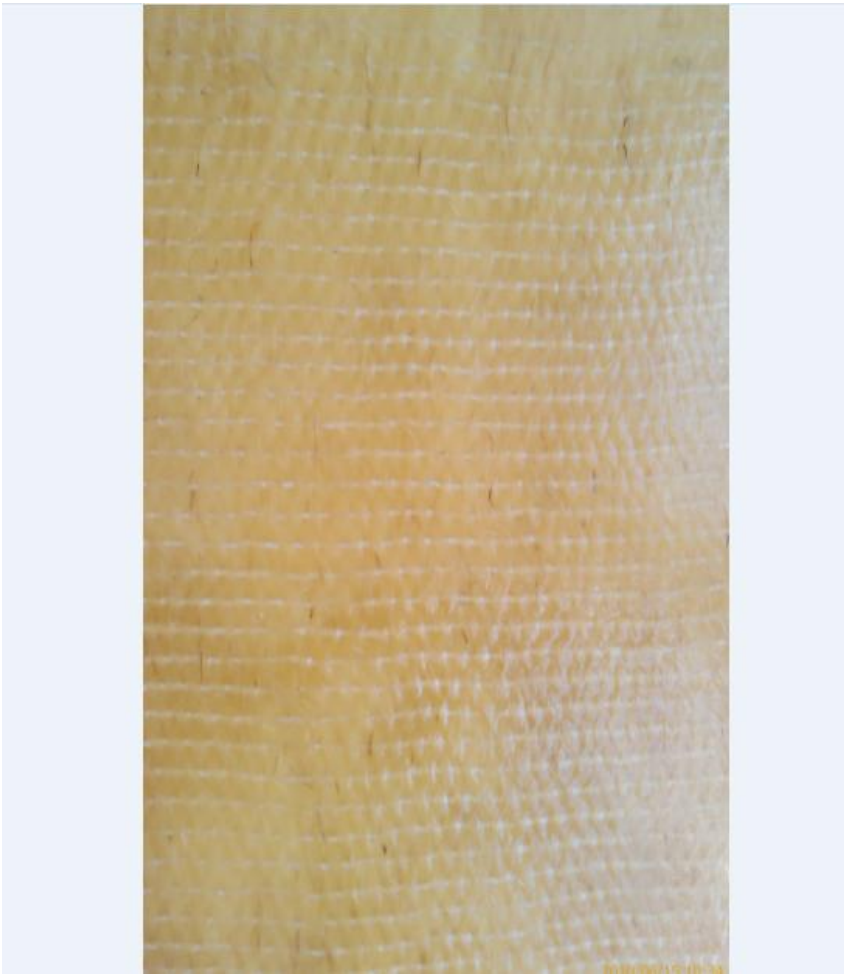

Figure 3.6: Moulded composite panel

3.2.2 Hydrothermal Ageing

Pre-ageing of test specimens was conducted on sisal fibre, neat polyester resin, and sisal-polyester composite specimens with the aim of establishing the ageing effects on the mechanical properties. These mechanical tests were carried out at regular intervals throughout the 6 months ageing period in order to establish retention of the mechanical properties as a function of exposure temperature and duration. This accelerated ageing was conducted in three (3) different aqueous environments in water baths (Figure 3.7) of distilled water at respective pre-set temperatures of 23°C, 40°C, and 60°C.

Prior to placement of end tabbing (where necessary) and running of tests, test specimens were first dried under vacuum in an autoclave in order to expel any possible available moisture.

3.3 Testing Procedures

This section describes the various mechanical test procedures carried out on composites (both micro and macro composite test specimens), neat cured polyester, and single sisal fibres specimens in order to assess the retention of their mechanical properties after being subjected to hydrothermal ageing process over specific time periods. The studies included the following: isothermal water uptake studies for the determination of the relative rates of absorption by the sisal-polyester composite in aqueous environments at different temperatures; tensile tests on single sisal fibres, neat cured polyester resin, sisal-polyester composite test specimens; fracture toughness tests; single fibre microbond pull-out tests; Dynamic Mechanical Analysis (DMA) of cured polyester resin specimens in order to assess impact of the ageing process on its viscoelastic properties.

3.3.1 Isothermal Water Uptake

Many polymeric matrices are known to be affected by absorbed moisture which tends to hydrolyse polymer bond resulting in the breakdown and leaching of its water soluble constituents. It further lowers the matrix's glass transition temperature through plasticisation of the matrix (Marom, 1976). Furthermore, prolonged exposure to this environment has an effect on the mechanical properties of the

composite. Moisture sorption to an extent triggers profound effects on both long and short term stability of composite systems. It is therefore inevitable that determination of the moisture content and rate at which its diffusion occurs into the composites when subjected to hydrothermal environment is accomplished (Surathi and Karbhari, 2006).

Isothermal water uptake studies were conducted for the determination of the relative rate of absorption of water by the sisal-polyester composite by immersing test specimens into distilled water at different pre-set temperatures. This study was conducted in accordance with ASTM D570-98 standard. This test method for the rate of water absorption is significant as a guide to the relative amount of water taken up by the composite material and consequently establish the correlation between absorbed moisture and mechanical properties as a function of the conditioning temperature and exposure duration is desired. This study is at times used as a control measure to determine the uniformity of the resultant laminate product.

In order to get an estimate of the diffusion coefficient of the composite material at a specific temperature and subsequently the diffusion coefficient as a function of exposure temperature, experiments were run in three (3) water baths at respective pre-set ideal operating temperatures of 23°C, 40°C, and 60°C shown in Figure 3.7.

Water uptake was monitored on three (3) samples consisting of three (3) specimens (with dimensions of 76.2mm x 25.5mm x 2.5mm) by gravimetric changes in the test specimens.

Figure 3.7: Three water baths used for specimen conditioning at respective temperatures of 23°C, 40°C, and 60°C.

3.3.2 Tensile Testing

Studies were conducted on hydrothermal aged sisal fibre, neat polyester resin, and sisal-polyester composite specimens with the aim of establishing the ageing effects on the samples' mechanical properties. These tests were carried out at five regular intervals throughout the 6 month ageing period.

3.3.2.1 Single Sisal Fibre

The individual sisal fibres were initially subjected to a 5% diluted NaOH treatment for duration of one (1) hour, a treatment usually carried out on reinforcing natural fibres in order to improve their surface in readiness for bonding with resins in composites. This treatment triggers the hydroxyl groups of the cellulose and lignin in the sisal fibre structure resulting in an enhancement in the tie created with the surrounding matrix (Puitel et al., 2011; Li et al., 2007).

After this treatment, the fibres were further subjected to a hydrothermal ageing treatment in 36 litre water baths at 23^{o}C, 40^{o}C, and 60^{o}C for a maximum period of 6 months. Periodical tests were conducted at regular intervals of 30 days in order to access the retention of their tensile strength properties. These tests were conducted in

accordance with ASTM D3822 standard. Tensile testing of non-hydrothermally treated fibre specimens was also conducted solely for the purpose of establishing a baseline for comparison and determining the effect of the ageing process on the tensile properties of the sisal fibre.

For tensile tests on conditioned single fibre to be conducted, the single fibres had to be first glued onto individual test cardboard coupons bearing an open gauge length of 30mm as shown in Figure 3.8(a). The glue was allowed to fully set before tests were conducted to eliminate any possible slippage when held between machine grips while performing the tests. Before each test was conducted, the fibre diameter was measured at three (3) different points along the fibre length with the help of an Olympus optical microscope and an average calculated.

The test specimen coupon was then held between the grips attached to an Instron 5564 tensile testing machine (see Figure. 3.8(b)) which was coupled with a 10N load cell. The specimen cardboard in Figure 3.8(a) was then cut along the cutting line on either sides of the fibre to allow the fibre to freely bridge the two pneumatic grips. The tests were conducted at a constant crosshead speed of 2 mm/min until complete failure of sisal fibre recorded. With the help of the testing machine's data acquisition systems, plots of the load-displacement were acquired from which the sisal fibre tensile strength properties were later determined. Due to the wide inconsistency in the sisal fibre tensile properties, each test sample consisted of not less than 23 test specimens.

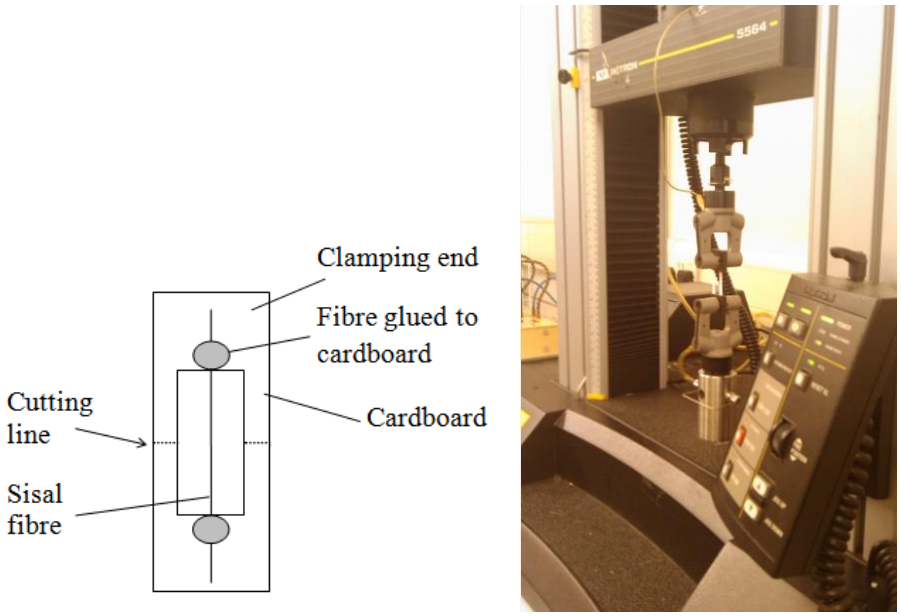

(a) (b)

Figure 3.8: (a) Single fibre tensile test specimen. (b) Single fibre testing Rig.

3.3.2.2 Neat Polyester Resin

The tests to determine tensile properties of both untreated and hydrothermally treated unreinforced cured polyester resin specimens were done in accordance with ASTM D 638-03 standard. Dumbbell-shaped tests specimens in Figure 3.9 were die casted in CNC-machined non-stick plastic (Teflon) moulds shown in APPENDIX K, machined to the profile specified in the ASTM D 638-03 standard. These experiments were carried out under constant laboratory conditions on an Instron 5569 tensile testing machine fitted with a 1kN load cell at a loading rate of 2mm/min. A mechanical extensometer was pre-set and placed at a gauge length of 25 mm on the mid portion of the test specimens. (See the neat polyester specimen testing arrangement in Appendix N).

Tensile test of these dumbbell shaped cured polyester resin test specimens were conducted under ambient conductions for both untreated and hydrothermally treated (treated by immersion in distilled water at 23^{o}C, 40^{o}C and 60^{o}C respective temperatures over time). Tests of untreated specimens were done first to establish a good baseline for comparison and to also determine the effect of the different ageing environments on the tensile properties of the cured resin material.

Prior to running the mechanical testing, test specimens were subjected to hydrothermal ageing in three water baths at pre-set temperatures of 23^{o}C, 40^{o}C and 60^{o}C respectively for specific periods of 30, 60, 90, 120 and 150 days. Temperature beyond 60^{o}C may not be ideal as operating temperature for the matrix as it tend to affect the viscoelastic properties of the matrix which would in turn result in misleading observations in the experiments. At the end of each ageing period, testing of samples was conducted to assess the retention of tensile properties after being subjected to this hydrothermal ageing environment.

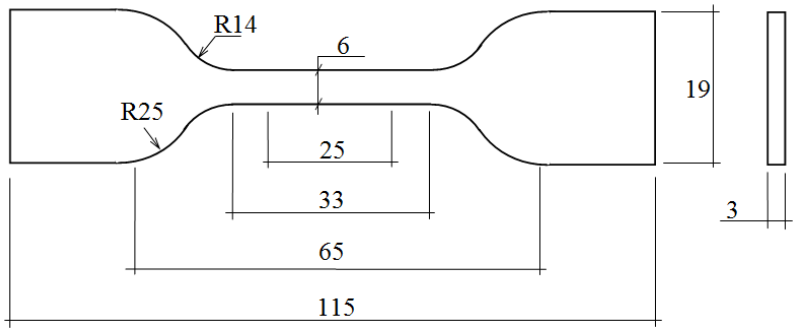

Figure 3.9: Neat polyester resin specimen geometry. (Dimensions in mm.)

3.3.2.3 Sisal-Polyester Composite

Tensile tests on the sisal fibre reinforced polyester composite test specimens were conducted in accordance with the requirements of BS EN ISO 527-5:2009 standard. The specimens used in this study were plain woven sisal fibre mat embedded in polyester resin matrix fabricated using vacuum assisted resin infusion process with a resultant fibre volume fraction of 50-55%. The tensile test specimens were cut from sisal-polyester composite panel after being released from the mould and edges of each specimen were polished using emery paper in order to avoid edge defects. The geometry for the tabbed test specimen is shown in Figure 3.10 which is based on the recommendation in the same standard. (Refer to APPENDIX L for the making of end tabbing material; curing cycle used when making the glass fibre prepreg end tabs; and actual tabbing).

These tests were carried out on an Instron 5569. Loading to test specimens was introduced through a 10kN load cell at a rate of 2mm/min^{-1}. An extensometer was set and placed at a gauge length of 50mm on the mid portion of the test specimens. All tests were conducted at a room temperature of 22.5^{o}C and 75% relative humidity.

All test specimens were hydrothermally treated at respective temperatures of 23°C, 40°C and 60°C for a maximum of 6 months period. Periodical monthly tests were conducted on the aged specimens, as detailed in Appendix M.

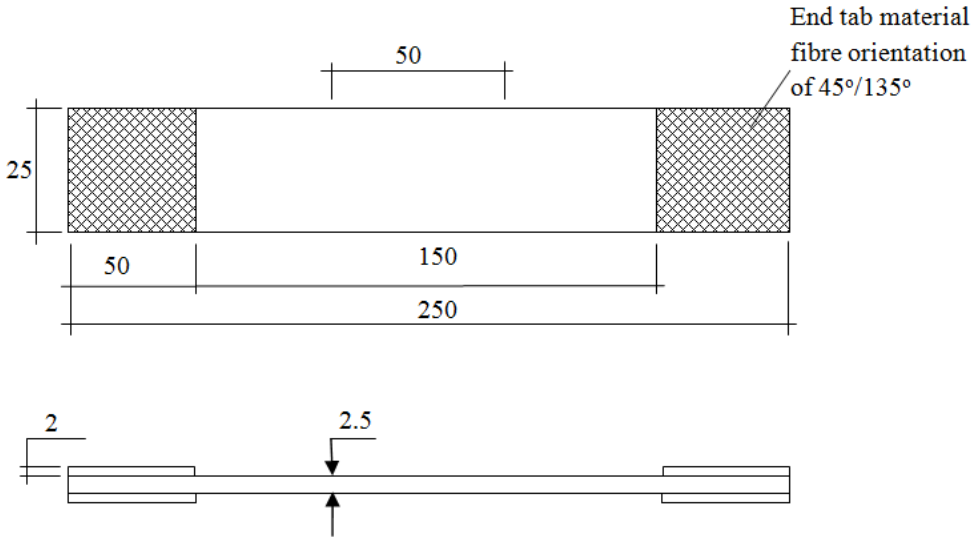

Figure 3.10: Tabbed tensile test specimen. (Dimensions in mm.)

3.3.3 Dynamic Mechanical Analysis

Dynamic Mechanical Analysis (DMA) is of great importance in the analysis of polymeric materials viscoelastic properties, locate the material glass transition temperatures and transitions corresponding to molecular motions: it is characterised by variations of stress cyclic frequencies and temperature changes. It is a well-established fact that the higher the Tg, the better will be the long term thermal stability of a material. It is for this reason that this research sought to examine the stability of the viscoelastic properties after subjecting it to an aqueous environment, for a range of operating temperatures, over time.

In this research, DMA of neat polyester resin was conducted in accordance with ASTM 4065-1 to evaluate the response of its transition temperature, Tg, and other viscoelastic properties after hydrothermal ageing for specified period of time. These test were conducted on a PerkinElmer® DMA 8000 machine shown in Figure 3.11a). The specimens used for DMA were neat polyester resin cast and cured in a non-stick Teflon mould and later cut on a diamond cutter into rectangular shaped bars of dimensions of 50 x 10 x 3mm. A minimum of 5 specimens were prepared for each test sample. The choice to use neat polyester specimens for the test as opposed to

sisal reinforced polyester specimens was arrived at after considering the fact that the polymer chains adjacent to the fibres in reinforced specimens are tightly adjoined thus, limiting this mobility. They cannot therefore partake in any transitions that are measurable by DMA. Furthermore, the inconsistencies in the reinforcing sisal fibre such as volume fraction across the test specimen, the mechanical properties from one fibre to the other, varying fibre diameter along its entire length and from fibre to fibre, would throw DMA results all over the spectrum creating huge standard deviations in the results, a view shared by other researchers.

The storage modulus $E^{/}$, loss modulus $E^{//}$, and glass transition temperature Tg (at times referred to as tan δ) were determined for hydrothermally treated test specimens. The treatment was done by initially immersing the specimens in distilled water-filled water baths at respective pre-set temperatures of 23^{o}C, 40^{o}C, and 60^{o}C for a maximum duration of 4320 hours (6 months). DMA tests were conducted at regular intervals throughout this period.

Similarly, DMA tests of non-hydrothermally treated test specimens were also carried out for the purpose of setting a comparative baseline and determining the effect the ageing process poses on the viscoelastic properties of cured polyester matrix material of the reinforced composite.

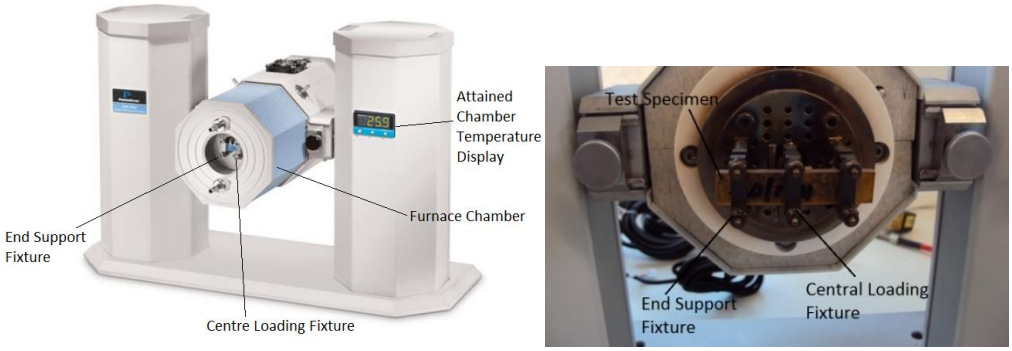

(a) (b)

Figure 3.11: (a) PerkinElmer® DMA 8000 machine. (b) Specimen mounting arrangement.

In the DMA testing machine, the specimens were tightly fitted centrally between two fixtures in a double cantilever arrangement located in the temperature controlled furnace chamber. The two support fixtures were spaced at 17.5mm from the centre

loading fixture (See Figure 3.11(b)). This centre fixture was driven to an oscillatory mode by an actuator at the set two frequencies of 1 and 10 Hz respectively and with set resultant dynamic displacement amplitude of 0.05mm. Measurement were carried out at multi frequencies for purposes of firstly, exploring the frequency dependence of a relaxation process and secondly, to provide data at specific frequencies. The two supports were connected to a transducer, which measures the stress level. The specimen was heated to temperature of up to 180^{o}C at steady a ramp rate of 3^{o}C/min. The temperature dependant $E^{/}$, $E^{//}$, and tan δ were measured from which the beginning and the end of the transition from a glassy state to rubbery state were established for tested specimens.

3.3.4 Composite Fracture

This section describes test procedures conducted to assess the fracture response of the sisal fibre-reinforced polyester composite after being subjected to hydrothermal ageing at both micro and macro composite levels.

3.3.4.1 Microbond Failure

Before the experiments commenced, the upper part of the test specimen coupon was held and suspended in grips attached to an Instron 5564 tensile testing machine (see Figure. 3.12(a)) which was coupled with a 10N load cell. It is imperative that the axis of the fibre coincides with that of the Instron machine in order to minimise errors in the results obtained. The specimen cardboard in Figure 3.12(b) was then cut along the cutting line on either sides of the fibre to allow the fibre to freely hang with the droplet held below the two knife-edges. The gap between the knife-edges was precisely set to 0.35mm through the rig micrometre as shown in Figure 3.13. The cured polyester resin droplet (the matrix) was then pulled down when the test started at a constant crosshead speed of 1 mm/min until failure by debonding of the interface occurred. With the help of the testing machine data acquisition system, plots of the load-displacement were acquired from which the debonding force was later determined.

(a)

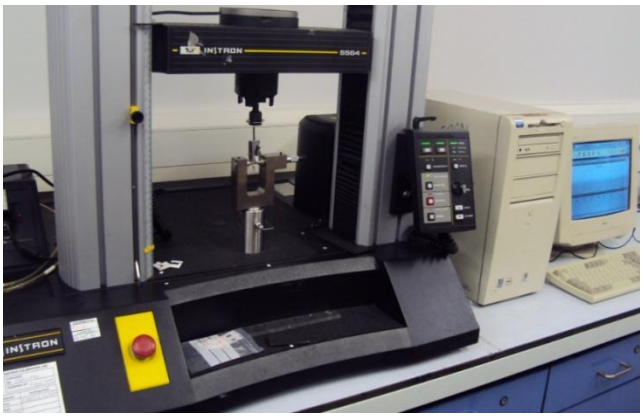

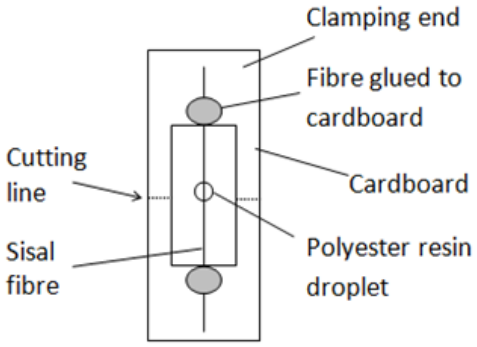

(b)

Figure 3.12: (a) Microbond Testing Rig. (b) Microbond test specimen arrangement.

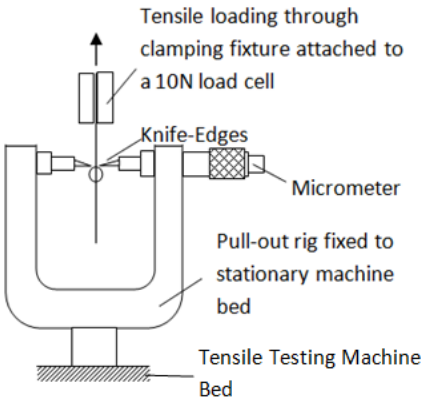

Figure 3.13: Close up on the microbond test grip arrangement.

3.3.4.2 Macro Composite Fracture Toughness

The assessment of the fracture toughness properties for fibre reinforced composites made from thermosetting matrices is normally conducted through the stress intensity factor approach, as a result of their common brittle tendencies (Zhao and Botsis, 1996). For this reason, periodic translaminar fracture toughness tests of hydrothermal

aged unidirectional sisal fibre reinforced polyester specimens were conducted in accordance with the ASTM Standard E1922-97 (last revised 2004). Prior to running these tests, test specimens were initially subjected to a hydrothermal ageing process in three (3) water baths at pre-set temperatures of 23^{o}C, 40^{o}C, and 60^{o}C respectively for a maximum period of six (6) months. This was aimed at assessing the effects hydrothermal ageing poses on the fracture toughness property of this reinforced composite throughout the ageing period.

Test specimens were prepared to the dimensions and tolerances prescribed in the test standard. The specimen specifications are illustrated in Figure 3.14. The notch in the specimen was cut using a diamond cutter to produce the required narrow slit.

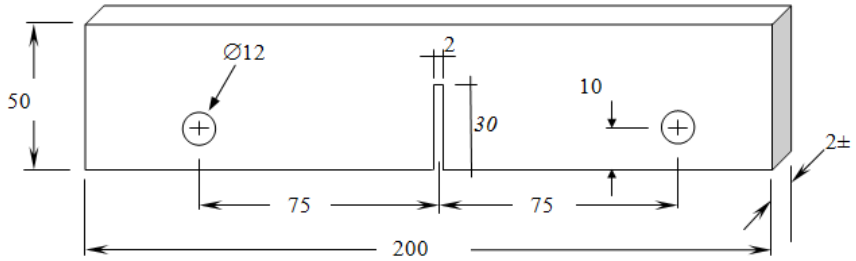

NOTE 1 — All dimensions +/– 0.01 *W*, except as noted.

NOTE 2 — All surfaces perpendicular and parallel as applicable within 0.01*W*.

Figure 3.14: Translaminar Fracture Toughness Test Single-Edge-Notch [ESE(T)] Specimen.

According to the standard, a single-edge-notch (ESE(T)) specimen was eccentrically loaded in tension (Mode I). The attained load was recorded with the help of a 10 kN load cell versus resultant displacement across the notch mouth at the specimen edge for all specimen tested. A displacement gauge model type MTS 634.31F-24 was used to simultaneously measure the notch-mouth displacement during loading. Knife edges affixed to test specimens at the notch mouth enabled attachment of the displacement gauge to the specimens.

From the acquired load-displacement data, the load corresponding to the prescribed increase in the normalised notch length was established. From this load, the

translaminar fracture toughness, K_{TL}, was further computed using the following equation (3.1) founded on the basis of elastic stress analysis of the modified single-edge notched specimen (ASTM E1922, 1997):

$$K_{TL} = \left[P/BW^{1/2}\right]\alpha^{1/2}[1.4+\alpha][3.97 - 10.88\alpha + 26.25\alpha^2 - 38.9\alpha^3 + 30.15\alpha^4 - 9.27\alpha^5]/[1-\alpha]^{3/2} \quad (3.1)$$

Where:

K_{TL}	-	Translaminar fracture toughness, MPa.m$^{1/2}$.
P	-	Applied load, MN.
α	-	a/W (dimensionless).
a_n	-	Notch length, m.
B	-	Specimen thickness, m.
W	-	Specimen width, m.

Tests were conducted on an Instron 5569 tensile testing machine that has provision for simultaneous recording of the applied load (through the attached load cell) to the specimen at a constant crosshead speed of 2 mm/min and the resulting notch-mouth displacement with the use of an extensometer attached to the notch mouth. A typical arrangement is shown in Figure 3.15. Typical pin-loading clevises (shown in Appendix A) similar to the type used in test method ASTM E 399 were used to apply the load on to the specimen.

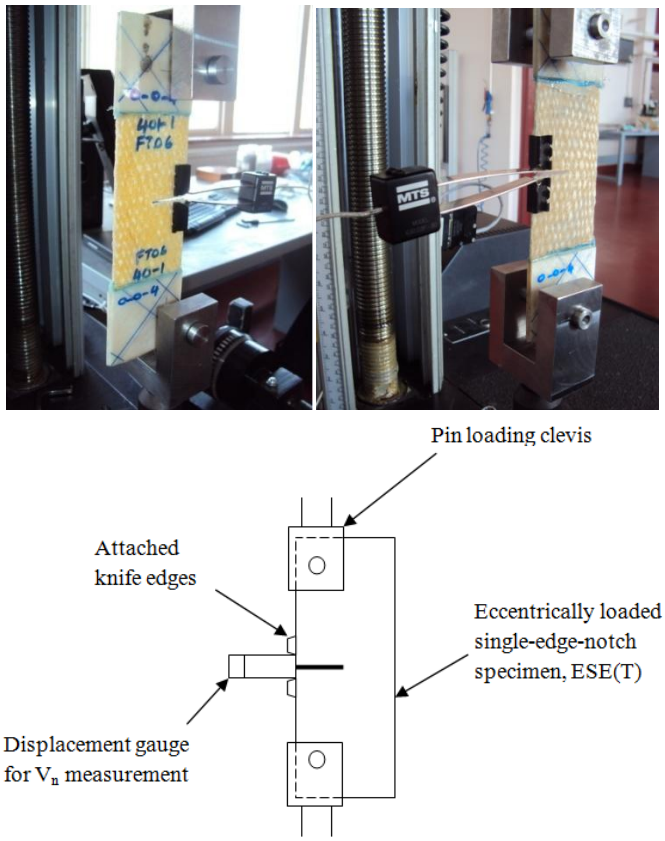

Figure 3.15: Test Arrangement for Translaminar Fracture Toughness Tests.

Fracture toughness tests of non-hydrothermally treated test specimens were also conducted. This was solely for the purpose of establishing a baseline for comparison and further establishing the effect of the ageing process on the fracture toughness property of the composite material.

In all, it was required by the standard that a minimum of five (5) tests were performed to produce a good average of test results for each sample provided that the results were reasonably close to each other within a small band of error. For this reason, five (5) tests specimens per sample were used. The testing standard requires a minimum of five specimens to be tested, hence this choice. This choice also took into consideration the limited available hydrothermal conditioning water bath capacity.

CHAPTER 4 EXPERIMENTAL RESULTS

4.1 Introduction

The objective of the experimental investigations in this work was to determine the effect of the environmental on the fracture damage of sisal fibre reinforced polyester composite. This chapter presents and discusses the results from experiments conducted on sisal fibre reinforced polyester composite and on its separate constituents with the aim of assessing the effects accelerated hydrothermal ageing poses on the mechanical properties. Constituents examined for the retention of mechanical properties with hydrothermal ageing were:

- Single reinforcing sisal fibres;
- Polyester matrix;
- Interface region between the matrix and the reinforcing fibres as functions of the hydrothermal ageing temperature and exposure time.

4.2 Isothermal Water Uptake

Results of the isothermal water uptake studies conducted on the sisal fibre reinforced polyester composite test specimens are given in Table 4.1. Average percentage moisture gains at time *t* for the samples were calculated and plotted against respective exposure time.

$$M = M(t) = \frac{Weight\ of\ specimen\ after\ immesion - Weight\ of\ dry\ specimen}{Weight\ of\ dry\ specimen} X\ 100 \quad (4.1)$$

Table 4.1: Average moisture percentage gain for Sisal/Polyester specimens immersed in water at 23°C, 40°C and 60°C.

Time (Hrs)	$\sqrt{Time}$, (Hrs$^{1/2}$)	Average Moisture Gain (%)		
		23°C	40°C	60°C
0	0	0	0	0
0.4992	0.7065	0.035	0.060	0.097
1.0008	1.0004	0.055	0.067	0.103
24	4.8989	0.125	0.237	0.410
48	6.9282	0.197	0.332	0.440
120	10.9544	0.287	0.360	0.437
144	12	0.315	0.365	0.440
168	12.9614	0.327	0.382	0.443
216	14.6969	0.362	0.385	0.443
288	16.9706	0.380	0.380	0.450
312	17.6635	0.375	0.372	0.447
336	18.3303	0.387	0.390	0.453
360	18.9737	0.4	0.375	0.447
456	21.3541	0.427	0.385	0.437
528	22.9782	0.445	0.392	0.433
552	23.4947	0.440	0.392	0.430
624	24.9780	0.447	0.395	0.427
720	26.8328	0.482	0.405	0.407
816	28.5657	0.470	0.392	0.397
888	29.7993	0.470	0.392	0.397
1032	32.1247	0.475	0.412	0.400
1200	34.6410	0.520	0.427	0.427
1392	37.3095	0.505	0.415	0.413
1656	40.6939	0.497	0.417	0.403
2016	44.8998	0.460	0.407	0.377
2376	48.7442	0.445	0.410	0.357
2712	52.0768	0.452	0.405	0.357
3120	55.8569	0.407	0.400	0.353
3600	60	0.402	0.405	0.370

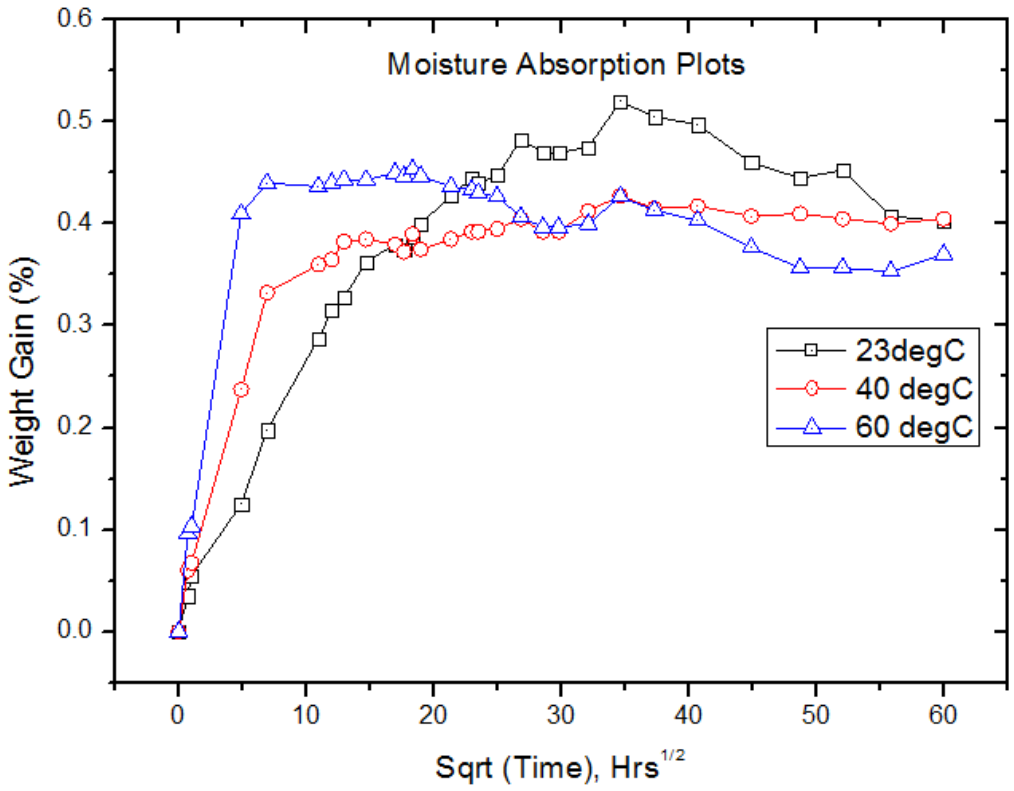

Figure 4.1: Moisture Absorption plots of Sisal fibre reinforced polyester composite immersed in water at temperatures of 23°C, 40°C and 60°C.

For the estimation of moisture contents at saturation (maximum moisture content, M_m) and subsequent determination of the Diffusion Coefficient (D) of the reinforced composite at the respective ageing temperatures, the data presented in Table 4.1 was further fitted using MathCAD to equations (2.11) and (2.12) of the Fickian Diffusion model. The fitted graphs are shown in Figure 4.2 through Figure 4.4. The MathCAD algorithm which was used to fit the given data is presented in Appendix B.

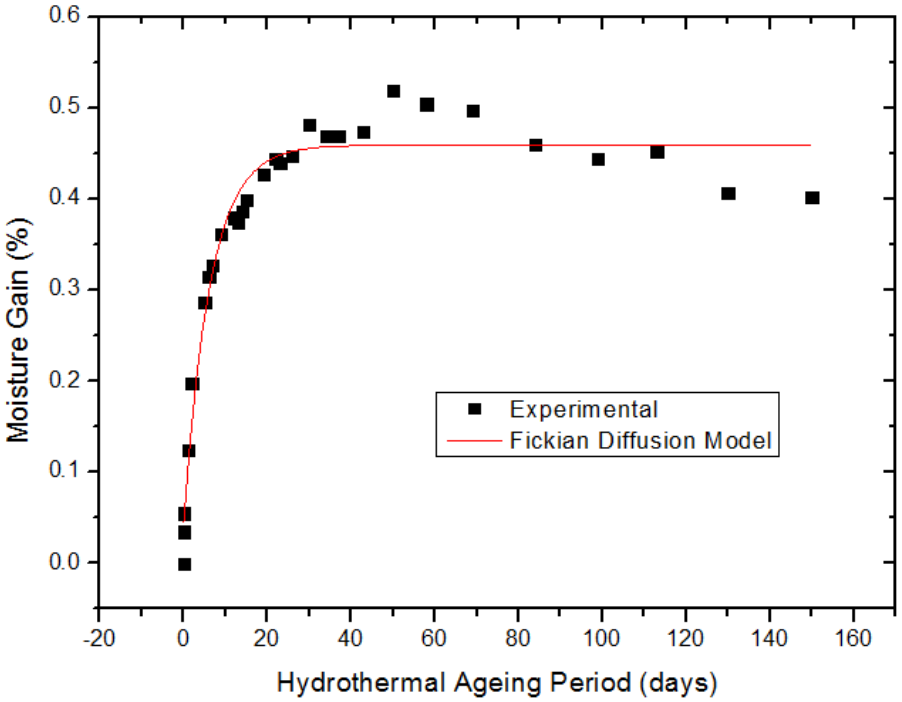

Figure 4.2: Moisture absorption plot of sisal fibre reinforced polyester composite specimens immersed in distilled water at 23^{o}C fitted based on the Fickian diffusion model.

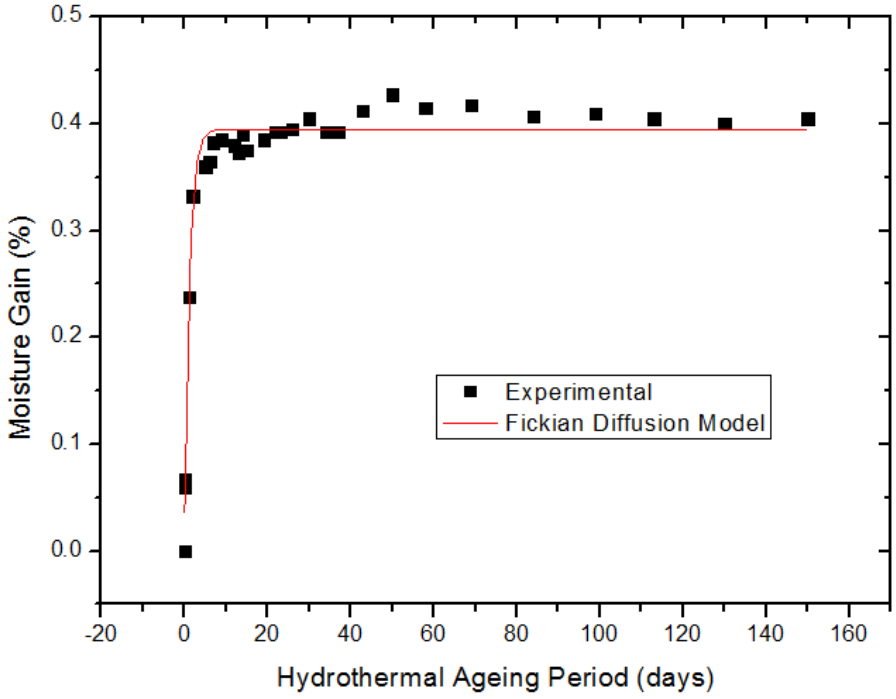

Figure 4.3: Moisture absorption plot of sisal fibre reinforced polyester composite specimens immersed in distilled water at 40^{o}C fitted based on the Fickian diffusion model.

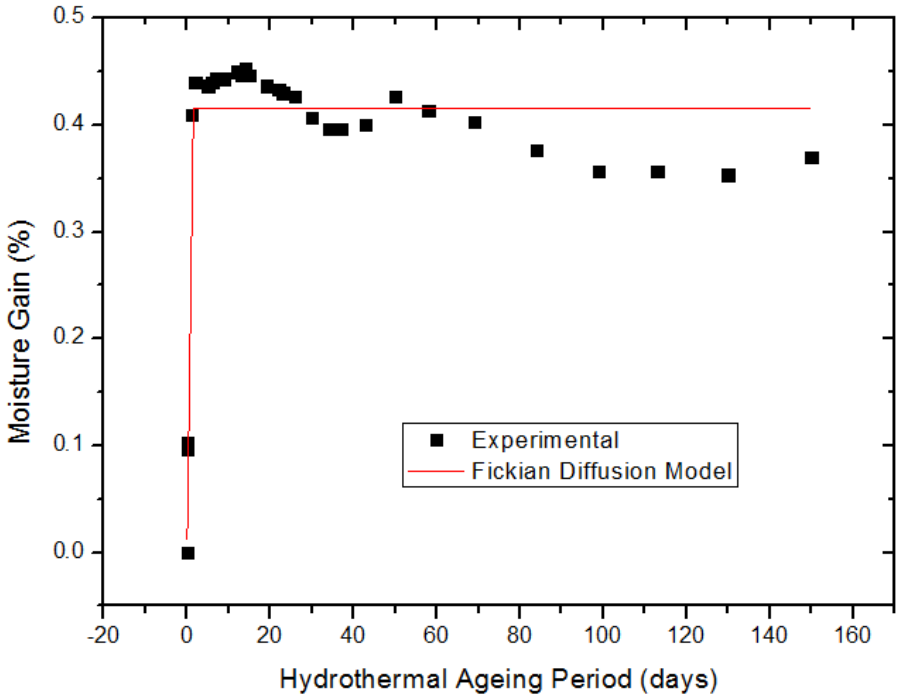

Figure 4.4: Moisture absorption plot of sisal fibre reinforced polyester composite specimens immersed in distilled water at 60°C fitted based on the Fickian diffusion model.

Table 4.2 lists the determined values of the maximum moisture contents and diffusion coefficients based on the Fickian diffusion model.

Table 4.2: Values of maximum moisture contents and diffusion coefficients determined based on the Fickian diffusion model.

Exposure Temp			Max Moisture	Diffusion Coefficient (mm^2/sec)	
				Fickian Diffusion Model	Edge Effect Correction
(°C)	(K)	(1000/K)	Content, Mm (%)	(D)	(Dx)
23	297.2	3.36530	0.45	0.003270242	0.002557241
40	314.2	3.18319	0.40	0.012771391	0.009986884
60	334.1	2.99266	0.42	0.036958302	0.028900399

According to Arrhenius life-stress relationship, the rate of a reaction (in this case diffusion) is proportional to the stimulus (temperature),

$$Rate(T) = Ae^{-E_a/RT} \tag{4.2}$$

Where Rate (T) – is the rate of the reaction

E_a – is the Activation Energy for the reaction

T – is the temperature, in Kelvin

A – is a factor which represents a frequency factor for the process

R – is the universal gas constant, in $J.mol^{-1}.K^{-1}$.

Equation (4.2) can be rewritten as

$$\ln(Rate) = l(A) + {}^{-E_a}/_{RT} \tag{4.3}$$

By substituting y for ln(Rate) and *x* for 1/T in equation (4.3), produces

$$y = \ln(A) + {}^{-E_a}/_{R(x)}$$

The resultant linear equation for the best fit line on the graph in Figure 4.5 is

$$y = -6.5x + 15.96$$

Where

$$Slope = -\frac{E_a}{R} = -6.5$$

$$y_{\text{Intercept}} = \ln(A) = 15.95$$

Therefore

$$A = 8.537681x10^6$$

The activation energy for absorption is

$$E_a = 54.044\ kJ$$

Table 4.3: Diffusion coefficient values for sisal fibre reinforced polyester composite when exposed to hydrothermal ageing environments at the three respective pre-set temperatures.

Exposure Temperature ($1000K^{-1}$)	3.3653	3.1832	2.9927
Diffusion Coefficient (ln(Dx))	-5.9688	-4.6065	-3.5439

Table 4.3 lists respective resultant diffusion coefficients for the sisal/polyester composite system for the three respective ageing environments.

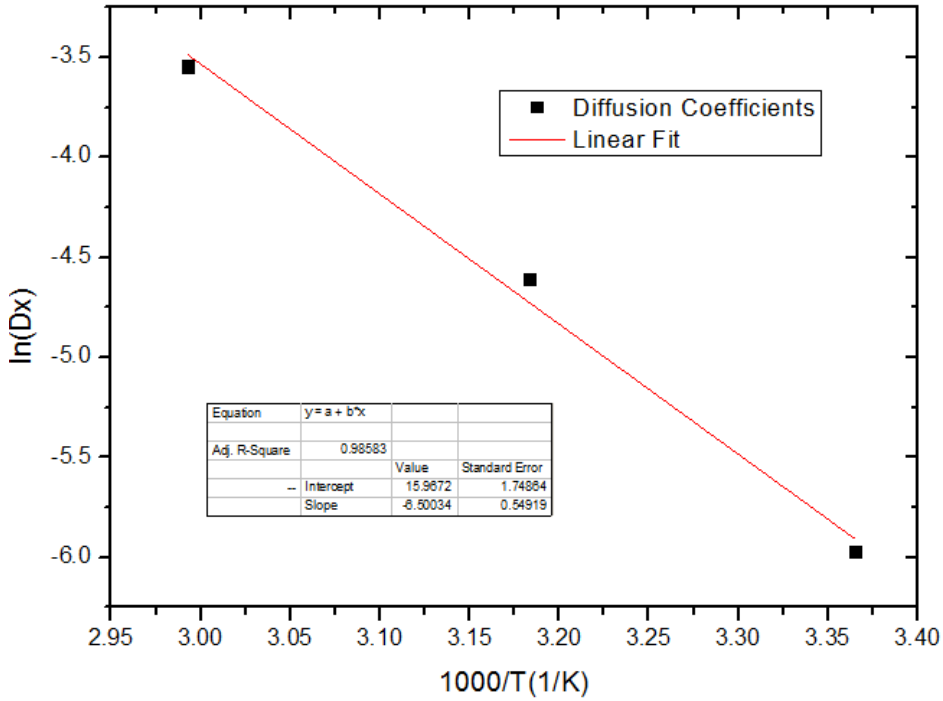

Figure 4.5: Arrhenius plot of natural log of edge-effect corrected Fickian diffusion coefficient against inverse temperature of aged sisal fibre reinforced composite specimens at different temperature environments.

4.3 Tensile Testing

This section presents the tensile tests results from experiments conducted on both sisal fibre reinforced polyester composite as a whole and also on its separate constituents.

4.3.1 Tensile Strength

Results pertaining to mechanical tests conducted on sisal fibres, neat cured polyester and sisal/polyester composite specimens with the aim of assessing the effect of moisture on their ultimate tensile strength after undergoing hydrothermal ageing treatment are now presented.

4.3.1.1 Sisal Fibre

Variation in the values of the ultimate tensile strength of hydrothermally treated single sisal fibre specimens are presented in Table 4.4 and subsequently in Figure 4.6. The contour plot is presented in Figure 4.7.

Table 4.4: Average values of ultimate tensile strength for hydrothermally treated single sisal fibres.

Time (Days)	Ultimate Tensile Strength (MPa)					
	23°C		40°C		60°C	
	σ_{TS} (MPa)	StdDev	σ_{TS} (MPa)	StdDev	σ_{TS} (MPa)	StdDev
0 (Untreated)	876.7	876.7	876.7	876.7	876.7	876.7
30	952.671	458.023	1104.6	477.414	980.228	346.683
60	655.641	327.676	642.247	249.422	636.16	147.373
90	689.492	169.151	925.404	538.713	875.612	394.039
120	762.178	327.121	724.32	183.996	600.394	190.269

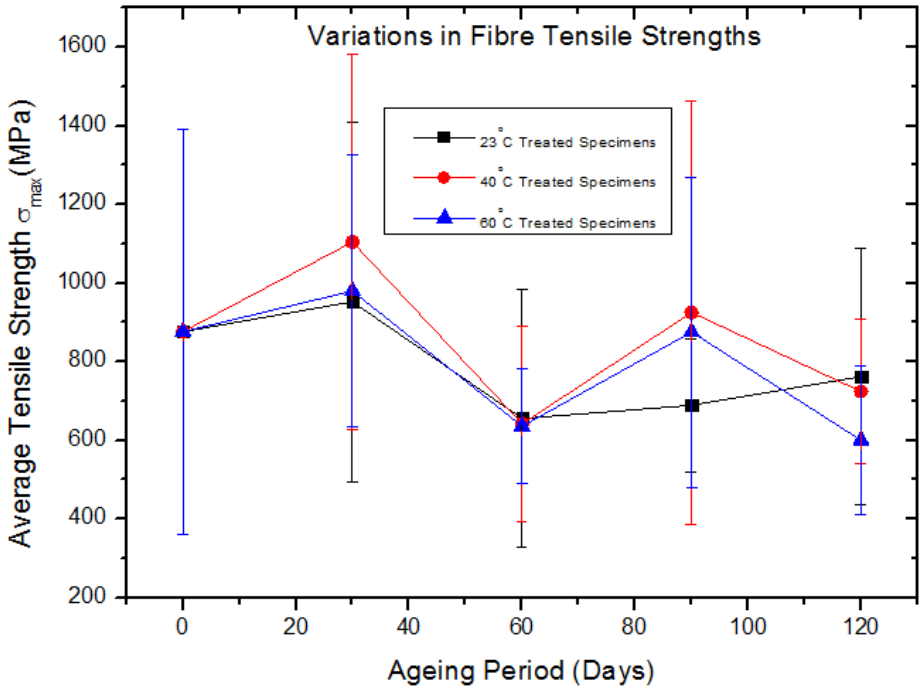

Figure 4.6: Average value of ultimate tensile strength plot for hydrothermally treated single sisal fibres.

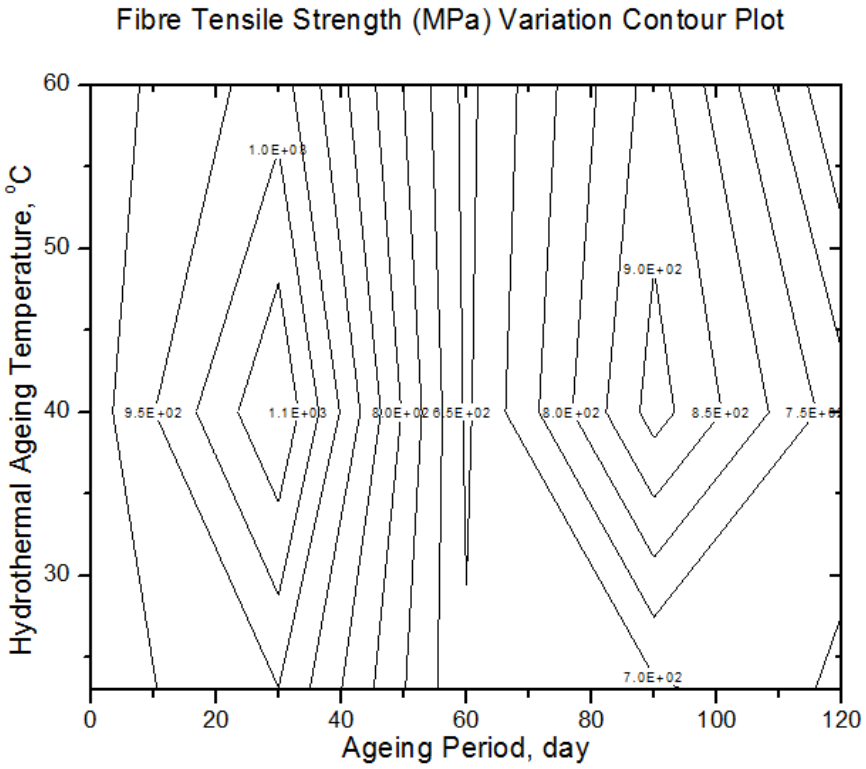

Figure 4.7: Contour plot describing variations in the single sisal fibre ultimate tensile strength as a function of hydrothermal ageing temperature and treatment period.

4.3.1.2 Neat Polyester Resin

Table 4.5: Average values of ultimate tensile strength for cured neat polyester resin specimens treated hydrothermally at temperature of 23°C, 40°C and 60°C over specific periods.

Time (Days)	Ultimate Tensile Strength (MPa)					
	23°C		40°C		60°C	
	σ_{TS} (MPa)	StdDev (MPa)	σ_{TS} (MPa)	StdDev (MPa)	σ_{TS} (MPa)	StdDev (MPa)
0 (Untreated)	30.552	3.8743	30.552	3.8743	30.55195	3.8743
30	19.9469	6.0057	15.8465	3.0142	16.4257	2.3865
60	23.6985	8.2616	15.6972	2.8743	12.27937	2.6914
90	17.1643	3.0558	12.9295	2.6190	9.27253	1.6336
120	19.6685	1.4578	13.4775	2.5271	6.35924	1.8939

Figure 4.8 shows neat polyester resin tensile test result plots of the values of ultimate tensile strength for dried polyester resin specimens as a function of immersion time and environment temperature presented in Table 4.5.

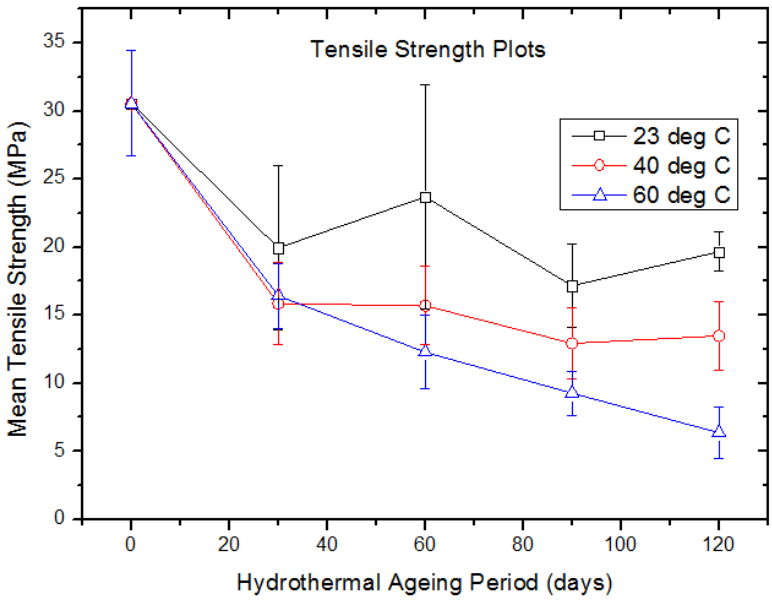

Figure 4.8: Changes in the ultimate tensile strength of neat polyester specimens hydrothermally treated in distilled water at different temperatures over time.

Figure 4.9 through Figure 4.11 show composite plots of average tensile strength retention and percentage moisture gain versus hydrothermal conditioning time for the same cured polyester resin specimens.

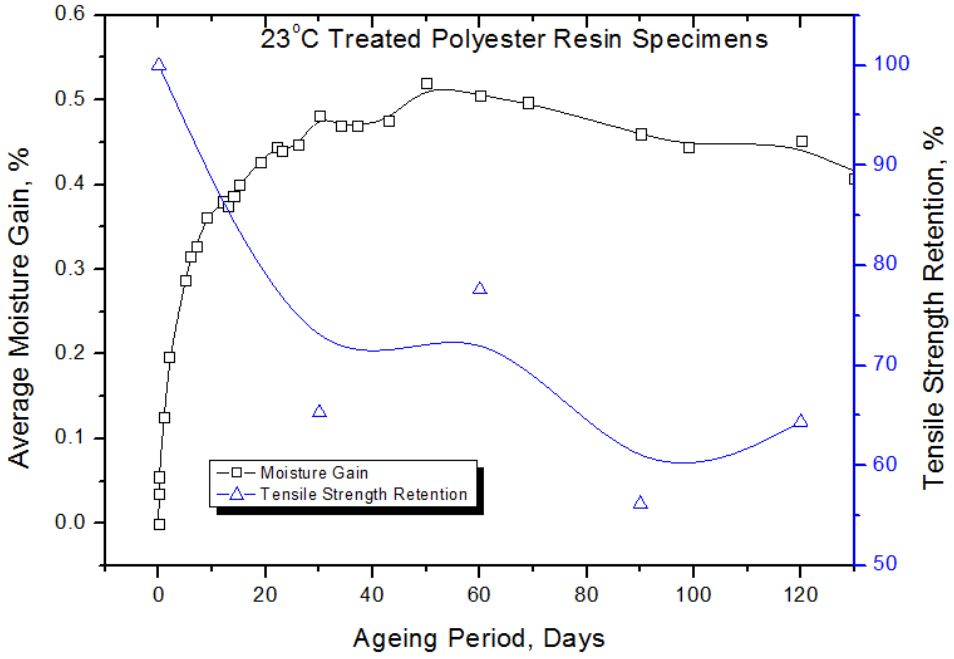

Figure 4.9: The relationship between % water absorption and tensile strength with increasing exposure times for neat cured polyester resin specimens hydrothermally treated at 23°C.

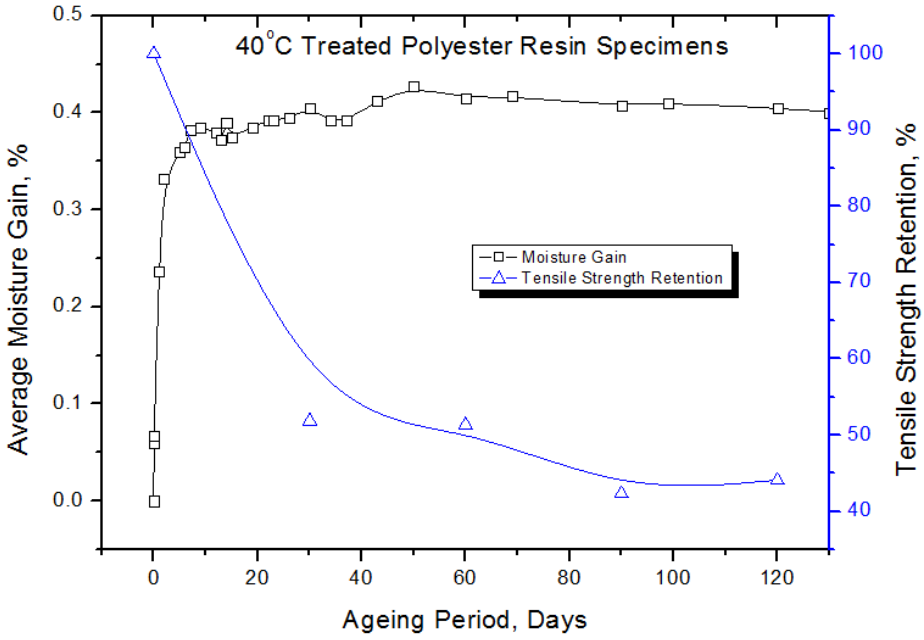

Figure 4.10: The relationship between % water absorption and tensile strength with increasing exposure times for neat cured polyester resin specimens hydrothermally treated at 40°C.

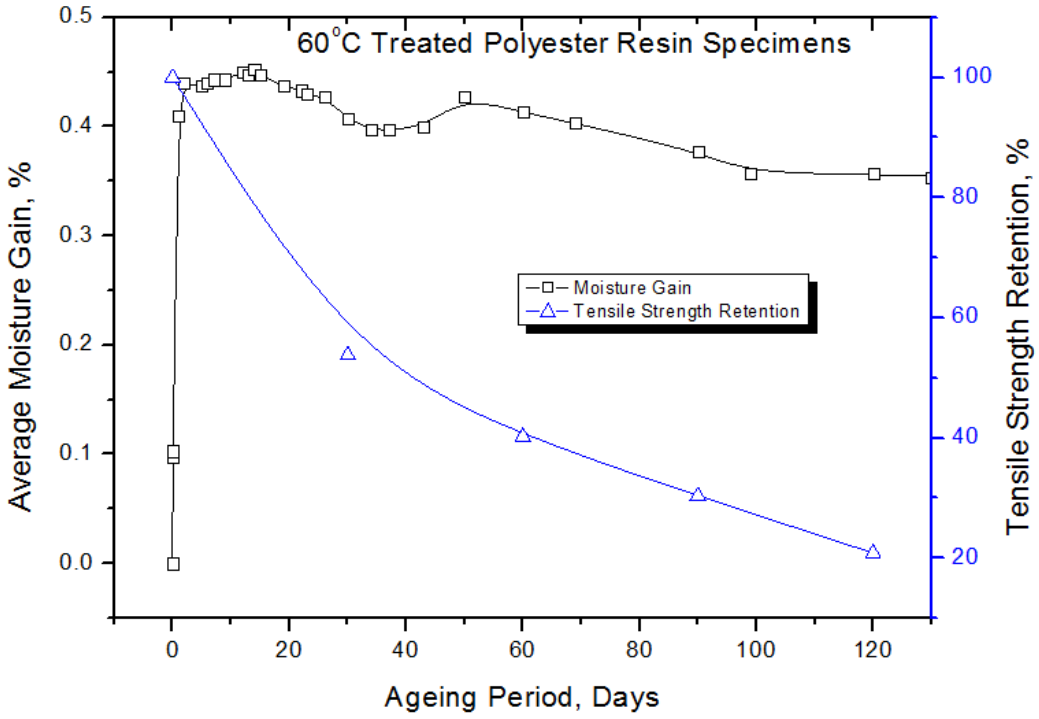

Figure 4.11: The relationship between % water absorption and tensile strength with increasing exposure times for neat cured polyester resin specimens hydrothermally treated at 60°C.

A resultant surface contour plot shown in Figure 4.12 depicts changes in the tensile strength of cured polyester resin specimens as a function of the hydrothermally treated water temperature and conditioning period.

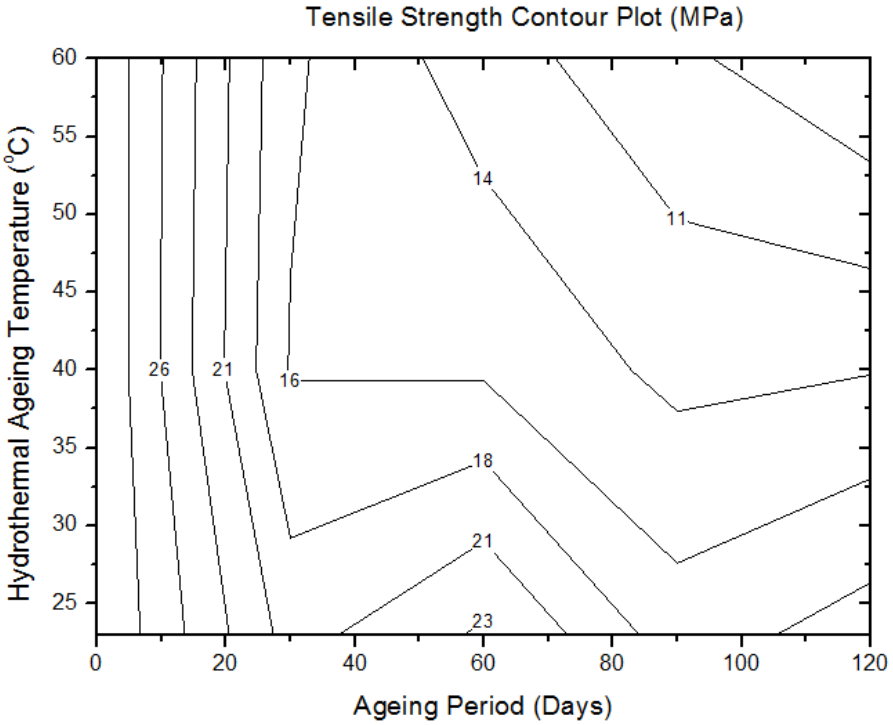

Figure 4.12: Resultant tensile strength surface contour plot as a function of the hydrothermal ageing temperature and ageing period.

4.3.1.3 Sisal-Polyester Composite

Figure 4.13 shows tensile test result plots of the variations in the values of tensile strength of sisal fibre reinforced polyester specimens, as a function of immersion time and environment temperature presented in Table 4.6.

Table 4.6: Average values of the ultimate tensile strength of sisal fibre reinforced polyester specimens treated hydrothermally at temperatures of 23°C, 40°C and 60°C over specific periods of time.

Time (Days)	Ultimate Tensile Strength (MPa)					
	23°C		40°C		60°C	
	σ_{TS} (MPa)	StdDev (MPa)	σ_{TS} (MPa)	StdDev (MPa)	σ_{TS} (MPa)	StdDev (MPa)
0	45.172	11.212	45.172	11.213	45.172	11.213
30	31.876	8.178	37.534	0.657	36.191	12.388
60	41.912	3.816	40.112	2.056	30.698	5.559
90	39.973	10.140	32.326	5.613	33.121	2.401
120	39.2087	2.897	35.284	2.584	22.902	7.127

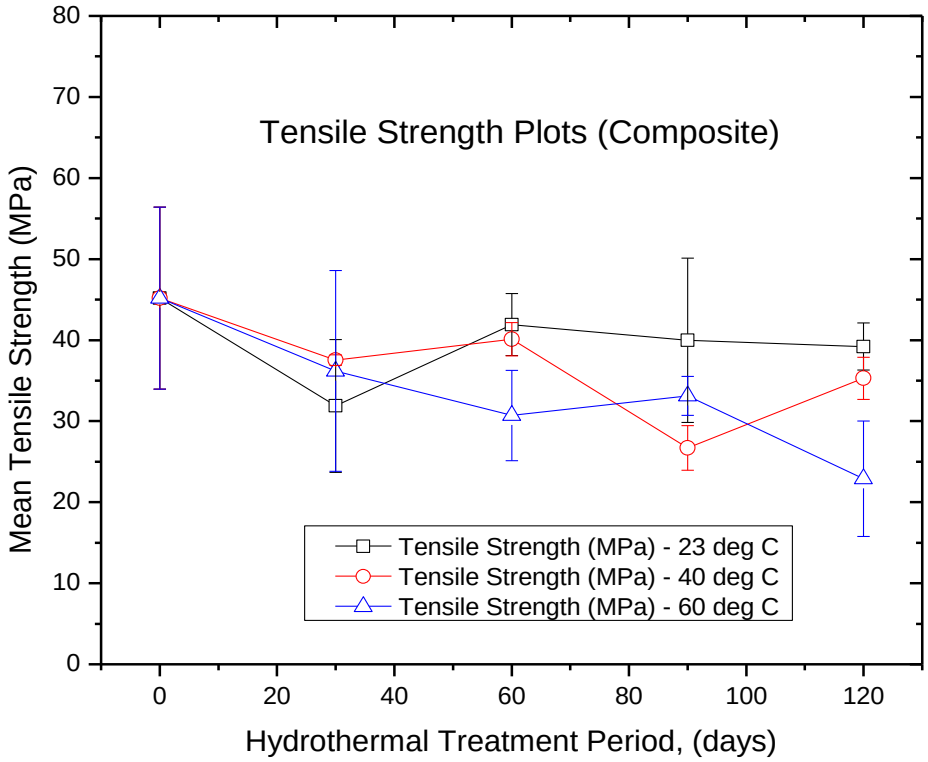

Figure 4.13: Changes in the tensile strength of sisal fibre reinforced polyester composite specimens that are treated hydrothermally in distilled water at different temperatures over specific periods of time.

Figure 4.14 through Figure 4.16 show the plots of average tensile strength and percentage moisture gain versus hydrothermal conditioning time for the same sisal fibre reinforced polyester composite specimens.

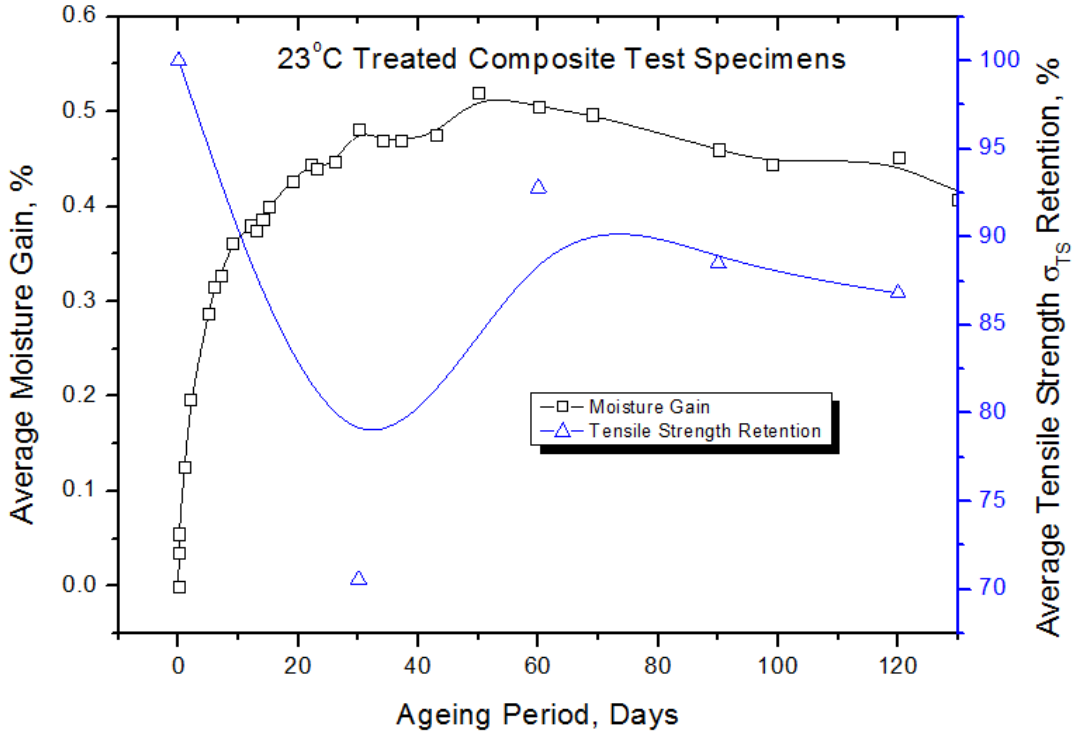

Figure 4.14: The relationship between water absorption and tensile strength with increasing exposure times for sisal fibre reinforced polyester composite specimens hydrothermally treated at 23°C.

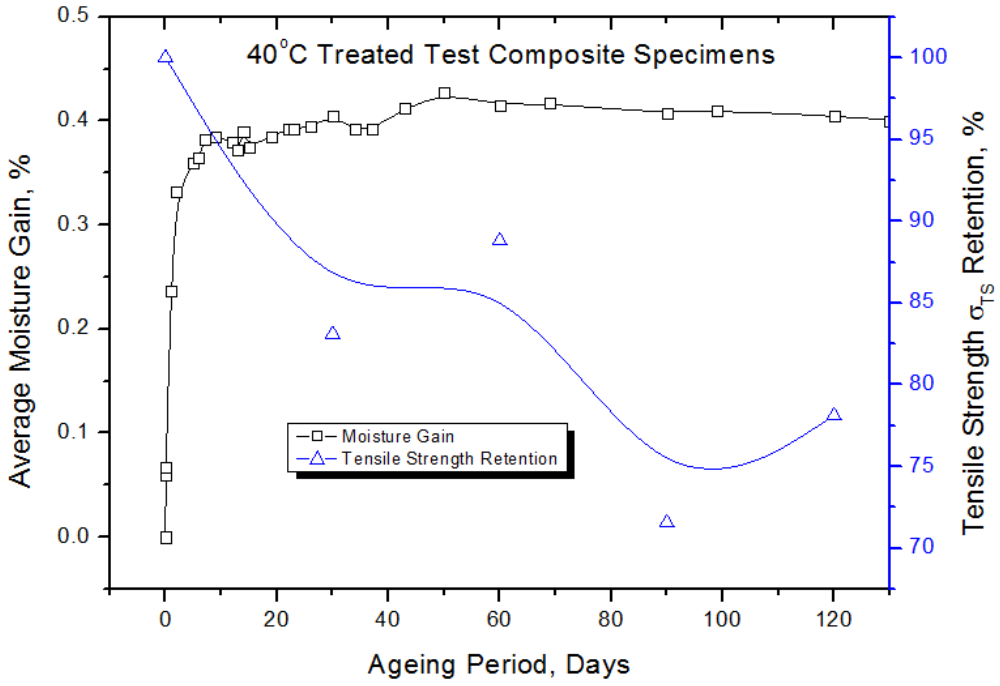

Figure 4.15: The relationship between % water absorption and tensile strength with increasing exposure times for sisal fibre reinforced polyester composite specimens hydrothermally treated at 40°C.

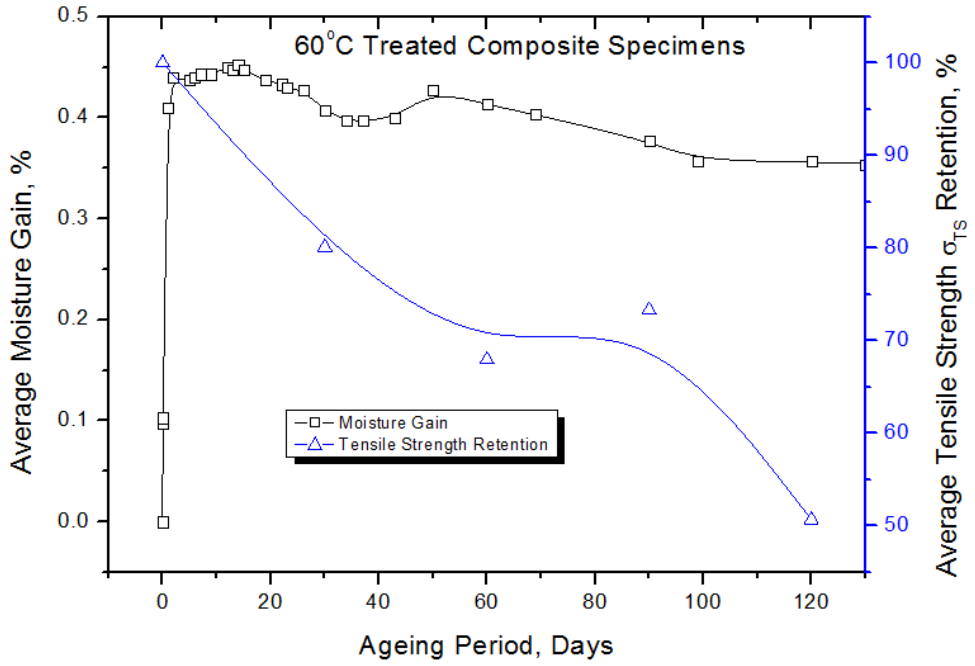

Figure 4.16: The relationship between % water absorption and tensile strength with increasing exposure times for sisal fibre reinforced polyester composite specimens hydrothermally treated at 60°C.

Figure 4.17 shows the resultant surface contour plot depicting changes in the tensile strength of sisal fibre reinforced polyester composite specimens with changes in the hydrothermally treated water temperature and conditioning period.

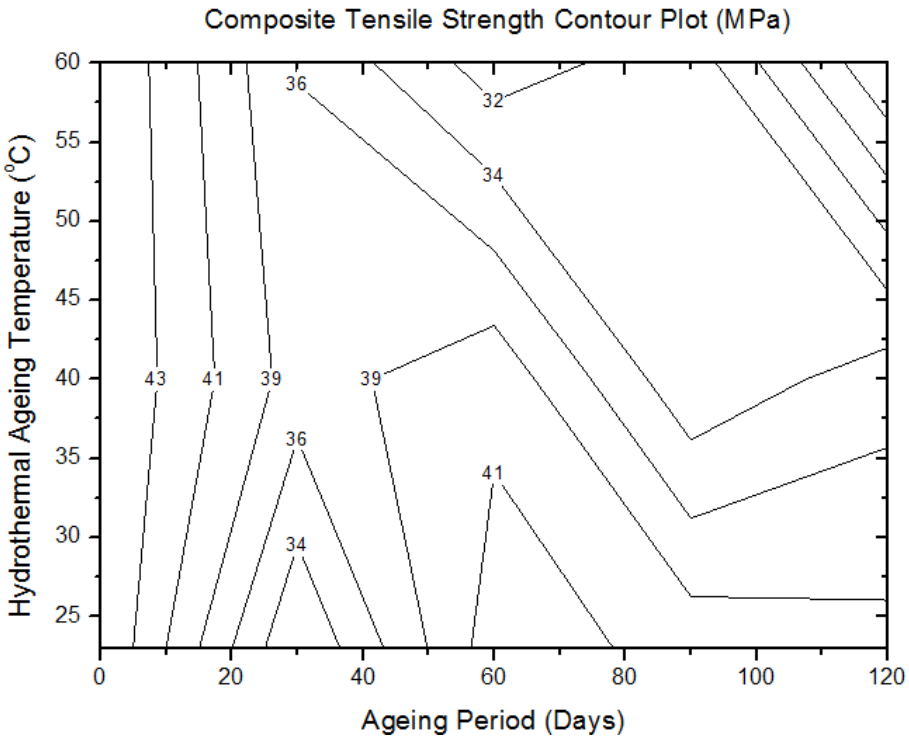

Figure 4.17: Resultant surface contour plot depicting changes in the tensile strength (MPa) of sisal fibre reinforced polyester composite specimens with changes in the hydrothermally treated water temperature and conditioning period.

4.3.2 Tensile Modulus

Results pertaining to mechanical tests conducted in order to assess the effect on the tensile modulus of sisal fibres, neat polyester and sisal/polyester composite system after undergoing hydrothermal treatment are presented.

4.3.2.1 Sisal Fibre

Changes in the values of modulus of elasticity for the single sisal fibre specimens, hydrothermally treated by immersion in distilled water at different temperatures of 23°C, 40°C and 60°C over specific durations are given in Table 4.7 and graphically in Figure 4.18 and Figure 4.19. (More detailed information on the effects of temperature and moisture content on the elastic modulus of single sisal fibres has been added in Appendix C).

Table 4.7: Average elastic modulus values for hydrothermally treated single sisal fibres.

Time (Days)	Elastic Modulus, E (GPa)					
	23°C		40°C		60°C	
	E	StdDev	E	StdDev	E	StdDev
0	40.881	21.098	40.881	21.097	40.881	21.097
30	35.318	18.621	41.555	11.939	29.612	8.807
60	29.298	13.539	27.046	9.535	26.886	7.373
90	32.537	8.595	38.219	19.187	42.639	18.484
120	29.921	13.081	31.401	5.579	29.003	6.984

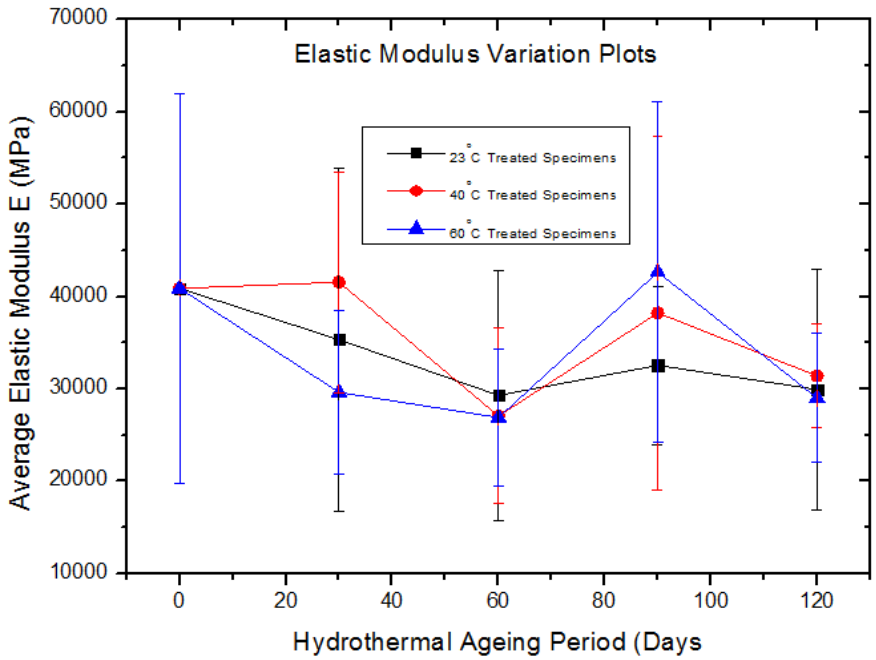

Figure 4.18: Average elastic modulus variation plot for hydrothermally treated single sisal fibres.

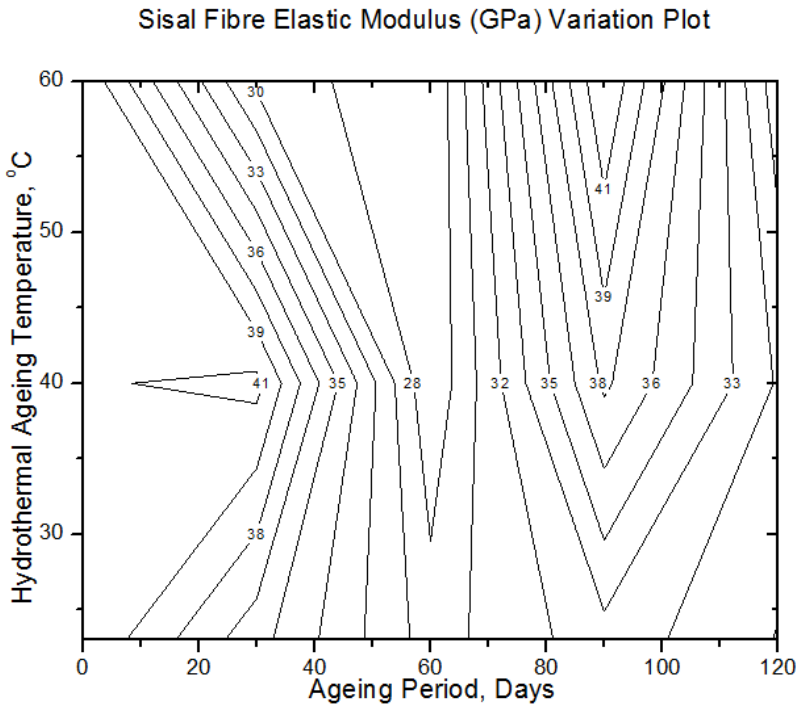

Figure 4.19: Resultant surface contour plot depicting changes in the elastic modulus of single fibre test specimens with changes in the hydrothermally treated water temperature and conditioning period.

4.3.2.2 Neat Polyester Resin

The changes in the values of modulus of elasticity of the neat polyester specimens hydrothermally treated by immersion in distilled water at different temperatures of 23°C, 40°C and 60°C for specific durations are given in Table 4.8 and graphically in Figure 4.20 through Figure 4.23.

Table 4.8: Values of Modulus of Elasticity for neat polyester specimens after being immersed in distilled water at different temperature over specified time periods.

Time (Days)	Elastic Modulus (GPa)					
	23°C		40°C		60°C	
	E (GPa)	StdDev (GPa)	E (GPa)	StdDev (GPa)	E (GPa)	StdDev (GPa)
0	2.186	0.21	2.186	0.21	2.186	0.21
30	3.193	0.38	3.003	0.22	3.163	0.25
60	2.622	0.23	2.593	0.21	2.664	0.14
90	2.798	0.13	2.711	0.41	2.191	0.52
120	2.872	0.13	2.759	0.13	1.932	0.12

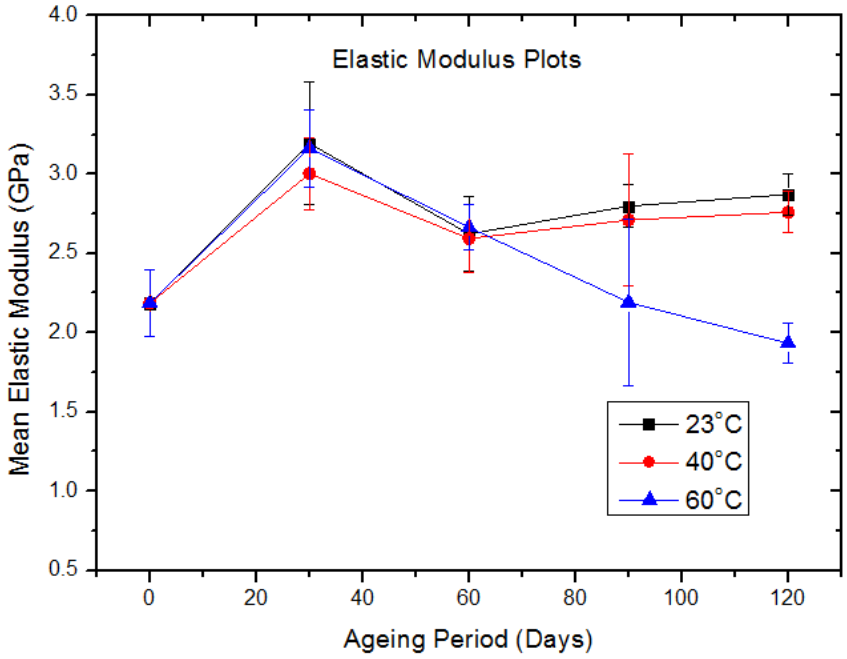

Figure 4.20: Changes in the Modulus of Elasticity of neat polyester resin specimens hydrothermally treated in distilled water at different temperature over time.

The surface contour plot shown in Figure 4.24 illustrates changes in the modulus of elasticity of post cured polyester resin specimens hydrothermally treated at temperatures ranging from 23°C to 60°C over a period of 120 days.

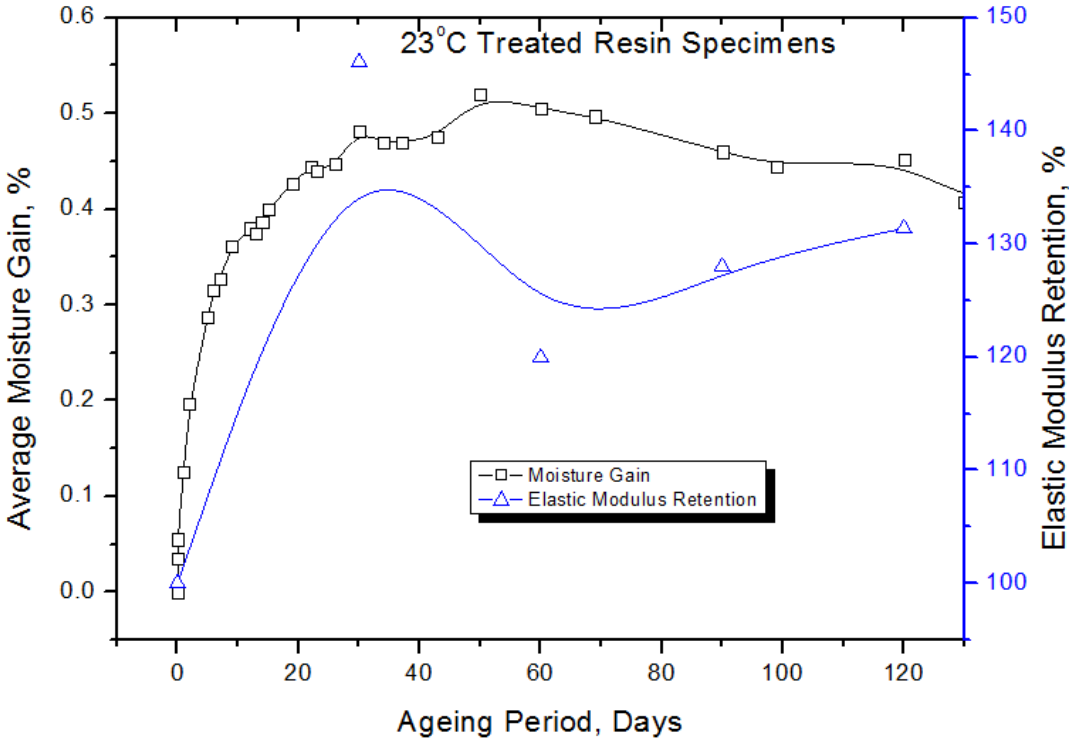

Figure 4.21: A relationship of water absorption and elastic modulus with increasing exposure times for neat cured polyester resin specimens hydrothermally treated at 23°C.

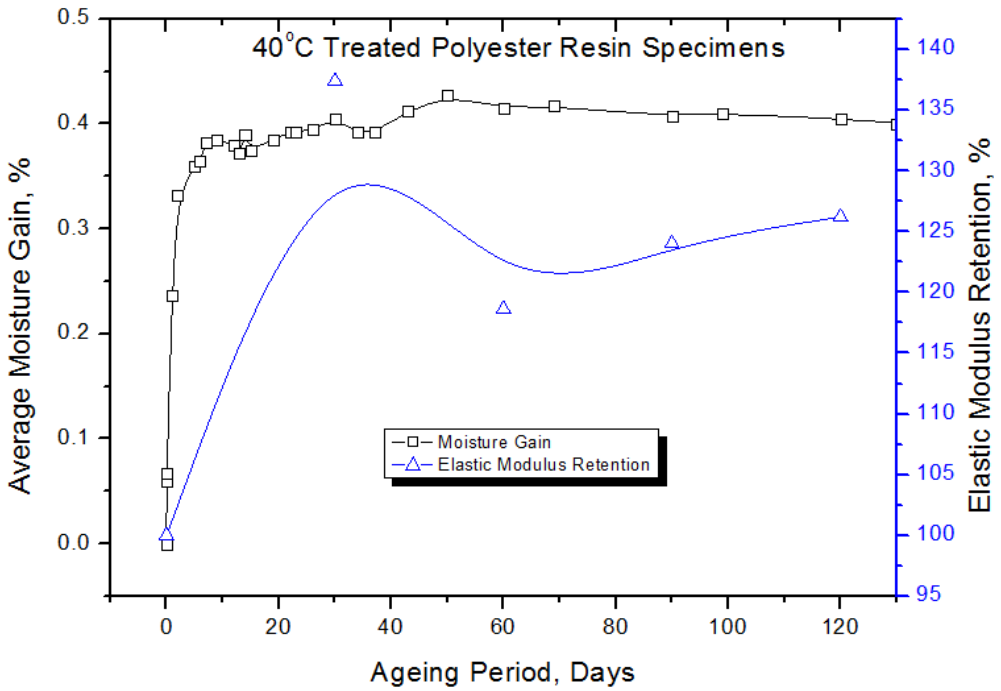

Figure 4.22: A relationship of water absorption and elastic modulus with increasing exposure times for neat cured polyester resin specimens hydrothermally treated at 40°C.

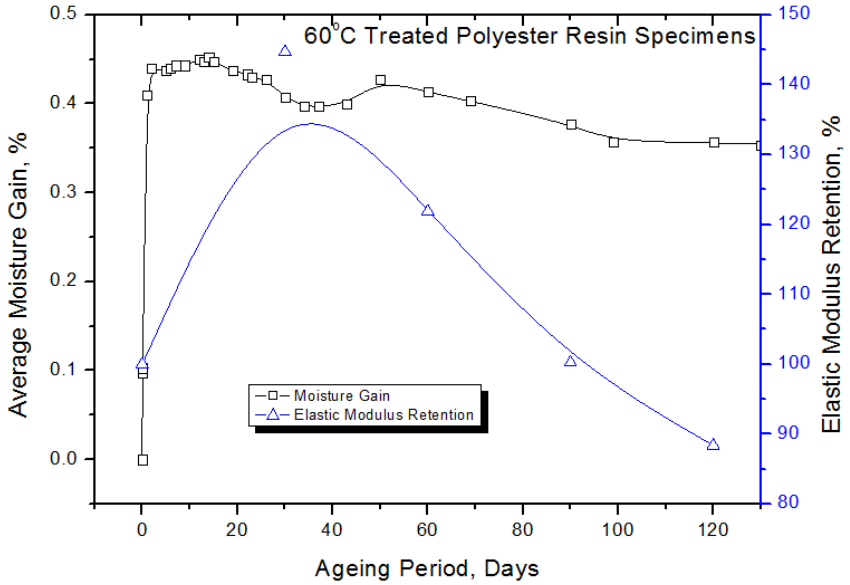

Figure 4.23: A relationship of water absorption and elastic modulus with increasing exposure times for neat cured polyester resin specimens hydrothermally treated at 60°C.

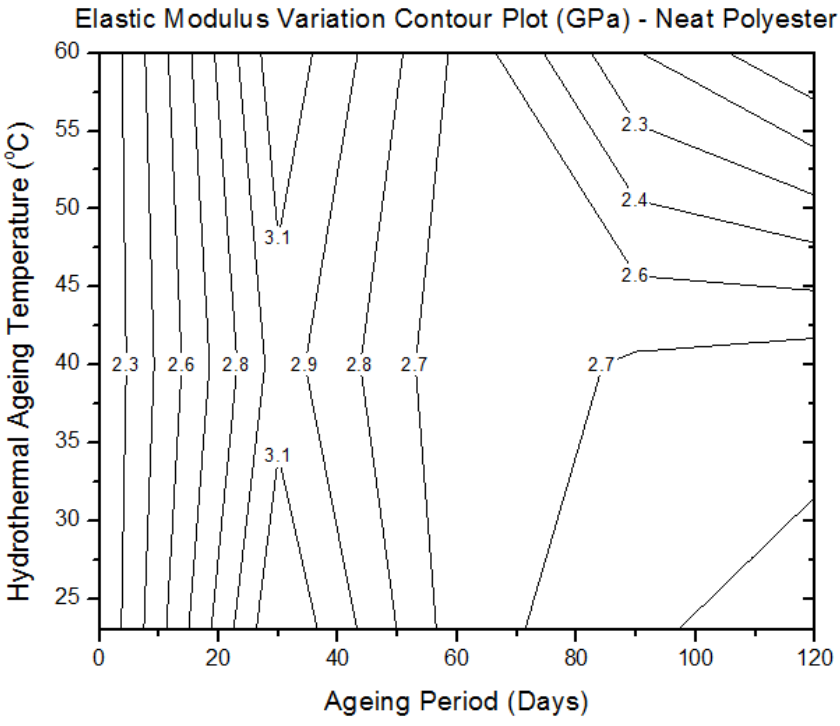

Figure 4.24: Surface contour plot depicting changes in the Modulus of Elasticity of cured polyester resin specimens hydrothermally treated in distilled water at temperatures ranging from 23°C to 60°C over a period of 120 days.

4.3.2.3 Sisal-Polyester Composite

The variations in the values of modulus of elasticity of the Sisal/Polyester composite specimens, hydrothermally treated by immersion in distilled water at respective temperatures of 23^{o}C, 40^{o}C and 60^{o}C for specific durations, are given in Table 4.9 and graphically in Figure 4.25 through Figure 4.29.

Table 4.9: Modulus of Elasticity values for Sisal/Polyester composite specimen after being in immersed on distilled water at different temperature over specified time periods.

Time (Days)	Elastic Modulus (GPa)					
	23°C		40°C		60°C	
	E (GPa)	StdDev (GPa)	E (GPa)	StdDev (GPa)	E (GPa)	StdDev (GPa)
0	3.749	0.46	3.749	0.46	3.749	0.46
30	3.736	0.61	3.747	0.92	3.277	1.1
60	4.905	0.25	4.404	0.17	4.015	0.22
90	5.149	0.66	5.171	1.15	3.844	1.19
120	4.084	0.48	3.603	0.49	3.283	1.1

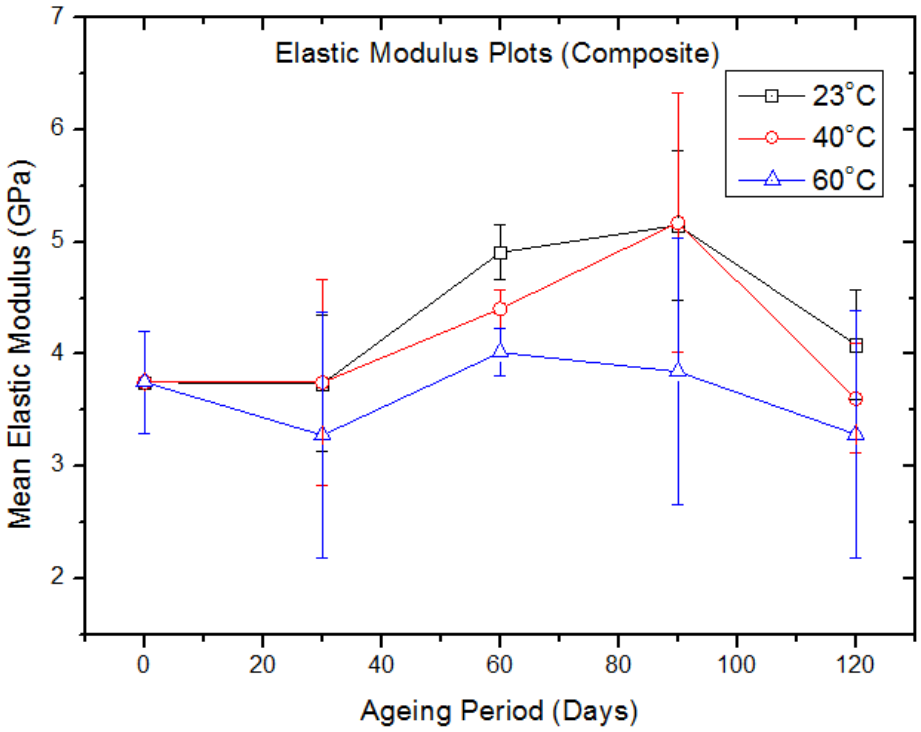

Figure 4.25: Changes in the modulus of elasticity of Sisal/Polyester composites hydrothermally treated in distilled water at different temperature over specific time periods.

The surface contour plot shown in Figure 4.24 illustrates changes in the modulus of elasticity of post cured polyester resin specimens hydrothermally treated at temperatures ranging from 23^{o}C to 60^{o}C over a period of 120 days.

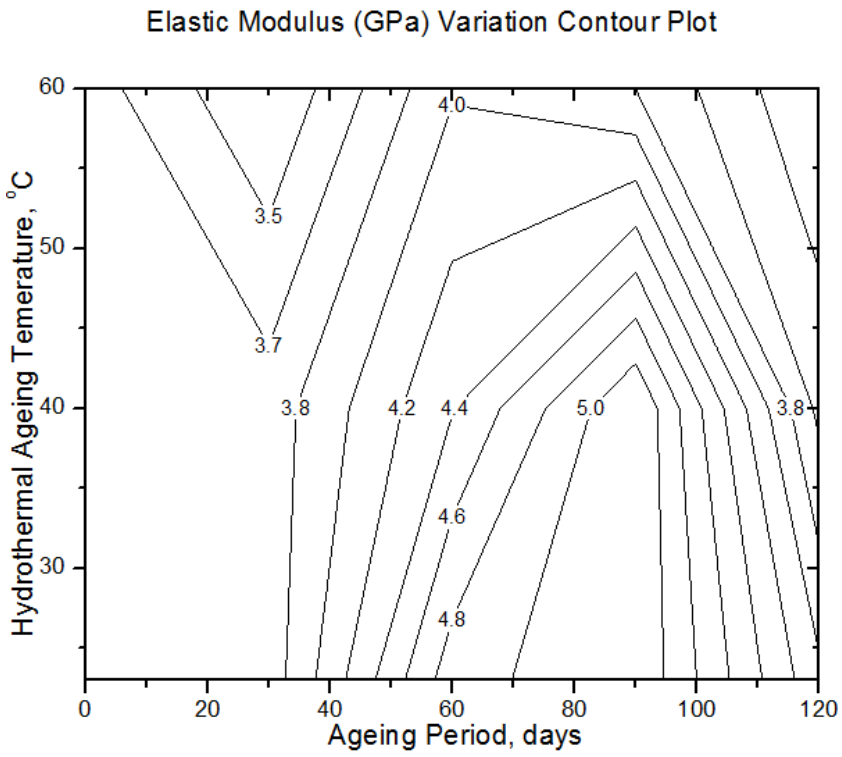

Figure 4.26: Resultant surface contour plot depicting changes in the elastic modulus of sisal/ polyester composite specimens with changes in the hydrothermally treated water temperature and conditioning period.

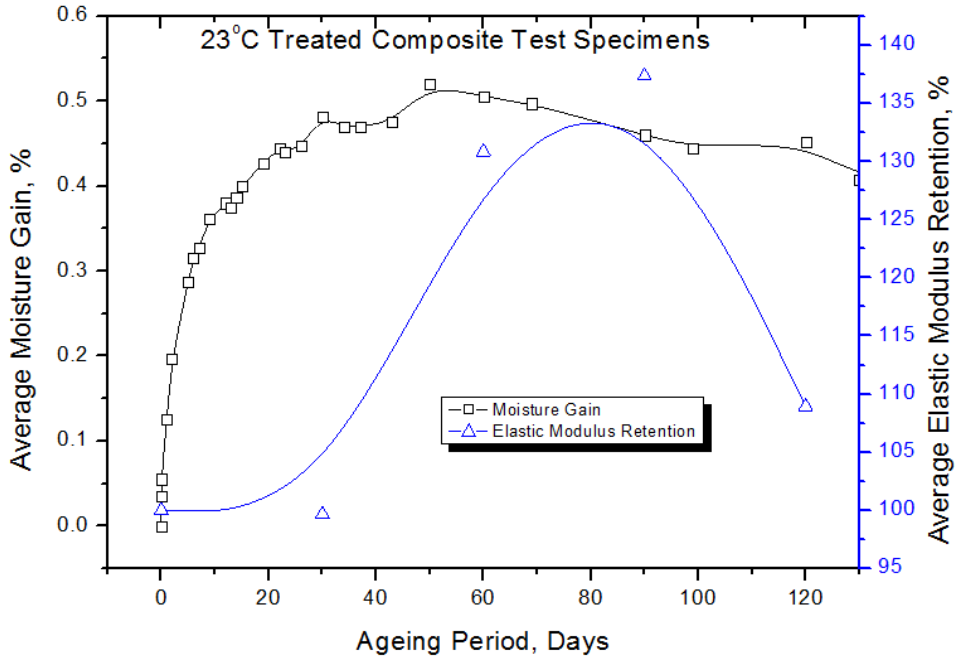

Figure 4.27: The relationship between water absorption and elastic modulus with increasing exposure times for sisal fibre reinforced polyester composite specimens hydrothermally treated at 23°C.

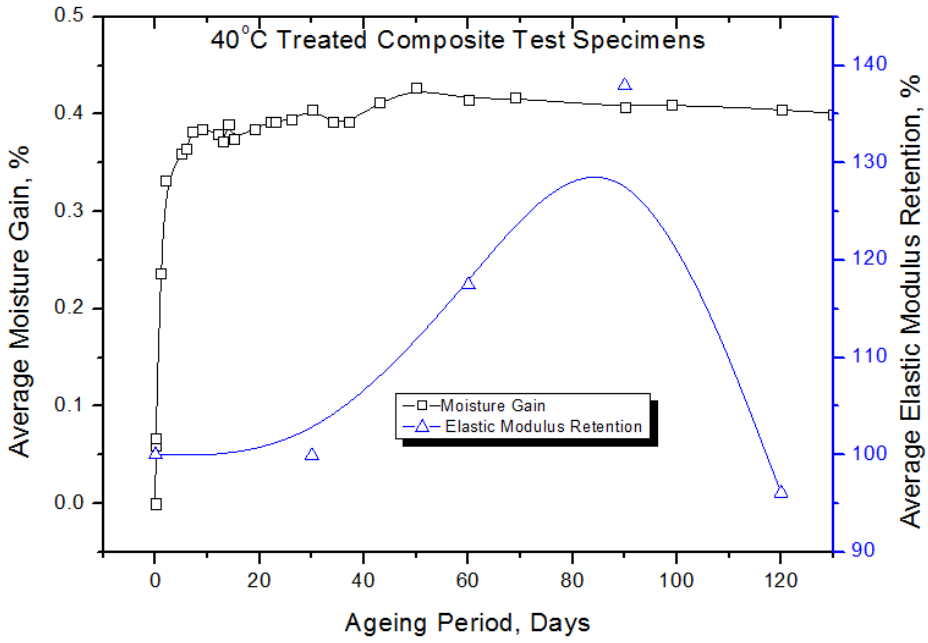

Figure 4.28: The relationship between water absorption and elastic modulus with increasing exposure times for sisal fibre reinforced polyester composite specimens hydrothermally treated at 40°C.

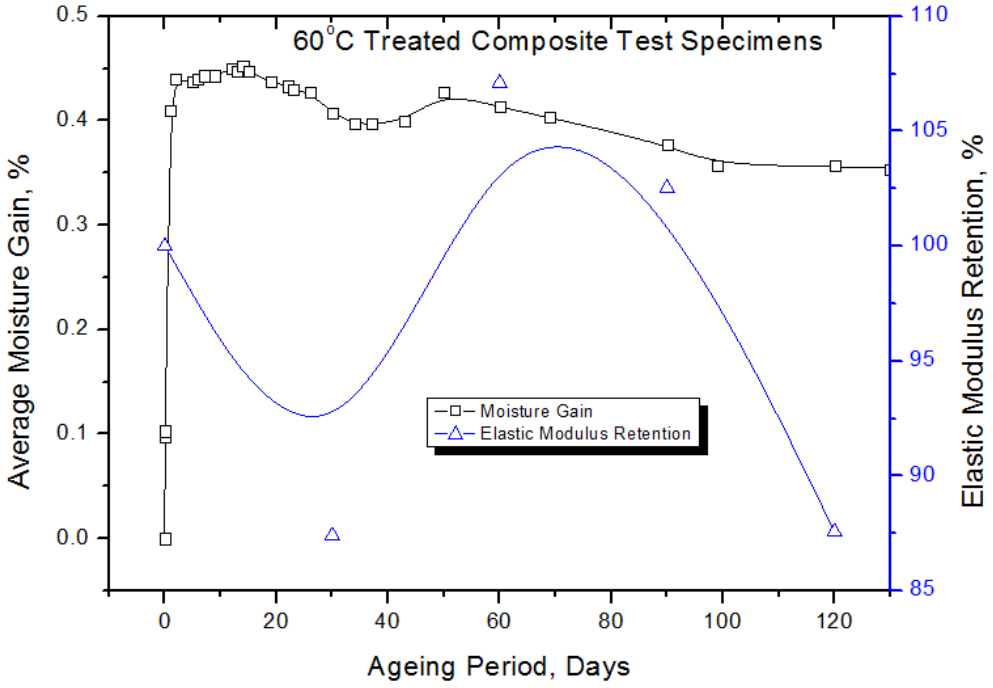

Figure 4.29: The relationship between water absorption and elastic modulus with increasing exposure times for sisal fibre reinforced polyester composite specimens hydrothermally treated at 60°C.

4.4 Dynamic Mechanical Analysis

Figure 4.30 shows a multi frequency DMA composite plot of the Storage Modulus, Loss Modulus and *Tan δ* resulted from an analysis conducted on one untreated polyester test specimen. Other result plots for the other test conducted on the same cured resin systems after hydrothermal treatment for different durations are presented in Appendix D.

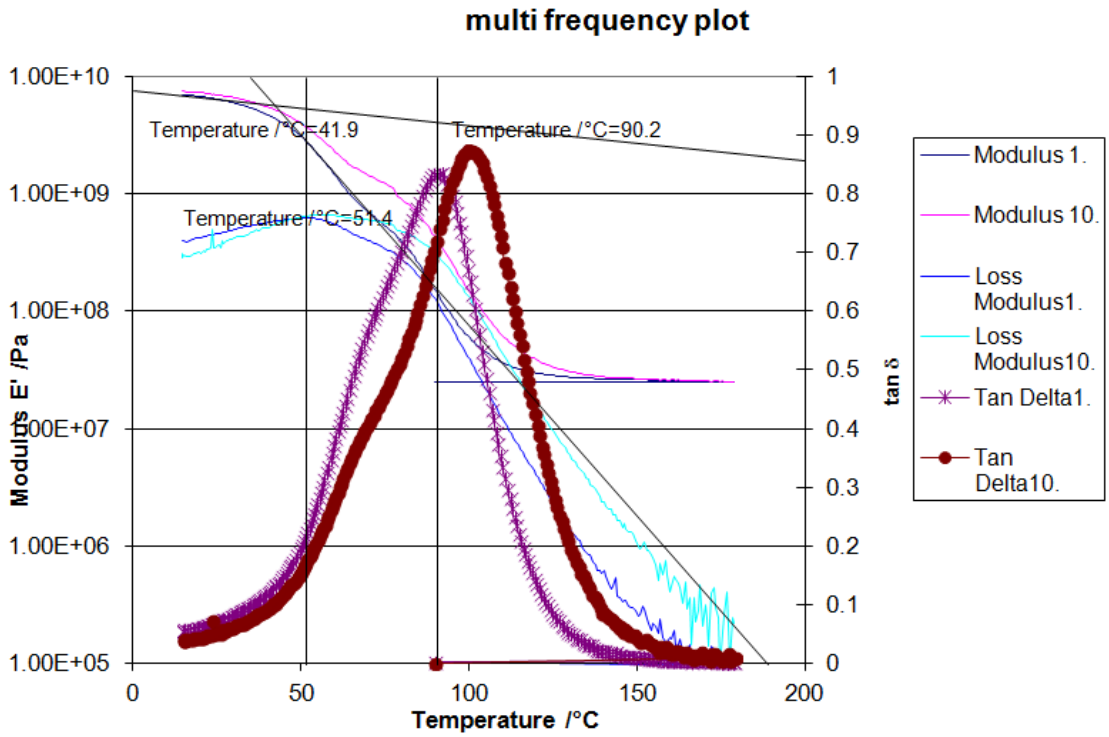

Figure 4.30: Multi frequency DMA plots of Storage Modulus, Loss Modulus and *Tan δ* of untreated polyester test specimen. Plots of the other results are shown in Appendix D.

Table 4.10 presents glass transition temperature (Tg) test results from the Dynamic Mechanical Analysis (DMA) of hydrothermally aged polyester specimens for a total period of 150 day at temperatures of 23°C, 40°, and 60°C. A more detailed table of results is presented in Appendix D.

Table 4.10: Glass transition temperature test results summary of hydrothermal treated polyester resin test specimens at respective temperature of 23°C, 40°C and 60°C over a maximum of 150 days.

Ageing Period, days	Glass Transition Temperature Tg, °C					
	23°C		40°C		60°C	
	Average	StdDev	Average	StdDev	Average	StdDev
0	89.966	0.251	89.966	0.252	89.966	0.252
30	78.966	0.577	83.575	4.661	82.35	3.270
60	82.275	2.826	86.325	3.171	83.433	0.896
90	80.1	0.458	85.2	3.112	85.375	2.696
120	79.6	0.1	84.225	3.386	84.625	3.047
150	79.1	0.271	87.75	0.636	82.925	0.537

Figure 4.31 further gives a graphical summary of the respective variations in the Tg throughout the review time period.

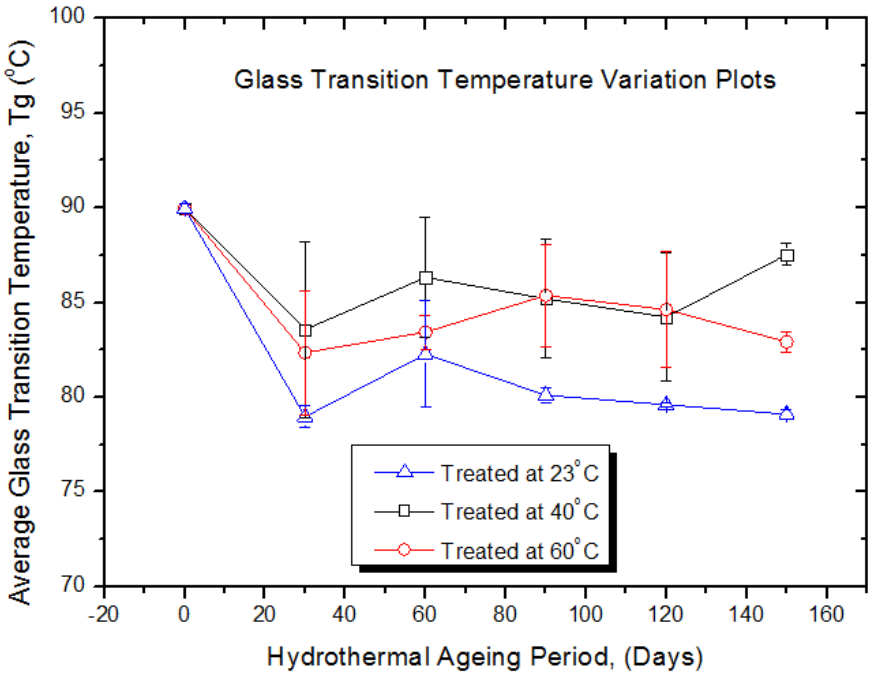

Figure 4.31: Glass transition temperature variation plots of hydrothermally treated specimens at respective water temperatures of 23°C, 40°C and 60°C over a period of 150 days of ageing.

Plots showing the relationships existing between water absorption and glass transition temperature over time for neat cured polyester resin specimens hydrothermally treated at 23°C, 40°C, and 60°C are shown in Figure 4.32 through Figure 4.34.

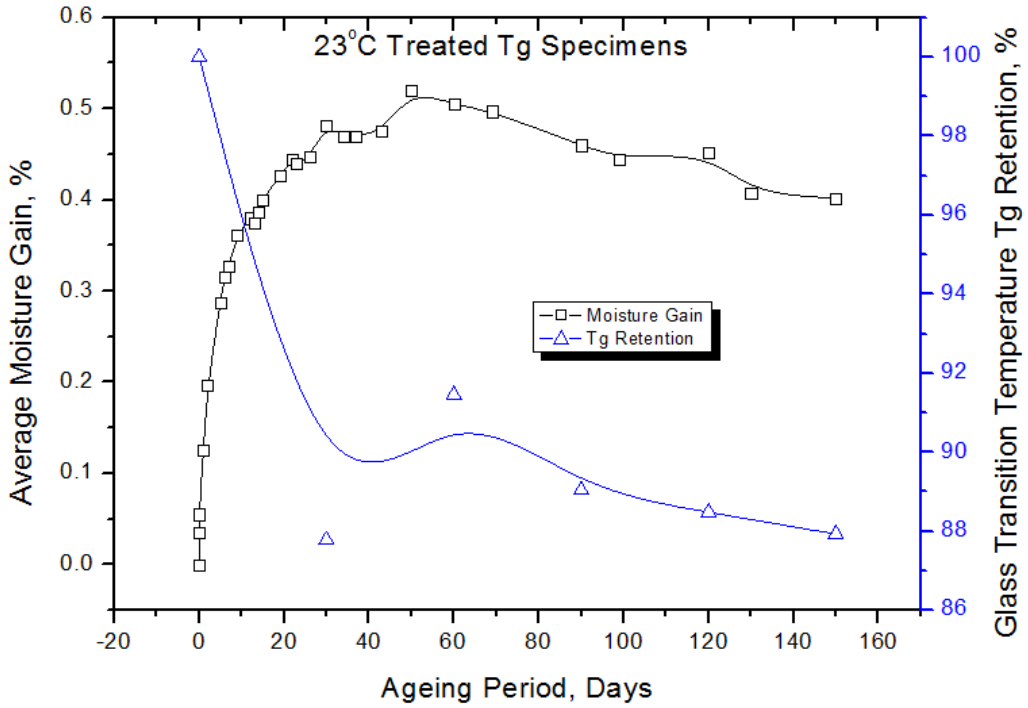

Figure 4.32: The relationship between water absorption and glass transition temperature with increasing exposure times for neat cured polyester resin specimens hydrothermally treated at 23°C.

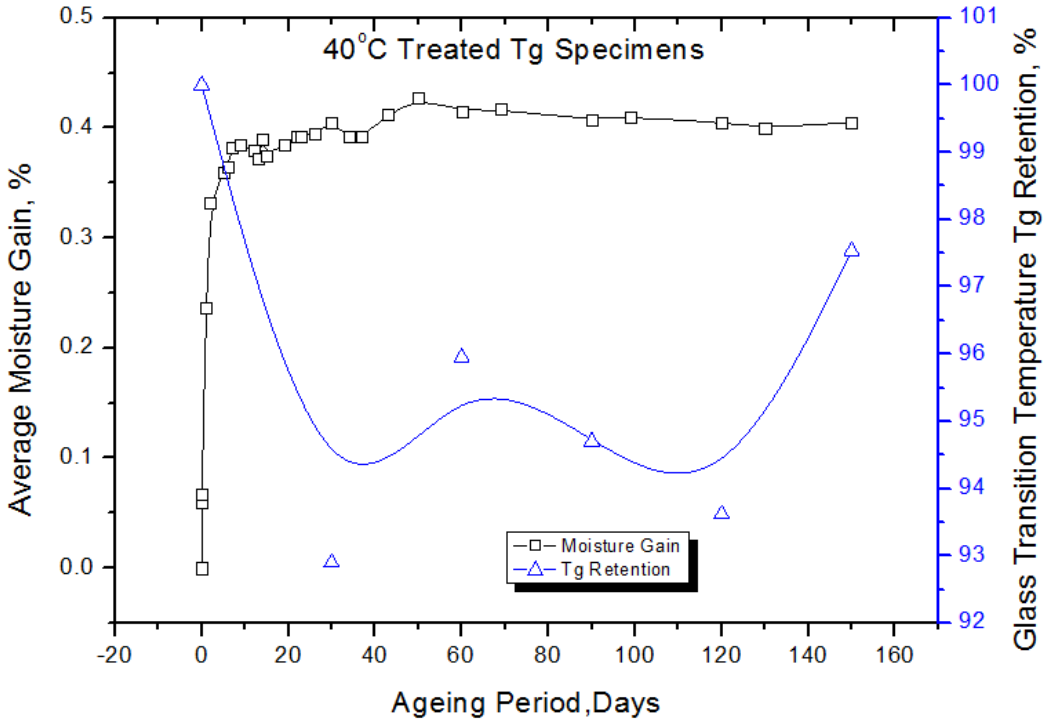

Figure 4.33: The relationship between water absorption and glass transition temperature with increasing exposure times for neat cured polyester resin specimens hydrothermally treated at 40°C.

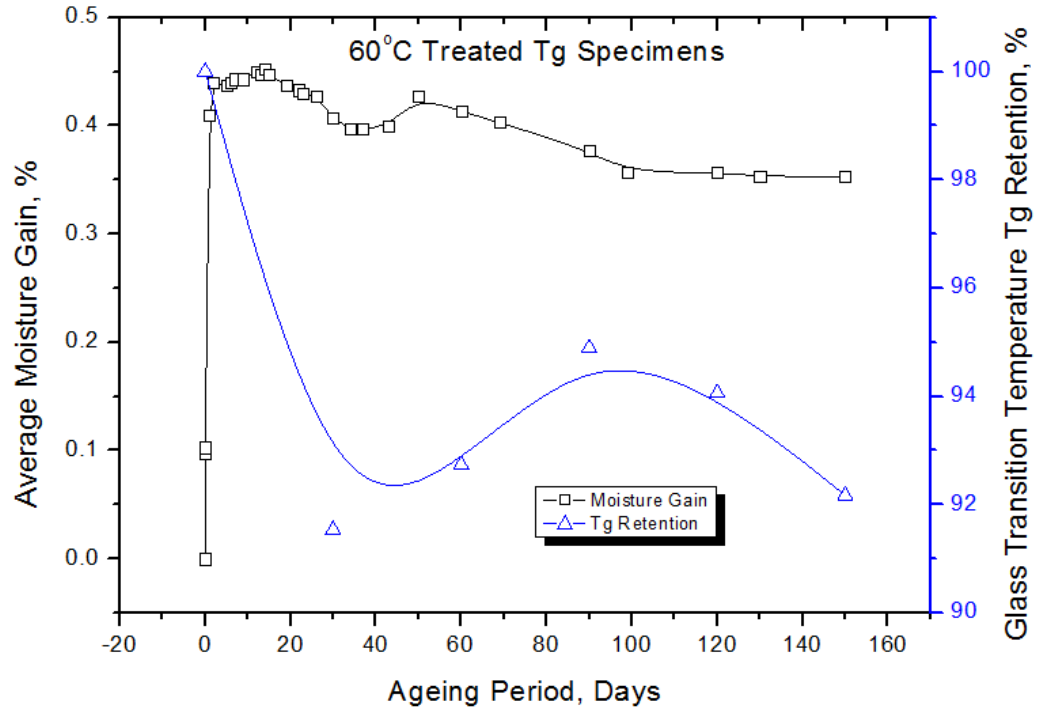

Figure 4.34: The relationship between water absorption and glass transition temperature with increasing exposure times for neat cured polyester resin specimens hydrothermally treated at 60°C.

This variation in the Tg is further shown in Figure 4.35 in the form of a contour plot describing clearly the variations in the same property as a function of the ageing conditions.

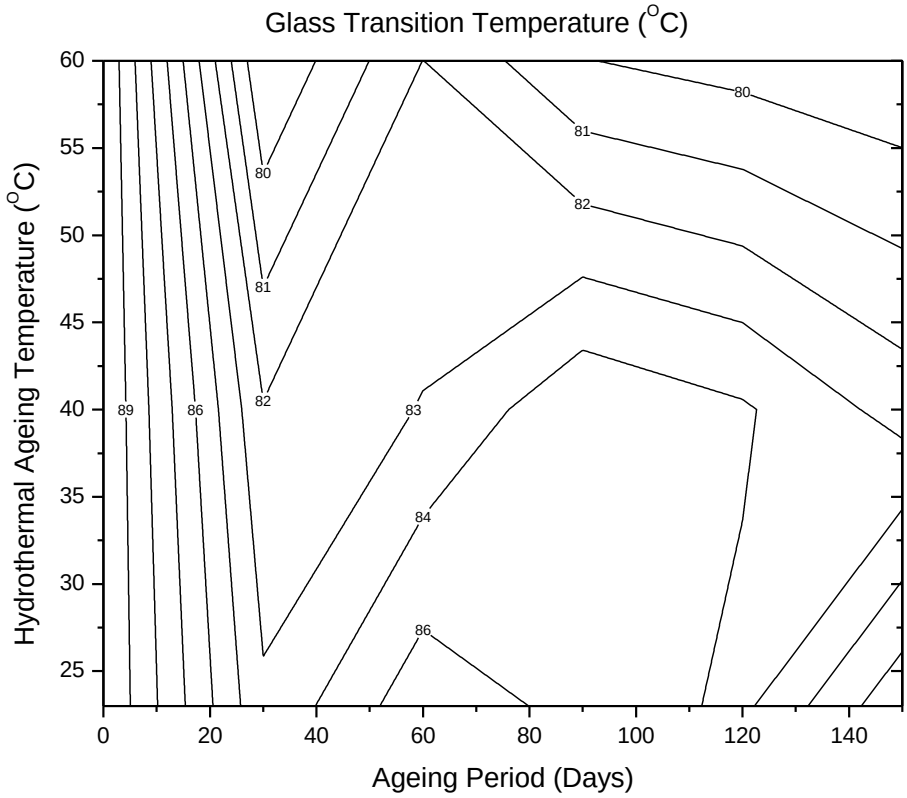

Figure 4.35: Contour plot describing variations in the glass transition temperature as a function of hydrothermal ageing temperature and treatment period based on the experiment values.

Figure 4.36 through Figure 4.38 show plots of glass transition temperature as a function of moisture content for hydrothermally treated cured resin test specimens at respective temperatures of 23°C, 40°C, and 60°C.

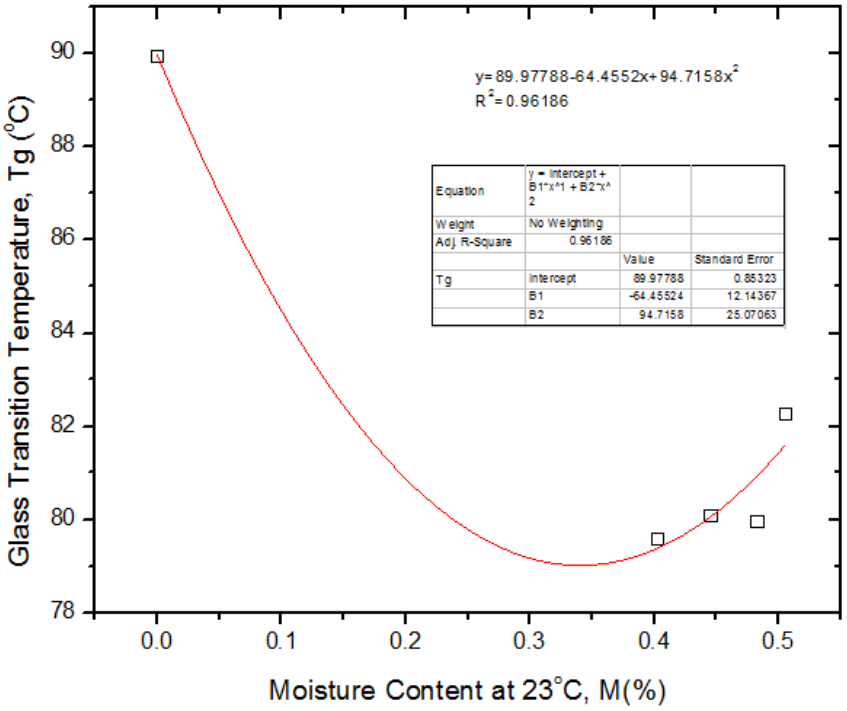

Figure 4.36: Glass transition temperature as a function of moisture content at hydrothermal conditioning temperature of 23°C.

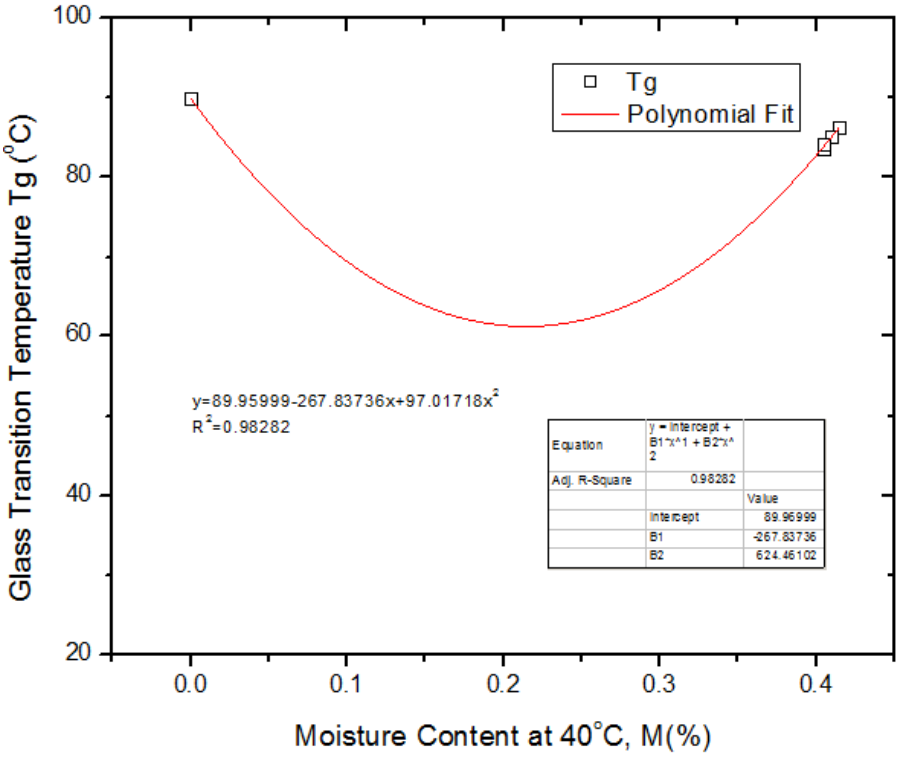

Figure 4.37: Glass transition temperature as a function of moisture content at hydrothermal conditioning temperature of 40°C.

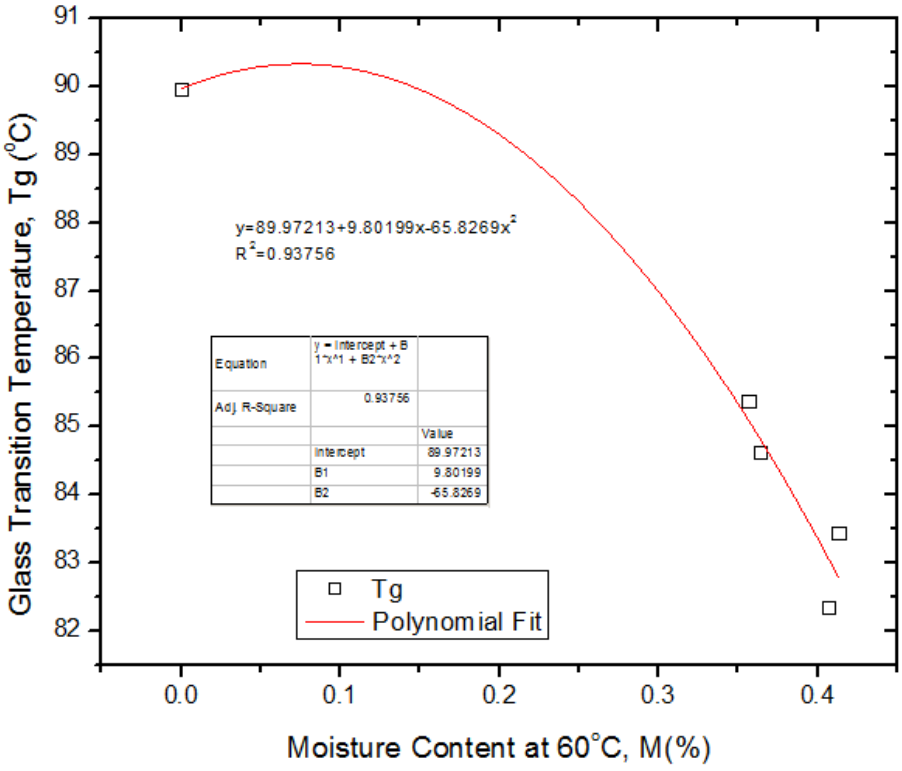

Figure 4.38: Glass transition temperature as a function of moisture content at hydrothermal conditioning temperature of 60°C.

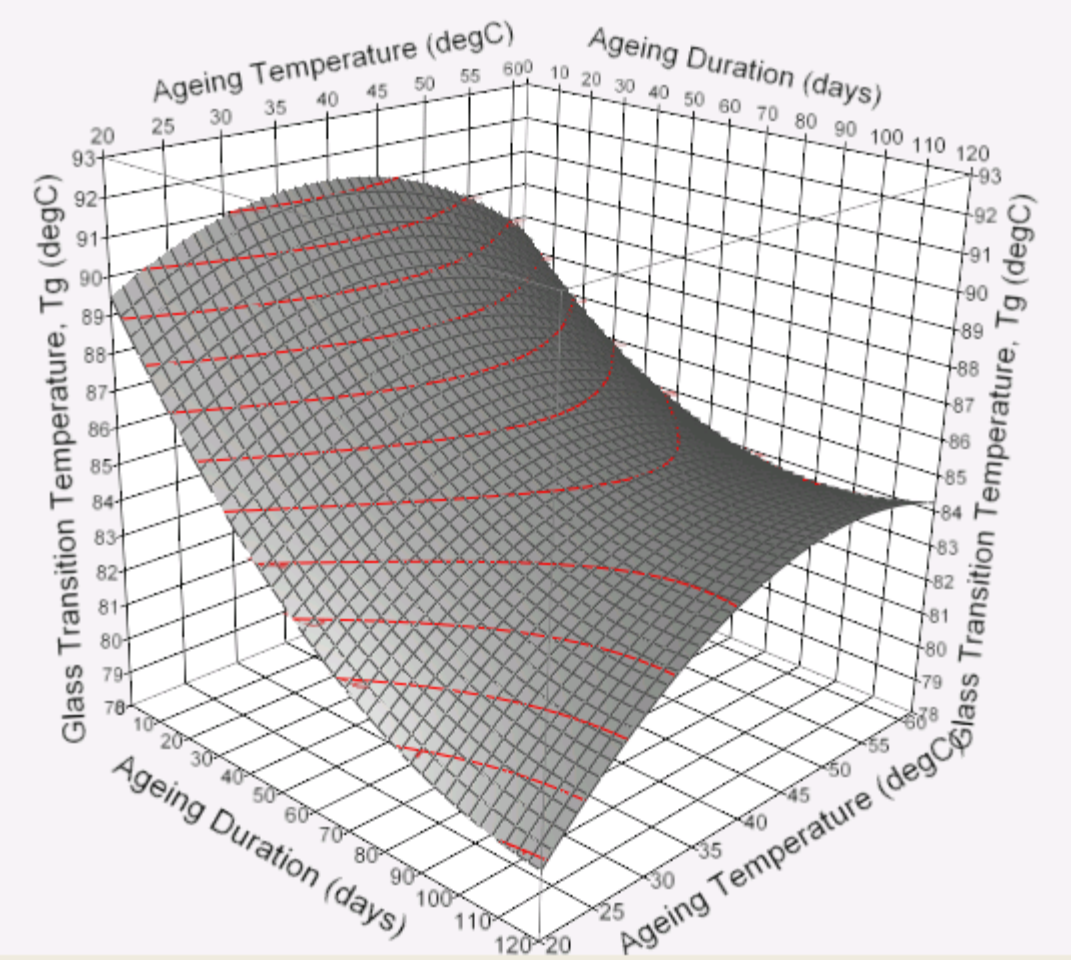

Figure 4.39: Fitted glass transition temperature surface plot.

The fitted surface plot in Figure 4.39 shows the variations in composite's glass transition temperature as a function of hydrothermal ageing temperature and treatment period based on the regression model. This regression analysis was conducted to determine the relationship existing between the hydrothermal treatment and exposure duration on the resultant glass transition temperature of the composite material for the three ageing conditions. This relationship can be described by model equation (4.4):

$$T_g = 85.63 + 1.034\alpha_{Temp} - 3.57\beta_{Time} + 1.25\alpha_{Temp}\beta_{Time} - 2.08\alpha_{Temp}^2 + 2.15\beta_{Time}^2 \quad (4.4)$$

Where

T_g – Glass transition temperature, ^{o}C.

α_{Temp} – is a temperature-based parameter which is equal to

$$\alpha_{Temp} = \frac{Temp - 40}{20}$$

For *Temp* ranges from 23°C to 60°C.

β_{Time} – is an ageing duration-based parameter which is equal to

$$\beta_{Time} = \frac{Duration - 60}{60}$$

For *Duration* ranges from 0 to 120 day.

A summary of the regression analysis has been in included in APPENDIX E for further reference.

4.5 Composite Fracture

This section presents results and analysis following studies conducted on hydrothermally aged microbond and fracture toughness test specimens with the aim of assessing the retention of their respective properties over specific periods.

4.5.1 Micro Composite Fracture

Figure 4.40 shows a microbond single fibre pull-out force trace plot of one unconditioned microbond specimen.

Assuming that this peak force is the shearing force and is evenly acting along the entire fibre embedded circumference, therefore the shear strength adhesive bond at the interface is calculated from equation (4.5),

$$\tau = \frac{F_p}{\pi D l} \tag{4.5}$$

Where F_p – Pull-out force

D – Fibre diameter

l – Fibre embedded length

Figure 4.40 through Figure 4.46 show samples of recorded plots of microbond shearing force versus corresponding droplet displacement for few selected test specimens, revealing effects of the respective hydrothermal ageing treatments on the resultant debonding force.

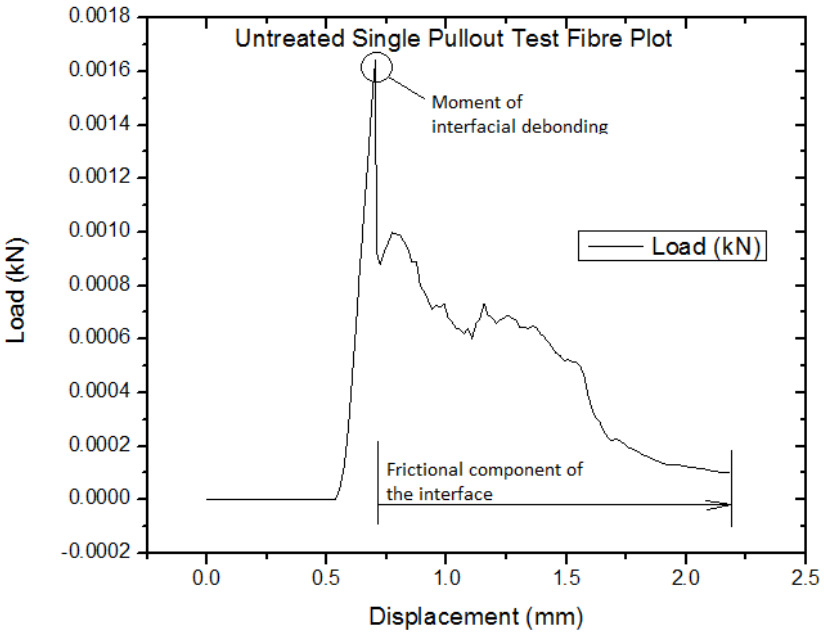

Figure 4.40: Single fibre pull-out test plot of a sisal/polyester micro composite (Non-hydrothermally treated)

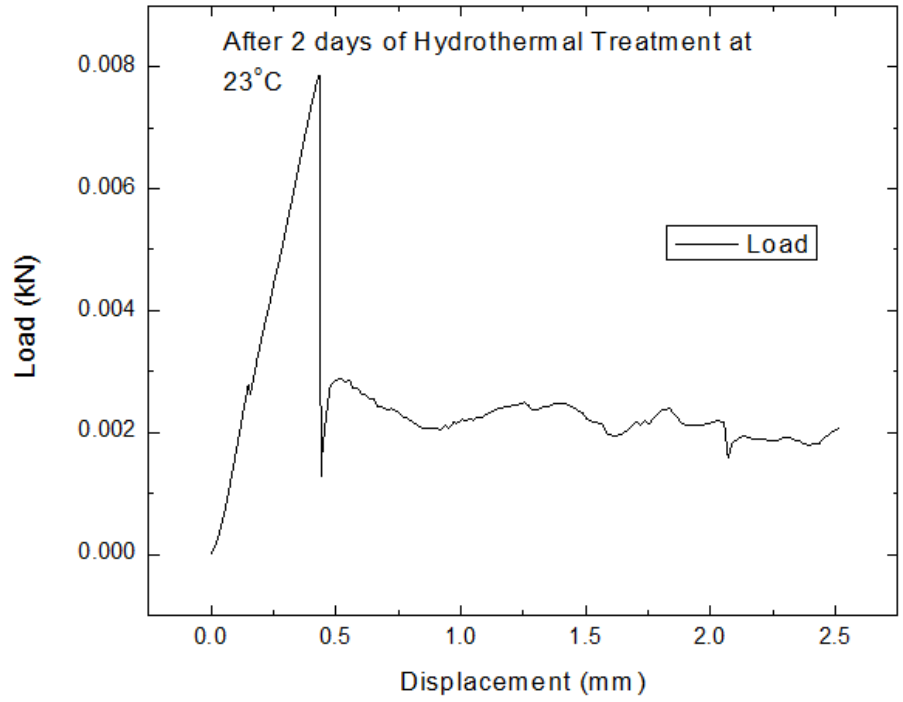

Figure 4.41: Microbond simple fibre pull-out test plot after 2 days (48hrs) of hydrothermal treatment at a temperature of 23°C.

Results of the first two days of hydrothermal treatment of microbond samples at the three ageing temperatures are further shown in Figures 4.41, 4.43 and 4.44.

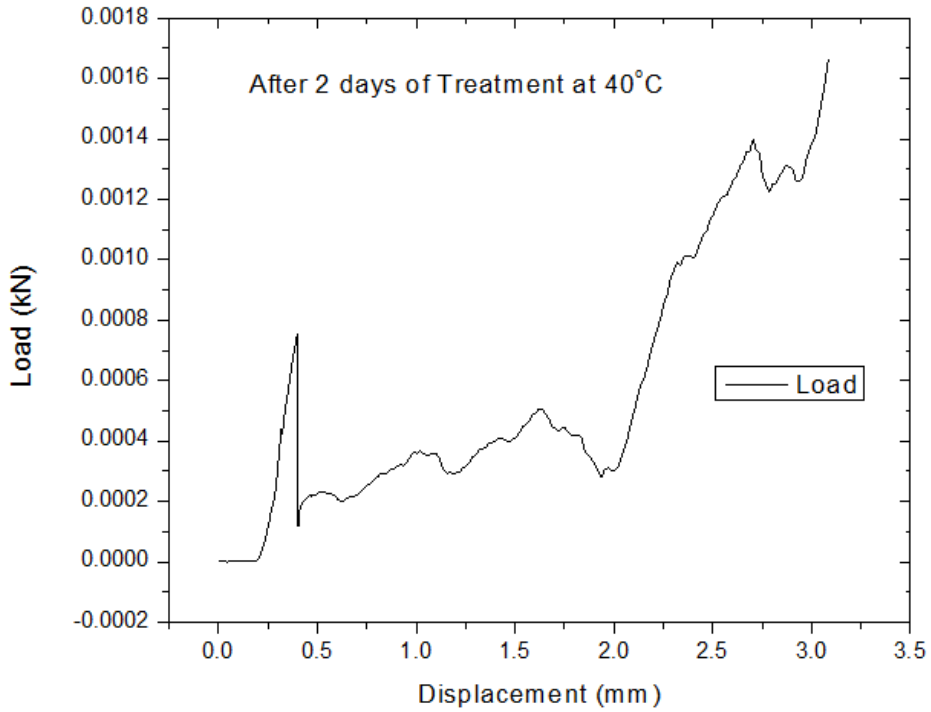

Figure 4.43: Microbond simple fibre pull-out test plot after 2 days (48hrs) of hydrothermal treatment at a temperature of 40°C.

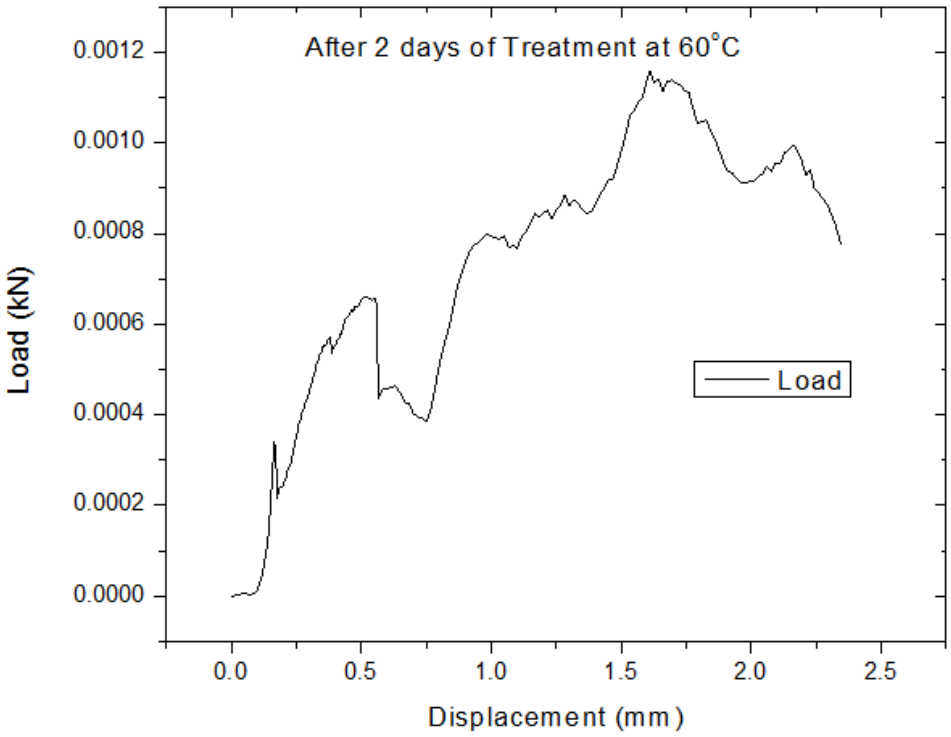

Figure 4.44: Microbond simple fibre pull-out test plot after 2 days (48hrs) of hydrothermal treatment at a temperature of 60°C.

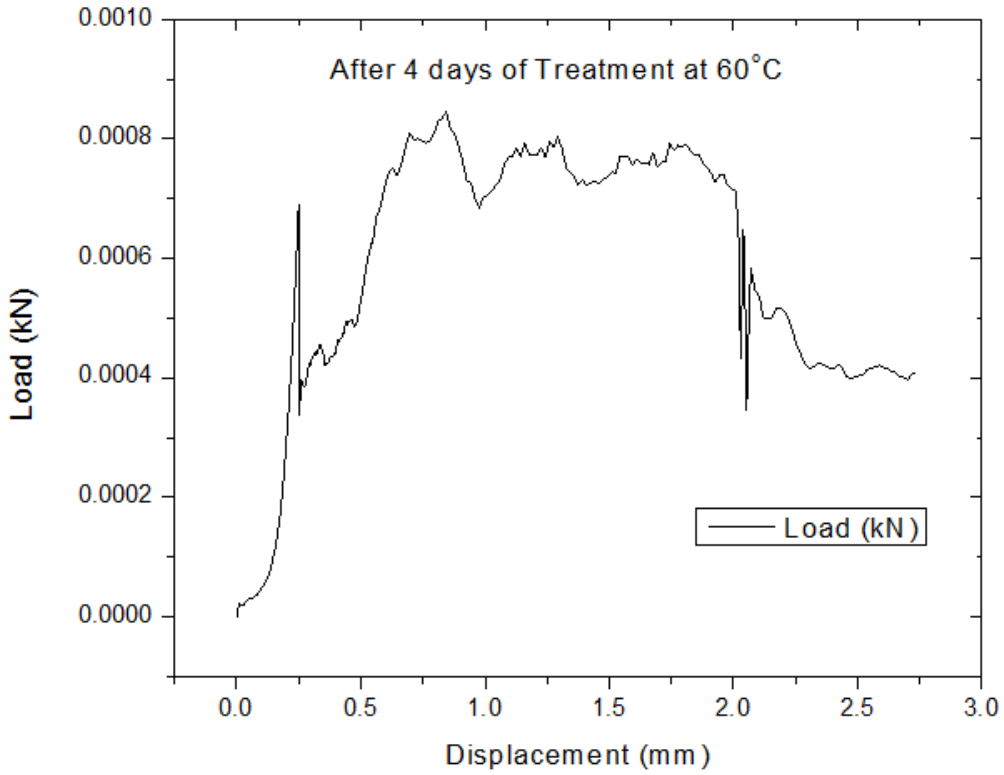

Figure 4.45: Microbond simple fibre pull-out test plot after 4 days (96hrs) of hydrothermal treatment at a temperature of 60°C.

The fibre diameters and microbond embedded lengths of each pull-out test specimen were measured prior to conducting of each destructive test. The shear debonding loads determined from the microbond pullout tests were then plotted against their corresponding interfacial embedded area for each particular fibre/matrix microbond system.

A collection of results from several microbond pull-out tests are shown in scatter plots in Figure 4.46 through Figure 4.58 for the different ageing temperatures and exposure durations.

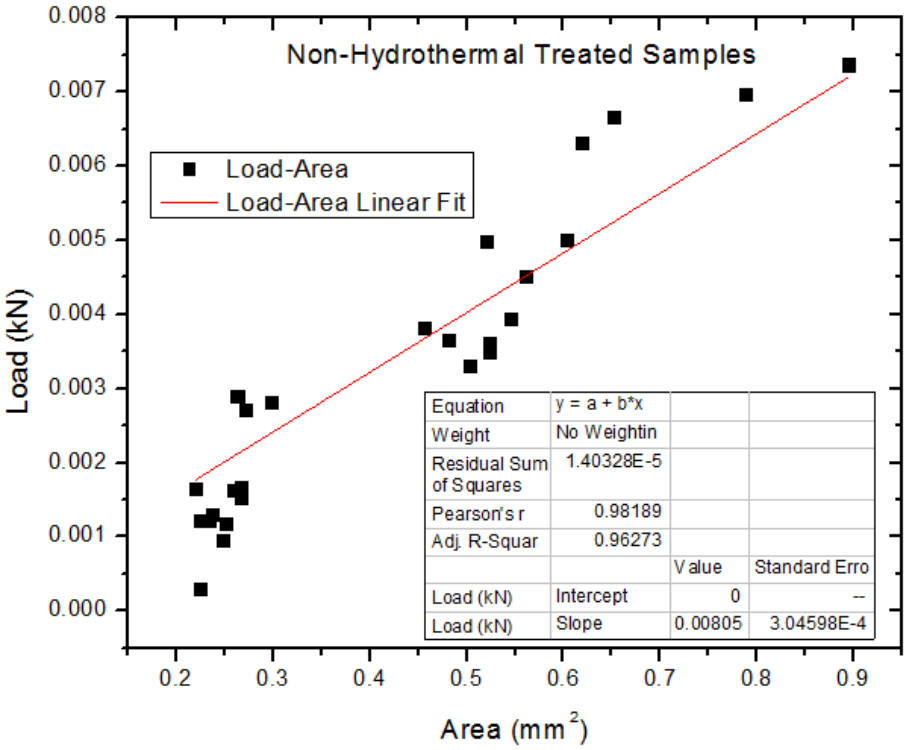

Figure 4.46: Microbond debonding load versus embedded area scatter plot for untreated polyester resin droplet/single sisal fibre composite system.

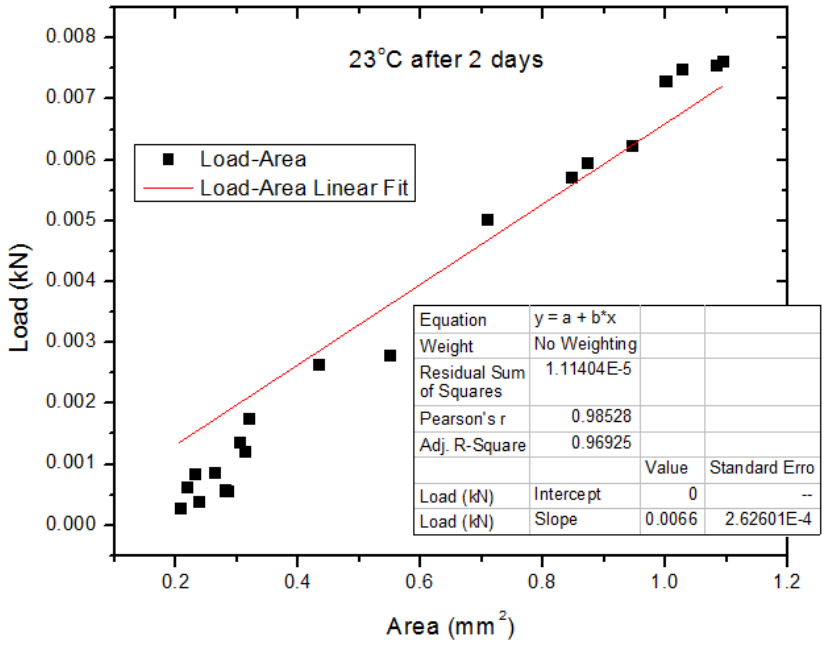

Figure 4.47: Microbond debonding load versus embedded area scatter plot for hydrothermally treated polyester resin droplet/single sisal fibre composite system at temperature of 23°C for a period of 2 days (48hrs).

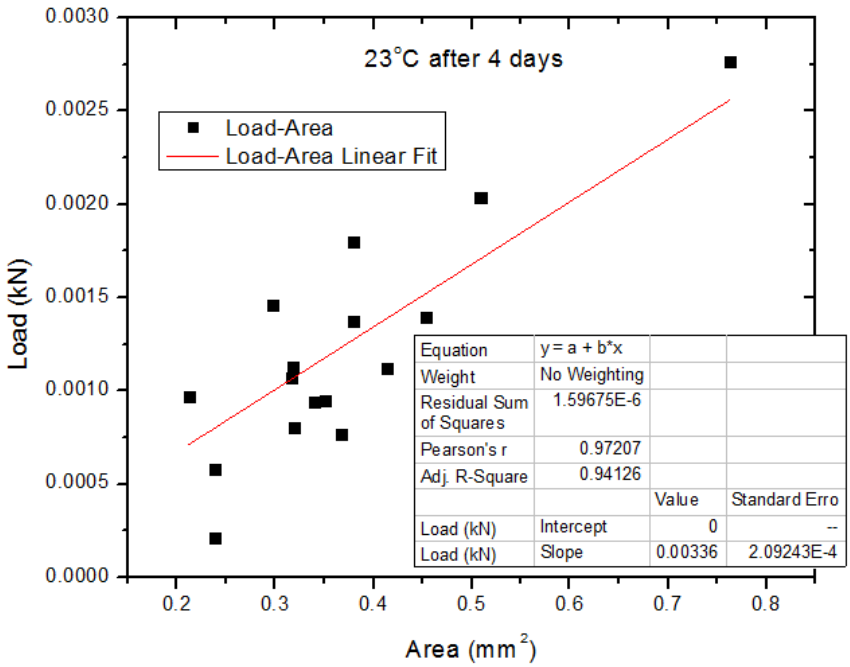

Figure 4.48: Microbond debonding load versus embedded area scatter plot for hydrothermally treated polyester resin droplet/single sisal fibre composite system at temperature of 23°C for a period of 4 days (96hrs).

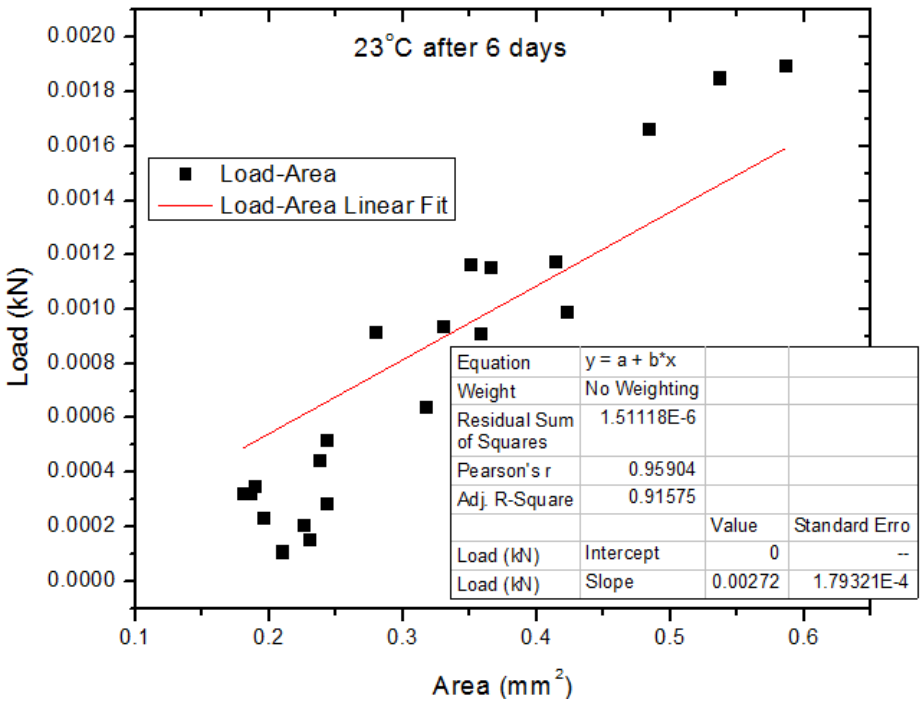

Figure 4.49: Microbond debonding load versus embedded area scatter plot for hydrothermally treated polyester resin droplet/single sisal fibre composite system at temperature of 23°C for a period of 6 days (144hrs).

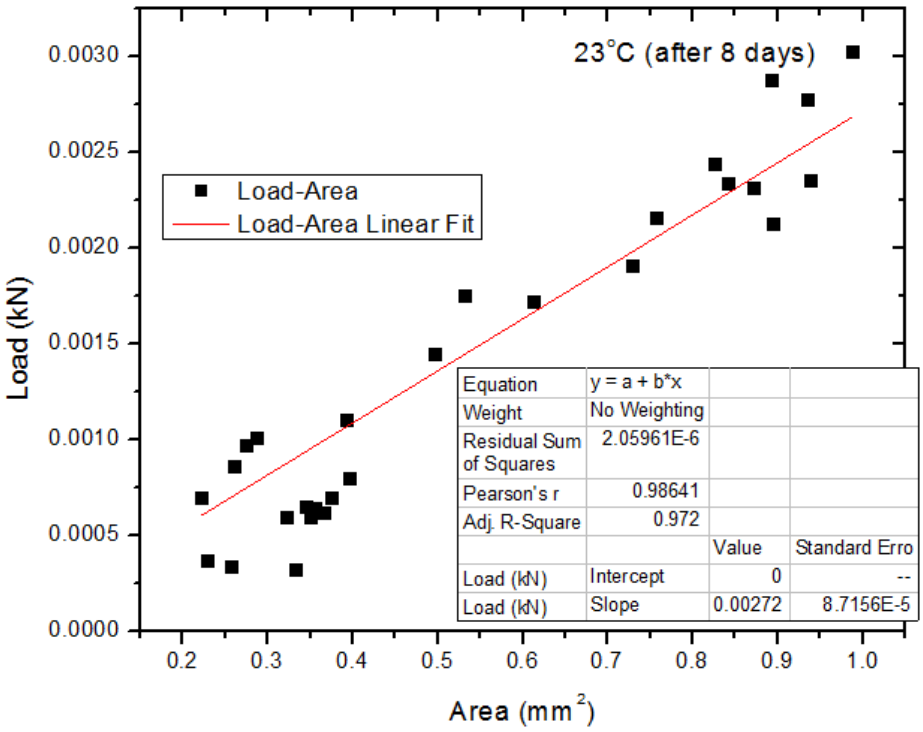

Figure 4.50: Microbond debonding load versus embedded area scatter plot for hydrothermally treated polyester resin droplet/single sisal fibre composite system at temperature of 23°C for a period of 8 days (192hrs).

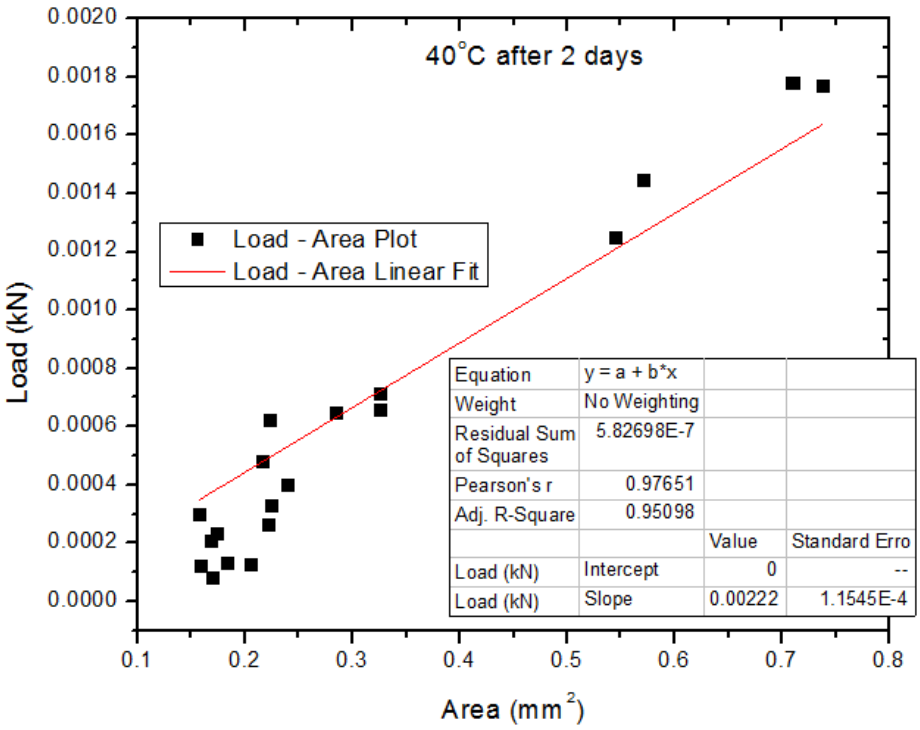

Figure 4.51: Microbond debonding load versus embedded area scatter plot for hydrothermally treated polyester resin droplet/single sisal fibre composite system at temperature of 40°C for a period of 2 days (48hrs).

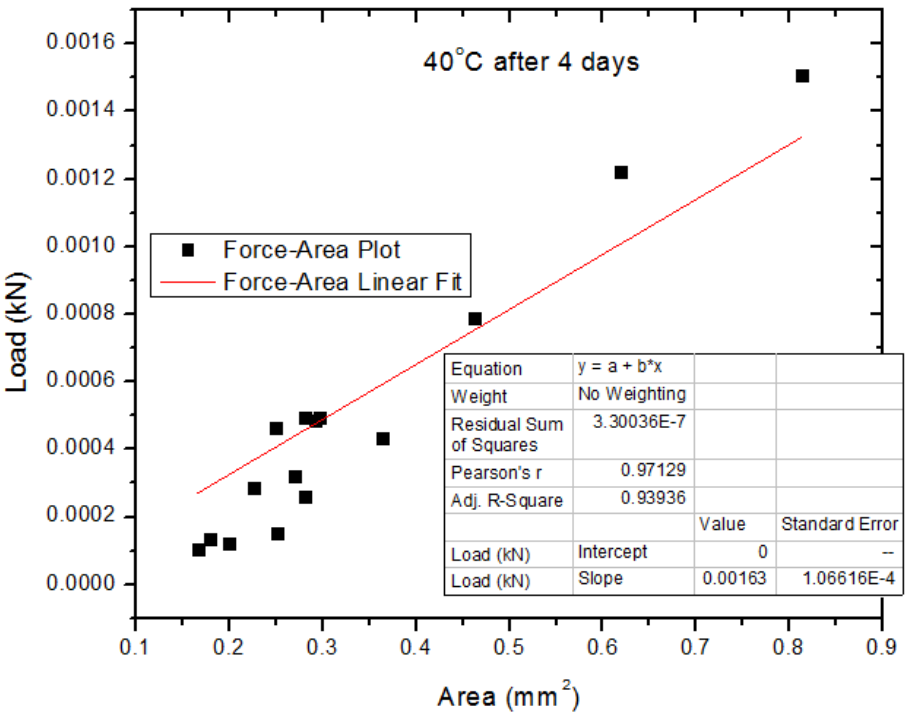

Figure 4.52: Microbond debonding load versus embedded area scatter plot for hydrothermally treated polyester resin droplet/single sisal fibre composite system at temperature of 40°C for a period of 4 days (96hrs).

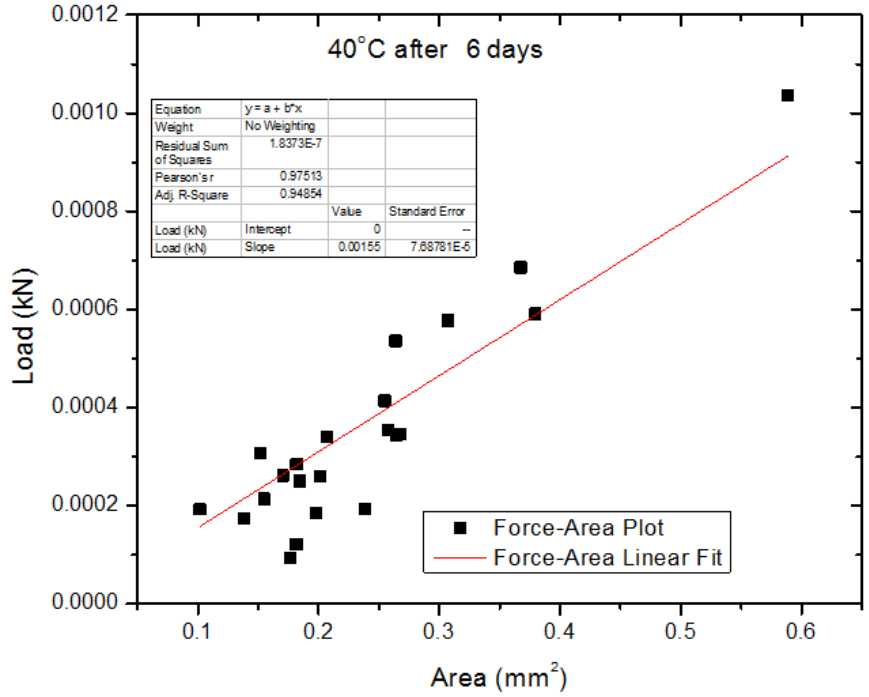

Figure 4.53: Microbond debonding load versus embedded area scatter plot for hydrothermally treated polyester resin droplet/single sisal fibre composite system at temperature of 40°C for a period of 6 days (144hrs).

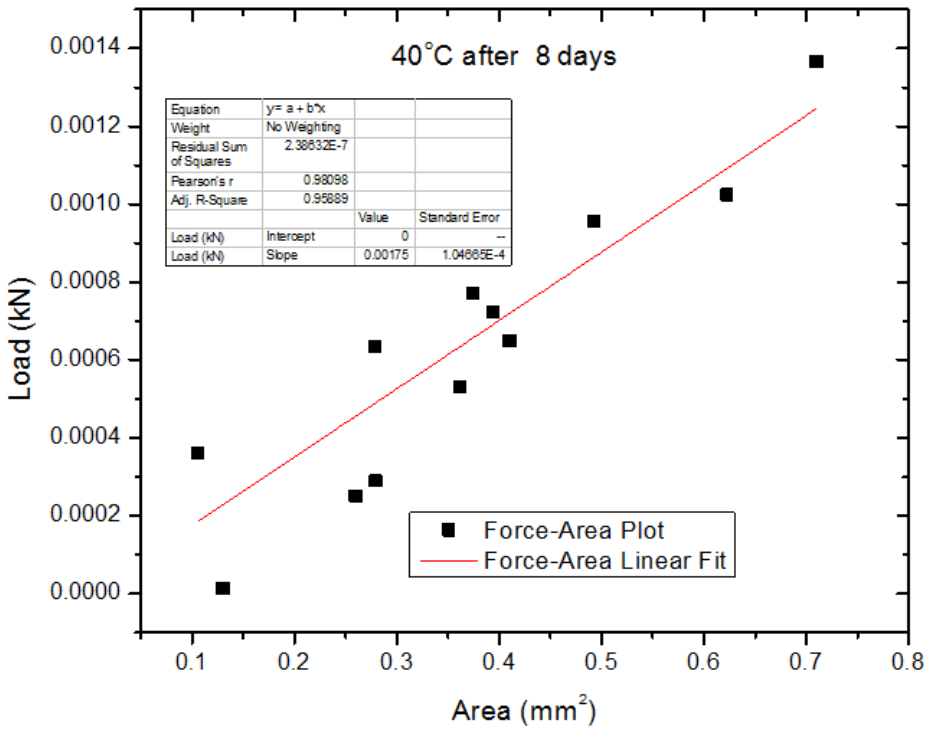

Figure 4.54: Microbond debonding load versus embedded area scatter plot for hydrothermally treated polyester resin droplet/single sisal fibre composite system at temperature of 40°C for a period of 8 days (192hrs).

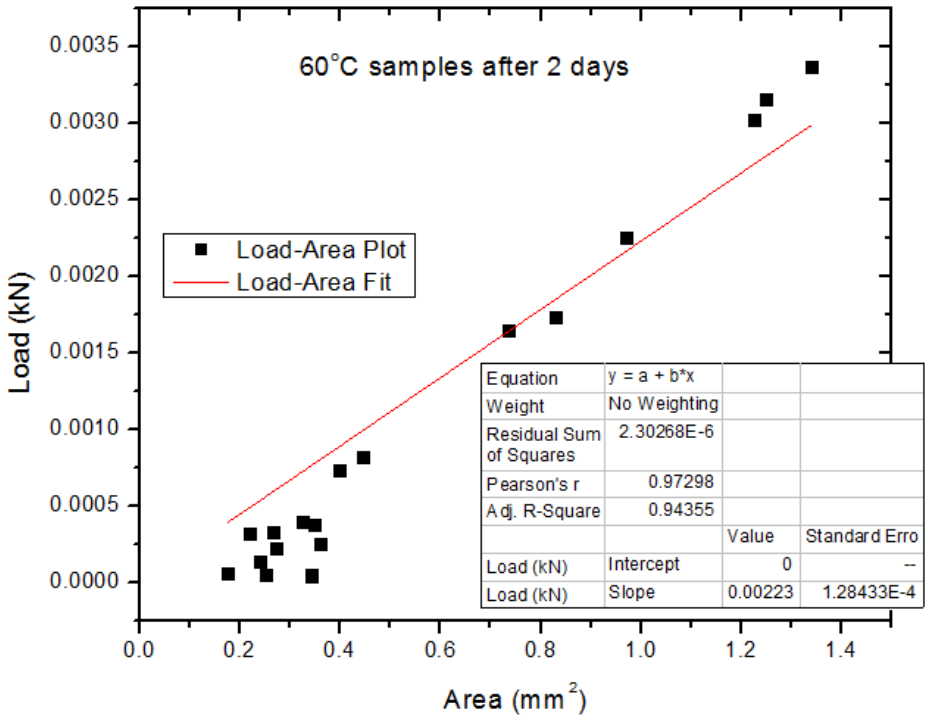

Figure 4.55: Microbond debonding load versus embedded area scatter plot for hydrothermally treated polyester resin droplet/single sisal fibre composite system at temperature of 60°C for a period of 2 days (48hrs).

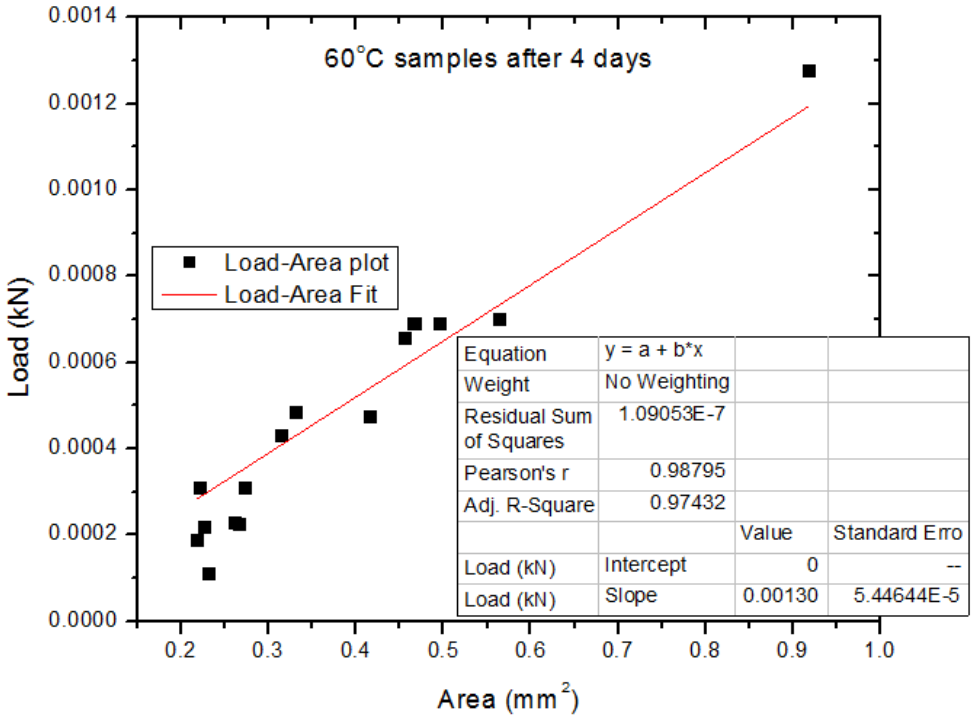

Figure 4.56: Microbond debonding load versus embedded area scatter plot for hydrothermally treated polyester resin droplet/single sisal fibre composite system at temperature of 60°C for a period of 4 days (96hrs).

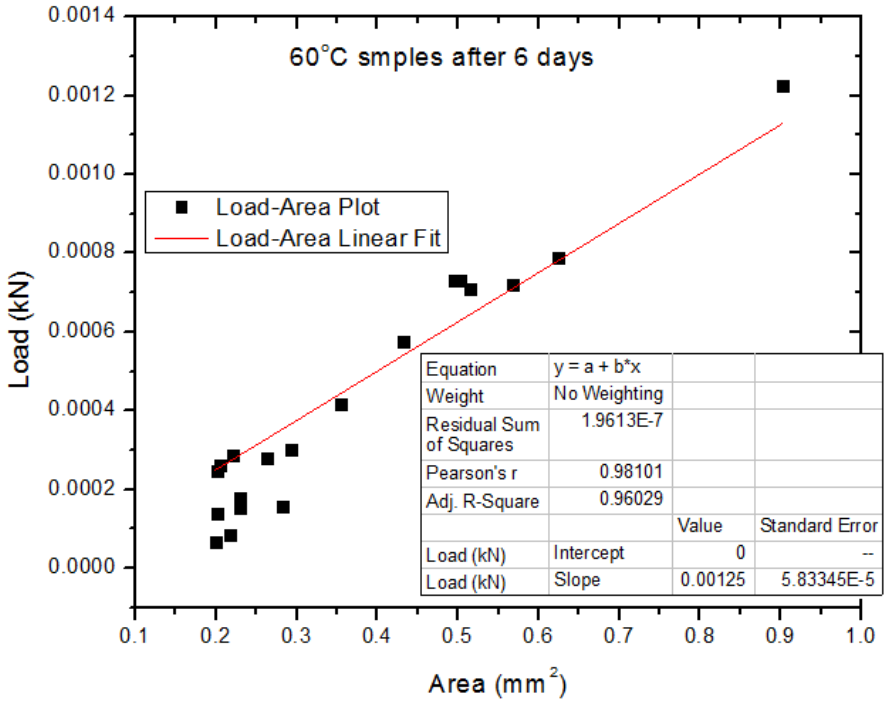

Figure 4.57: Microbond debonding load versus embedded area scatter plot for hydrothermally treated polyester resin droplet/single sisal fibre composite system at temperature of 60°C for a period of 6 days (144hrs).

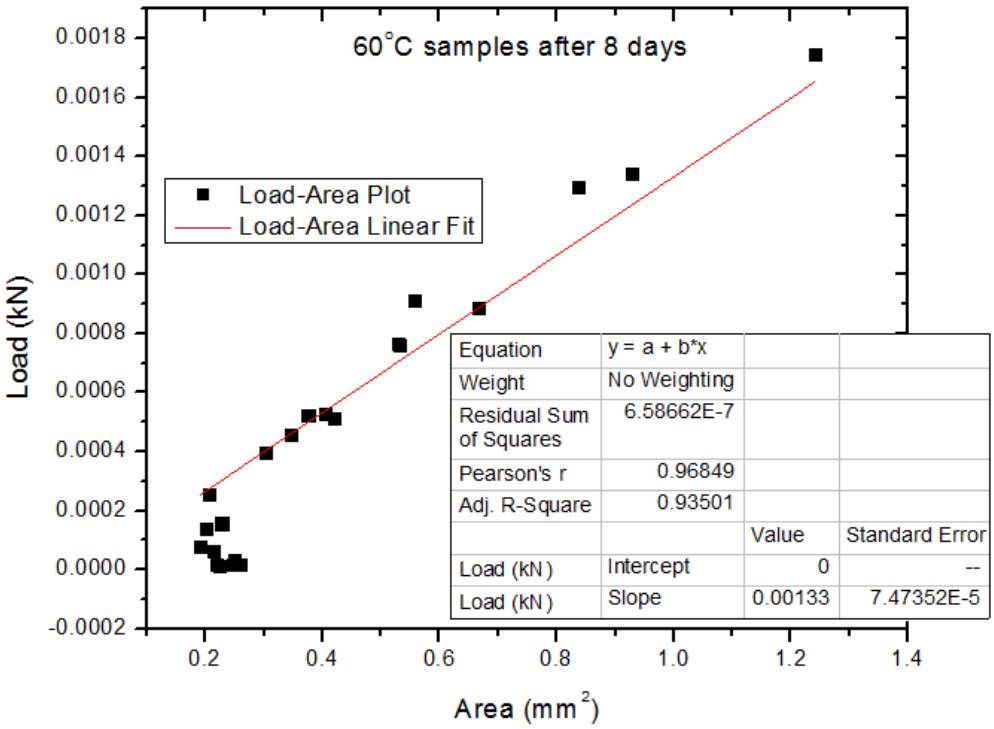

Figure 4.58: Microbond debonding load versus embedded area scatter plot for hydrothermally treated polyester resin droplet/single sisal fibre composite system at temperature of 60°C for a period of 8 days (192hrs).

Table 4.11 shows the average resultant microbond strength data for samples hydrothermally treated at respective temperatures of 23°C, 40°C and 60°C at 5 regular intervals over a total period of 8 days. A corresponding surface contour plot showing graphically the variation in the property is shown in Figure 4.59.

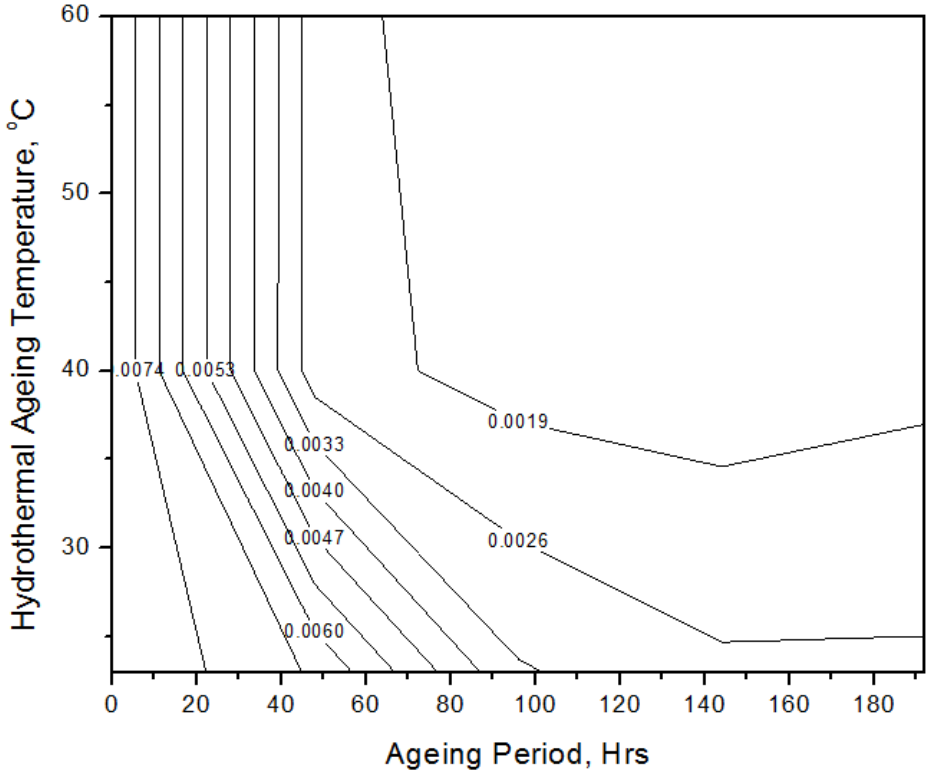

Figure 4.59: Resultant surface contour plot depicting changes in the interfacial shear strength of microbond sisal/polyester composite system test specimens with changes in the hydrothermally treated water temperature and conditioning period.

Table 4.11: Average values of microbond shear strength at different ageing temperatures and period.

Treatment Period (Hours)	Average Microbond Shear Strength (kN/mm^2)					
	23^oC		40^oC		60^oC	
	τ_{Int}	StdDev	τ_{Int}	StdDev	τ_{Int}	StdDev
0 (Untreated)	0.00805	3.0459E-4	0.00805	3.0459E-4	0.00805	3.0459E-4
48	0.0066	2.626E-4	0.00222	1.154E-4	0.00223	1.2843E-4
96	0.00336	2.0923E-4	0.00163	1.06616E-4	0.001301	5.4464E-5
144	0.00272	1.7932E-4	0.00155	7.6878E-5	0.00125	5.83345E-5
192	0.00272	8.7156E-5	0.00175	1.0466E-4	0.00133	7.4735E-5

Figure 4.60 shows combined plots of drops shear bond strength for single fibre microbond tests after specimen were hydrothermally treated at respective temperatures of 23^{o}C, 40^{o}C and 60^{o}C for a maximum period of 8 days. Polynomial functions listed in Table 4.12 were applied to fit the plotted curves. The drops in the shear strengths appear to be steep in the beginning of observation for all the three ageing conditions.

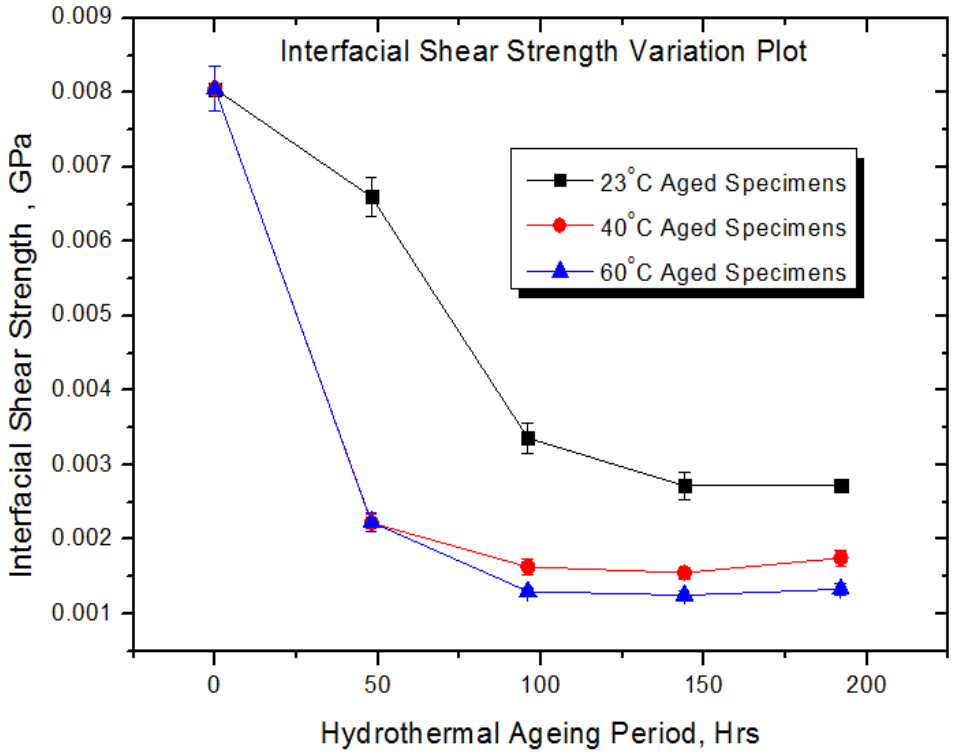

Figure 4.60: Plots of variations of microbond shear strength for hydrothermally aged single fibre micro composite specimens treated at 23^{o}C, 40^{o}C, and 60^{o}C, over a maximum period of 8days (192 hours).

Table 4.12: Values of microbond shear strength and polynomial curve fitting functions for hydrothermally aged single fibre micro composite specimens treated at 23°C, 40°C and 60°C over a maximum period of 8 days (192 hours).

Resultant Interfacial Shear Strength Values (GPa)							
Temp (°C)	Ageing Periods (hours)					Shear Strength Function	R^2
	0	48	96	144	192		
23	8.05E-03	6.60E-03	3.36E-03	2.72E-03	2.72E-03	$F(x) = 0.00823 - 3.8x10^{-5} x - 1.93x10^{-7}x^2 + 1.27x10^{-9}x^3$	0.892
40	8.05E-03	2.22E-03	1.63E-03	1.55E-03	1.75E-03	$F(x) = 0.0077 - 1.586x10^{-4} x + 1.273x10^{-6} x^{-4} - 3.154x10^{-9} x^3$	0.777
60	8.05E-03	2.23E-03	1.30E-03	1.25E-03	1.33E-03	$F(x) = 0.007 - 1.481x10^{-4} x + 1.119x10^{-6}x^2 - 2.684x10^{-9}x^3$	0.845

Where in the derived function x is the ageing period (in hours).

A corresponding model function is shown in equation (4.6) which describes the variation.

$$\tau_{Int} = 0.00179 - 0.00057\alpha_{Temp} - 0.00306\beta_{Time} - 0.00035\alpha_{Temp}\beta_{Time} + 0.00039\alpha_{Temp}^2 + 0.00295\beta_{Time}^2 \quad (4.6)$$

Where

τ_{Int} - Microbond Interfacial Strength, GPa.

α_{Temp} – Temperature based parameter which is equal to,

$$\alpha_{Temp} = \frac{T - 40}{20}$$

T – Ageing temperature, ^{o}C.

β_{Time} – Duration based parameter which is equal to,

$$\beta_{Time} = \frac{d - 96}{96}$$

d – Ageing duration, hours.

Following a regression analysis of the microbond pull-out tests results, a more comprehensive model description of the effects of temperatures and absorbed water on the microbond interfacial strength over time was developed. Figure 4.61 and Figure 4.61show a much clearer picture of the effect hydrothermal treatment has on the sisal reinforced polyester composite system, in the combined plots of the three resultant ageing environments and also a plot in the form of a 3-dimensional plot of the microbond strength as a function of ageing period and hydrothermal ageing temperature. This plot is based on a generated regression model of the experiment data. A corresponding model function is presented as in equation (4.6). A summary of results of the regression conducted is presented in APPENDIX F.

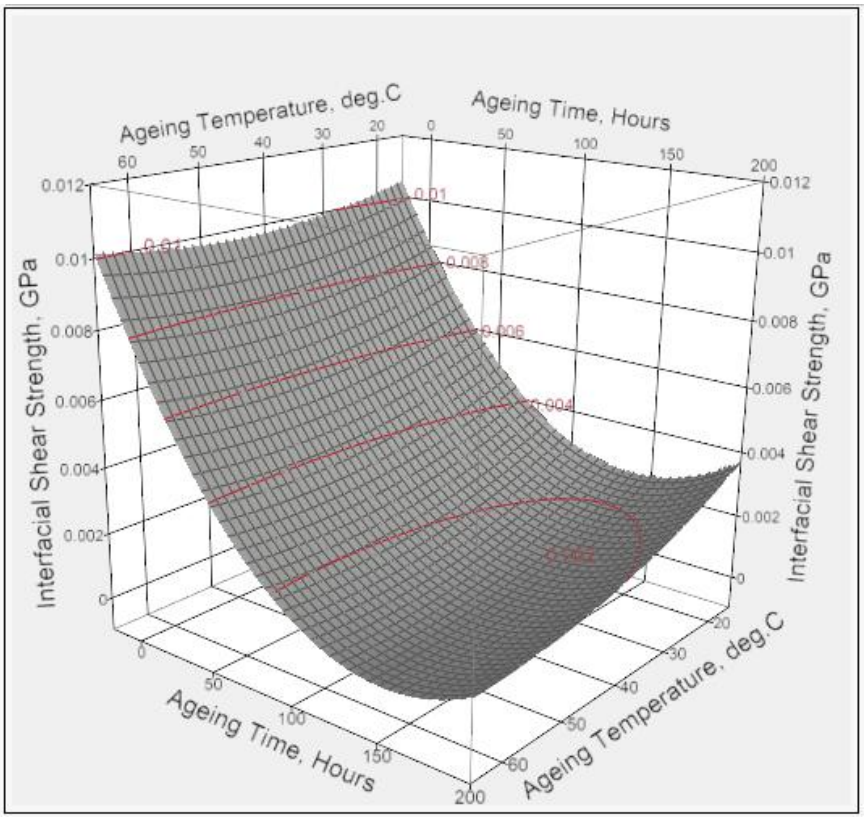

Figure 4.61: The fitted surface plot describing variations in microbond interfacial strength as a function of hydrothermal ageing temperature and treatment period based on the derived empirical model.

Figure 4.62 through Figure 4.64 show the relationship between water absorption and microbond interfacial strength with increasing exposure times for single sisal fibre/polyester microbond composite specimens hydrothermally treated at 23^{o}C, 40^{o}C and 60^{o}C respectively.

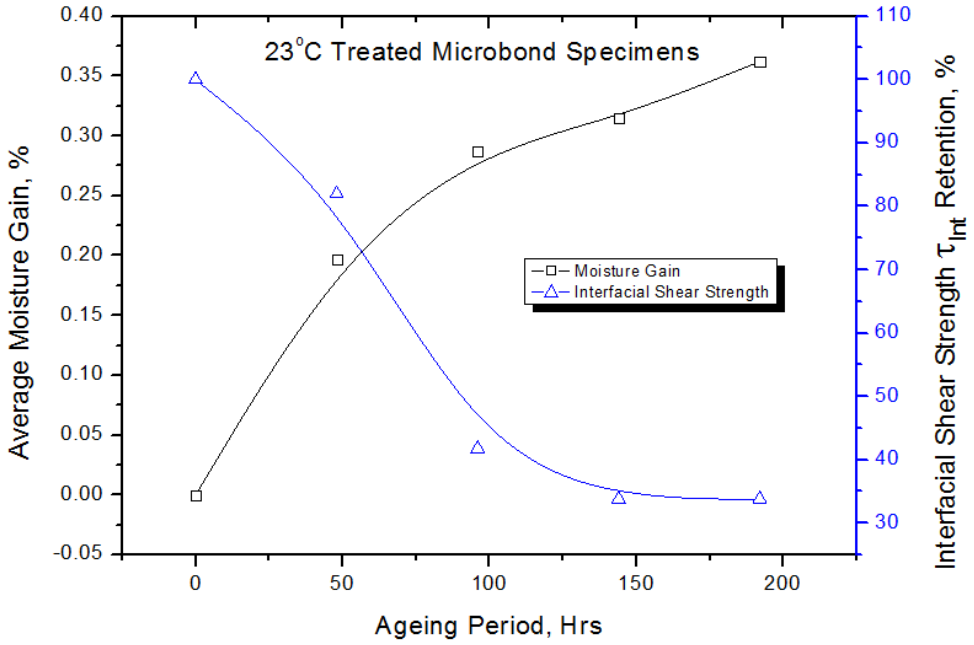

Figure 4.62: The relationship between water absorption and microbond interfacial strength with increasing exposure times for single sisal fibre - polyester micro composite specimens hydrothermally treated at 23°C.

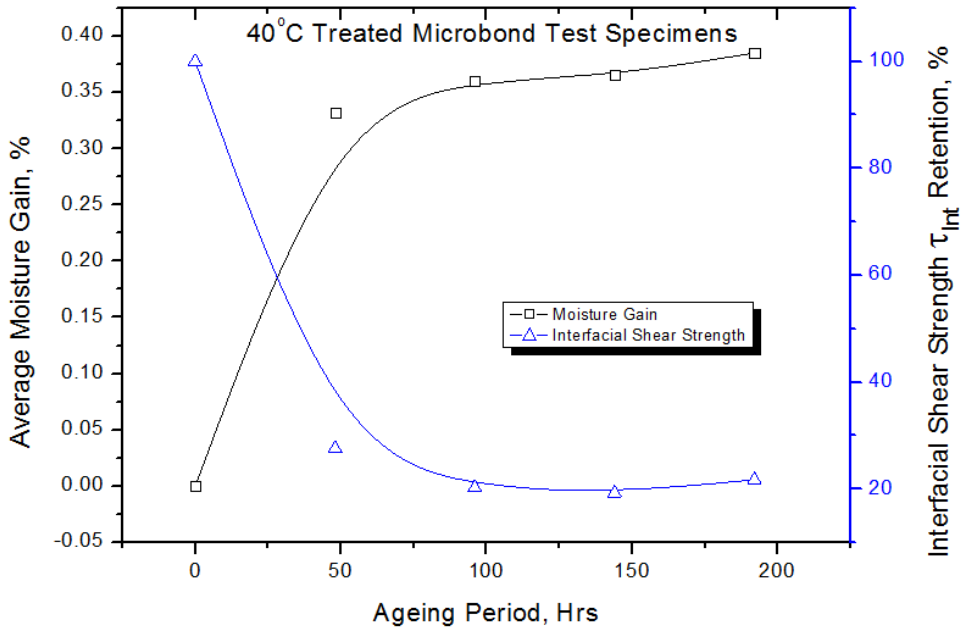

Figure 4.63: The relationship between water absorption and microbond interfacial strength with increasing exposure times for single sisal fibre - polyester micro composite specimens hydrothermally treated at 40°C.

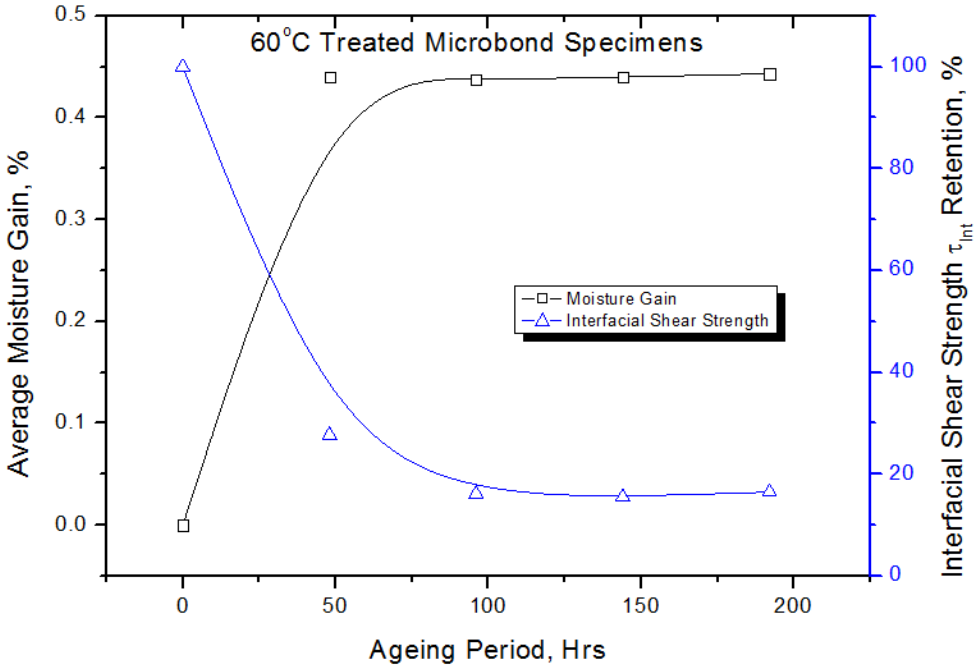

Figure 4.64: The relationship between water absorption and microbond interfacial strength with increasing exposure times for single sisal fibre - polyester micro composite specimens hydrothermally treated at 60°C.

For each hydrothermal treatment, microbond pulled-out specimen fibres were further examined on a NeoScope JCM 5000 Scanning Electron Microscope (SEM) for presence of residual polyester matrix crystal on the fibre surface after debonding. Resultant SEM images are shown in Figure 4.65(More images are in Appendix G).

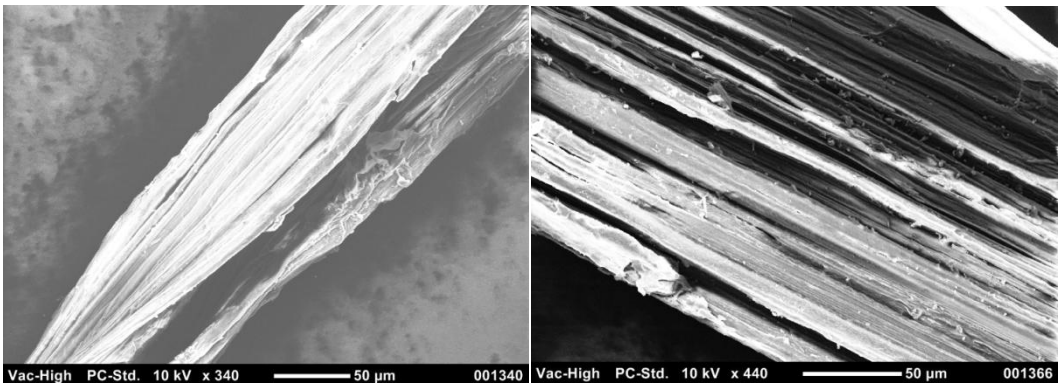

(a) (b)

Figure 4.65: Scanning Microscopic images of the surfaces of a sisal fibre following interfacial debonding of sisal/polyester microbond composite systems (a) untreated treated; (b) hydrothermally treated at temperature of 23°C for a period of two days.

4.5.2 Macro Composite Fracture

The following is a presentation of results and analyses of experimental tests on fracture toughness.

A sample result plot obtained from a single fracture toughness test is shown in Figure 4.66. (See Appendix H for plots of all fracture toughness tests result. Appendix I further provides a summary of both attained maximum force, P_{max} during fracture tests and resultant fracture toughness, K_{TL}, for all test conducted).

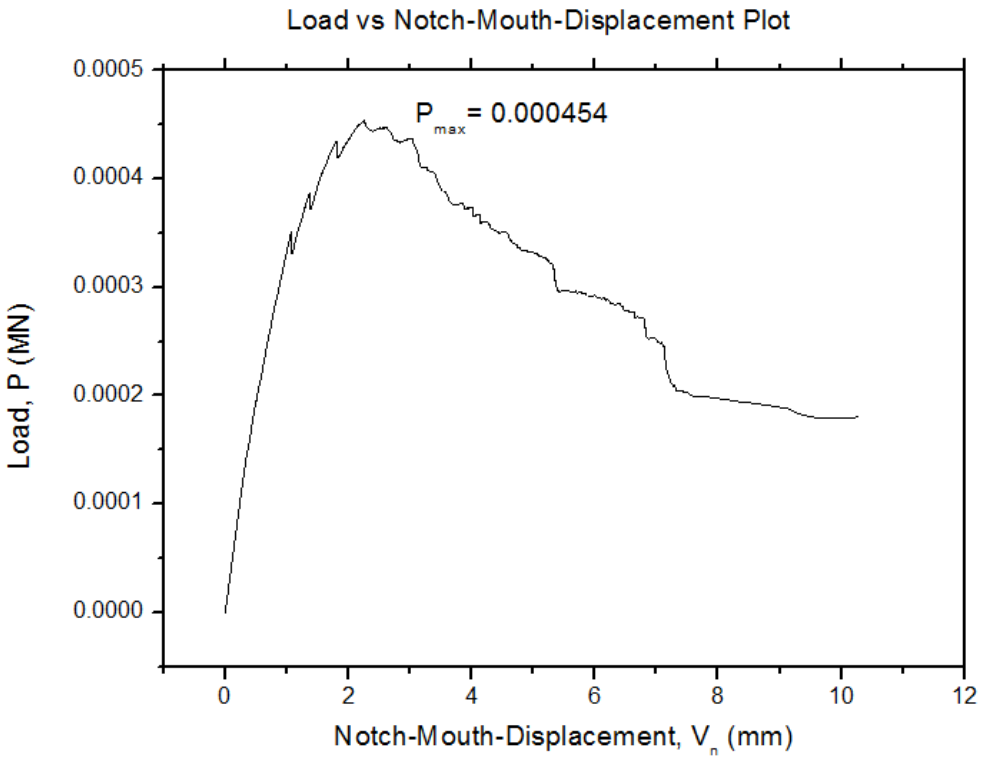

Figure 4.66: A sample Load vs. Notch-mouth displacement plot of a translaminar fracture toughness test.

A summary of results obtained from all fracture toughness experiments is given in Table 4.13.

Table 4.13: Summarised fracture toughness experimental results of hydrothermally treated sisal fibre reinforced polyester composite.

Time (Days)	Fracture Toughness ($MPa.m^{1/2}$)					
	23°C		40°C		60°C	
	K_{TL} ($MPa.m^{1/2}$)	StdDev ($MPa.m^{1/2}$)	K_{TL} ($MPa.m^{1/2}$)	StdDev ($MPa.m^{1/2}$)	K_{TL} ($MPa.m^{1/2}$)	StdDev ($MPa.m^{1/2}$)
0 (Untreated)	6.265	0.9171	6.265	0.9171	6.265	0.9171
30	4.717	1.1492	5.23	0.4706	3.82	0.0565
60	4.167	0.8154	3.962	0.5116	3.456	0.2050
90	4.397	0.6147	4.122	0.8501	2.987	0.2615
120	4.247	0.1347	3.785	0.4872	3.341	0.3885

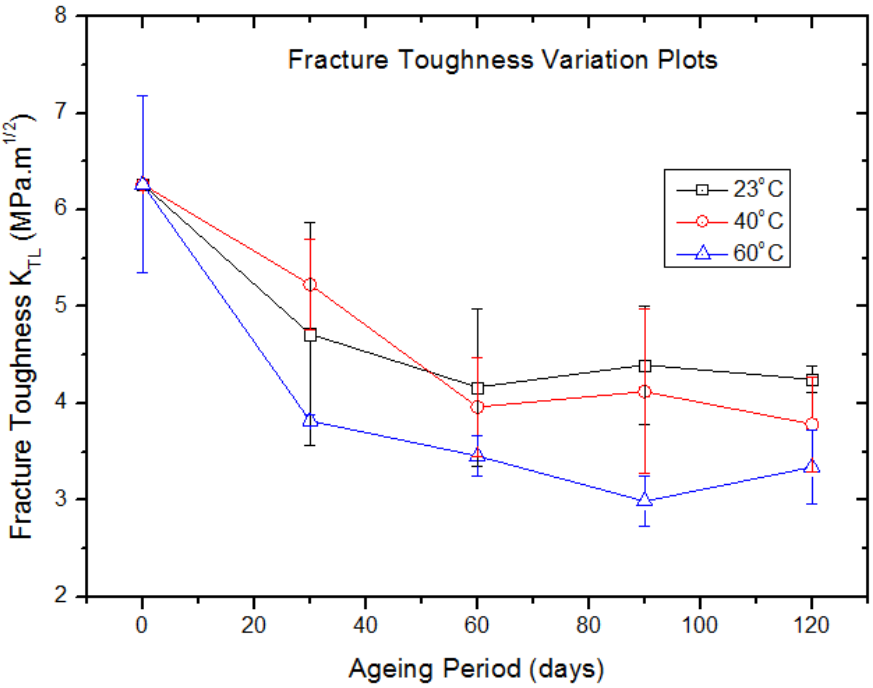

Figure 4.67: Variation of fracture toughness with ageing period for hydrothermally treated sisal fibre reinforced polyester composite specimens.

Figure 4.67 shows fracture toughness plots of hydrothermally treated sisal fibre reinforced polyester composite specimens at different temperatures. Figure 4.68 through Figure 4.70 show plots of the variation of the fracture toughness at respective temperatures of 23^{o}C, 40^{o}C and 60^{o}C, with changes in the amount of absorbed moisture by the same composite.

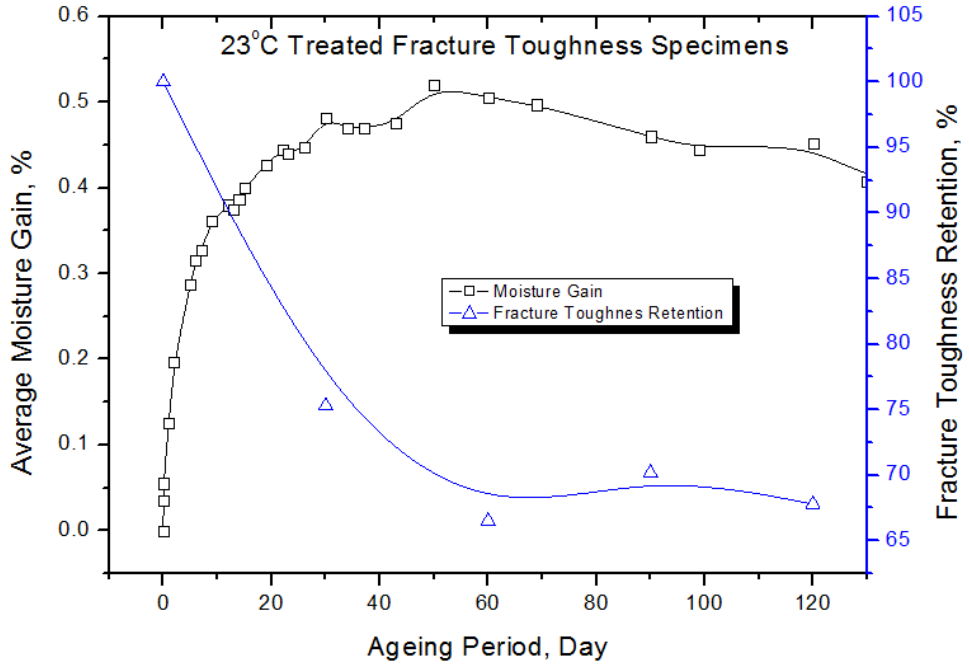

Figure 4.68: The relationship between water absorption and fracture toughness with increasing exposure times for sisal fibre reinforced polyester composite specimens hydrothermally treated at 23°C.

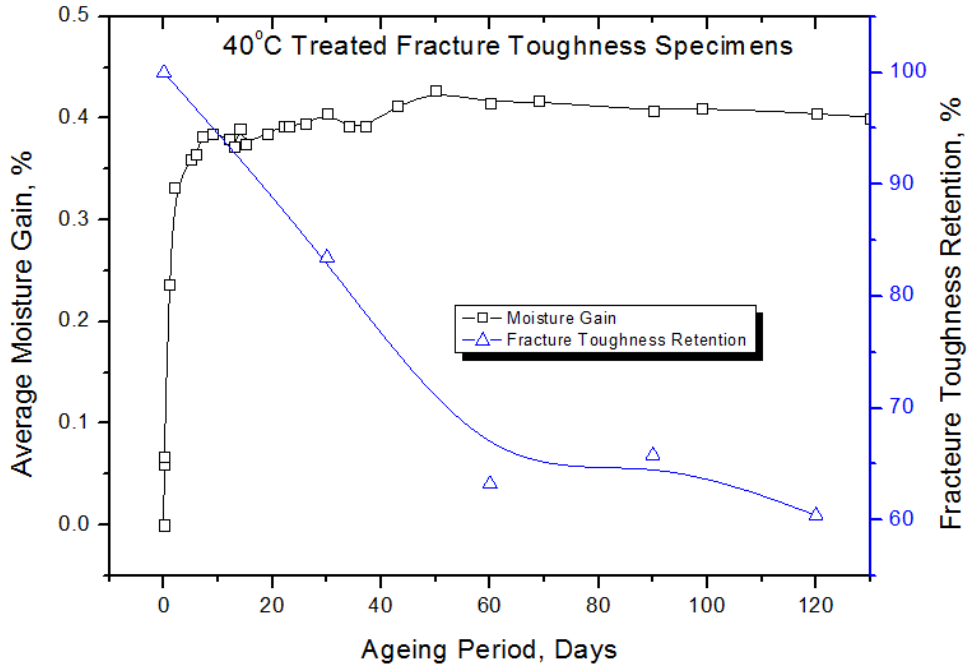

Figure 4.69: The relationship between water absorption and fracture toughness with increasing exposure times for sisal fibre reinforced polyester composite specimens hydrothermally treated at 40°C.

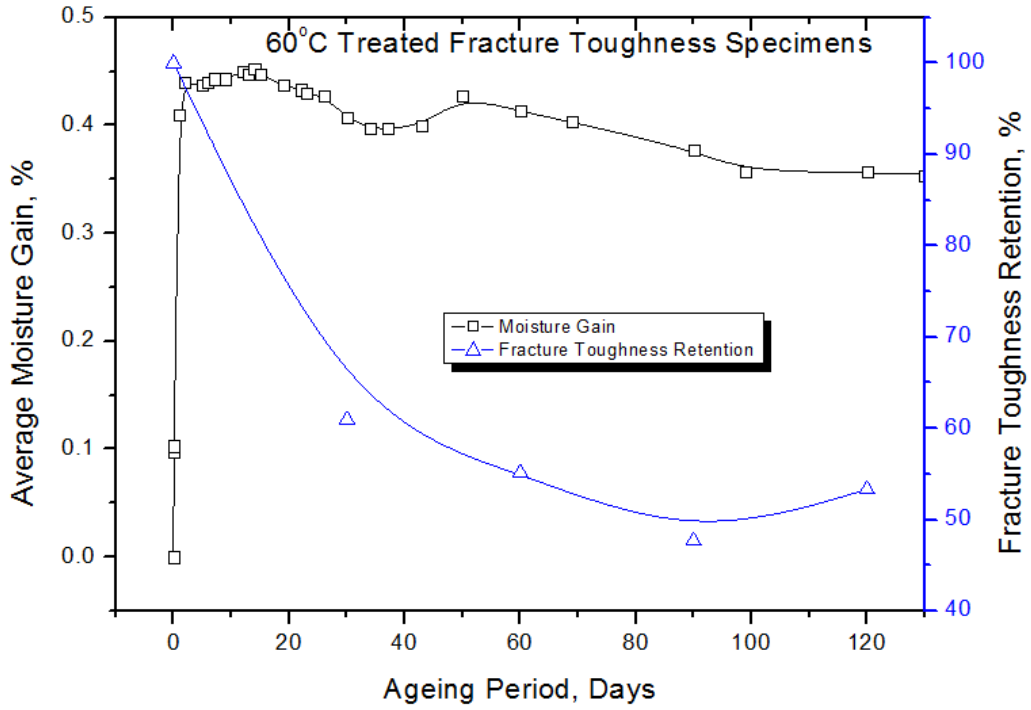

Figure 4.70: The relationship between water absorption and fracture toughness with increasing exposure times for sisal fibre reinforced polyester composite specimens hydrothermally treated at 60°C.

But for a more comprehensive description of effects intermediate temperatures pose on the fracture toughness, refer to Figure 4.71 depicting a contour plot based on experiment values of the fracture toughness as a function of ageing period and hydrothermal ageing temperature.

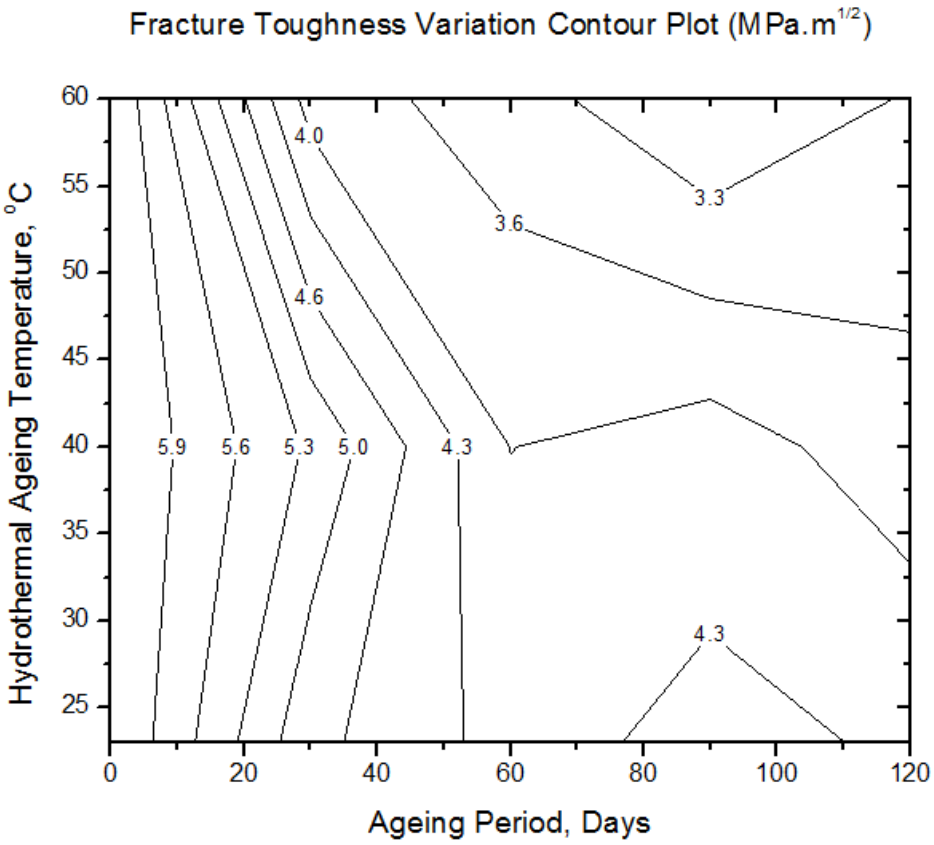

Figure 4.71: Contour plot describing variations in the fracture toughness as a function of hydrothermal ageing temperature and treatment period based on the experiment values.

4.5.3 Fracture Toughness Predictive Modelling

This sub-section presents results obtained from empirical and theoretical modelling of the fracture toughness of the sisal fibre reinforced polyester composite. Furthermore, a comparison of empirical and theoretical model predicted values with those of experimentally obtained fracture toughness is presented.

4.5.3.1 Empirical Model

JMP8 statistical analysis software was used to conduct regression analysis and analysis of variance of the fracture toughness. A corresponding empirical predictive model function was further developed using the Response Surface Methodology (RSM) Centre Composite Design (CCD) and is shown in equation (4.7). This model describes comprehensively, for a given pre-hydrothermal ageing composite specimen tensile strength, the relationship the fracture toughness and hydrothermal ageing conditions (ageing temperature and ageing period), taking into account intermediate

values. Its resultant fitted surface plot is shown in Figure 4.72 for clarity bringing out the general trends between cause and effect based on this very model. Refer to Appendix J for details of the regression and analysis of variance.

$K_{TL} = 0.087\sigma_{TS_o} - 0.27\alpha_{Temp} - 1.24\beta_{Time} - 0.23\alpha_{Temp}\beta_{Time} - 0.061\alpha_{Temp}^2 + 1.15\beta_{Time}^2$, MPa.m$^{1/2}$

(4.7)

Where α_{Temp} – Temperature based parameter which is equal to

$$\alpha_{Temp} = \frac{AgeingTemperature - 40}{20}$$

Ageing temperature, ^{o}C.

β_{Time} – Time based parameter which is equal to

$$\beta_{Time} = \frac{AgeingTime - 60}{60}$$

Ageing time, days.

σ_{TSo} – Pre-ageing tensile strength of the composite in MPa.

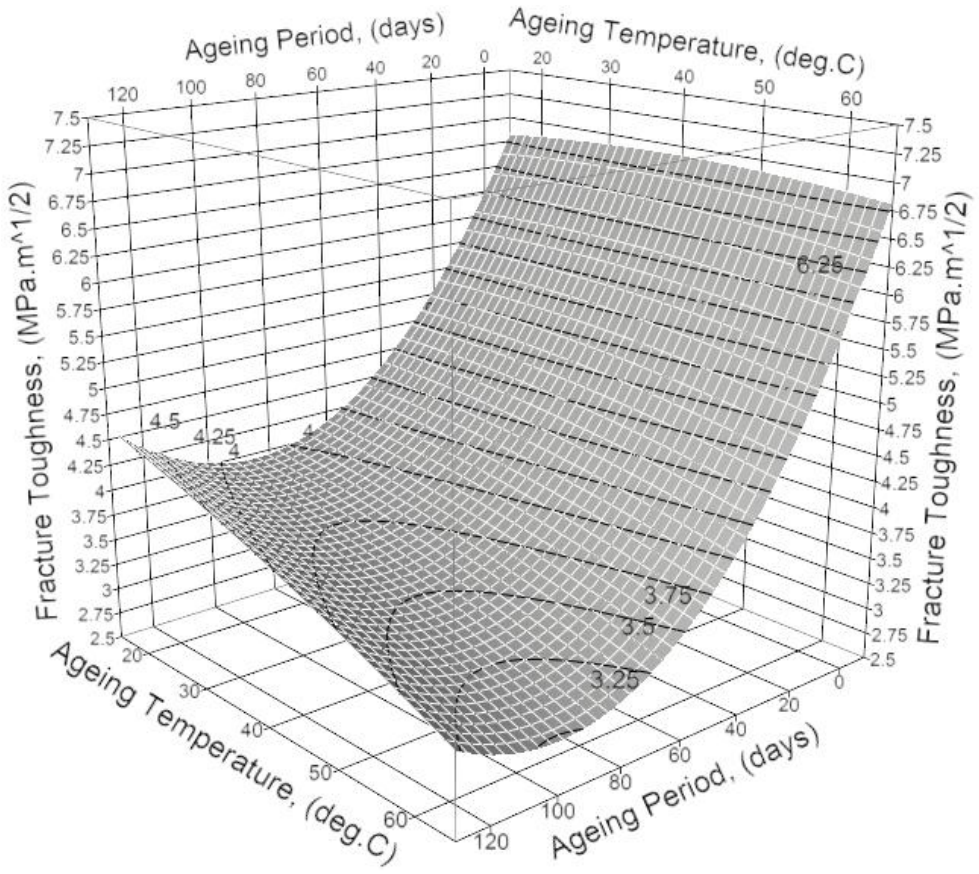

Figure 4.72: The fitted surface plot describing variations in fracture toughness as a function of hydrothermal ageing temperature and treatment period based on the model.

As recommended by ASTM D 5510 – 94 Standard, the F statistic for 95% confidence was used to determine significance of the model. The significance of F value (in Appendix J) shows that there is only less that 1% chance that the regression output was merely a chance occurrence. In other words, this means that there is over 99% confidence in the ability of the model to explain the dependent variable (observed response).

Predicted values based on the model equation (4.7) were applied to the data obtained experimentally for the three hydrothermal ageing conditions and presented in order to have an estimate of the effective predictive capability of the model. A comparison between empirical model predicted fracture toughness values and experimentally obtained values is shown in Table 4.14 for the three hydrothermal ageing environments.

Table 4.14: Predicted values of the fracture toughness in comparison with experimentally obtained values.

Time (days)	23°C			40°C			60°C		
	Pred. Values ($MPa.m^{1/2}$)	Exp. Values ($MPa.m^{1/2}$)	% Variance	Pred. Values ($MPa.m^{1/2}$)	Exp. Values ($MPa.m^{1/2}$)	% Variance	Pred. Values ($MPa.m^{1/2}$)	Exp. Values ($MPa.m^{1/2}$)	% Variance
0	6.308	6.265	0.681	6.316	6.265	0.807	6.211	6.265	-0.869
30	4.923	4.717	4.184	4.835	5.23	-8.169	4.617	3.82	17.262
60	4.113	4.167	-1.312	3.929	3.962	-0.852	3.598	3.456	3.922
90	3.878	4.397	-13.383	3.598	4.122	-14.56	3.154	2.987	5.279
120	4.218	4.247	-0.687	3.842	3.785	1.4836	3.285	3.341	-1.71
Mean			-2.103			-4.258			4.779
StdDev			6.655			6.923			7.595

Figure 4.73 through Figure 4.75 graphically show these comparisons between experimental and predicted fracture toughness values for specimens accelerated aged in distilled water at 23°C, 40°C and 60°C respectively.

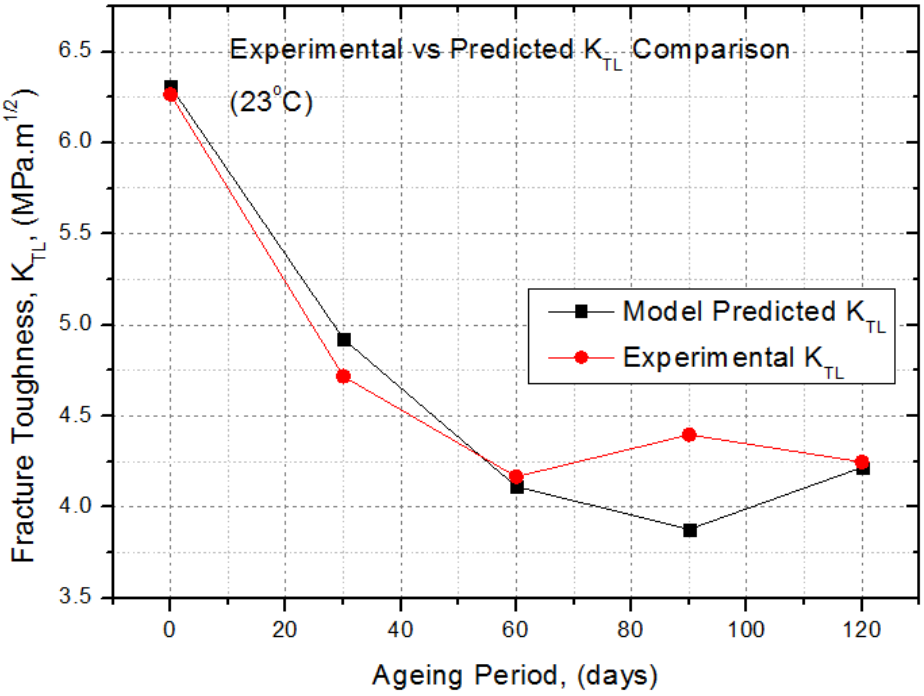

Figure 4.73: Comparison between experimental and predicted values of fracture toughness values for specimens that were accelerated aged in distilled water at 23°C.

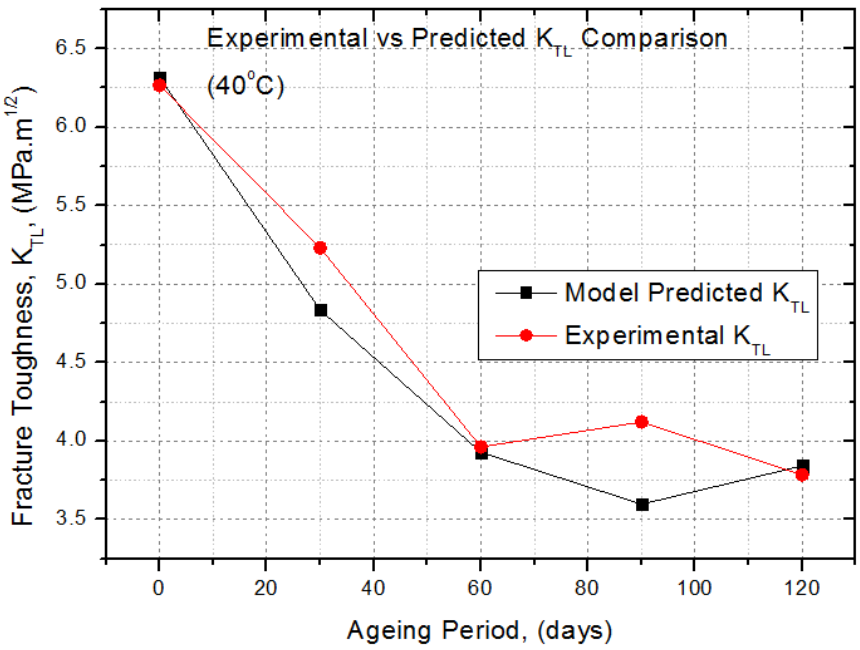

Figure 4.74: Comparison between experimental and predicted values of fracture toughness values for specimens that were accelerated aged in distilled water at 40°C.

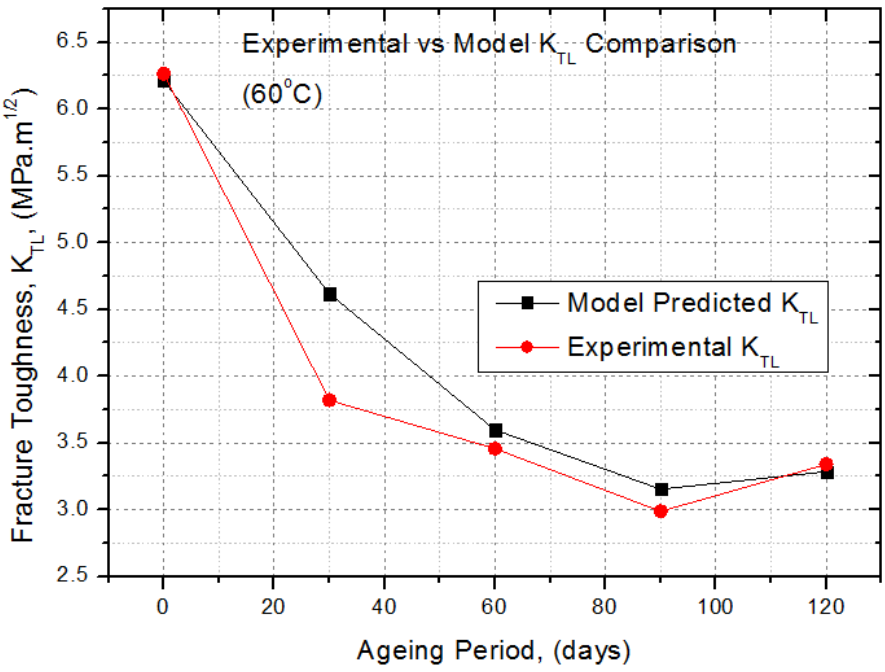

Figure 4.75: Comparison between experimental and predicted values of fracture toughness values for specimens that were accelerated aged in distilled water at 60°C.

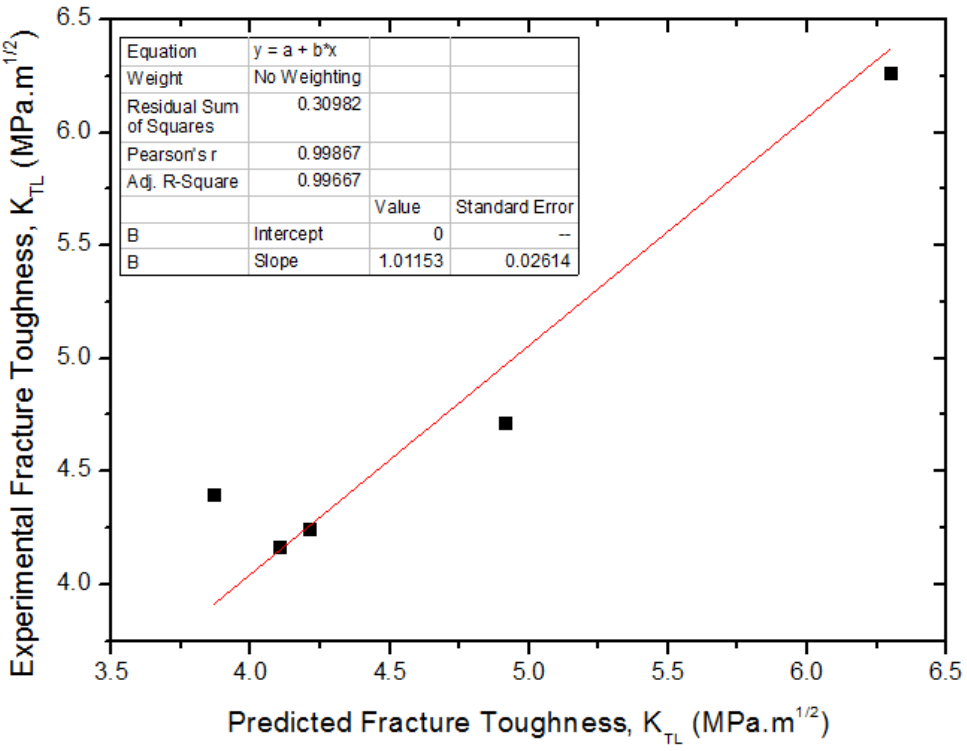

Figure 4.76: Scatter plot of average experimental versus predicted values of fracture toughness values for specimens that were accelerated treated in distilled water at 23^{o}C.

In Figure 4.76 through Figure 4.78, the model is further validated by plotting scatter plots of observed values against predicted ones for the different ageing environments.

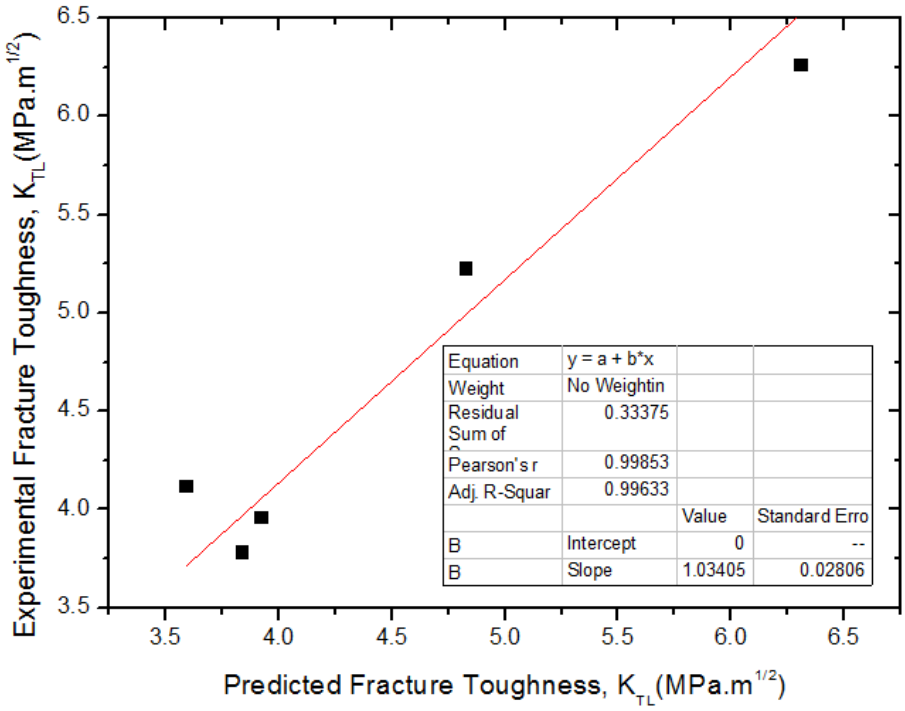

Figure 4.77: Scatter plot of average experimental versus predicted values of fracture toughness values for specimens that were accelerated treated in distilled water at 40^{o}C.

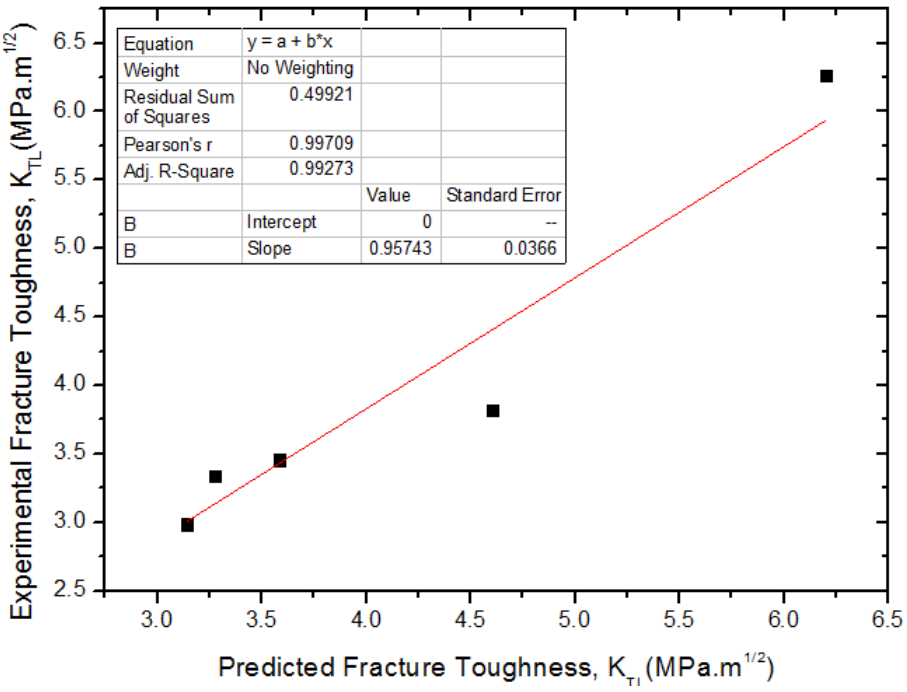

Figure 4.78: Scatter plot of average experimental versus predicted values of fracture toughness values for specimens that were accelerated treated in distilled water at 60^{o}C.

4.5.3.2 Theoretical Model

This sub section presents the practical implementation of the Arrhenius Life-Stress analysis procedure explained in Section 2.1.2.1 in the generation of the theoretical model. This is for the purpose of making long-term predictions of the durability of the composite with the help of values of facture toughness determined using the accelerated ageing model.

Table 4.15 shows model predicted ageing data of fracture toughness tests as determined by the model in equation (4.7). Details have already been presented in sub Section 4.5.3.1. The corresponding percentage retention of the fracture toughness by the composite throughout the 120 days of accelerated ageing at respective temperature of 23^{o}C, 40^{o}C and 60^{o}C are presented in Figure 4.79. It was assumed that post curing effects on the composite specimens during this ageing period were at minimum as they were dominated over by the ageing deterioration and as such were neglected in the calculation of percentage retention of the fracture toughness.

Table 4.15: Results of model determined fracture toughness of hydrothermally treated sisal fibre reinforced polyester composite.

Period		23^{o}C		40^{o}C		60^{o}C	
Time, Days	ln(Time)	K_{TL}, MPa.m$^{1/2}$	% Retention	K_{TL}, MPa.m$^{1/2}$	% Retention	K_{TL}, MPa.m$^{1/2}$	% Retention
0	0	6.308	100	6.316	100	6.211	100
30	3.4012	4.923	78.044	4.835	76.552	4.617	74.336
60	4.0943	4.113	65.203	3.929	62.207	3.598	57.929
90	4.4998	3.878	61.477	3.598	56.966	3.154	50.781
120	4.7875	4.218	66.867	3.842	60.829	3.285	52.890

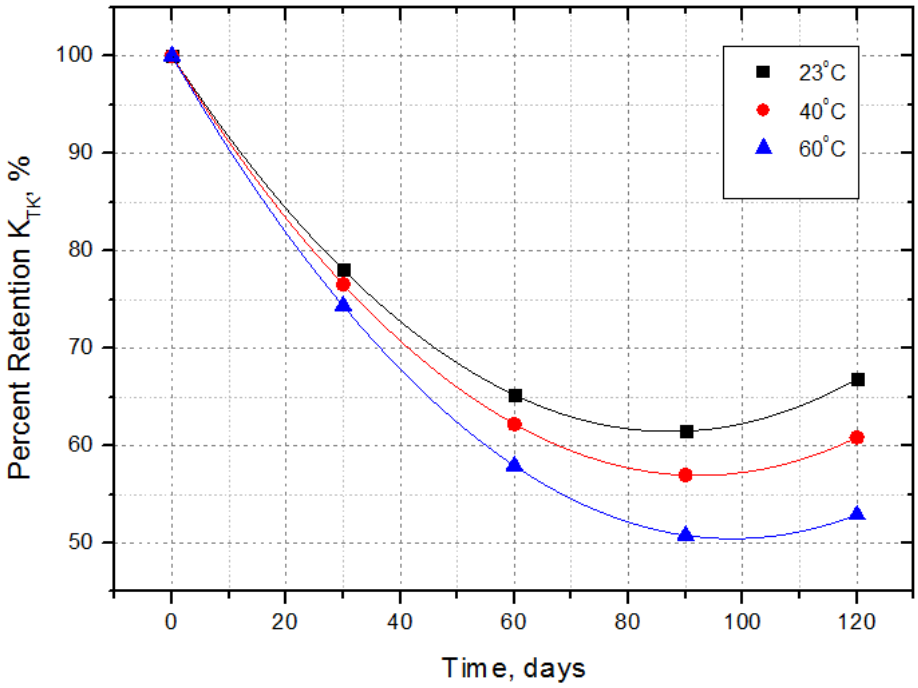

Figure 4.79: Percentage retention of the fracture toughness for sisal fibre reinforced polyester composite specimens.

Figure 4.80 shows a linearised form of the relationship between percentage retention of fracture toughness and time. Note that as a result of the mathematical undefined nature of the natural logarithm of zero, for computation purpose, the initial value is approximated equal to that of day one, assuming that no notable degradation in the fracture toughness property of the composite occurs. It is worth noting from the linear trend lines the influence of activation energy on the acceleration factor, specifically higher gradients with higher ageing temperatures.

A tabulation of the respective fit equations for the three ageing environments is presented in Table 4.16.

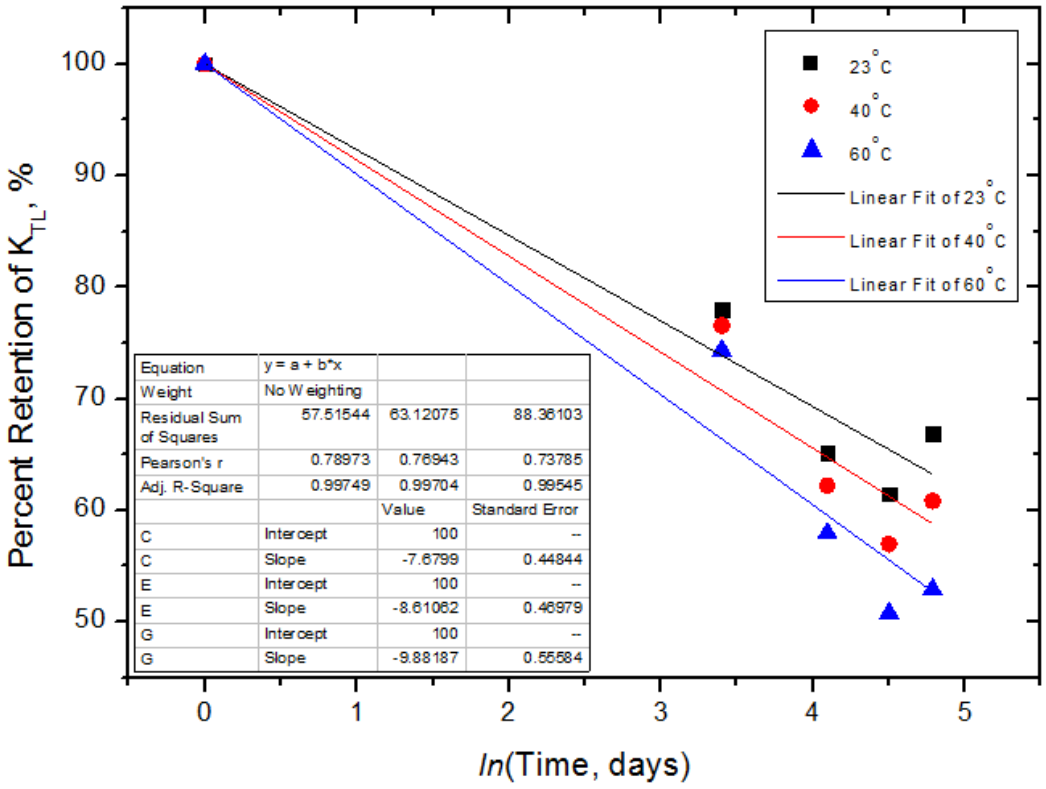

Figure 4.80: Arrhenius plot for reduction in percentage retention of the fracture toughness for the sisal fibre reinforced polyester composite specimen over time at different ageing temperatures.

Table 4.16: Linear relationship between the fracture toughness and time for sisal fibre-reinforced polyester composite specimens that are treated hydrothermally.

Ageing Temperature, ^{o}C	Fit Equation	Adj.R^2
23^{o}C	Y(Time)=100-7.679*ln(Time)	0.997
40^{o}C	Y(Time)=100-8.6101*ln(Time)	0.997
60^{o}C	Y(Time)=100-9.8818*ln(Time)	0.995

The equations in Table 4.16 predict the fracture toughness response of the composite specimens when subjected to the respective hydrothermal treatments with time.

The percentage retention values are used to establish a relationship between percentage fracture toughness retention and temperature. The relationship existing between fracture toughness retention and temperature is different for each time step.

Sub Section 2.1.2.1 described life of a material as being proportional to the inverse of the process reaction rate. And as such, Figure 4.81 shows the per cent retention rate of the fracture toughness plotted against the inverse of temperature for different time steps. Figure 4.82 shows a combined Arrhenius Life-Stress model predicted retention values plot of K_{TL} for aged specimens at respective temperatures of 23^{o}C, 40^{o}C, and 60^{o}C for a maximum period of 150 years.

A comparison between Arrhenius Life-Stress (theoretical) model predicted fracture toughness retention values and experimentally obtained values is shown in Table 4.17 through Table 4.19 for the three hydrothermal ageing environments.

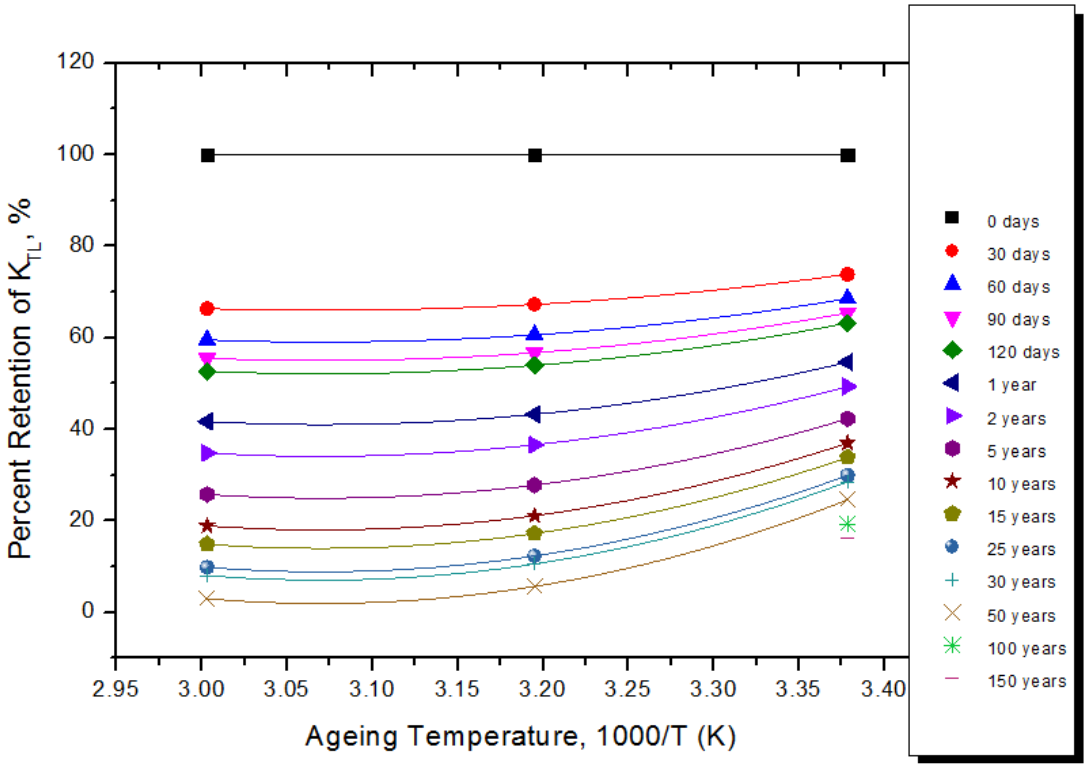

Figure 4.81: Percentage retention of the translaminar fracture toughness K_{TL} against inverse of temperature.

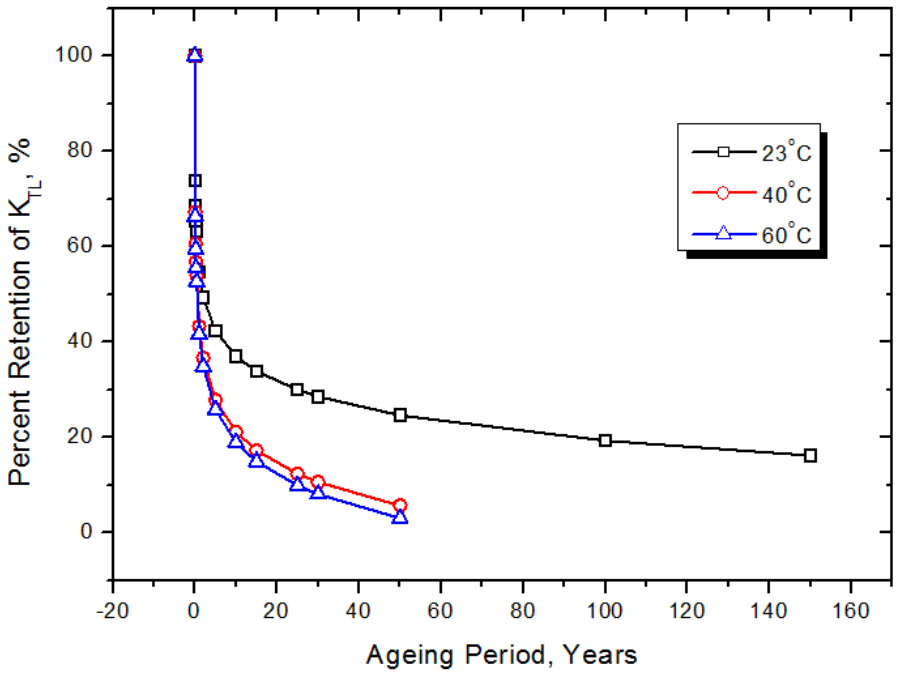

Figure 4.82: Arrhenius Life-Stress (theoretical) model predicted retention values of K_{TL} for specimens that were treated hydrothermally at temperatures of 23°C, 40°C, and 60°C.

Table 4.17: Comparison between experimental and the Arrhenius Life-Stress model predicted retention values of K_{TL} for specimens treated hydrothermally in distilled water at a temperature of 23°C.

Ageing Time, Years	Arrhenius Model Predicted Retention Values	Experimental Values	Variance, %
0	100	100	0
0.0821	73.88	75.29	-1.87
0.1643	68.55	66.52	3.05
0.2465	65.44	70.19	-6.76
0.3287	63.23	67.79	-6.72

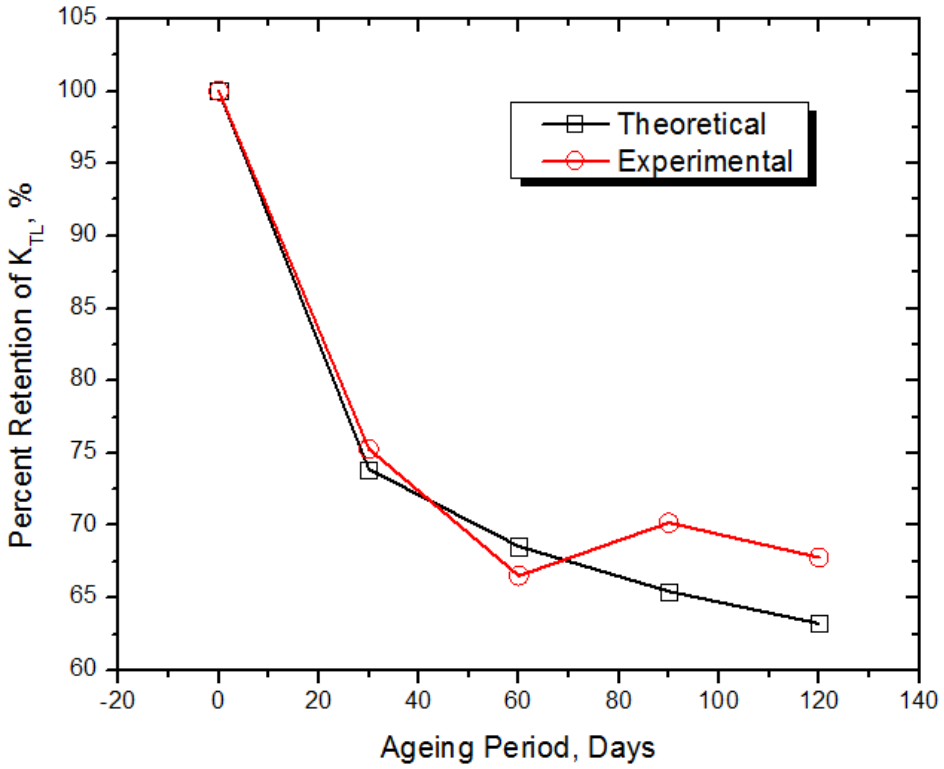

Figure 4.83: Comparison between experimental and Arrhenius Life-Stress (theoretical) predicted model retention values of K_{TL} for specimens that were treated hydrothermally in distilled water at a temperature of 23°C.

Table 4.18: Comparison between experimental and the Arrhenius Life-Stress model predicted retention values of K_{TL} for specimens treated hydrothermally in distilled water at a temperature of 40°C.

Ageing Time, Years	Arrhenius Model Predicted Retention Values	Experimental Values	Variance, %
0	100	100	0
0.0821	67.31	83.47	-19.36
0.1643	60.65	63.24	-4.09
0.2465	56.75	65.8	-13.75
0.3287	53.98	60.41	-10.64

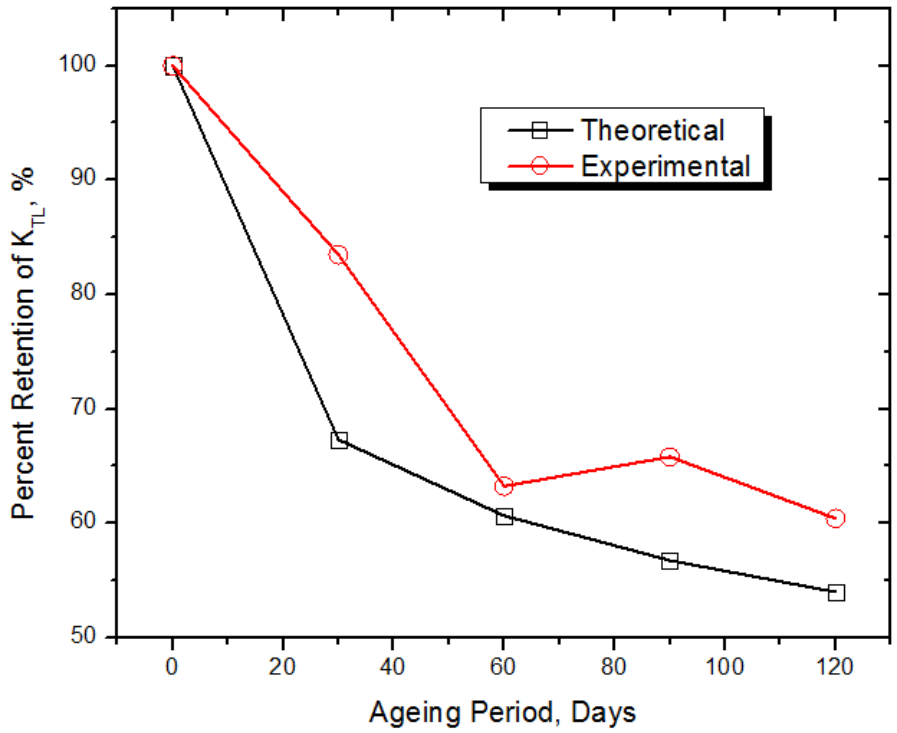

Figure 4.84: Comparison between experimental and Arrhenius Life-Stress (theoretical) predicted model retention values of K_{TL} for specimens that were treated hydrothermally in distilled water at a temperature of 40^{o}C.

Table 4.19: Comparison between experimental and the Arrhenius Life-Stress model predicted retention values of K_{TL} for specimens treated hydrothermally in distilled water at a temperature of 60^{o}C.

Ageing Time, Years	Arrhenius Model Predicted Retention Values	Experimental Values	Variance, %
0	100	100	0
0.0821	66.39	60.97	8.89
0.1643	59.54	55.17	7.92
0.2465	55.53	47.68	16.46
0.3287	52.69	53.33	-1.20

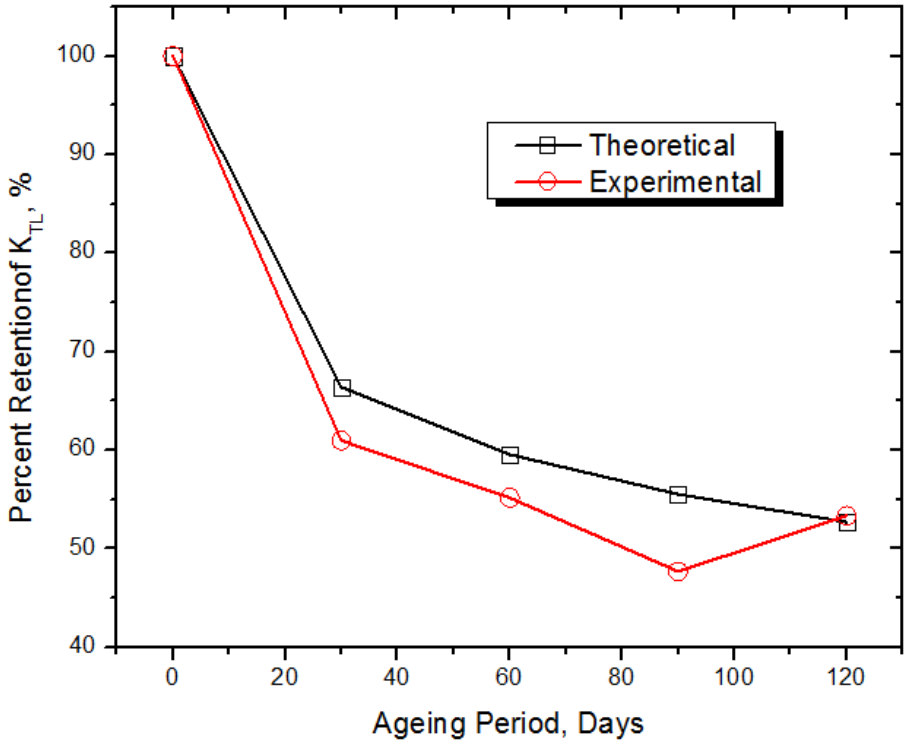

Figure 4.85: Comparison between experimental and Arrhenius Life-Stress (theoretical) predicted model retention values of K_{TL} for specimens that were treated hydrothermally in distilled water at a temperature of 60^{o}C.

In Figure 4.86 through Figure 4.88, the model results are further validated by scatter plots of observed values against predicted ones for the different ageing environments.

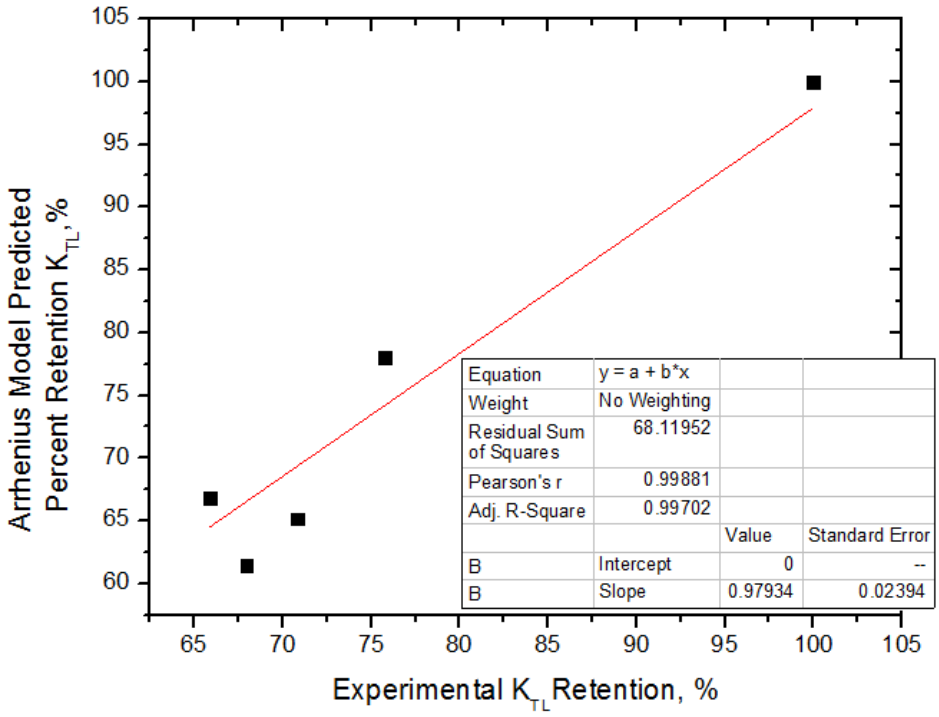

Figure 4.86: Scatter plot of average experimental versus theoretically predicted retention percentage values of fracture toughness for test specimens that were treated hydrothermally 23^{o}C.

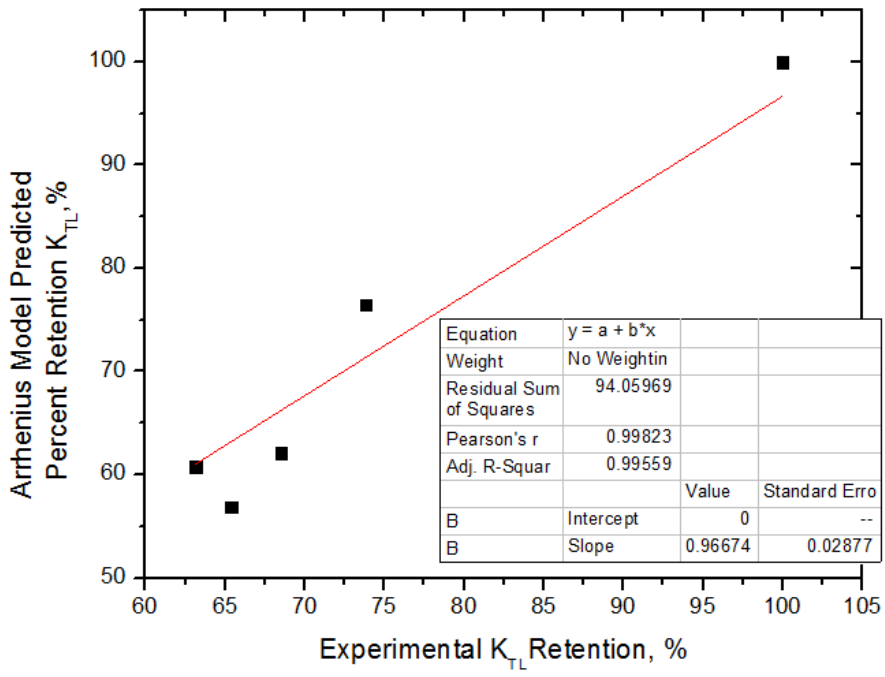

Figure 4.87: Scatter plot of average experimental versus theoretically predicted retention percentage values of fracture toughness for test specimens that were treated hydrothermally 40^{o}C.

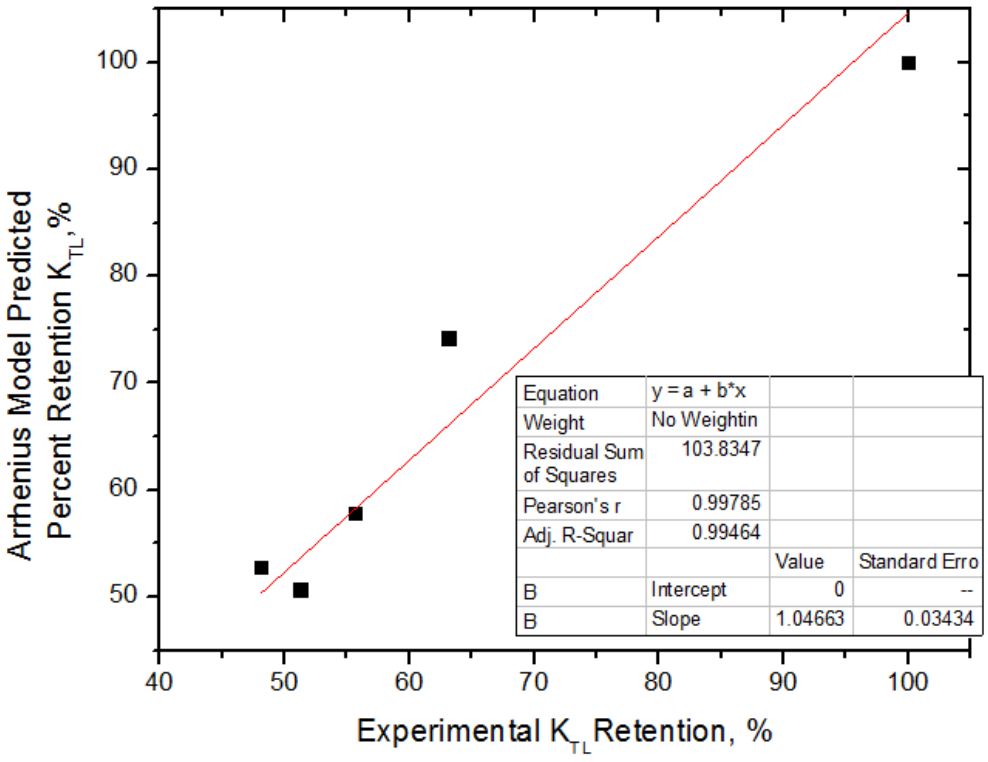

Figure 4.88: Scatter plot of average experimental versus theoretically predicted retention percentage values of fracture toughness for test specimens that were treated hydrothermally 60°C.

4.5.3.3 Comparison of Theoretical, Empirical Predicted and Experimental Results Fracture Toughness

A comparison between Arrhenius Life-Stress (theoretical) model-predicted, Empirical model predicted, and experimental retention values of K_{TL} for specimens hydrothermally treated at respective ageing environments of 23°C, 40°C and 60°C for the first 120 days are presented in Figure 4.89 through Figure 4.91.

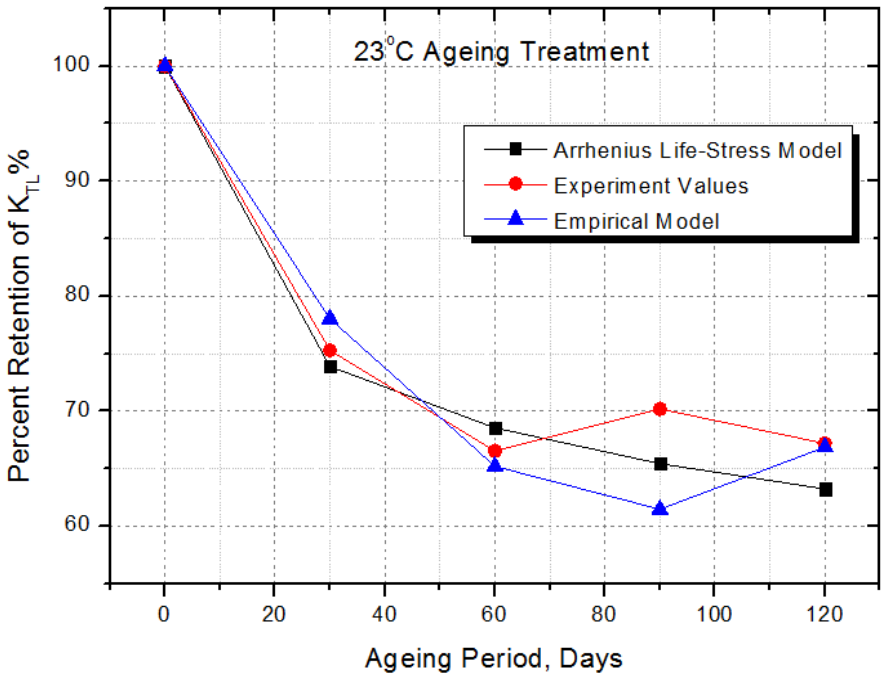

Figure 4.89: Comparison between Arrhenius Life-Stress (theoretical) model, Empirical model and experimental retention values of K_{TL} for specimens that were treated hydrothermally in distilled water at temperature of 23°C.

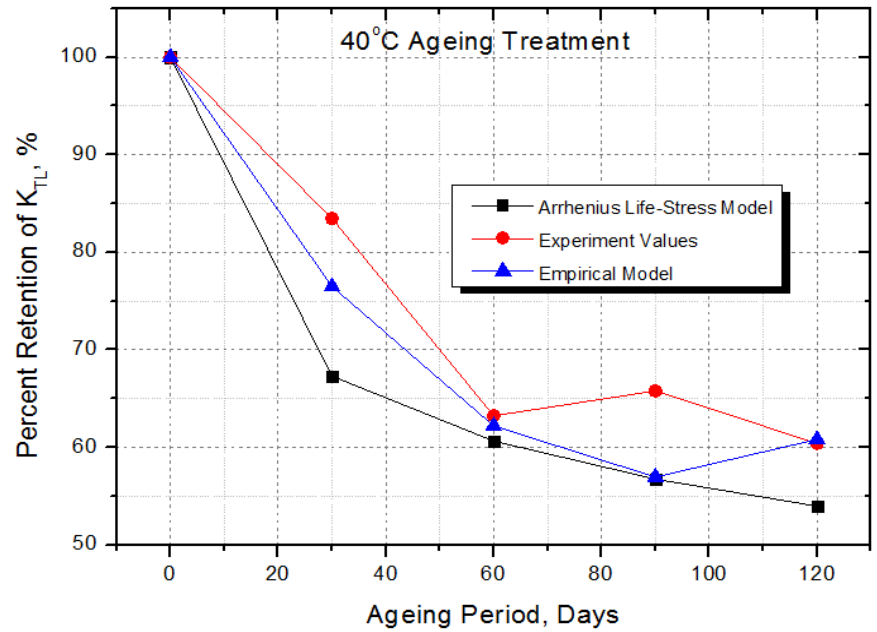

Figure 4.90: Comparison between Arrhenius Life-Stress model, Empirical model and experimental retention values of K_{TL} for specimens that were treated hydrothermally in distilled water at temperature of 40°C.

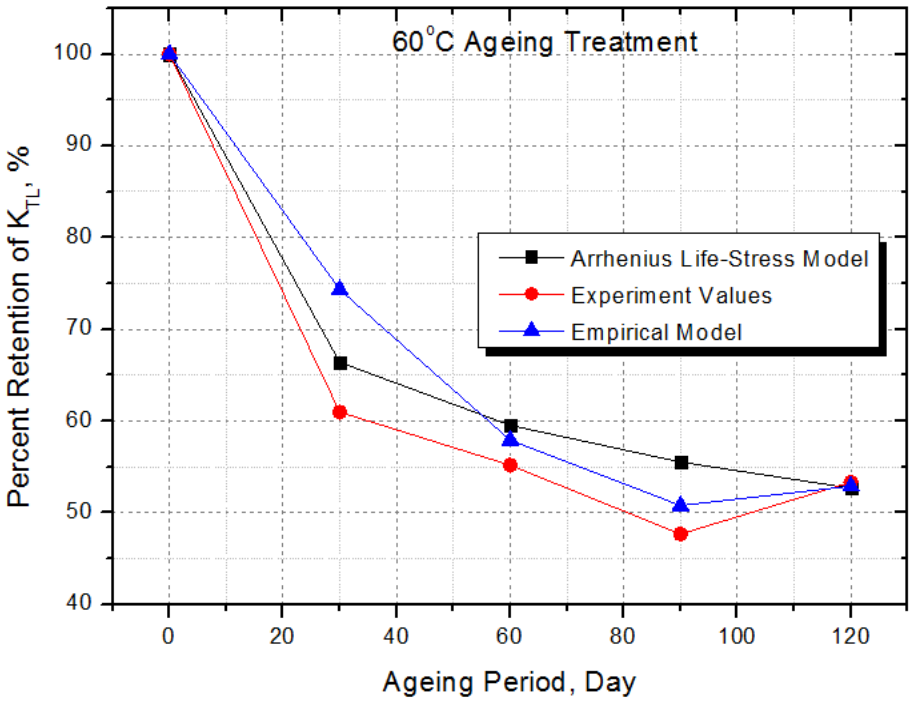

Figure 4.91: Comparison between Arrhenius Life-Stress model, Empirical model and experimental retention values of K_{TL} for specimens that were treated hydrothermally in distilled water at temperature of 60°C.

CHAPTER 5 DISCUSIONS

5.1 Introduction

This chapter discusses the results presented in Chapter 4 from experiments conducted on both sisal fibre reinforced polyester composite as a whole and also on its separate constituents with the aim of assessing the effects accelerated hydrothermal ageing poses on the fractural strength.

5.2 Isothermal Water Uptake

From Figure 4.1 of moisture absorption plots of sisal fibre reinforced polyester composite immersed in water at temperatures of 23^{o}C, 40^{o}C and 60^{o}C, it can be seen that there are 3 distinct regions just as observed by Verghese et al. (1999)which areas follows:

During the first 48 hours of the test specimens being immersed in water, all the three graphs exhibit Fickian diffusion tendencies. In this first stage, the rate of change of absorption is linear with respect to time as prescribed by equation (2.7). This is often referred to in literature as the initial absorption process. In terms of diffusion, this is the region where concentration gradients of the water and that of the reinforced composite test specimens are equilibrating and as such, its termed as a “diffusion controlled” region. In this stage the temperature of the water environment, will directly affect the diffusion coefficient resulting in either an increase or decrease in the rate of water uptake depending upon the direction of temperature change.

A non-linear region of the Fickian moisture absorption curve follows the linear section which is characterised by a long spell of equilibrated of concentration gradients, and therefore a stagnation of moisture content in the composite specimen. This leads to the final stage in the Fickian moisture absorption curve marking the transition into the chemical equilibrium where equilibration between liquid phase and the reinforced polymer is established. This region is describes as being extremely sensitive to external factors such as temperature as there are specific interactions between water and the chemical polymeric structure.

From the same plots, it can further be seen that the water uptake in the composite material is indeed enhanced by the existence of a thermal gradient as was suggested reportedly by both Gautier et al. (1999b) and Mula et al. (2006). This thermal gradient functions as an active accelerator which boosts the water uptake in its initial phase. This is evident from the increase in slope with the increase in the temperature of water temperature. The greatest gradient is observed in the 60^{o}C plot. At higher exposure durations, water absorption levels up as the moisture level inside the composite reaches its point of saturation, at which stage where there is no more water uptake. This comes as a result of the fact that during absorption, the maximum quantity of water uptake by composites is a function of thermodynamic potentials of the surrounding water and the immersed composite material.

Figure 4.1 shows that specimens immersed in distilled water at temperature of 23^{o}C gained maximum amount of moisture amounting to 0.52% after 1200 hours of treatment, while specimens treated at 40^{o}C and 60^{o}C reached their maximum contents of 0.4275% and 0.4533% after 1200 and 336 hours respectively. Thereafter, the 23^{o}C and 60^{o}C specimens experienced continuous weight losses, signalling irreversible damages in the composite specimens as suggested by Surathi and Karghari (2006). The specimens treated in water at 40^{o}C maintain a plateau with negligible signs of weight loss through to the end of the study at 3600 hours.

Note that the distinction arising in Figure 4.2 through Figure 4.4 between experimental result plot and the Fickian predicted fitted trend line is as a result of the non-uniformity of the composite panel as absorbed moisture infiltrates deeper.

Arrhenius plot of natural log of edge-effect corrected Fickian diffusion coefficient against inverse temperature of aged sisal fibre reinforced composite specimens at different temperature environments in Figure 4.5 shows, when fitted, that a linear relationship is exhibited, with a resulting correlation coefficient (R^2) of 0.98583. This therefore, confirms Arrhenius equation that diffusion coefficient depends on temperature. This implies that temperature is an acceleration factor in the ageing environments. Therefore, from the above analysis, it can be concluded that the activation energy of diffusion for this NaOH treated fibre reinforced composite system equals to 54.04 kJ.mol^{-1}. Pavlidou et al.(2005) obtained 49 kJ.mol^{-1} for silane

treated glass fibre reinforced polyester composite, which is not different from the one obtained here.

5.3 Tensile Testing

This section discusses tensile tests results presented in Section 4 from experiments conducted on both sisal fibre reinforced polyester composite as a whole and also on its separate constituents.

5.3.1 Tensile Strength

5.3.1.1 Sisal Fibre

From the summarized data presented in Figure 4.6 (more detailed information has been added in Appendix C) on the effects of temperature and moisture content on the tensile strength of single sisal fibres, the following deductions can be made:

For single sisal fibres that are treated hydrothermally, changes in water temperature appear to have had mixed but perceptible effects on the fibre tensile strength over the observation period. As is evident from the data presented, the tensile strength exhibits a general to be decline with the increase in environmental ageing period. Fibre tensile strength reductions of 13.06%, 17.3% and 31.5% for the 23^{o}C, 40^{o}C and 60^{o}C treatment environments respectively were seen. From these results, it is apparent that temperature also plays a role in the deterioration of the fibre tensile strength in a sisal fibre reinforced composite, while in service, when continuously taking in moisture over a long period.

It is worth noting that the standard deviations in all the tested samples appear to be rather wide. This is largely because of the inherent variability in the cross-sectional geometry and tensile properties along the lengths of sisal fibres (Inacio et al.,2010). Li et al.(2000a) reported that the tensile strength of the sisal fibres in a given sample obtained from the same source would range between 400–1000 MPa.

5.3.1.2 Neat Polyester Resin

From Figure 4.8, it is observed that the initial moisture levels taken up rapidly give rise to a continuous reduction of the tensile strength of the neat polyester specimens with increase in hydrothermal conditioning temperature during the first 30 days of conditioning. This is more pronounced in the specimen treated at the higher temperatures of 40^{o}C and 60^{o}C.

But after the first 30 days of treatment, the results show a slowdown in the drop of the tensile strength, with specimens immersed in water at temperatures of 23^{o}C and 40^{o}C recording much improved reduction (with an increase in the property recorded with specimens treated at 23^{o}C) in the property, while specimens immersed in water at temperature of 60^{o}C recorded the least improvement. This trend continues up to the end of the observation period for specimens treated at 60^{o}C.

This slowdown in the drop of the tensile strength can be attributed to the absorbed moisture which causes swelling stress build-up due to expansion of the matrix, which in turn opposes the curing stresses resulting in the increases in the tensile strength. Continued uptake of moisture by the resin specimen tends to further reduce the tensile strength possibly as a result of the reduction of the adhesion between the molecules, just as concluded by Panigrahi and Mallick(2009) from studies conducted on various composite systems. Further increases in the tensile strength are later experienced as a result of the hydrolysis of polymer chains. Broken covalent bonds join forces with the soaked up moisture forming rather stronger hydrogen bonds with the hydrophilic groups in the polyester network. The double hydrogen bonds in water molecules function as a physical crosslink.

It was found that these ageing environments yielded overall reductions in the cured neat polyester resin tensile strengths averaging 30.552%, 55.88% and 79.18% for the 23^{o}C, 40^{o}C and 60^{o}C ageing environments respectively over the observation period.

5.3.1.3 Sisal-Polyester Composite

In the initial stages of moisture absorption, the tensile strength of the composite dropped followed by raises in its magnitude for 23^{o}C and 40^{o}C treated specimens.

Meanwhile specimens treated hydrothermally at 60^{o}C continued experiencing further reduction in the tensile strength. This may be attributed to relief of residual stresses resulting from the curing process causing further drops in the tensile property. The absorbed moisture causes swelling stress owing to the matrix expansion which in turn opposes the curing stresses hence the increases in the tensile strength. Continued uptake of moisture by the composite decreases the tensile strength due to reduction of the adhesion between the molecules of the matrix, an occurrence similarly observed by Panigrahi and Mallick(2009) during studies conducted on various composite systems. Further increases in the tensile strength are later experienced as a result of the hydrolysis of polymer chains. Broken covalent bonds join forces with the soaked up moisture forming rather stronger hydrogen bonds with the hydrophilic groups in the polyester network. The double hydrogen bonds in water molecules function as a physical crosslink. The formation of hydrogen bonds in the polyester matrix also causes at the same period an increase in the Glass Transition Temperature (Tg).

However, prolonged immersion of test specimens in water at higher temperatures resulted in further reduction of tensile strength due to plasticisation of the matrix material and also the penetration of large amounts of water at the interface region which consequently deteriorated the fibre/matrix bond (Jeffrey et al., 2011; Schutte, 1994). As mentioned earlier, water uptake in the composite material is enhanced by the existence of a thermal gradient.

Figure 4.14 through Figure 4.16 point out that as water moisture increase as a result of the presence of a thermal gradient reaching almost constant levels, the tensile strength initially rapidly reduced during the first 40 days of exposure to these ageing environments. This was then followed by gradual reductions in the same property; although a significant appreciation was recorded in specimens treated at 23^{o}C which also later drops gradually. However, the specimens treated at 60^{o}C (Figure 4.16) showed a much steeper continuous reduction in the mechanical property throughout the rest of the conditioning period just as observed with the case of cured neat polyester resin specimens. This effect can be attributed due to high levels of plasticisation in specimens treated hydrothermally at 60^{o}C which has a tendency of lowering the tensile strength of a polymeric composite. Whereas in the case of the

23^{o}C treated specimens, successive creation and later dissolution of hydrolysed segments in its polymer chains results in this observed steeper recovery of the tensile strength.

It was found that these ageing environments yielded reductions in the tensile strengths of treated composite test specimens averaging 13.2%, 21.88% and 49.3% for the 23^{o}C, 40^{o}C and 60^{o}C treatment environments respectively over the observation period.

Other consequences on the composite of this accelerated hydrothermal ageing treatment were more pronounced surface degradation and particularly yellowing, loss of glossiness coupled with decreased transparency for the otherwise transparent polyester matrix material. Also visible mild signs of chalking were observed.

5.3.2 Tensile Modulus

Results pertaining to mechanical tests conducted in order to assess the effect on the tensile modulus of sisal fibres, neat polyester and sisal/polyester composite system after undergoing hydrothermal treatment are discussed.

5.3.2.1 Sisal Fibre

On the effects of temperature and moisture content on the elastic modulus of single sisal fibres, the following deductions can be made from the data obtained: For single sisal fibre hydrothermally treated, changes in water temperature appear to have had effects on the fibre elastic moduli over the observation period. As is evident from the plotted data presented in Figure 4.18, the elastic modulus declines with the increase in the environmental ageing. These ageing environments yielded reductions in fibre elastic moduli averaging 26.8%, 23.2% and 29% for the 23^{o}C, 40^{o}C and 60^{o}C treatment environment respectively over the 120 days ageing period. From these results, it is correct to state that temperature also plays a role in the deterioration of the fibre elastic modulus in a sisal fibre, which continuously takes in moisture over a period.

It is also worth mentioning that the value of standard deviation values in the results for all the tested samples appear to be large. This is largely because of the inherent inconsistency in the cross-sectional geometry and tensile properties along the lengths of sisal fibres, an opinion equally made by Inacio et al. (2010). This variation differs from fibre to fibre obtained from the same source.

5.3.2.2 Neat Polyester Resin

During the initial phase of moisture absorption, hydrolysis dominates over plasticisation. Hydrolysis has a tendency of increasing the elastic modulus of the neat resin test specimens during continued exposure to this very environment as portrayed for all the three ageing environments in Figure 4.20. This phenomenon leads to a misconception as it is presumed that there is some kind of enhancement of some mechanical properties during the early stage of moisture uptake. The perceived initial rise in the elastic modulus values is typical with hydrolytic dilapidation of the matrix and successive dissolution of hydrolysed segments. It has been suggested by Chin et al. (2001) that the lack of the hydrolysed segments in the matrix material, leads to its embrittlement and for this reason a rise in both elastic modulus and glass transition temperature (T_g) of the matrix occurs. But afterward, it has been observed that prolonged exposure to the ageing environments tends to have an opposite effect on the T_g, leading to its reduction as explained in Section 5.4. This is mainly caused by plasticisation which also leads to deterioration of the matrix.

Plasticisation normally takes into effect after prolonged moisture absorption during continued exposure to this very ageing environment and also at higher hydrothermal ageing temperatures resulting in deterioration of the matrix as observed in Figure 4.23.

5.3.2.3 Sisal-Polyester Composite

Variations in the modulus of elasticity of the treated sisal/polyester composite system plotted in Figure 4.25 showed similar trends to that of the cured polyester resins discussed in sub Section 5.3.2.2 where the effect of hydrolysis caused enhancements in the modulus during the initial phase of moisture absorption, typical with hydrolytic dilapidation of the matrix and successive dissolution of hydrolysed

segments. Further exposure to the ageing environments leads to some reductions in modulus due to possible onset of plasticization resulting in further dilapidation of the matrix material of the composite system.

An enhancement of the mechanical property appears to have taken place in the hydrothermally aged composite test specimens during the early periods of moisture uptake as seen in Figure 4.27 through Figure 4.29. This perceived enhancement of the elastic modulus is attributed to the dilapidation of the matrix material and successive dissolution of hydrolysed segments, leading to its embrittlement and for this reason a rise in the mechanical property. Plasticisation normally takes into effect after prolonged moisture absorption during continued exposure to this very ageing environment resulting in deterioration of the matrix and subsequent reduction in its elastic modulus as observed in specimens hydrothermally treated at 60^{o}C.

The primary elastic modulus of a composite of a unidirectionally reinforced composite loaded along the reinforcement depends on the elastic moduli and volume fraction of the constituents making up the composite, and the bonding that exists in between the reinforcing fibre and the surrounding matrix. If it is assumed that sufficient load transfer occurs between the fibre and matrix, then the elastic modulus should be equal to that predicted from the rule of mixtures, and should be independent of the interfacial shear strength.

5.4 Dynamic Mechanical Analysis

Glass transition temperatures (T_g) of cured polyester resin specimens, after being subjected to accelerated ageing by hydrothermal treatment at respective temperatures of 23^{o}C, 40^{o}C, and 60^{o}C, were determined through Dynamic Mechanical Analysis (DMA). This was done using neat (unreinforced) polyester resin specimens instead of the actual sisal fibre reinforced composited test specimens. This is because polyester polymer chains nearest to the reinforcing fibre are tightly bound and are so highly restricted in mobility such that they cannot participate in any transitions that are measurable by DMA. Furthermore, the inconsistency in the fibre geometrical properties would as such throw test results all over the chart. Therefore, for a much more comprehensive and accurate understanding of the exact onset, peak and end of the glass transition, neat polyester resin specimens were used in this study.

Measurements were carried out for a different number of frequencies for purposes of firstly, exploring the frequency dependence of the relaxation process and secondly, to provide data at specific frequencies. For the purpose of determining T_g of the resin material, a single loading frequency of 1Hz was used in accordance to ASTM 4065-1 standard. Complex viscosity has a dependence on the frequency in the denominator so that at 1 Hz, complex viscosity will overlap the complex modulus (Menard, 1999). And from the obtained graph (Figure 4.30), Modulus 1, Loss modulus 1 and Tan Delta1 plots were used to study and interpret the onset, peak and end temperatures of the glass transition, respectively.

From Figure 4.30 it is worth noting that at the moment where the storage modulus, $E^{/}$ (labelled as Modulus 1 in the plot) declined sharply, the damping curve (labelled as *Tan δ*) experienced its peak. However, this decline in the storage modulus as the furnace chamber temperature intensifies is an indication that the resin system may be showing signs of becoming thermally unstable. These signs are equally observed through the gradual increasing amounts of noise at higher temperatures in the Loss Modulus plots. At about the same moment the loss modulus, $E^{//}$ also went through its peak, but its peak was not as prominent as that of the damping curve peak. The peak in the loss modulus curve was reached at a temperature which is somewhat lower than the peak in the *Tan δ* curve.

In practice, the *Tan δ* is regarded, for the most part as the sensitive gauge of the presence of molecular motions which are happening in the material. The *Tan δ* peak is to a greater extent related with the main transition of the material from a glass state to a rather rubbery state. It is the point which signifies the completion of the transition. The temperature at which *Tan δ* goes through its highest point in the plot is hence referred to as the glass transition temperature, Tg of the material, of which in this case is $90.2^{o}C$ for the untreated polyester test specimen whose analysis is presented in Figure 4.30.

It is also worth noting that the maximum value of *Tan δ* peak is higher than that obtained from the use of the $E^{//}$ plot. This comes as a result of the fact that *Tan δ* peak takes place at the end of the transition region between elastic and viscoelastic

zones, whereas the $E^{//}$ maximum takes place somewhere in the middle of this very transition zone.

DMA results in Figure 4.31 coupled with the percentage average moisture gain and T_g retention composite plots in Figure 4.32 through Figure 4.34 of treated neat polyester resin specimens at different temperatures reveal that during the first 30 days of hydrothermal treatment, the Tg initially decreased but further exposure to these very environments resulted in increases in its values. Ahmad et al. (2011) while studying other resin systems reported similar occurrences even to an extent where after continued exposure, the Tg values appreciated beyond that of the dry untreated resin material. This can be explained by the formation of additional cross-links in the wet polyester resin molecules. The observed initial increase in Tg is in harmony with hydrolytic degradation and later dissolution of hydrolysed fragments. It was assumed by Apicella et al. (1983) and Chin et al. (2001) that the loss of the hydrolysed, low molecular weight segments, which make the matrix flexible, lead to embrittlement resulting in an increase in the Tg. And as such, observing from Figure 4.31, greater increases in the Tg were observed in specimens treated at higher ageing temperatures as water absorption by this composite system happens to be enhanced by the existence of a thermal gradient.

Hydrolysis has a similar influence on the elastic modulus as observed in sub Section 5.3.2.2, yielding appreciation in the mechanical properties which is often misconstrued as some kind of enhancement of some mechanical properties during the first stage of moisture absorption. But extended exposure to these very ageing environments tend to have an opposite effect on the Tg as plasticization of the matrix sets in, resulting in the deterioration of the composite matrix.

Plots of the variation of the glass transition temperature (T_g) with the moisture content in the resin specimens are shown in Figure 4.36 through Figure 4.38. Second order polynomial curve fits were applied to the given plots. Caution must be taken as interpretations and further use of the model functions as they are limited to the indicated maximum moisture contents shown on the plots.

Specimens hydrothermally treated at 60^oC (Figure 4.38) appear to be in agreement with lubrication and gelation theory (also referred to as The Gel Theory) for plasticisation sighted by Verghese et al. (1999) where at first the drop in the Tg starts

off gradually but then begins to intensify with increase in the absorbed moisture content signifying possible occurrence of plasticization of the matrix material. This is not the case with specimens hydrothermally treated at temperatures of 23^{o}C and 40^{o}C which show signs of enhancements in the viscoelastic property as seen in the respective Figure 4.36 and Figure 4.37. This is as a result of the presence of hydrolysis due to the creation of additional cross-links in the wet resin molecules resulting in the enhancement in the property.

The interfacial adhesive bond strength and strain show dependence, especially near the glass transition temperature (Tg) of the composite matrix. Similarly, the fracture toughness is expected to show temperature dependence as observed in Section 5.5. As such, downward changes to Tg points pose a negative effect to the resultant fracture toughness of the composite product. (Banea *et al*, 2011)

5.5 Composite Fracture

This section discusses results and analysis following studies conducted on hydrothermally aged microbond and fracture toughness test specimens with the aim of assessing the retention of their respective properties over specific periods.

5.5.1 Micro Composite Fracture

It is worth noting from Figure 4.40 which shows a microbond single fibre pull-out force trace plot of one unconditioned microbond specimen that the interfacial bond experienced shearing due to the applied pull-out force, resulting in a steady rise in the force from the initial frictional force to a peak value of 0.00165kN. This peak defines the maximum adhesive bonding force existing at the polyester/sisal fibre interface. An abrupt drop to a certain lower frictional force level was then observed. This drop is indicative of the subsequent failure in the interface that binds the droplet to the sisal fibre. The droplet was further pushed down the fibre with only the frictional force exerted by the fibre counteracting its downward movement. It is then followed by a drop back abruptly to some lower frictional force level as the resin droplet is pulled down the fibre. For sisal fibres, this level varies from one fibre to another and is dependent upon the variations in the fibre diameter along its entire

length. This variation in fibre diameter also defines the profile type of the frictional resistance the pull out test will exhibit post debonding.

From Figure 4.40 through 4.46, it was observed that in cases where a low microbond shearing force was recorded mainly due to subsequent deterioration of interfacial bond which was as a result of the applied hydrothermal treatment on the composite, higher frictional forces exerted by the fibre were recorded which to a lesser extent tended to continue providing bonding. It is further worth noting, from Figure 4.41 through Figure 4.45 of selected plots of the first 4 days (96hrs) of hydrothermal ageing of the microbond test specimens, that the shearing force reduced further as the ageing process progressed when compared with untreated specimen in Figure 4.40. This deterioration was more pronounced in samples treated at higher conditioning temperature as observed with specimens hydrothermally treated at 60^{o}C. This was due to the existing of a thermal gradient in the moisture diffusion process in the micro composite and subsequently increase of the rate of the deterioration of the bonding existing between the fibre and its surrounding matrix.

A collection of results from several microbond pull-out tests are shown in scatter plots in Figure 4.46 through Figure 4.58 for the different ageing temperatures and exposure durations. All scatter plots yield a well-defined linear relationships from which average shear bonding strengths were determined from the resultant slopes of the linear trend lines. In these figures, each data point represents the average of not less than 20 microbond test results.

The relationship between interfacial shear stress and direct stress is based on analysis first developed by Cox (1952) and applied to fibre pull-out tests by other investigators (Bartos, 1980; Greszczuk, 1969; Takaku and Arridge, 1973; Lawrence, 1972) which highlights the proportionality of the debonding force to the hyperbolic tangent of the embedded length. The stress distribution over short embedded fibre lengths is assumed to be in effect uniform, which is consistent with these resultant scatter plots.

It is worth stating that the major source of the observed distributions of interfacial shear bonding strength values around the trend line emanates from variations in the

surface characteristics from one position on the surface to the other along the length sisal fibres extracted from the same batch.

Preliminary bond strength measurements on non-hydrothermally treated microbond specimens yielded an average interfacial shear strength of about 8 MPa as shown from the slope of the trend line in Figure 4.46 and resultant Table 4.11. Significant reductions in the interfacial strengths was observed in all of the three ageing conditions during the initial period, with steeper declines experienced in test samples which were subjected to 40^{o}C and 60^{o}C of hydrothermal ageing treatment. The strength dropped and settled to an average value of about 2.72 MPa for the 23^{o}C treated test specimens, whereas for the 40^{o}C and 60^{o}C treated samples their strengths further settle down to values of about 1.75 and 1.33 MPa respectively. This amount to 66.2%, 78.2%, and 83.4% interfacial strength drops respectively. These drops in bond strength can be attributed to plasticisation of the resin by the water as well as reduction in the mechanical interlocking pressures arising from thermal expansion mismatching of the fibre and matrix as suggested by Biro (1993).

Following a regression analysis of the microbond pull-out tests results, a more comprehensive model description of the effects of temperatures and absorbed water on the microbond interfacial strength over time was developed. A corresponding model function is presented as equation (4.6) which describes the variation with correlation coefficient of 0.97718. This suggests that this empirical model fits the experiment data well.

Composite plots in Figure 4.62 through Figure 4.64 point out that as moisture increased inside the composites due to the influence of the presence of a thermal gradient reaching almost constant levels, the interfacial shear strength initially reduced rapidly during the first 4 days (for 40^{o}C and 60^{o}C treated specimens) and about 8 days (for the 23^{o}C specimens) of exposure to these ageing environments. This was then followed by a gradual levelling of the property until the end of the observation period for specimens treated at 23^{o}C. Whereas for specimens treated at 40^{o}C and 60^{o}C experienced steeper rapid reductions in interfacial shear strengths during the first 3 days which was followed by sudden levelling of the property for the remainder of the conditioning period. In all, the 23^{o}C and 40^{o}C hydrothermally treated specimens registered average reductions in the interfacial shear strength

amounting to 66.2%, 78.2% respectively, while the 60^{o}C treated specimens yielding the highest reduction of 83.4%.

Isothermal water uptake studies presented in the composite plots were conducted, as described in Section 3.3.1 and whose results are in Section 4.2, in the same ageing chambers along-side microbond test specimens. This was done in order to determine the relative rate of absorption of water by the sisal-polyester composite by immersing standard test specimens into distilled water at different pre-set temperatures of 23^{o}C, 40^{o}C and 60^{o}C respectively. Based on the Fickian diffusion model, the isothermal water uptake study yielded diffusion coefficients amounting to 0.00327mm^{2}.sec^{-1}, 0.01277mm^{2}.sec^{-1} and 0.03695mm^{2}.sec^{-1} for specimens placed in their respective study hydrothermal ageing environments.

For each hydrothermal treatment, microbond pulled-out specimen fibres were further examined on a NeoScope JCM 5000 Scanning Electron Microscope (SEM) for presence of residual polyester matrix crystal on the fibre surface after debonding.

Results of these scans indicate little to no traces of the residual matrix material present on the sisal fibre at the original location of the polyester resin droplet along the fibre. (The presence of this residual matrix appears to be dependent on the duration of the applied hydrothermal ageing as seen in the SEM images in Figure 4.65, with more Appendix G). From these microbond fractographs, it can be concluded that complete interfacial bond failure occurred during the pull-out tests in the 40^{o}C and 60^{o}C treated test specimens as a result of the hydrothermal ageing process. Gautier et al. (1999a) in their findings associated osmotic cracking in the matrix, as well as at the interface and subsequent interfacial debonding to the overall composite failure when subjected to hydrothermal treatment.

Undoubtedly, the ultimate tensile strength of the composite is for the most part controlled by the collective reinforcing fibre strength. The fibre strength primarily is also a function of gauge length and decreases with increasing gauge length. Any factors which affect individual fibre properties generally also affect fibre bundle strength. Certainly, the loss of ultimate tensile strength of the sisal fibre reinforced

polyester composite might also be attributed to the loss of bundle strength of fibres. However, the data shown in Figure 4.13 and Table 4.11indicate that ultimate tensile strength of the bulk composite reduced significantly with decreasing interfacial shear strength, suggesting that the loss in interfacial strength may be more important than the loss in individual fibre strength. Although the theoretical reasoning for such a relationship is not fully understood as yet, one possible interpretation is that loss of interfacial shear strength increases the effective gauge length of the fibre bundle in the composite which in turn has a direct influence on the ultimate tensile strength of the composite as suggested by Ramakrishna (1990).

5.5.2 Macro Composite Fracture

From results presented in sub section 4.5.2, it is observed that sisal fibre reinforced polyester composite exhibits an almost linear characteristic response during the initial phase of testing up to approximately, which in this case of the example plot in Figure 4.65, $0.7P_{max}$ of loading. Internal microcracking, which subsequently develops inside the composite, leads to a nonlinear response which continues up to the pick load, P_{max}. Upon reaching this critical load, fracture propagated continuously as the applied load reduced to some lower value of about $0.5P_{max}$ before the test was stopped.

These composite plots in Figure 4.68 through Figure 4.70 point out the fact that as the percentage of moisture increased to saturation as a result of the presence of a thermal gradient, the fracture toughness reduced rapidly initially. This was then followed by a levelling of the property until the end of the observation period for specimens treated at 23^oC. Specimens that were kept at 40^oC experienced a gradual reduction in fracture toughness throughout the rest of the conditioning period while the 60^oC treated specimens showed marginal recovery in the tested property. In all, the 23^oC and 40^oC hydrothermally treated specimens registered reductions in the fracture toughness amounting to 32.2%, 39.5% respectively, while the 60^oC treated specimens yielded the highest reduction of 46.7%.

Isothermal water uptake studies results presented in the composite plots were conducted along-side in the same ageing chambers with fracture toughness test specimens in order to determine the relative rate of absorption of water by the sisal-polyester composite by immersing standard composite test specimens into distilled water at different pre-set temperatures of 23^{o}C, 40^{o}C and 60^{o}C respectively. (For further details on this study, refer to sub Section 3.3.1 and whose results are in sub Section 4.2).

Further fractographic analyses of SEM images which were conducted on fracture toughness test specimens revealed and placed interfacial debonding as the major fracture mechanism, indicative of a strong influence of hydrothermal degradation on fracture toughness test results. This observation is in line with findings following the single fibre microbond pullout studies in sub Section 4.5.1. (See also SEM fractographic images in Appendix G).

Results of regression had a correlation coefficient of 0.9933776. This suggests that the estimated model equation (equation 4.7) fits the experiment data well. Note that any predictions based on values of the ageing duration and exposure temperature that fall significantly outside the bounds of fracture toughness experiments may be inaccurate.

5.5.3 Fracture Toughness Predictive Model

5.5.3.1 Empirical Modelling

Results of regression had a correlation coefficient of 0.9933776. This suggests that the estimated empirical model equation (equation 4.7) fits the experiment data well. Note that any predictions based on values of the ageing duration and exposure temperature that fall significantly outside the bounds of fracture toughness experiments may be inaccurate.

From the comparison plots in Figure 4.73 through Figure 4.75 between experimental and predicted fracture toughness values and data in the accompanying Table 4.14, it can be seen that predicted results which are based on the model compare well with

the experimental results, with the maximum difference remaining below 14% for specimens treated at 23^{o}C and 40^{o}C. Specimens that were aged at 60^{o}C specimens recording maximum percentage difference not exceeding 17%. It is observed that the fitted lines in Figure 4.76 through Figure 4.78 display respective slopes of 1.009, 1.03182, and 0.95518, all symbolising almost perfect 45^{o} angle line fits. This observation is consistent with the fact that in all the three ageing environments, both the experimental and predicted values of the responses are spread in close proximity to the fitted lines in the coefficients of correlation (Adjusted R^2) of 0.9967, 0.99637 and 0.99271 respectively, signifying a nearly perfect fit of the developed empirical model to the experimental results.

This model can therefore suitably be used to predict fracture toughness property changes in test specimens subjected to hydrothermal environments for as long the specimen are of the same material, undergo same fibre surface treatment, and possess geometrical configurations as prescribed in accordance with ASTM E1922-97 testing standard for translaminar fracture toughness.

5.5.3.2 Theoretical Modelling

It is apparent from results presented in Table 4.17 through Table 4.19 and Figure 4.83 through Figure 4.85 for the respective ageing environments that the Arrhenius model predicted K_{TL} retention values compare very well with experiment ones as they are within average experimental scatter bounds.

It is worth noting in Figure 4.86 through 4.88 that the fitted lines display respective slope values of 0.97934, 0.96674, and 1.04663, all symbolising almost perfect 45^{o} angle line fits. This observation is consistent with the fact that in all the three respective scatter plots, both the experimental and the theoretically predicted values of the responses are spread in close proximity to the fitted lines with the respective values of the coefficient of determination (Adjusted R^2) of 0.99881, 0.99559 and 0.99464. This signifies a nearly perfect fit of the theoretical model to the experimental results.

5.5.3.3 Comparison of Empirical, Theoretical Model Predicted, and with Experimental Fracture Toughness Results.

From the plotted result in Figure 4.89 through Figure 4.91, it is apparent that the theoretical results (Arrhenius Life-Stress model) were closely correlated with both observed and empirical data, thus confirming the assumption in the Arrhenius' Life-Stress theoretical model, that the life is inversely proportional to the reaction rate of the process. The slight discrepancy is most likely due to the fact that the two models are not taking into account of the slight notable periodic appreciations and depreciations of the K_{TL} owing to the successive creation and dissolution of the hydrolysed segments in the resin material molecule chains throughout the test period as observed experiment results. Despite this, all the three approaches trend towards the same direction.

5.5.4 Summary

The effect of hydrothermal aging on the fractural strength of sisal fibre reinforced polyester composites specimens treated in water at 23^{o}C, 40^{o}C and 60^{o}C for specific periods was assessed from the composite's macro and micro behaviour through the translaminar fracture toughness (K_{TL}) of the composite and single fibre microbond interfacial shear strength respectively. The results, obtained by means of an eccentrically loaded single-edge-notch fracture toughness test specimen, revealed that hydrothermal ageing yields significant changes in K_{TL}, with more pronounced decrease in the property recorded with increase in ageing temperature. The resultant empirical model generated compares well with K_{TL} values obtained from experiments. K_{TL} results determined by the empirical model were further used with the help of the Arrhenius Life-Stress analysis in determining the composite's long-term performance.

Results from the single fibre microbond pullout tests of hydrothermally treated test specimens revealed reductions in the interfacial microbond strengths as the absorbed moisture levels intensified. This interface plays a major role in the adhesion created between the NaOH treated sisal fibre surface and the polyester matrix in order to establish the desired macroscopic mechanical properties of the composite. As such,

with its failure resulted in the reduction of both the tensile strength and fracture toughness of the composite.

It is generally understood that for the production of quality reinforced composite materials, the creation of a durable fibre/matrix interfacial region is imperative for the excellent transfer of applied loads between one fibre to the other through the surrounding matrix while at the same time offering resistance against moisture attack from the surrounding environment. From results presented, it is therefore essential to identify and use a suitable coupling agent during fibre treatment prior to infusion in order to improve both the fibre/matrix interfacial bonding and further resistance against moisture attack and subsequently maintaining the overall fractural strength over time.

CHAPTER 6 CONCLUSION AND SUGGESTIONS FOR FUTURE WORKS

The conclusions presented in this chapter are applicable to unidirectional sisal fibre reinforced polyester composite made from Sodium Hydroxide treated natural sisal fibres and general purpose polyester laminating resin.

6.1 Summary of Findings

1. Polymeric composite materials, when subjected to hydrothermal environment, take up moisture, eventually leading to the deterioration of their mechanical properties. The rate of deterioration can vary from one composite system to the other, depending on factors which include the temperature and length of exposure to such environment. The quantity of moisture absorbed intensifies with the length of the exposure time to this hydrothermal ageing treatment, while the rate of its uptake increases with increase in exposure.

2. The resultant Arrhenius analysis of moisture absorption studies yielded a correlation coefficient of 0.98583, confirming that water absorption was related to the prevailing temperature. Therefore, from the analysis it can be concluded that the activation energy of absorption for this NaOH treated composite system is equal to 54.04 $kJ.mol^{-1}$.

3. It was found that these ageing environments yielded reductions in the reinforcing sisal fibre tensile strengths averaging 13.06%, 17.3% and 31.5% for the 23^{o}C, 40^{o}C and 60^{o}C treatment environments respectively over the observation period. The overall reduction in the cured neat polyester resin tensile strength averaging 30.552%, 55.88% and 79.18% for the same respective ageing environments. The sisal fibre – polyester interface suffered 66.2%, 78.2% and 83% average reductions in the

interfacial strengths for the respective ageing environments. As expected, reductions in the tensile strength property of hydrothermally treated sisal fibre reinforced polyester composite averaged 13.2%, 21.88% and 49.3% for the same respective ageing environments. From these results, it can be stated that temperature plays a big role in the deterioration of the strength of the three constituents making up the fibre reinforced composite, and consequently lead to an overall reduction in the tensile strength of the reinforced composite.

4. Environmental ageing studies on single sisal fibres also produced deterioration of the fibre elastic moduli averaging 26.8%, 23.2% and 29% for the 23^{o}C, 40^{o}C and 60^{o}C treatment environment respectively over the study period. Similarly, changes in the values of modulus of elasticity of the neat polyester specimens hydrothermally treated under same respective environments yielded enhancement of the property amounting to averages of 31.33% and 26.2% for test specimens treated at 23^{o}C and 40^{o}C respectively, whereas the 60^{o}C treated specimen resulted in property deterioration of 13.14%. The perceived initial rise in the elastic modulus values is typical with hydrolytic dilapidation of the matrix and successive dissolution of hydrolysed segments. It is suggested that the lack of the hydrolysed segments in the matrix material, leads to its embrittlement and for this reason a raise in both the elastic modulus and glass transition temperature (Tg) of the matrix occurs. But afterward, it has been observed that prolonged exposure to the ageing environments tends to have an opposite effect on the Tg, leading to its reduction. This is mainly caused by plasticisation which also leads to deterioration of the matrix. Plasticisation is responsible for the observed continued reduction of the elastic modulus in the 60^{o}C treated specimens. As such, continued exposure to the environment would result in the eventual deterioration of the matrix, in respect of stiffness.

5. The interfacial shearing strength in microbond composite specimens tend to reduce as the ageing process progresses and this deterioration is more pronounced in samples treated at higher conditioning temperature. It can

further be observed that in cases where a low microbond shearing force is recorded mainly due to subsequent deterioration of interfacial bond which is as a result of applied hydrothermal treatment to the composite. When compared with the remaining interfacial bond strength, higher frictional forces have been recorded which to a lesser extent tend to continue providing bond strength.

6. Scanned Electron Microscopic (SEM) images on the surface of the fibre extracted from the fractured specimens (non-aged and the other after the ageing of the test specimens in the hydrothermal ageing environments), revealed the effect posed by the infused moisture through microcracks along the fibre-matrix interfacial bonding. The absence of resin material on the surfaces of the debonded fibres signify a strong influence of water degradation on the fracture toughness and overall strength of the composite.

6.2 Conclusions

This research has successfully developed and used both empirical and theoretical models to predict the effects of the environment on fracture of a sisal fibre-reinforced polyester composite and its subsequent life performance. From the modelling conducted, it is apparent that the theoretical results gave a close correlation with both observed and empirical data confirming Arrhenius' Life-Stress theoretical assumption that the life is proportional to the inverse reaction rate of the process.

6.3 Summary of Contributions

An empirical relationship existing between the fracture toughness and hydrothermal ageing period has been established for this composite system and successfully validated using theoretical model and experimentally obtained values. The use of each one of the two, empirical and theoretical models, has successfully enabled life-time prediction of this composite system to be made.

6.4 Suggestions for Further Research

A number of investigations have been conducted in the past on various composites under hydrothermal ageing. Few of these have investigated the same in conditions of reverse thermal effects. However, once a composite is in close proximity of its saturation plateau, the moisture uptake is largelyunpredictablemore especially when the ambient temperature is dropped. This result in the composite taking in more moisture thus creating a new higher saturation plateau in a phenomenon often termed as reverse thermal effect. It is therefore suggested that further future work with this same composite system be conducted in environments that would create these effects.

REFERENCES

ADAMSON, M. J. 1983. "A conceptual model of the thermal-spike mechanism in graphite-epoxy laminates, Long-Term Behaviour of Composites". *ASTM STP*, 813**,** 179 - 191.

AHMAD, Z., ANSELL, M. P. & SMEDLEY, D. 2011. "Moisture Absorption Characteristics of Epoxy Based Adhesive Reinforced with CTBN and Ceramic Particles for Bonded-in Timber Connection: Fickian or Non-Fickian Behaviour". *Material Science and Engineering.*

ALESSI, S., CONDURUTA, D., PITARRESI, G., DISPENZA, C. & SPADARO, G. 2010. "Hydrothermal Ageing of Radiation Cured Epoxy Resin-Polyether Sulfone Blends as Matrices for Structural Composites". *Polymer Degradation and Stability,* 95**,** 677 - 683.

APICELLA, A., MIGLIARESI, C., NICOLAIS, L., IACCARINO, L. & S.ROCCOTELLING 1983. "The water ageing of unsaturated polyester based composites: Influence of resin chemical structure". *Composites,* 14**,** 387.

ASTM Standard E1922, 1997, "Test Method for Translaminar Fracture Toughness of Laminated Polymer Matrix Composite Materials", ASTM International, West Conshohocken, PA, 1997, DOI: 10.1520/E1922-97, www.astm.org

AVESTON, J., COOPER, G. A. & KELLY, A. 1971. Single and Multiple Fracture. *The Properties of Fibre Composites.* Surrey: IPC Science And Technology Press.

BAGHEPOUR, S. 2012. Fibre Reinforced Polyester Composites. *Polyester,* Dr. Hosam El-Din Saleh (Ed.), InTech, DOI: 10.5772/48697. Available from: http://www.intechopen.com/books/polyester/fibre-reinforced-polyester-composites.

BAI, S. L., WU, C. M. L., MAI, Y. W., ZENG, H. M. & LI, R. K. Y. 1999. "Failure Mechanisms of Sisal Fibres in Composites". *Advanced Composites Letters,* 8**,** 13 - 17.

BANEA, M. D., da SILVA, L. F. M., & CAMPILHO, R. D. S. G. 2011. "Effect of Temperature on Tensile Strength and Mode I Fracture Toughness of High Temperature Epoxy Adhensive". *Journal of Adhesion Sienceand Technology*, 26, 939 – 953.

BARTOS, P. 1980. "Analysis of Pull-out Tests on Fibre Embedded in Brittle Matrices". *Journal of Material Science,* 15**,** 3122-28

BESSEL, T. J. & MUTULI, S. M. 1982. "The Interfacial Bond Strength of Sisal Cement Composites using a Tensile Test". *Journal of Material Science Letters,* 1**,** 5 - 16.

BIRO, D. A., PLEIZIER, G. & DESLANDES, Y. 1993. "Application of the Microbond Technique: Effects of Hydrothermal Exposure on Carbon Fibre/Epoxy Interfaces". *Composite Science and Technology,* 46**,** 293 - 301.

BIRON, M. (ed.) 2003. *Thermoplastics and Thermoplastic Composites,* Amsterdam: ELSEVIER.

BISANDA, E. T. N. & ANSELL, M. P. 1991. "The Effect of Silane Treatment on the Mechanical and Physical Properties of Sisal-Epoxy Composites". *Composites Science and Technology,* 41**,** 165 - 178.

BOUALEM, N. & SEREIR, Z. 2011. "Accelerated Ageing of Unidirectional Hybrid Composites under the Long-Term Elevated Temperature and Moisture Concentration". *Theoretical and Applied Fracture Mechanics,* 55**,** 68 - 75.

BROWN, R. P., KOCKOTT, D., TRUBIROHA, P., KETOLA, W. & SHORTHOUSE, J. 1995. "A Review of Accelerated Durability Tests". *In:* BROWN, R. P. (ed.) *VAMAS Report No.18.* Versailles Project on Advanced Materials and Standards.

BUDUANSKY, B., EVANS, A. G. & HUTCHINGSON, J. W. 1995. "Fibre-Matrix Debonding Effectes on Cracking in Alighned Fibre Ceramic Composites". *International journal of Solid and Structures,* 32**,** 315 - 328.

BUDUANSKY, B., HUTCHINSON, J. W. & EVANS, A. G. 1986. "Matrix Fracture in Fibre-Reinforced Ceramics". *Journal of the Mechanics and Physics of Solids,* 34**,** 167-189.

CARTER, H. G. & KIBLER, K. G. 1978. "Langmuir-Type Model for Anomalous Moisture Diffusion In Composite Resins". *Journal of Composite Materials,* 12**,** 118 - 131.

CARVALHO, L. H. 1997. "Chemical Modification of Fibres for Plastics Reinforcement in Composites". *Lignocellulosic-Plastics Composites.* São Paulo: USP and UNESP.

CAUICH-CUPUL, J.I., PEREZ-PACHECO, E., VALADEZ-GONZALES, A., HERRERA-FRANCO, P.J. 2011. "Effect of Moisture Absorption on the Micromechanical Behaviour of Carbon Fibre/Epoxy Matrix Composites". *Journal of Material Science,* 46, 6664 – 6672.

CHAND, N., TIWARY, R. K. & ROHATGI, P. K. 1988. "Bibliography Resource Structure Properties of Natural Fibres – An Annotates Bibliography". *International Journal of Material Science,* 23**,** 381 – 387.

CHIN, J. W., HUGHES, W. L. & SIGNOR, A. 2001. "Elevated Temperature Ageing of Glass Fibre Reinforced Vinyl Ester and Isophthalic Polyester Composites in Water, Salt water and Concrete Pore Solution". *In:* American Society for Composites, 2001 Blacksburg, VA. The National Institute of Standards and Technology (NIST), 1-12.

COX, H. L. 1952. “The Elasticity and Strength of Paper and other Fibrous Materials”. *British Journal of Applied Physics,* 3.

CRAVEN, J. P., CRIPPS, R. & VINEY, C. 2000. “Evaluating the Silk/Epoxy Interface by means of the Microbond Test”. *Composites,* Part A**,** 653 – 660.

GAUR, U., CHOU, C. T. & MILLER, B. 1994. “Effect of Hydrothermal Ageing on Bond Strength”. *Composites,* 25**,** 609 - 612.

GAUR, U. & MILLER, B. 1990. “Effects of Environmental Exposure on Fiber/Epoxy Interfacial Shear Strength”. *Polymer Composites,* 11**,** 217 - 222.

GAUTIER, L., MORTAIGNE, B. & BELLENGER, V. 1999a. “Interface Damage Study of Hydrothermally Aged Glass-Fibre-Reinforced Polyester Composites”. *Composite Science and Technology,* 59**,** 2329 - 2337.

GAUTIER, L., MORTAIGNE, B. & BELLENGER, V. 1999b. “Interfacial Damage Studies of Hydrothermally Aged Glass Fibre Reinforced Polyester Matrix Composites”. *Composite Science and Technology,* 59**,** 2329 - 2337.

GEO, Y. C. & COTTERELL, B. 1988. “Fracture of Fibre-Reinforced Materials”. *ZAMP(Journal of Applied Mathematics and Physics),* 39**,** 550 -572.

GHORBEL, I. & VALENTIN, D. 1993. “Hydrothermal Effects on the Physico-Chemical Properties of Pure and Glass Fiber Reinforced Polyester and Vinylester Resins”.*Polymer Composites,* 14**,** 324 – 334.

GILLAT, O. & BROUTMAN, L. J. 1978. “Effect of an external stress on moisture diffusion and degradation in a graphite-reinforced epoxy laminate”. *Advanced Composite Materials—Environmental Effects, ASTM STP,* 658**,** 61 - 83.

GOPALAN, R., SOMASHEKAR, B. R. & DATTAGURU, B. 1989. “Environmental Effects on Fibre-Polymer Composites”. *Polymer Degradation and Stability,* 24**,** 361 - 371.

GRESZCZUK, L. B. 1969. “Theoretical Studies of the Mechanics of the Fiber–Matrix Interface in Composites”. *Interface in Composites,* ASTM STP 452**,** 49.

HORNSBY, P. R., HINRICHSEN, E. & TARVERDI, K. 1997. “Preparation and Properties of Polypropylene Composites Reinforced with Wheat and Flax Straw Fibres”. *Journal of Materials Science,* 32**,** 443 - 449.

INACIO, W. P., LOPES, F. P. D. & MONTEIRO, S. N. 2010. “Diameter Dependence of Tensile Strength by Weibull Analysis: Part III Sisal Fibre2. *Matéria (Rio J.),* 15**,** 124 - 130.

JEFFREY, K. J. T, TARLOCHIN, F, & RAHMAN M. M. 2011. “Residual Strength of Copped Strand Mat Glass Fibre/Epoxy Composite Structures: Effect of

Temperature and Water Absorption". *International Journal of Automobile and Mechanical Engineering.* Vol. 4, 504 – 419.

JOSEPH, K., PAVITHRAN, C., THOMAS, S., BABY, K. & PREMALATHA, C. K. 1994. "Melt Rheological Behaviour of Short Sisal Fibre Reinforced Polyethylene Composites". *Plastics, Rubber and Composites Processing and Applications,* 21**,** 237–245.

JOSEPH, K., THOMAS, S. & PAVITHRAN, C. 1992. "Viscoelastic Properties of Short Sisal Fibre Filled Low Density Polyethylene Composites". *Material Letters,15***,** 224 - 228.

JOSEPH, K., THOMAS, S. & PAVITHRAN, C. 1993. "Tensile Properties of Short Sisal Fibre Reinforced Polyethylene Composites". *Journal of Applied Polymer Science,* 47**,** 1731 - 1739.

JOSEPH, K., THOMAS, S. & PAVITHRAN, C. 1995. "Effects of Ageing on the Physical and Mechanical Properties of Sisal Fibre Reinforced Polyethylene Composites". *Composite Science and Technology,* 53**,** 99 - 110.

JOSEPH, K., THOMAS, S. & PAVITHRAN, C. 1996. "Influence of Interfacial Addition on the Mechanical Properties and Fracture Behaviour of Short Sisal Fibre Reinforced Polymer Composites". *European Polymer Journal,* 32**,** 1243 - 1250.

KALAPRASAD, G., JOSEPH, K. & THOMAS, S. 1997. "Influence of Short Glass Fibre Addition on the Mechanical Properties of Sisal Reinforced Low Density Polyethylene Composites". *Journal of Composite Materials,* 31**,** 5.

KANYANGA, S. B. 1988. *Fatigue and Fracture Behaviour of Carbon Fibre Reinforced Plastics.* PhD Thesis, University of Sheffield.

KARBHARI, V. M. 2004." E-Glass/Vinylester Composites in Aqueous Environments: Effects on Short-Beam Shear Strength". *Journal of Composites for Construction,* 8**,** 148 - 156.

KENNEDY, K. C., CHEN, T. & KUSY, R. P. 1998. "Behaviour of Photopolymerised Silicate Glass Fibre-Reinforced Dimethacrylate Composites Subjected to Hydrothermal Ageing: Part II. Hydrolytic Stability of Mechanical Properties". *Journal of Materials Science: Material Medicine,* 9**,** 651 - 660.

KIM, J. K. & MAI, Y. W. (eds.) 1998. *Engineered Interfaces in Fibre Reinforced Composites,* Oxford: Elsevier Science Ltd.

KOTANI, M., YASUFUKU, Y., TAMAISHI, Y. & KAWANDA, H. 2010. "Study of Strength Degradation Mechanism of Woven GFRP in Water Environment". *Journal of Solid Mechanics and Materials Engineering,* 4**,** 1574 - 1584.

KUMAR, R. P., AMMA, M. L. G. & THOMAS, S. 1995. "Short Sisal Fibre Reinforced Styrene- Butadiene Rubber Composites". *Journal of Applied Polymer Science,* 58**,** 597 – 612.

LAWRENCE, P. 1972. "Some Theoretical Considerations of Fibre Pull-out From an Elastic Matrix". *Journal of Material Science,* 7, 1 – 6.

LI, H., ZADORECKI, P. & FLODIN, P. 1987. "Cellulose Fibre-Polyester Composites with Reduced Water Sensitivity, Chemical Treatment and Mechanical Properties". *Polymer Composites,* 8**,** 199 – 207.

LI, X., TABIL, L. G. & PANIGRAHI, S. 2007. "Chemical Treatments of Natural Fiber for Use in Natural Fiber-Reinforced Composites: A Review". *Journal of Polymers and the Environment,* 15**,** 25 - 33.

LI, Y., MAI, Y. & YE, L. 2000a. "Sisal Fibre and its Composites: A Review of Recent Developments". *Composites Science and Technology,* 60**,** 2037 - 2055.

LI, Y., MAI, Y. W. & YE, L. 2000b "Microstructure and Mechanical Properties of Sisal Fibre and Adhesion to Vinyl Ester Resin". *In:* Proceedings of the 9th European Conference on Composite Materials (ECCM-9), Brighton, UK. IOM Communications Ltd, London.

LI, Y., MAI, Y. W. & YE, L. 2006. "Fracture properties and characteristics of sisal textile reinforced epoxy composites". *Key Engineering Materials,*, 312**,** 167-172.

LIANG, K., SHI, S.Q., NICHOLAS, D.D., & SITES, L.2013. "Accelerated weathering test of kenaf fibre unsaturated polyester sheet moulding compounds". *Wood and Fibre Science,* 45, 1, 42–48.

LUYT, A. S. & MALUNKA, M. E. 2005. "Composites of Low-Density Polyethylene and Short Sisal Fibres: The Effect of Wax Addition and Peroxid Treatment on the Thermal Properties". *Thermochimica Acta,* 426**,** 101 – 107.

MANIKANDAN, K. C., NAIR, S. M. D. & THOMAS, S. 1996. "Tensile Properties of Short Sisal Fibre Reinforced Polystyrene Composites". *Journal of Applied Polymer Science,* 60**,** 1483 - 1497.

MARCOVICH, N., REBOREDO, M. M. & ARANGUREN, M. I. 1997. "Chemical Modification of Lignocellulosic Materials: The Utilisation of Natural Fibers as Polymer Reinforcement". *Lignocellulosic-Plastics Composites.* São Paulo: USP/UNESP.

MAROM, G. 1976. "The Role of Water Transport in Composite Materials". *Journal of Composite Materials,* 10**,** 341 - 374.

MAROM, G. & BROUTMAN, L. J. 1981. "Moisture in epoxy resin composites". *Journal of Adhesives,* 12**,** 153 - 164.

MARSHALL, D. B. & COX, B. N. 1987. "Tensile Properties of Brittle Matrix Composites: Influence of Fibre Strength". *Acta Metallurgica et Materialia,* 35**,** 2607 - 2619.

MARSHALL, D. B., COX, B. N. & EVANS, A. G. 1985. "The Mechanics of Matrix Cracking in Brittle-Matrix Fibre composites". *Acta Metallurgica et Materialia,* 33**,** 2013 - 2021.

MATSAGAR, V. 2014. "Advances in Structural Engineering: Materials, Volume Three". Springer. pp 1656 – 1657.

MAXWELL, A. S., BROUGHTON, W. R., DEAN, G. & SIMS, G. D. 2005. "Review of Accelerated Ageing Methods and Lifetime Prediction Techniques for Polymeric Materials", NPL Report DEPC MPR 016, National Physical Laborotory.

MENARD, K. P. 1999. "Dynamic Mechanical Analysis: A Practical Introduction". London, CRC Press.

MILLER, B., MURI, P. & REBENFELD, L. 1987. "A Microbond Method for Determination of the Shear Strength of a Fiber/Resin Interface", *Composite Scienceand Technology*, 28**,** 17 - 32.

MOUZAKIS, D. E., ZOGA, H. & GALIOTIS, C. 2007. "Accelerated Environmental Ageing Study of Polyester/glass Fibre Reinforced Composites (GFRPCs)". *Composites,* 39**,** 467 – 475.

MUKHERJEE, P. S. & SATYANARAYANA, K. G. 1984. "Structure and Properties of some Vegetable Fibres". *Journal of Materials Science,* 19**,** 3925 - 3934.

MULA, S., BERA, T., RAY, P. K. & RAY, B. C. 2006. "Effects of Hydrothermal Aging on Mechanical Behaviour of Sub-zero Weathered GFRP Composites". *Journal of Reinforced Plastics and Composites,* 25**,** 673 - 680.

NATURAL FIBRES. August 2014**.** "Sisal - Too coarse for clothing and upholstery, sisal is replacing glass fibres in composite materials used to make cars and furniture", http://www.naturalfibres2009.org/en/fibres/sisal.html

BABY N. S., SAKTHIESWARAN N., BRINTHA G. S., & BABU O. G., 2016. " A Review on Hybrid Composites Reinfroced with Sisal Fibres, Glass Fibres, Steel Fibres and Prosopis Luliflora". *International Journal for Research in Applied Science & Engineering Technology*, 4(5), 449 – 451,

PAGANO, N. J. & KIM, R. Y. 1994. “Progressive Microcracking in Unidirectional Brittle Matrix Composite”. *Mechanics of Composite Materials and Structures,* 30**,** 3 - 29.

PAI, S. & CHANDRA, K. L. 2013. “Analysis of Polyester Fibre-Reinforced Concrete Subjected toElevated Temperatures”. *International Journal of Civil, Structural, Environmental and Infrastructure Engineering Research and Development,* 3**,** 1-10.

PANIGRAHI, A. & MALLICK, S. R. 2009. *Characterisation of Hybrid FRP Composite with Hydrothermal Exposure Under Varied Ambient Conditions.* MSc Metallurgical and Materials Engineering, National Institute of Technology.

PARAMASIVAM, T. & ABDULKALAM, A. P. J. 1974. “On the Study of Natural Fibre Composites”. *Fibre Science and Technology,* 7**,** 85-98.

PAVITHRAN, C., MUKHERJEE, P. S., BRAHMAKUMAR, M. & DAMONDARAN, A. D. 1987. “Impact Properties of Natural Fibre Composites”. *Journal of Materials Science Letters,* 6**,** 882 - 884.

PAVITHRAN, C., MUKHERJEE, P. S., BRAHMAKUMAR, M. & DAMONDARAN, A. D. 1988. “Impact Performance of Sisal – Polyester Composites”. *Journal of Materials Science Letters,* 7**,** 825 - 826.

PAVLIDOU, S., KRASSA, K. & PAPASPYRIDES, C. D. 2005. “Woven Glass Fabric/Polyester Composites: Effect of Interface Tailoring on Water Absorption”. *Journal of Applied Polymer Science,* 98**,** 843 - 851.

PHANI, K. K. & BOSE, N. R. 1987. “Temperature Dependence of Hydrothermal Ageing of CSM- Laminate During Water Immersion”. *Composites Science and Technology,* 29**,** 79 - 87.

PITKETHLY, M. J., FAVRE, J. P., GAUR, U., JAKUBOWSKI, J., MUDRICH, S. F., CALDWELL, D. L., DRZAL, L. T., NARDIN, M., WAGNER, H. D., LANDRO, L. D., HAMPE, A., ARMISTEAD, J. P. & VERPOEST, M. D. I. 1993. “A Round-Robin Programme on Interfacial Test Methodes”. *Composite Science and Technology,* 48**,** 205 - 214.

PUITEL, A. C., TOFANICA, B. M., GAVRILESCU, D. & PETREA, P. V. 2011. “Environmentally Sound Vegetal Fiber–Polymer Matrix Composites”. *Cellulose Chemistry and Technology,* 45**,** 265 - 274.

RAMAKRISHNA, T. B. 1990. “*Influence of Interfacial Shear Strength on the Mechanical Properties of SiC Fibre Reinforced Reaction-Bonded Silicon Nitride Matrix Composites”.* Advanced Metals and Ceramic Material Composites Symposium, Technical Report 90-C-003.

RAY, B. C. 2006. “Effects of Changing Environment and Loading Speed on Mechanical Behaviour of FRP Composites”. *Journal of Reinforced Plastics and Composites,* 25**,** 1227 - 1240.

RONG, M. Z., ZHANG, M. Q., YANG, G. C. & ZENG, H. M. 2001. “Treatment on the Mechanical Properties of Unidirectional Sisal Reinforced Epoxy Composites”. *Composite Science Technology,* 61**,** 1437 – 1447.

ROSATO, D. V., ROSATO, D. V. & ROSATO, M. V. 2004. *Plastic Product Material and Process Selection Handbook,* Oxford, Elsevier Science & Technology Books.

ROY, R., SARKAR, B. K. & BOSE, N. R. 2001. “Effects of Moisture on the Mechanical Properties of Glass Fibre Reinforced Vinylester Resin Composites”. *Bulletin of Materials Science,* 24**,** 87 - 94.

SATYANARAYANA, K. G., SUKUMARAN, K., MUKHERJEE, P. S., PAVITHRAN, C. & PILLAI, S. G. K. 1984”. Possibility of using Natural Fibre Composites as Building Materials”. *In:* International Conference on Low Cost Housing for Developing Countries, 177-181.

SATYANARAYANA, K. G., SUKUMARAN, K., MUKHERJEE, P. S., PAVITHRAN, C. & PILLAI, S. G. K. 1990. “Natural Fiber-polymer Composites”. *Journal of Cement and Concrete Composites,* 12**,** 117 - 136.

SHEN, C. H. & SPRINGER, G. S. 1976a. “Moisture absorption and desorption of composite Materials”. *Journal of Composite Materials,* 10**,** 2-20.

SHEN, C. H. & SPRINGER, G. S. 1976b. “Moisture Absorption and Desorption of Composite Materials”. *Journal of Composite Materials,* 10**,** 2 - 20.

SHEN, C. H. & SPRINGER, G. S. 1977. “Effects of moisture and temperature on the tensile strength of composite materials”. *Journal of Composite Materials,* 11**,** 2–16.

SHIRRELL, C. D., HALPIN, J. C. & BROWNING, C. E. 1976. “Moisture—an assessment of its impact on the design of resin based advanced composites”. *NASA Technical Report.* NASA.

SINGH, B., GUPTA, M. & VERMA, A. 1996. “Influence of Fibre Surface Treatment on the Properties of Sisal-Polyester Composites”. *Polymer Composites,* 17**,** 910 - 918.

SPRINGER, G. S., TUNG, R. W. & SANDERS, B. A. 1980. “Moisture Absorption of Polyester-E Glass Composites”. *Journal of Composite Materials,* 14**,** 142-154.

SREEKALA, M. S. & THOMAS, S. 2003. “Effects of Fibre Surface Modification on Water-Sorption Characteristics of Oil Palm Fibres”. *Composite Science Technology* 63**,** 861–869.

SURATHI, P. & KARBHARI, V. M. 2006. “Hygrothermal Effects on Durability and moisture Kinetics of Fiber-Reinforced Polymer Composites”. *Technical Report.* California: University of California.

SURATHI, P. & KARGHARI, V. M. 2006. “Hydrothermal Effects on Durability and Moisture Kinematics of Fibre Reinforced Polymer Composites”. San Diego: University of California.

TAKAKU, A. & ARRIDGE, R. G. E. 1973. “The Effect of Interfacial Radial and Shear Stress on Fiber Pull-out in Composite Materials”. *Journal of Applied Physics,* 6**,** 2038-47.

THAIS, H. D., SYDENSTRICKER, S. M. & SANDRO, C. A. 2003. “Pull-out and other Evaluations in Sisal Reinforced Polyester Biocomposites”. *Polymer Testing,* 22**,** 375 – 380.

THOMASON,J.L. 1995a. “The Interface Region in Glass Fibre-Reinforced Epoxy Resin Composites:1 Sample Preparation, Void Content and Interfacial Strength”. *Composites,* 26,467–475.

THOMASON,J.L. 1995b. “The Interface Regionin Glass Fibre-Reinforced Epoxy Resin Composites:2 Water Absorption, Void Content and Interface”. *Composites,* 26, 477–485.

THOMASON, J. L. & SCHOOLENBERG, G. E. 1994. “An Investigation of Glass Fibre/Polypropylene Interface Strength and its Effect on Composite Properties”. *Composites,* 25**,** 197 - 203.

SCHUTTE, C. L. 1994. “Environmental Durability of Glass Fibre Composites”. *Material Science and Engineering Report,* 13(7): 265 – 324.

VALADEZ-GONZALEZ, A., CERVANTES, J. M., OLAYO, R. & HERRERA-FRANCO, P. J. 1999. “Effects of Fibre Surface Treatment on Fibre-Matrix Bond Strength of Natural Fibre Reinforced Composites”. *Composites* 30**,** 300 – 320.

VERGHESE, K. N. E., HAYES, M. D., GARCIA, K., WOOD, J., RIFFLE, J. S. & LESKO, J. J. 1999. “Influence of Matrix Chemistry on the Short Term, Hydrothermal Aging of Vinyl Ester Matrix and Composites Under Both Isothermal and Thermal Spiking Conditions”. *Journal of Composite Materials,* 33**,** 1918 - 1938.

Wan, Y.Z., Wang, Y.L., Luo, H.L, Dong, X.H. & Cheng G.X. 2002. “Moisture absorption behaviour of C_{3D}/EP composite and effect of external stress”. *Material Science and Engineering,* 326, 2, 324 – 329.

WEAVING – University of Texas. August 2014. https://classes.lt.unt.edu/Spring_2011/CECS_5420_020/cmv0046/assign5/floor.html

WRIGHT, W. W. 1981. "The effect of diffusion of water into epoxy resins and their carbon fibre reinforced composites". *Composites,* 12**,** 201-205.

YANG, L. & THOMASON, J. L. 2010. "Interface Strength in Glass Fibre–Polypropylene Measured using the Fibre Pull-Out and Microbond Methods". *Composites,* Part A**,** 1077 – 1083.

YILMAZ, T. & SINMAZCELIK, T. 2010. "Effects of Hydrothermal Aging on Glass–Fibre/Polyetherimide (PEI) Composites". *Journal of Materials Science,* 45**,** 399 – 404.

ZHANDAROV, S. & MADER, E. 2005. "Characterization of fiber/matrix interface strength: applicability of different tests, approaches and parameters". *Composite Science and Technology,* 65**,** 149 - 160.

ZHANG, S. 2010. "Handbook of Nanostructured Thin Films and Coatings: Mechanical Properties - Volume 1". London: CRC Press. pp 512.

ZHAO, D. & BOTSIS, J. 1996. "Experimental and Numerical Studies in Model Composites, Part I: Experimental Results". *International Journal of Fracture,* 86**,** 153–174.

U.S. Congress, Office of Technology Assessment. 1998. "Advanced Materials by Design". , OTA- E-351. Washington, DC: U.S. Government Printing Office.

APPENDICES

APPENDIX A

CLEVISES FOR THE COMPACT TENSION SPECIMEN TEST FIXTURES FOR THE K_{IC} TEST SPECIMENS.

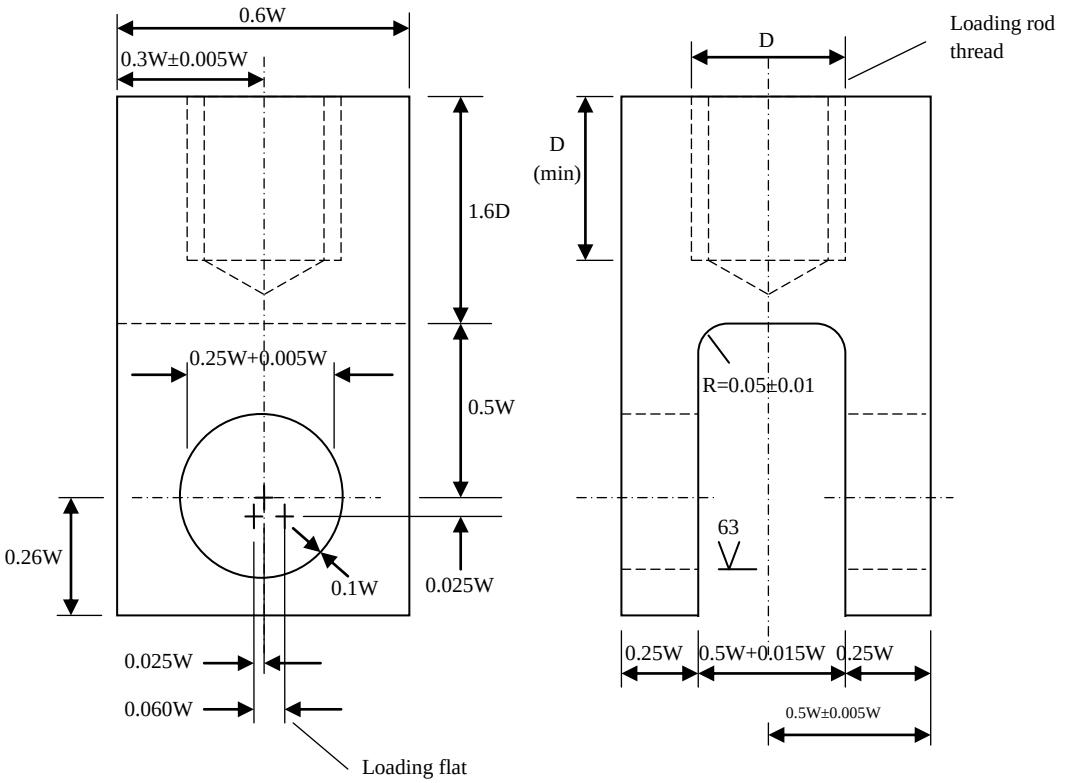

Figure A1: Clevises for the compact tension testing fixture.

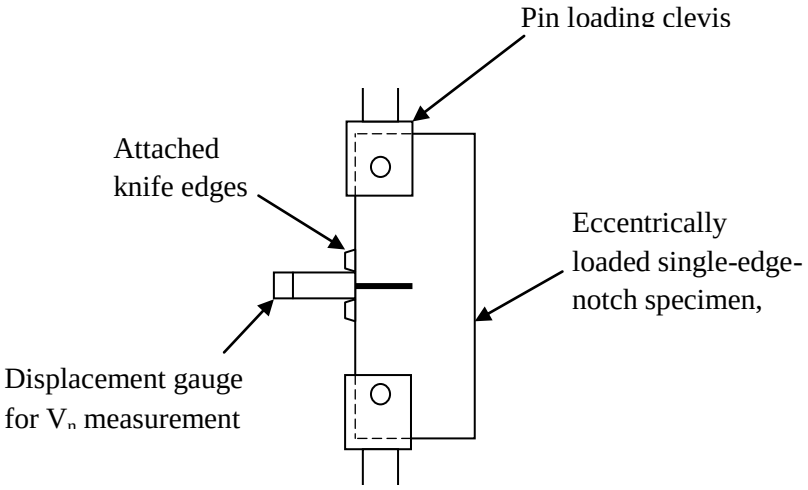

Figure A2: Fracture Toughness Testing Fixture arrangement

APPENDIX B

MathCAD MOISTURE DIFFUSION DATA FITTING ALGORITHM.

B.1. Fickian Diffusion model - 23^{o}C Treated Specimens

The MathCAD's genfit function was used to find the corresponding fitting parameters for the nonlinear fit. The function genfit (vx, vy, vg, f) denotes the vector having the parameters that make a function of x and parameters uo and u1(maximum moisture content and diffusion coefficients respectively) which best approximate the data in vx and vy.

vx = time(days)(Input)
vy = percentage moisture gain after immersion in water
vg = vector of guess values for Mm and Dc (Input) (guess values vector for M_m and D_c)
l = thickness of the specimen in m (specimen thickness (m))
nmax = maximum number of iterations (maximum amount of iterations)
g(r, p)0 = function which gives the values of the percentage moisture gain fitted to the data in vx and vy (Output)
r = is the vector of time increments for which genfit calculates the percentage moisture gain

$$vx := \begin{bmatrix} 0 \\ 1 \\ 2 \\ 5 \\ 6 \\ 7 \\ 9 \\ 12 \\ 13 \\ 14 \\ 15 \\ 19 \\ 22 \\ 23 \\ 37 \\ 43 \\ 50 \\ 58 \\ 69 \\ 84 \\ 113 \\ 150 \end{bmatrix} \qquad vy := \begin{bmatrix} 0 \\ 0.125 \\ 0.1975 \\ 0.2875 \\ 0.315 \\ 0.3275 \\ 0.3625 \\ 0.38 \\ 0.375 \\ 0.3875 \\ 0.4 \\ 0.4275 \\ 0.445 \\ 0.44 \\ 0.47 \\ 0.475 \\ 0.52 \\ 0.505 \\ 0.4975 \\ 0.46 \\ 0.4525 \\ 0.4025 \end{bmatrix}$$

$$f(z,u) := \begin{bmatrix} u_0 \cdot \left[1 - \frac{8}{\pi^2} \cdot \sum_{n=0}^{nmax} \left[\frac{1}{(2 \cdot n + 1)^2} \, exp\left[\frac{-u}{1^2} \cdot (2 \cdot n + 1)^2 \right] \right] \right] \\ 1 - \frac{8}{\pi^2} \cdot \sum_{n=0}^{nmax} \left[\frac{1}{2 \cdot n + (1)^2} \cdot exp\left[\frac{-u_1}{1^2} \cdot z \cdot \pi^2 \cdot (2 \cdot n + 1)^2 \right] \right] \\ \frac{-8}{\pi^2} \cdot u_0 \cdot \sum_{n=0}^{nmax} \left[\frac{-z \cdot n^2}{1^2} \cdot exp\left[\frac{-u_1}{1^2} \cdot z \cdot \pi^2 (2 \cdot n + 1)^2 \right] \right] \end{bmatrix}$$

$$p := genfit(vx, vy, vg, f)$$

$$vg := \begin{bmatrix} 0.7 \\ 0.00000005 \end{bmatrix}$$

$$r := 0, 1 .. 150$$

$$g(r) := f(r, p)$$

$$nmax := 21$$

B.2. Fickian Diffusion model - 40°C Specimens

$$vx := \begin{bmatrix} 0 \\ 1 \\ 2 \\ 5 \\ 6 \\ 7 \\ 9 \\ 12 \\ 13 \\ 14 \\ 15 \\ 19 \\ 22 \\ 23 \\ 37 \\ 43 \\ 50 \\ 58 \\ 69 \\ 84 \\ 113 \\ 150 \end{bmatrix} \qquad vy := \begin{bmatrix} 0 \\ 0.2375 \\ 0.3325 \\ 0.36 \\ 0.365 \\ 0.3825 \\ 0.385 \\ 0.38 \\ 0.3725 \\ 0.39 \\ 0.375 \\ 0.385 \\ 0.3925 \\ 0.3925 \\ 0.3925 \\ 0.4125 \\ 0.4275 \\ 0.415 \\ 0.4175 \\ 0.4075 \\ 0.405 \\ 0.405 \end{bmatrix}$$

$$f(z,u) := \begin{bmatrix} u_0 \cdot \left[1 - \frac{8}{\pi^2} \cdot \sum_{n=0}^{nmax} \left[\frac{1}{(2 \cdot n + 1)^2} \, exp\left[\frac{-u}{1^2} \cdot (2 \cdot n + 1)^2 \right] \right] \right] \\ 1 - \frac{8}{\pi^2} \cdot \sum_{n=0}^{nmax} \left[\frac{1}{2 \cdot n + (1)^2} \cdot exp\left[\frac{-u_1 \cdot z \cdot \pi^2}{1^2} \cdot (2 \cdot n + 1)^2 \right] \right] \\ \frac{-8}{\pi^2} \cdot u_0 \cdot \sum_{n=0}^{nmax} \left[\frac{-z \cdot n^2}{1^2} \cdot exp\left[\frac{-u_1}{1^2} \cdot z \cdot \pi^2 (2 \cdot n + 1)^2 \right] \right] \end{bmatrix}$$

$p := genfit(vx, vy, vg, f)$

$vg := \begin{bmatrix} 0.7 \\ 0.00000005 \end{bmatrix}$

$r := 0,1..150$

$g(r) := f(r, p)$

$nmax := 21$

B.3. Fickian Diffusion model - 60°C Specimens

$$vx := \begin{bmatrix} 0 \\ 1 \\ 2 \\ 5 \\ 6 \\ 7 \\ 9 \\ 12 \\ 13 \\ 14 \\ 15 \\ 19 \\ 22 \\ 23 \\ 37 \\ 43 \\ 50 \\ 58 \\ 69 \\ 84 \\ 113 \\ 150 \end{bmatrix} \qquad vy := \begin{bmatrix} 0 \\ 0.41 \\ 0.44 \\ 0.4366 \\ 0.44 \\ 0.4433 \\ 0.4433 \\ 0.45 \\ 0.4466 \\ 0.4533 \\ 0.4466 \\ 0.4366 \\ 0.4333 \\ 0.43 \\ 0.3966 \\ 0.4 \\ 0.4266 \\ 0.4133 \\ 0.4033 \\ 0.3766 \\ 0.3566 \\ 0.37 \end{bmatrix}$$

$$f(z,u) := \begin{bmatrix} u_0 \cdot \left[1 - \frac{8}{\pi^2} \cdot \sum_{n=0}^{nmax} \left[\frac{1}{(2 \cdot n + 1)^2} \, exp\left[\frac{-u}{1^2} \cdot (2 \cdot n + 1)^2 \right] \right] \right] \\ 1 - \frac{8}{\pi^2} \cdot \sum_{n=0}^{nmax} \left[\frac{1}{2 \cdot n + (1)^2} \cdot exp\left[\frac{-u_1 \cdot z \cdot \pi^2}{1^2} \cdot (2 \cdot n + 1)^2 \right] \right] \\ \frac{-8}{\pi^2} \cdot u_0 \cdot \sum_{n=0}^{nmax} \left[\frac{-z \cdot n^2}{1^2} \cdot exp\left[\frac{-u_1}{1^2} \cdot z \cdot \pi^2 (2 \cdot n + 1)^2 \right] \right] \end{bmatrix}$$

$p := genfit(vx, vy, vg, f)$

$$vg := \begin{bmatrix} 0.7 \\ 0.00000005 \end{bmatrix}$$

$r := 0, 1 .. 150$

$g(r) := f(r, p)$

$nmax := 21$

APPENDIX C

SINGLE FIBRE TENSILE TEST RESULTS

Untreated sisal fibre tensile test results

Table C1: Single sisal fibre tensile test results. (Non-hydrothermally treated)

Sample ID	Fmax (mN)	DisplMax (um)	StrainMax (%)	E (MPa)	σ_{Max} (MPa)
1	2550	609.1	2.03	13480	273.3
2	4958	747.4	2.491	22950	572.6
3	4739	737.9	2.46	20660	507.9
4	4152	833.2	2.777	16020	445
5	5295	719.9	2.4	49960	1198
6	3080	584	1.947	35810	697.1
7	4002	773.9	2.58	35150	906
8	3779	541.2	1.804	47450	855.3
9	4651	648.6	2.162	48820	1053
10	5004	595.1	1.984	57350	1133
11	2013	573.2	1.911	58650	372.3
12	3143	760.7	2.536	23570	528.7
13	3592	787.7	2.626	23050	604.3
14	4377	783.6	2.612	28240	736.3
15	4863	707.7	2.359	34680	818
16	7584	761.6	2.539	34580	875.9
17	3659	409.6	1.365	30990	422.6
18	1371	348.1	1.16	15900	158.3
19	2403	586.6	1.955	15450	277.5
20	8297	713.4	2.378	78990	1878
21	8291	682.1	2.274	82510	1877
22	7655	667.2	2.223	78090	1733
23	6912	770.5	2.568	61670	1733
24	9561	683.7	2.279	63460	1438
25	5473	556.5	1.855	44540	823.4

Sample ID	Fmax (mN)	DisplMax (um)	StrainMax (%)	E (MPa)	σ_{Max} (MPa)
Avg	4856.16	663.3	2.211	40880.8	869.98
StdDev	2133.442	119.1845	0.39736	21097.76	503.8904
Max	9561	833.2	2.777	82510	1878
Min	1371	348.1	1.16	13480	158.3

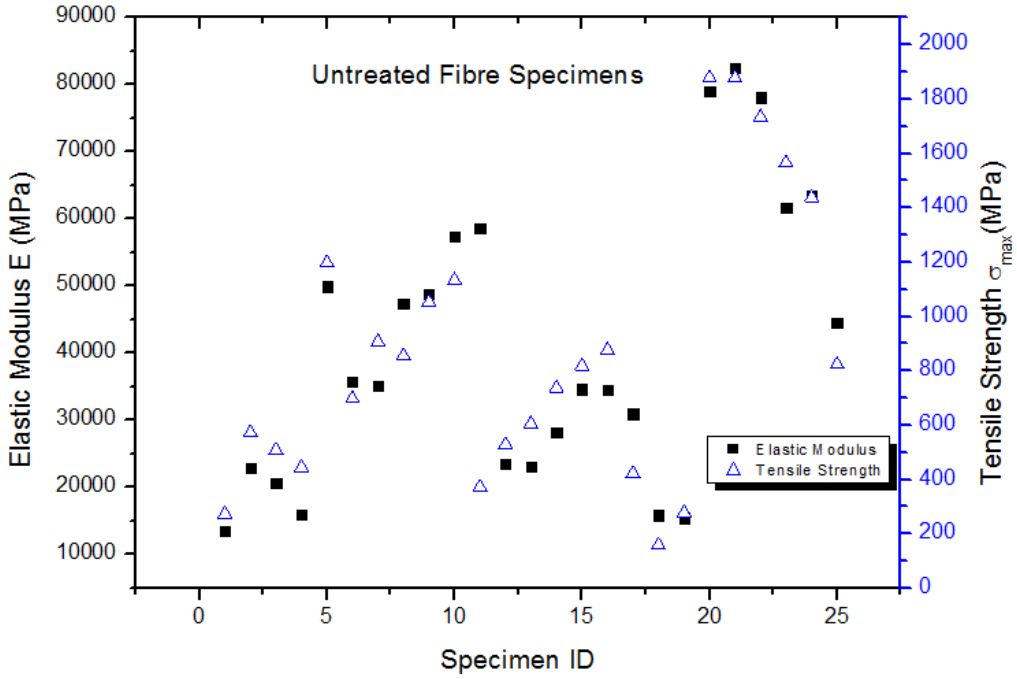

Figure C1: Tensile properties distribution for non-hydrothermally aged single sisal fibre tested specimens.

After one month of hydrothermal treatment of single sisal fibre samples

23^{o}C Samples

Table C2: Single sisal fibre tensile test results after 30 days of hydrothermal treatment of test specimens at 23^{o}C.

Sample Code	Max Load (mN)	Max Disp (um)	Max Strain (%)	E (MPa)	σ_{Max} (MPa)
3	9326	779.8	2.599	2599	515.2

Sample Code	Max Load	Max Disp	Max Strain	E	σ_{Max}
8	9911	849.5	2.832	55240	1558
4	8077	801.9	2.673	16020	428.1
9	8790	881.4	2.938	47550	1382
2	10000	7740	2.58	20540	530
6	8872	748.1	2.494	55940	1395
10	10000	871.3	2.904	54120	1572
13	9879	784.6	2.615	33420	873.5
7	10000	748.4	2.495	63020	1572
5	8484	802.7	2.676	16830	449.6
12	10000	766.7	2.556	34760	884
1	7726	724.8	2.416	16970	409.5
14	10000	784.1	2.614	33839	884.3
11	10000	608.2	2.027	43610	884.2
Avg	**9361.785714**	**1277.964**	**2.601357**	**35318.43**	**952.6714**
StdDev	**817.0367828**	**1861.126**	**0.22511**	**18620.38**	**458.0231**
Max	**10000**	**7740**	**2.938**	**63020**	**1572**
Min	**7726**	**608.2**	**2.027**	**2599**	**409.5**

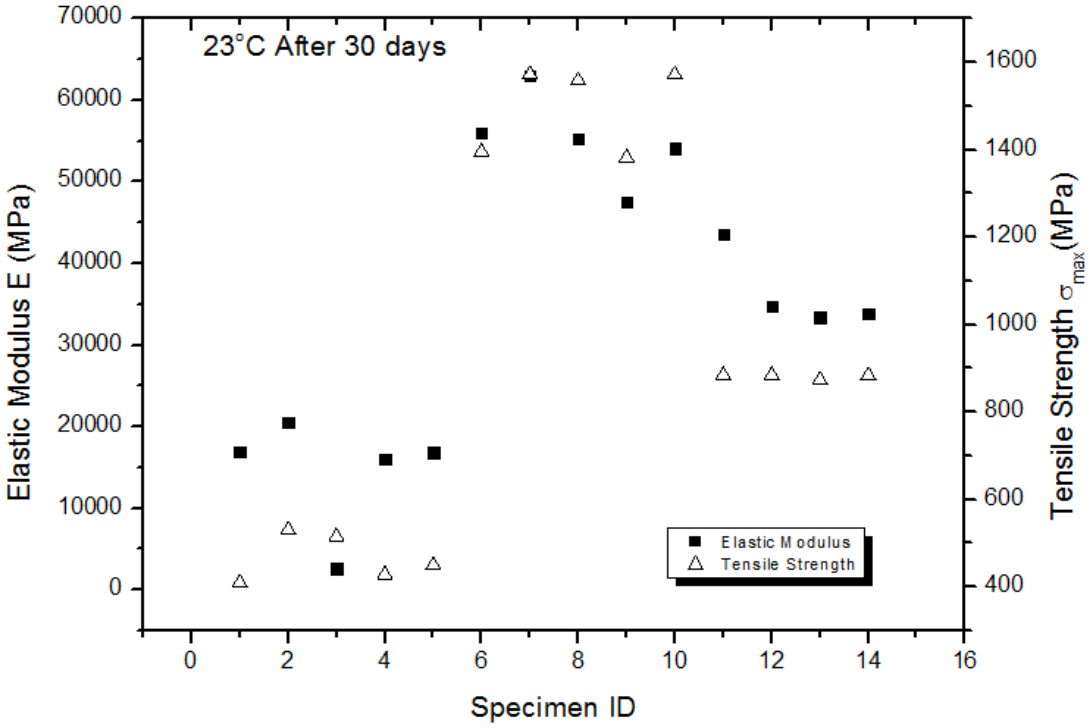

Figure C2: Tensile properties distribution for single sisal fibre test specimens after 30 days of hydrothermal ageing at 23°C.

40°C Specimens

Table C3: Single sisal fibre tensile test results after 30 days of hydrothermal treatment of test specimens at 40°C.

Sample Code	Max Load	Max Disp	Max Strain	E	σ_{Max}
	(mN)	(um)	(%)	(MPa)	(MPa)
8	6483	616.4	2.055	36770	748.7
10	10000	643.1	2.144	59380	1273
6	4770	644.1	2.147	34980	749.8
5	4255	886.2	2.954	32630	963.1
2	6820	919.5	3.065	50340	1544
1	9386	1049	3.496	60800	2125
4	3028	726.1	2.42	28400	685.5
7	4707	587.6	1.959	27750	543.9

Sample Code	Max Load	Max Disp	Max Strain	E	σ_{Max}
	(mN)	(um)	(%)	(MPa)	(MPa)
3	5558	854	2.847	44170	1258
9	10000	858.9	2.863	40330	1155
Avg	**6500.7**	**778.49**	**2.595**	**41555**	**1104.6**
StdDev	**2519.29448**	**155.8762**	**0.519373**	**11939.8**	**477.4141**
Max	**10000**	**1049**	**3.496**	**60800**	**2125**
Min	**3028**	**587.6**	**1.959**	**27750**	**543.9**

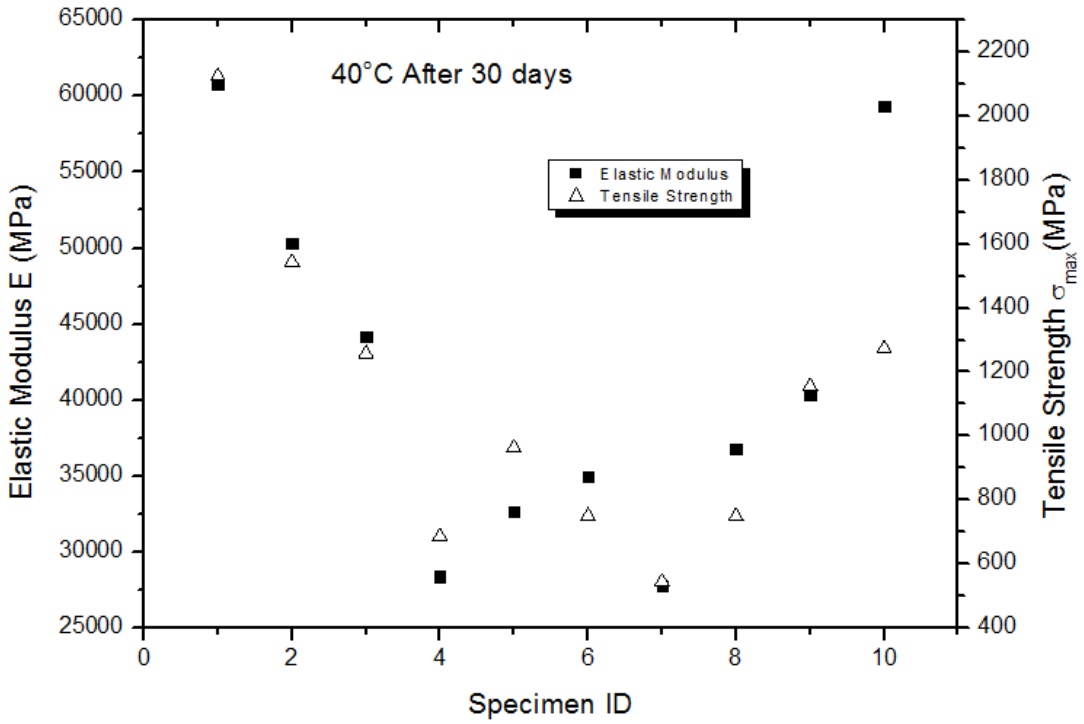

Figure C3: Tensile properties distribution for single sisal fibre test specimens after 30 days of hydrothermal ageing at 40^{o}C.

60^{o}C Samples

Table C4: Single sisal fibre tensile test results after 30 days of hydrothermal treatment of test specimens at 60^{o}C.

Sample Code	Max Load	Max Disp	Max Strain	E	σ_{Max}
	(mN)	(um)	(%)	(MPa)	(MPa)
6	9095	3180	10.6	19820	1430
12	8044	1028	3.428	27140	929
8	8140	1126	3.754	34080	1280
11	7546	1904	6.347	16150	871.4
4	10000	801.8	2.673	17640	605.4
5	10000	594.7	1.982	30550	605.6
1	10000	634.3	2.114	28620	605.6
14	10000	1103	3.677	31610	1155
3	10000	628	2.093	28900	605.6
15	10000	943.9	3.146	36820	1155
10	9909	900	3	51980	1558
13	8140	953.6	3.179	29560	940
7	8763	1643	5.478	31250	1377
2	10000	596.9	1.99	30450	605.6
Avg	**9259.785714**	**1145.514**	**3.818643**	**29612.14**	**980.2286**
StdDev	**938.6523219**	**699.8546**	**2.332955**	**8807.972**	**346.6836**
Max	**10000**	**3180**	**10.6**	**51980**	**1558**
Min	**7546**	**594.7**	**1.982**	**16150**	**605.4**

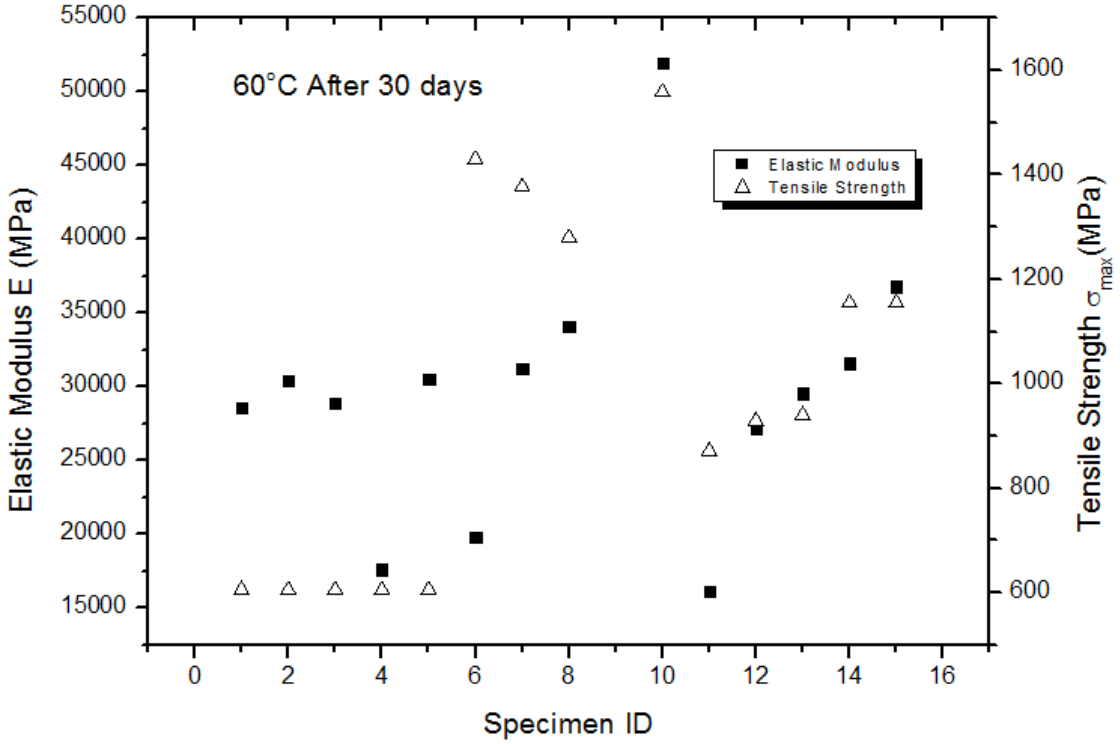

Figure C4: Tensile properties distribution for single sisal fibre test specimens after 30 days of hydrothermal ageing at 60^{o}C.

After two (2) month of hydrothermal treatment of single sisal fibre samples

23^{o}C treated specimens

Table C5: Single sisal fibre tensile test results after 60 days of hydrothermal treatment of test specimens at 23^{o}C.

Sample ID	Fmax (mN)	DisplMax (um)	StrainMax (%)	E (Mpa)	σ_{Max} (Mpa)
1	2476	354.2	1.181	69390	820
2	4210	1087	3.625	38410	1395
3	2203	679.4	2.265	19330	438.3
4	2435	785.3	2.618	18590	484.4
5	4299	892.2	2.974	28710	855.2
6	2854	802.7	2.676	21220	567.9
7	3424	746	2.487	28540	681.1

Sample ID	Fmax (mN)	DisplMax (um)	StrainMax (%)	E (Mpa)	σ_{Max} (Mpa)
8	5979	722.6	2.409	35070	843.5
9	6324	787	2.623	34180	892.1
10	6856	830.3	2.768	35000	967.3
11	6424	871.3	2.904	43470	906.2
12	4529	652.5	2.175	29940	639
13	9615	738.5	2.462	26260	642.9
14	10000	780.6	2.602	25700	668.6
15	10000	756.5	2.522	26490	668.6
16	10000	682.4	2.275	29400	668.6
17	8329	833.5	2.778	21590	556.8
18	10000	560.6	1.869	26600	497.4
19	10000	616.7	2.056	24210	497.4
20	4906	418.6	1.395	17520	244
21	9664	603.5	2.012	23970	480.6
22	10000	629.7	2.099	23690	497.4
23	10000	760.5	2.535	12810	324.8
24	10000	638.2	2.127	15270	324.8
25	10000	595.4	1.985	16350	324.8
26	10000	572.7	1.909	17030	324.8
27	10000	637	2.123	26640	565.9
28	10000	621.7	2.072	27300	565.9
29	10000	611.4	2.038	27780	565.9
30	10000	564.2	1.881	30090	565.9
31	10000	556.6	1.855	30500	565.9
32	4377	400.2	1.334	58290	771.4
33	9510	786.7	2.622	63860	1762
34	7628	694.6	2.315	58040	1344
35	6989	807.6	2.692	46060	1232
36	5224	745	2.483	37100	920.6
37	5734	676.6	2.255	14380	324.5
38	5077	560.4	1.868	15570	287.3

Sample ID	Fmax (mN)	DisplMax (um)	StrainMax (%)	E (Mpa)	σ_{Max} (Mpa)
39	4991	522.6	1.742	16300	282.4
40	7214	640.3	2.134	19190	408.2
41	8975	713.7	2.379	21400	507.9
Avg	**7551.35714**	**635.8285714**	**2.119285714**	**33275.71**	**721.7071429**
StdDev	**2179.55837**	**111.5007929**	**0.371590641**	**16948.72**	**443.1063173**
Max	**10000**	**1087**	**3.625**	**69390**	**1762**
Min	**2203**	**354.2**	**1.181**	**12810**	**244**

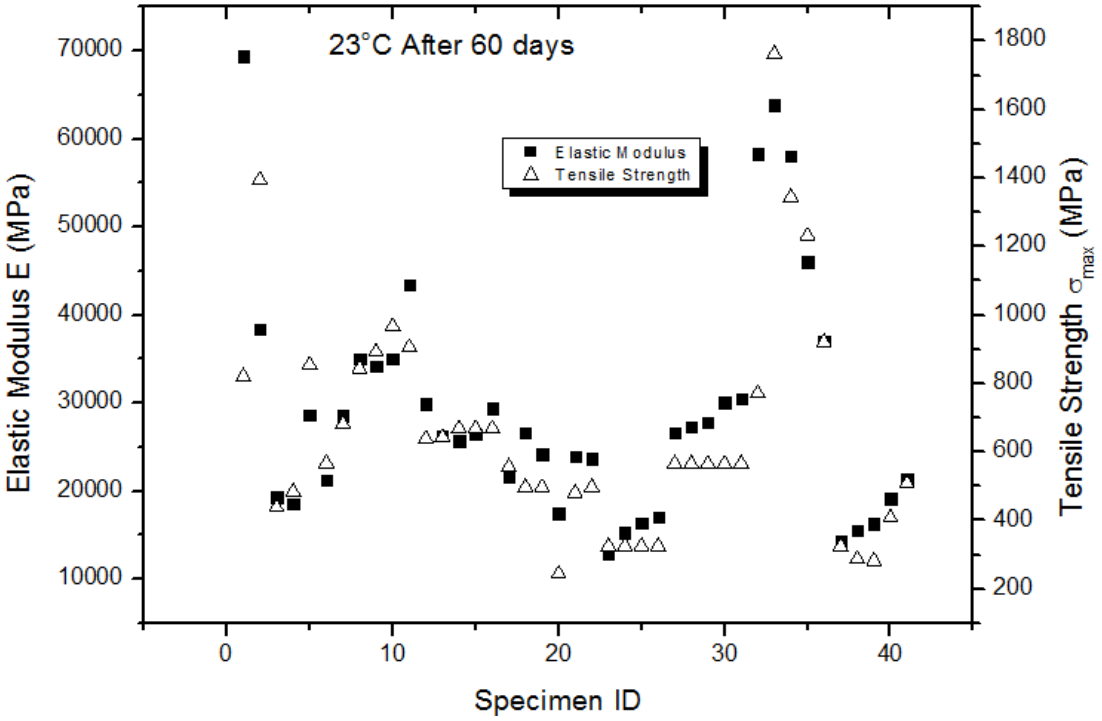

Figure C5: Tensile properties distribution for single sisal fibre test specimens after 60 days of hydrothermal ageing at 23^{o}C.

40^{o}C treated specimens

Table C6: Single sisal fibre tensile test results after 60 days of hydrothermal treatment of test specimens at 40^{o}C.

Sample ID	Fmax (mN)	Displ Max (um)	Strain Max (%)	E (Mpa)	σMax (Mpa)
1	8991	928.7	3.096	25700	795
2	10000	845.3	2.818	31360	884.2
3	7606	913.9	3.046	35250	1073
4	7801	1005	3.35	25440	851.6
5	7054	789.2	2.631	29300	770
6	6474	766.8	2.556	27700	706.7
7	4569	586.6	1.955	25540	498.8
8	6554	810.9	2.7	26480	715.5
9	10000	657.2	2.191	49830	1092
10	10000	652.6	2.175	35890	62.01
11	10000	612.8	2.043	38140	777.2
12	10000	566.4	1.888	41150	777.2
13	10000	586.5	1.955	16600	324.8
14	10000	599.9	2	16250	324.8
15	10000	682.8	2.276	14260	324.8
16	9998	675	2.25	14430	324.7
17	8275	1065	3.549	20630	468.3
18	6403	665.9	2.22	16390	362.3
19	10000	658.8	2.196	25770	565.9
20	10000	684.6	2.282	24810	565.9
Avg	**8686.25**	**737.695**	**2.45885**	**27046**	**651.0280532**
StdDev	**1708.53036**	**147.082127**	**0.490078004**	**9534.954**	**275.2657224**
Max	**10000**	**1065**	**3.549**	**49830**	**1092**
Min	**4569**	**566.4**	**1.888**	**14260**	**62.01**

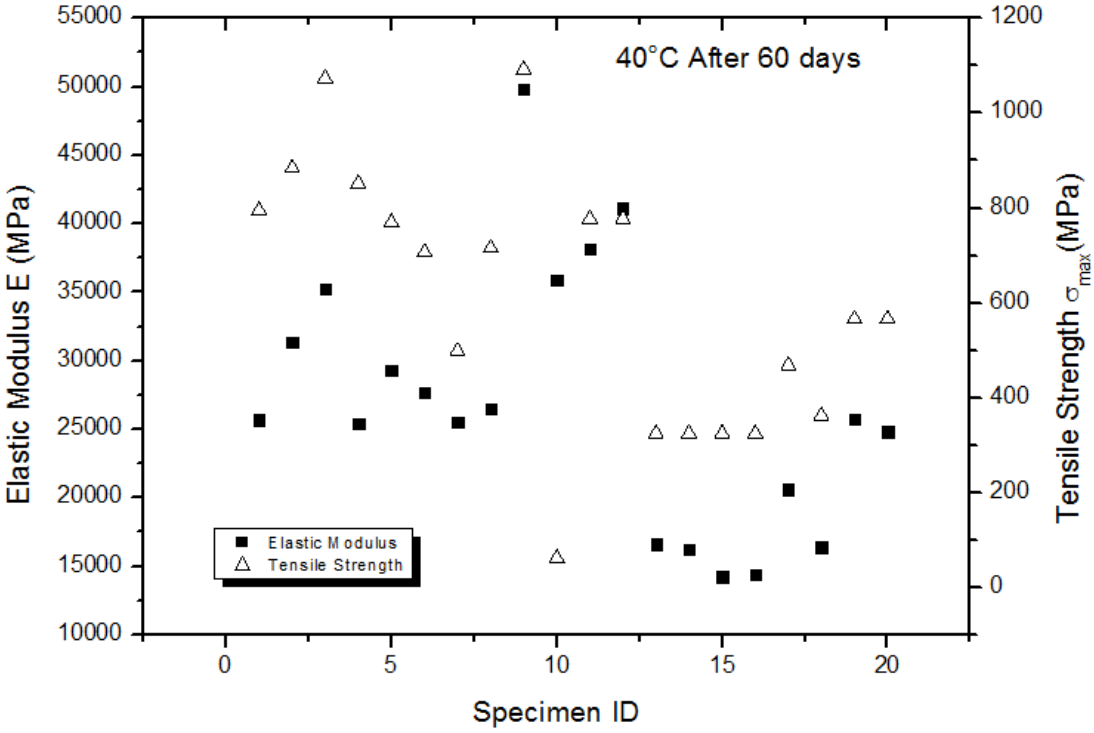

Figure C6: Tensile properties distribution for single sisal fibre test specimens after 60 days of hydrothermal ageing at 40^{o}C.

60^{o}C treated specimens

Table C7: Single sisal fibre tensile test results after 60 days of hydrothermal treatment of test specimens at 60^{o}C.

Sample ID	Fmax (mN)	Displ Max (um)	Strain Max (%)	E (Mpa)	σ_{Max} (Mpa)
1	4676	346.3	1.154	28690	331.6
2	9533	606.3	2.021	33470	675.9
3	8271	507.6	1.62	34990	586.5
4	10000	535.3	1.784	39720	709.2
5	6926	562.2	1.874	37500	612.4
6	6144	533.5	1.778	30580	543.3
7	8316	679.7	2.266	32450	735.3
8	7399	672.8	2.243	29190	654.2
9	5752	1029	3.431	14930	508.6

Sample ID	Fmax (mN)	Displ Max (um)	Strain Max (%)	E (Mpa)	σ_{Max} (Mpa)
10	7747	815.8	2.719	30020	815.2
11	7289	785	2.617	29360	767
12	6937	753.5	2.512	29050	730
13	8255	916.7	3.056	28500	868.6
14	8946	703.3	2.344	36140	846.5
15	7559	665.2	2.217	32250	715.3
16	7447	672.1	2.24	31360	704.6
17	8935	747.9	2.493	33910	845.4
18	8086	761.8	2.539	30160	765.1
19	9405	643.6	2.145	22530	467.8
20	9473	666.9	2.223	21550	471.2
21	9524	705.7	2.352	20160	473.7
22	6808	628.5	2.095	16150	338.6
23	10000	813.8	2.713	17550	467.7
24	10000	721.7	2.406	19450	467.7
25	7207	695.7	2.319	25740	596.8
26	9185	1230	4.1	15890	760
27	8025	833.9	2.78	23970	664.5
28	6718	1044	3.479	10110	556.3
29	9340	805.7	2.686	27900	749.1
30	8188	845.6	2.819	23310	656.7
Avg	**8069.7**	**730.97**	**2.434166667**	**26886**	**636.16**
StdDev	**1350.30326**	**173.8335493**	**0.582867175**	**7373.295**	**147.3734749**
Max	**10000**	**1230**	**4.1**	**39720**	**868.6**
Min	**4676**	**346.3**	**1.154**	**10110**	**331.6**

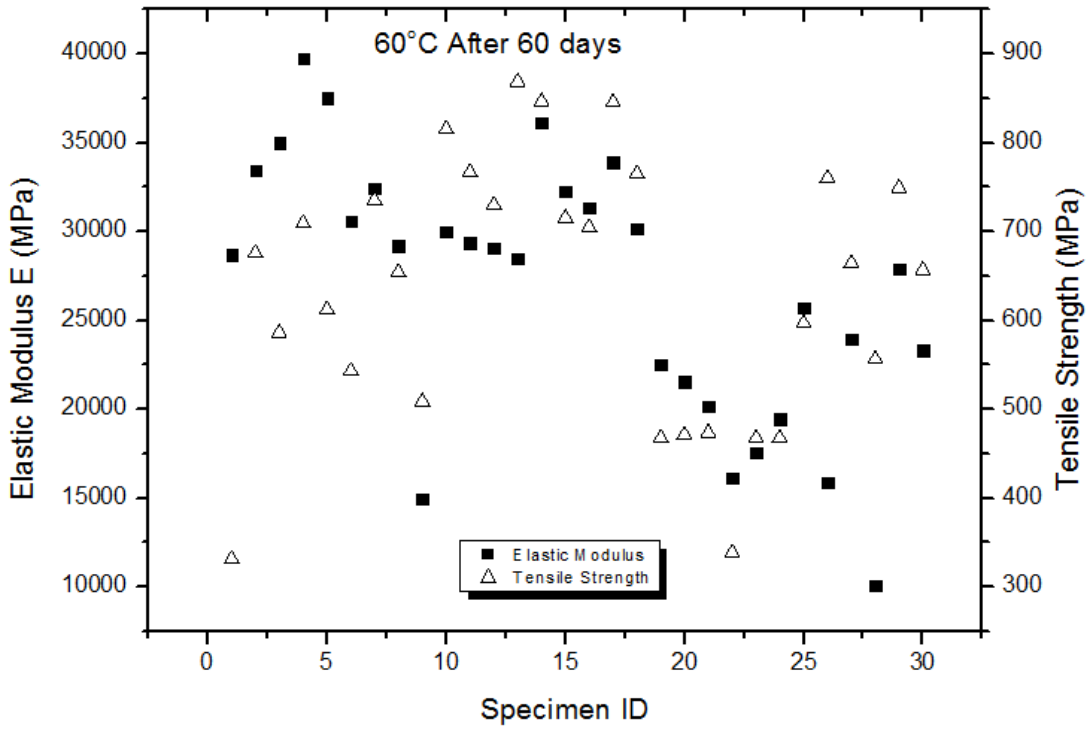

Figure C7: Tensile properties distribution for single sisal fibre test specimens after 60 days of hydrothermal ageing at 60^{o}C.

After 90 days of hydrothermal treatment of single sisal fibre samples

23^{o}C treated specimens

Table C8: Single sisal fibre tensile test results after 90 days of hydrothermal treatment of test specimens at 23^{o}C.

Sample ID	Fmax (mN)	DisplMax (um)	StrainMax (%)	E (Mpa)	σ_{Max} (Mpa)
1	7887	776.4	2.588	25240	653.1
2	9172	828.7	2.762	27490	759.5
3	7535	800	2.667	23620	623.9
4	8795	852.8	2.843	30580	728.3
5	7180	578.1	1.927	30880	594.6
6	8870	781.6	2.605	39350	1024
7	8454	623.3	2.078	47030	976.3

Sample ID	Fmax (mN)	DisplMax (um)	StrainMax (%)	E (Mpa)	σ_{Max} (Mpa)
8	7116	544.1	1.814	45410	821.9
9	7126	625.1	2.084	39500	823
10	5906	544.7	1.816	37630	682.1
11	3417	412.5	1.375	16190	218.8
12	8211	782.1	2.607	20220	525.9
13	8955	766.1	2.554	22640	573.5
14	9300	724.4	2.415	24680	595.6
15	8467	579.8	1.933	28110	542.3
16	9473	689.6	2.299	26170	598.2
17	10000	622.6	2.075	30420	631.4
18	10000	565.7	1.886	33500	631.5
19	10000	519.3	1.731	36480	631.4
20	10000	571.9	1.906	33110	631.5
21	7130	829.2	2.764	35970	945.2
22	4909	564.6	1.882	41870	650.8
23	6031	703.4	2.345	44070	799.6
24	5117	813.4	2.711	26990	678.3
25	6763	834	2.78	46280	896.6
Avg	**7832.56**	**677.336**	**2.25788**	**32537.2**	**689.492**
StdDev	**1769.74**	**124.5326**	**0.415071**	**8595.019**	**169.1509**
Max	**10000**	**852.8**	**2.843**	**47030**	**1024**
Min	**3417**	**412.5**	**1.375**	**16190**	**218.8**

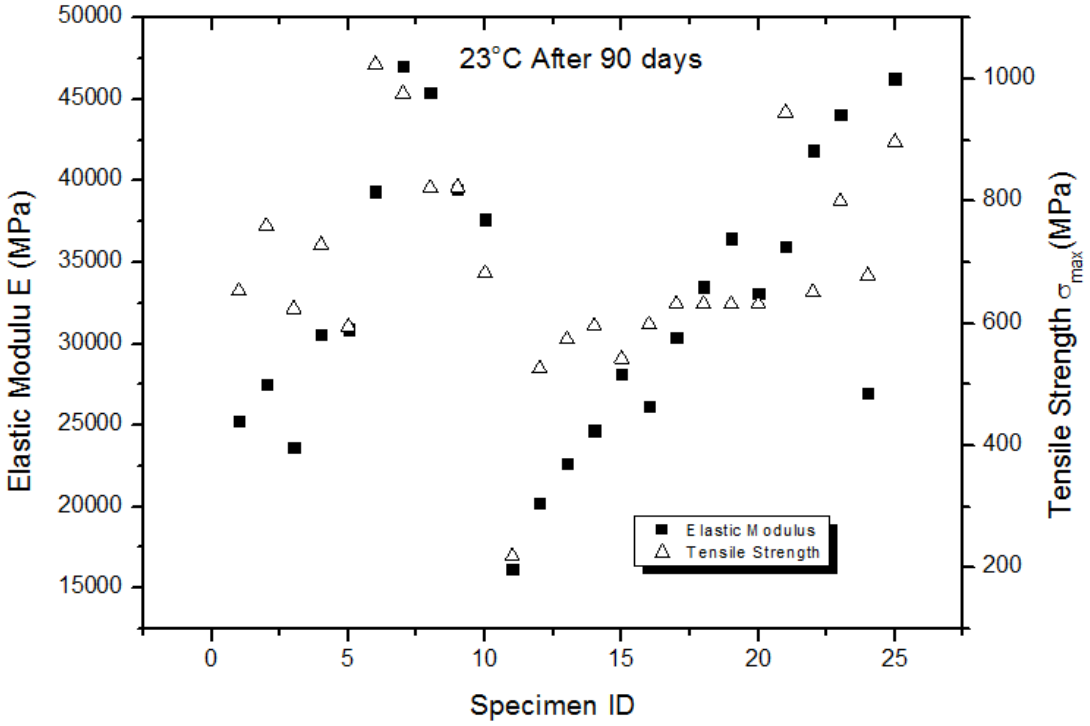

Figure C8: Tensile properties distribution for single sisal fibre test specimens after 90 days of hydrothermal ageing at 23^{o}C.

40^{o}C treated specimens

Table C9: Single sisal fibre tensile test results after 90 days of hydrothermal treatment of test specimens at 40^{o}C.

Sample ID	Fmax (mN)	DisplMax (um)	StrainMax (%)	E (Mpa)	σ_{Max} (Mpa)
1	8315	714.1	2.38	19510	464.3
2	10000	728.8	2.429	22990	558.5
3	10000	681.6	2.272	24590	558.4
4	10000	648.4	2.161	25840	558.5
5	10000	622.5	2.075	27220	558.4
6	10000	876.7	2.922	63240	1848
7	10000	832.4	2.775	66720	1848
8	8771	853.9	2.846	56940	1621
9	8374	791.3	2.638	58660	1548

Sample ID	Fmax (mN)	DisplMax (um)	StrainMax (%)	E (Mpa)	σ_{Max} (Mpa)
10	6916	760.8	2.536	50340	1278
11	8289	592.5	1.975	29750	587.8
12	9301	586.1	1.954	33760	659.5
13	4276	476	1.587	19110	303.2
14	4222	383	1.277	23450	299.3
15	9388	773.6	2.579	25850	665.7
16	5858	816.8	2.723	13630	369.9
17	7806	833.8	2.779	17740	492.9
18	7525	698	2.327	20430	475.2
19	10000	791	2.637	23950	631.5
20	10000	679	2.236	28230	631.5
21	6468	707.7	2.359	62060	1464
22	6883	784.1	2.614	59640	1558
23	7425	717.9	2.393	70380	1681
24	6709	671.7	2.239	67840	1518
25	4226	658.3	2.194	43620	956.5
Avg	**8030.08**	**707.2**	**2.35628**	**38219.6**	**925.404**
StdDev	**1942.042**	**116.2046**	**0.387604**	**19186.99**	**538.7135**
Max	**10000**	**876.7**	**2.922**	**70380**	**1848**
Min	**4222**	**383**	**1.277**	**13630**	**299.3**

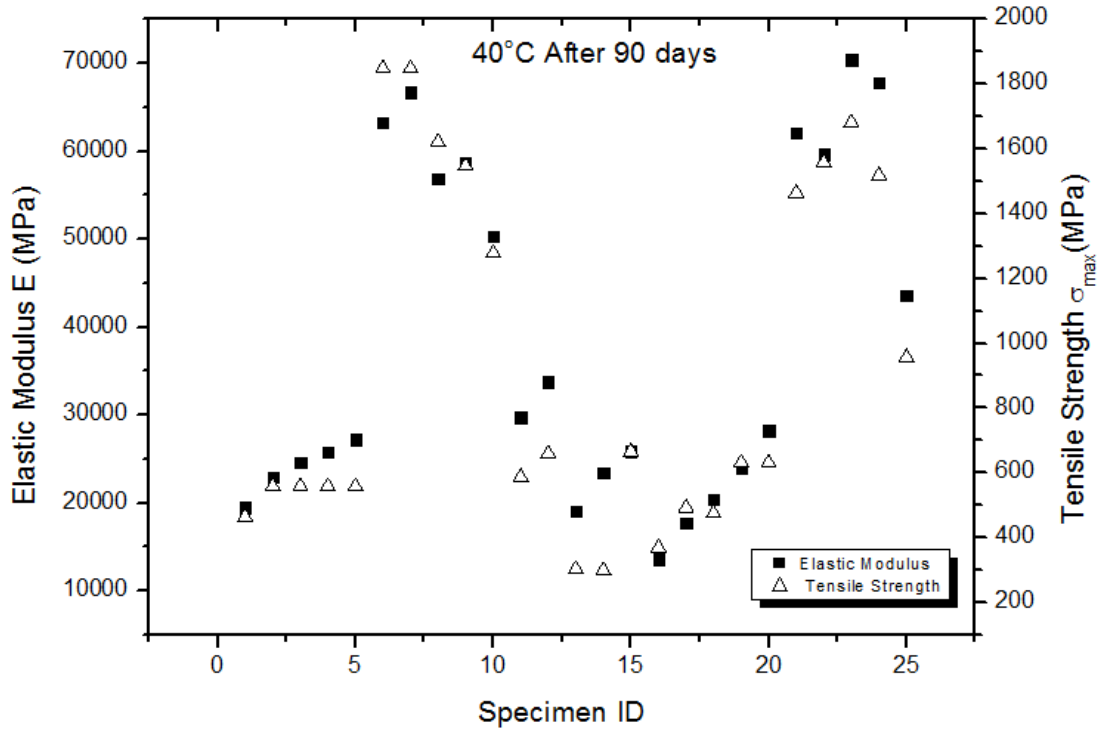

Figure C9: Tensile properties distribution for single sisal fibre test specimens after 90 days of hydrothermal ageing at 40^{o}C.

60^{o}C treated specimens

Table C10: Single sisal fibre tensile test results after 90 days of hydrothermal treatment of test specimens at 60^{o}C.

Sample ID	Fmax (mN)	DisplMax (um)	StrainMax (%)	E (Mpa)	σ_{Max} (Mpa)
1	10000	640	2.133	31780	678.4
2	10000	604.9	2.016	33670	678.4
3	10000	687.5	2.292	29600	678.4
4	10000	745.4	2.485	27310	678.4
5	10000	717.5	2.395	28310	678.4
6	5838	666	2.22	40630	897.6
7	4714	690.7	2.302	31510	724.7
8	7925	838.4	2.795	43670	1219
9	8072	743.9	2.48	51840	1241

Sample ID	Fmax (mN)	DisplMax (um)	StrainMax (%)	E (Mpa)	σ_{Max} (Mpa)
10	9383	786.3	2.621	55080	1443
11	7146	613.3	2.044	53930	1099
12	6548	674.8	2.249	25310	569.4
13	4994	496.8	1.656	27450	434.3
14	5831	549.5	1.832	28630	507.1
15	5533	504.8	1.683	28780	481.2
16	5603	474.7	1.582	37940	600.5
17	7031	531.5	1.772	42930	753.5
18	7213	557.6	1.859	42000	773
19	4930	494.2	1.647	32210	528.3
20	5047	531.4	1.771	30520	540
21	3114	496.5	1.655	33160	548.7
22	7840	721	2.403	57870	1382
23	7597	564	1.88	71300	1339
24	9394	568.5	1.895	87400	1655
25	10000	567.3	1.891	93150	1762
Avg	**7350.12**	**618.66**	**2.06232**	**42639.2**	**875.612**
StdDev	**1942.042**	**116.2046**	**0.387604**	**19186.99**	**538.7135**
Max	**10000**	**838.4**	**2.795**	**93150**	**1762**
Min	**3114**	**474.7**	**1.582**	**25310**	**434.3**

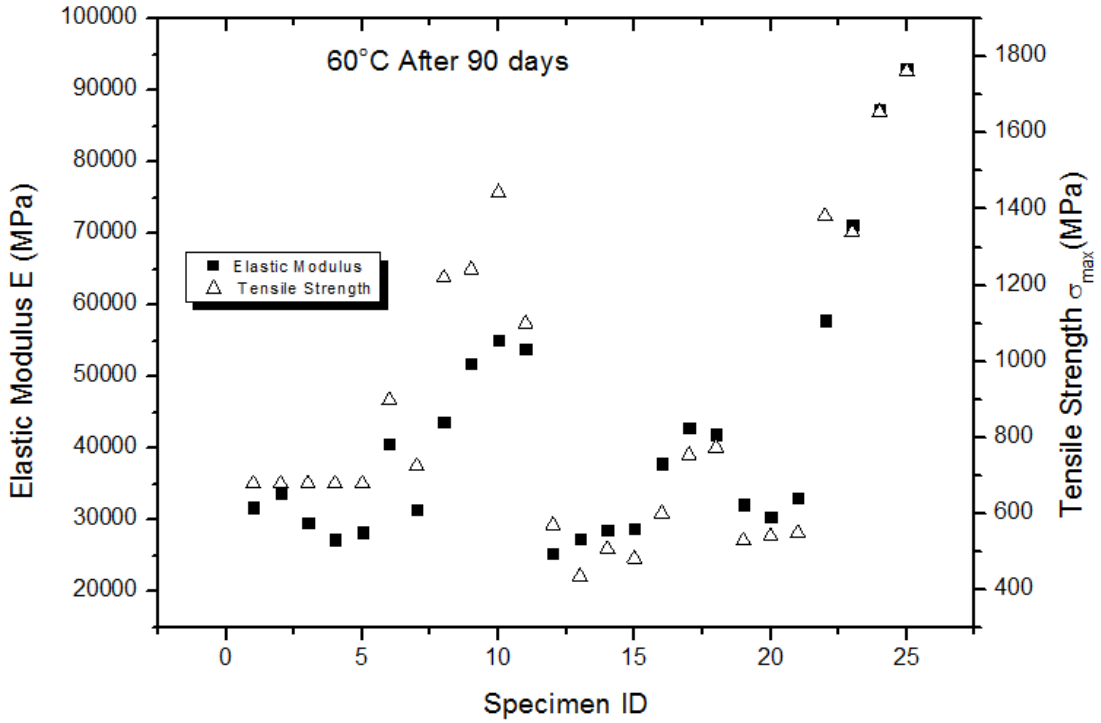

Figure C10: Tensile properties distribution for single sisal fibre test specimens after 90 days of hydrothermal ageing at 60^{o}C.

After 120 days of hydrothermal treatment of single sisal fibre samples

23^{o}C treated specimens

Table C11: Single sisal fibre tensile test results after 120 days of hydrothermal treatment of test specimens at 23^{o}C.

Sample ID	**Fmax (mN)**	**DisplMax (um)**	**StrainMax (%)**	**E (Mpa)**	**σ^{Max} (Mpa)**
1	7226	650.5	2.168	17670	383
2	7886	682	2.273	18390	417.9
3	7527	509.4	1.698	23560	398.9
4	10000	659.6	2.199	24100	530
5	10000	582.7	1.942	27290	530
6	5088	1273	4.244	19310	817.8
7	5160	570.9	1.903	43620	829.5

Sample ID	Fmax (mN)	DisplMax (um)	StrainMax (%)	E (Mpa)	σ^{Max} (Mpa)
8	9499	776.1	2.587	59120	1527
9	6353	643.6	2.145	47640	1021
10	8275	807.8	2.693	49420	1330
11	6005	851.5	2.838	20220	568.2
12	8155	939.6	3.132	24700	771.7
13	8669	792.8	2.643	31060	820.3
14	8704	766.9	2.556	32220	823.6
15	8503	872.2	2.907	16610	450.6
16	3985	740.7	2.469	47240	1165
17	3278	750.2	2.501	38480	958.1
18	2066	832.3	2.774	21820	604
19	1830	1024	3.413	15670	534.8
20	1343	914.9	3.05	20280	392.6
Avg	6477.6	782.035	2.60675	29921	743.7
StdDev	2765.169	174.9326	0.583222	13081.39	327.1212

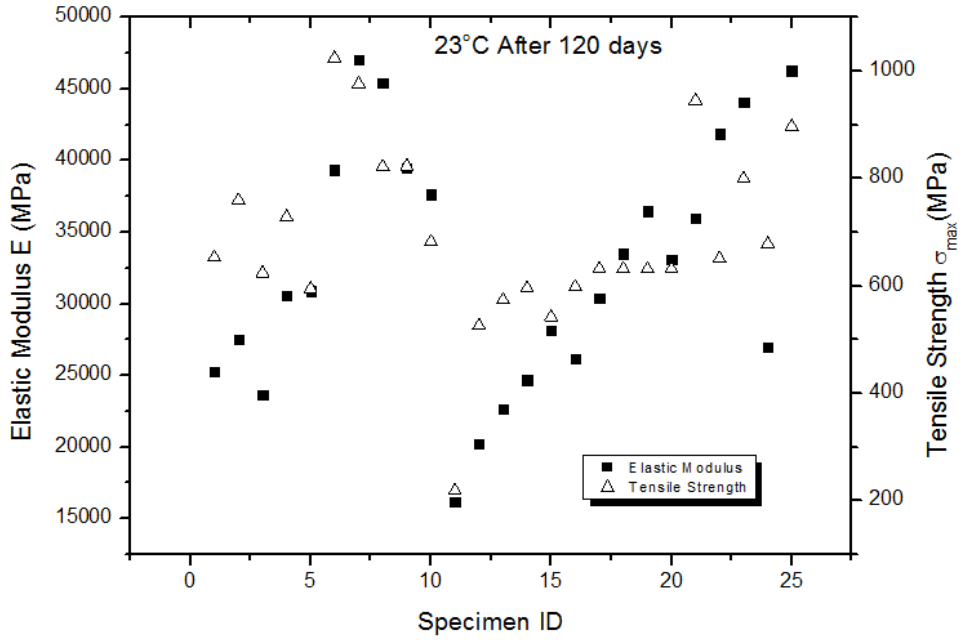

Figure C11: Tensile properties distribution for single sisal fibre test specimens after 120 days of hydrothermal ageing at 23^{o}C.

40^{o}C treated specimens

Table C12: Single sisal fibre tensile test results after 120 days of hydrothermal treatment of test specimens at 40^{o}C.

Sample ID	Fmax (mN)	DisplMax (um)	StrainMax (%)	E (Mpa)	σ_{Max} (Mpa)
1	8952	821.1	2.737	24700	674.4
2	9384	769.6	2.565	27620	707
3	8353	686.6	2.289	27560	629.3
4	9653	665.6	2.219	32810	727.2
5	9741	656.4	2.188	33650	733.9
6	7972	480.8	1.603	39930	639.4
7	9442	554.9	1.85	41090	757.3
8	8743	639.7	2.132	32890	701.2
9	8826	664.7	2.216	31960	707.9
10	5514	509.4	1.698	26250	442.2
11	3688	549.6	1.832	33860	620.3
12	3462	669.3	2.231	26130	582.4
13	4227	618.5	2.062	34480	711.1
14	3820	668.1	2.227	28930	642.6
15	3300	704	2.347	23660	555.1
16	9288	980.9	3.27	37650	1231
17	8004	857	2.857	37240	1061
18	7664	850.3	2.834	35900	1016
19	5752	741.1	2.47	30890	762.6
20	4409	1059	3.53	20830	584.5
Avg	7009.7	707.33	2.35785	31401.5	724.32
StdDev	2420.265	148.6721	0.495535	5579.145	183.996

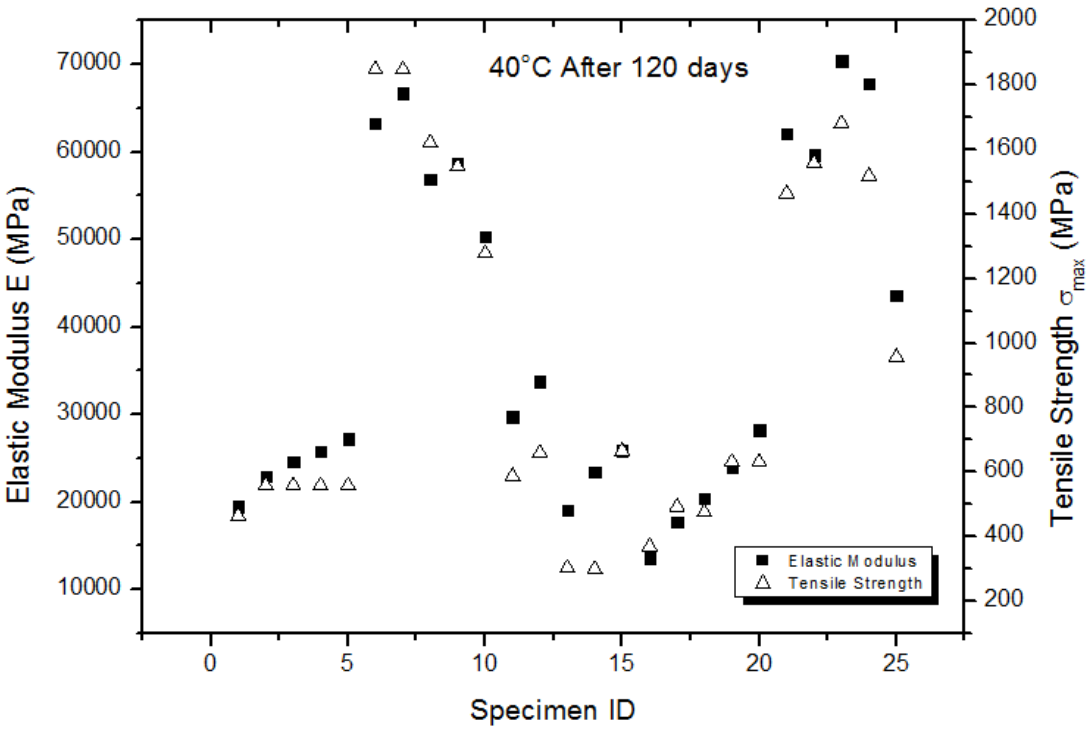

Figure C12: Tensile properties distribution for single sisal fibre test specimens after 120 days of hydrothermal ageing at 40^{o}C.

60^{o} C treated specimens

Table C13: Single sisal fibre tensile test results after 120 days of hydrothermal treatment of test specimens at 60^{o}C.

Sample ID	Fmax (mN)	DisplMax (um)	StrainMax (%)	E (Mpa)	σ_{Max} (Mpa)
1	5307	667.7	2.226	23760	520
2	7925	804.3	2.681	29120	776.4
3	6989	729.7	2.432	28190	684.8
4	5575	687.4	2.291	23850	546.1
5	4004	713.4	2.378	16500	392.3
6	4586	556.3	1.854	19440	293.7
7	8939	730.6	2.435	35280	716.9
8	9069	730.5	2.435	23870	580.8
9	10000	767.3	2.558	31350	802

Sample ID	Fmax (mN)	DisplMax (um)	StrainMax (%)	E (Mpa)	σ_{Max} (Mpa)
10	7205	616.1	2.054	22490	461.4
11	5887	557.3	1.858	30640	566.8
12	9877	674.3	2.248	42800	950.9
13	10000	627.9	2.093	37130	777.2
14	10000	683.6	2.279	42320	962.8
15	4629	432.7	1.442	25060	359.7
16	5571	481.4	1.605	27690	432.9
17	7273	574.4	1.915	29580	565.2
18	6114	460.9	1.536	31030	475.2
19	6980	529	1.763	30970	542.4
Avg	7154.211	632.8842	2.109632	29003.68	600.3947
StdDev	2016.959	107.8972	0.359703	6984.819	190.2695

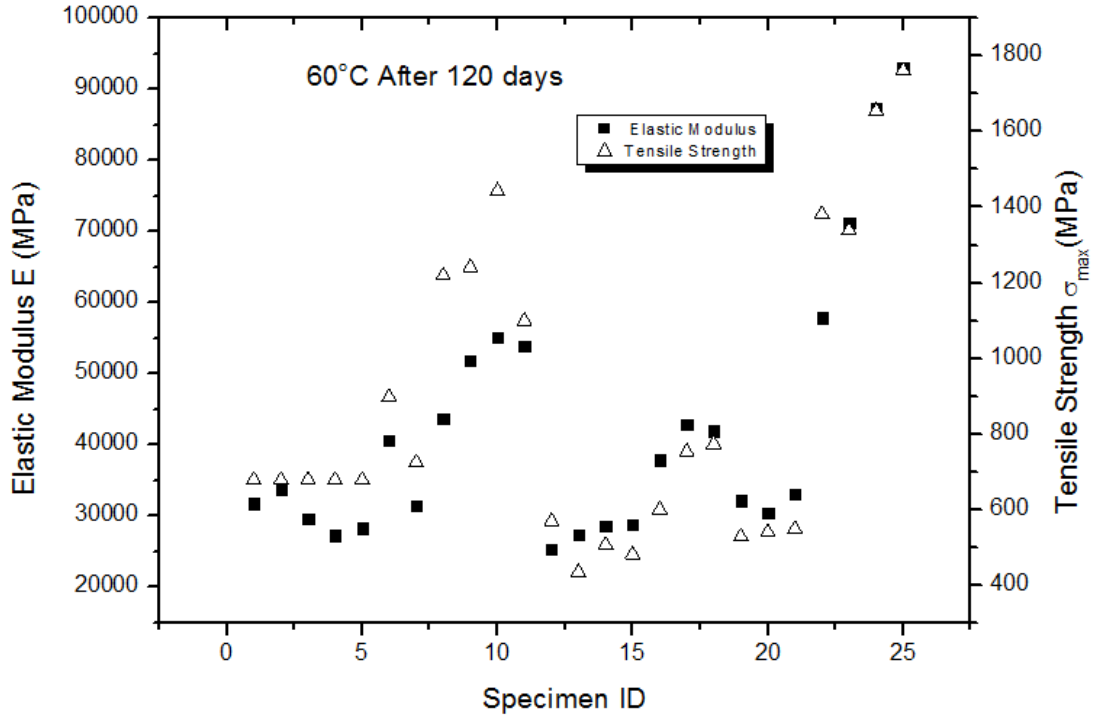

Figure C13: Tensile properties distribution for single sisal fibre test specimens after 120 days of hydrothermal ageing at 60°C.

APPENDIX D

DMA TEST RESULTS

1. A few selected Dynamic Mechanical Analysis (DMA) plots for untreated polyester resin specimens.

Specimen 0-0-1 (Untreated)

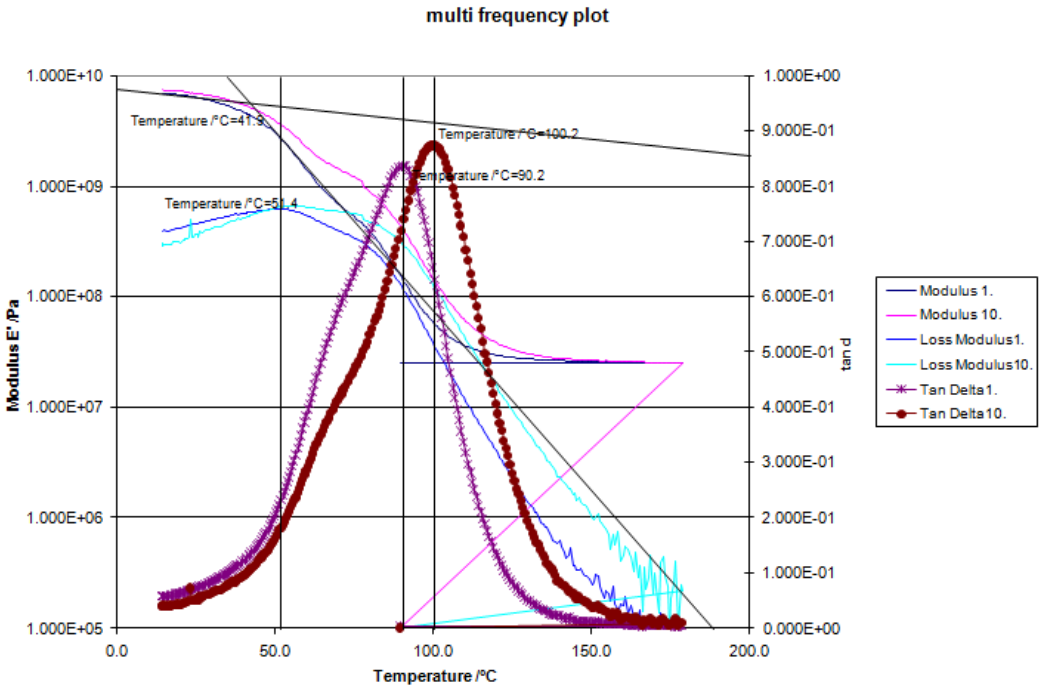

Specimen 0-02 (Untreated)

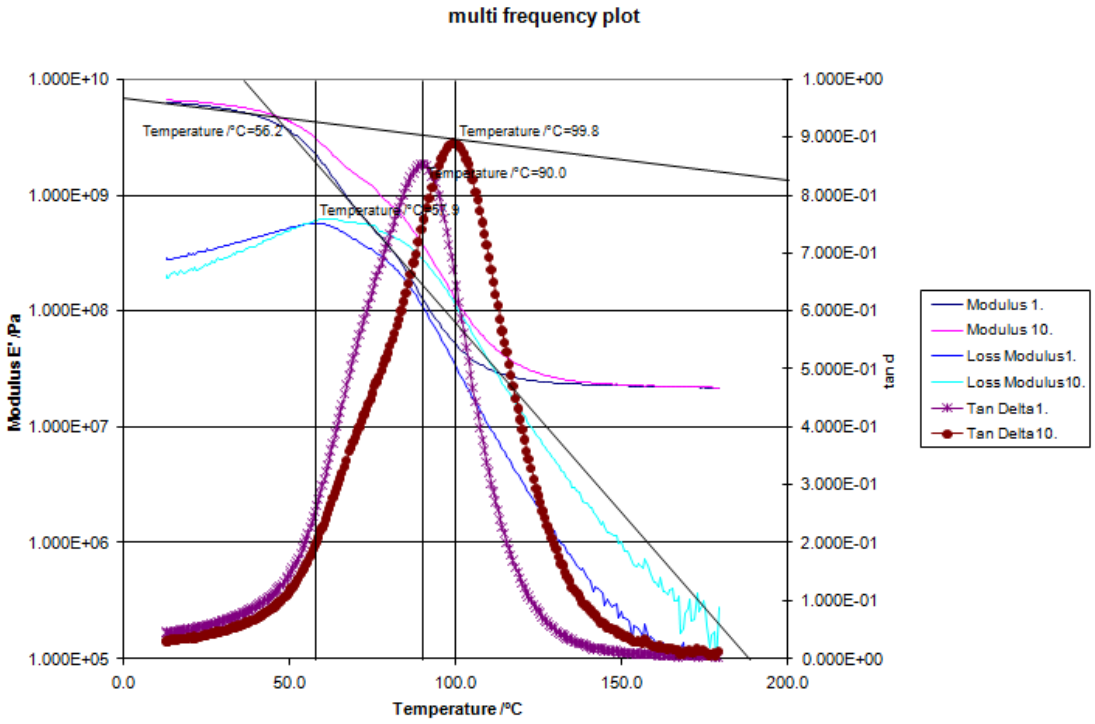

2. A few selected Dynamic Mechanical Analysis (DMA) plots for hydrothermally treated polyester resin specimens

   a) After 1 month of hydrothermal ageing at temperature of 23^{o}C.

Specimen 23-1-1

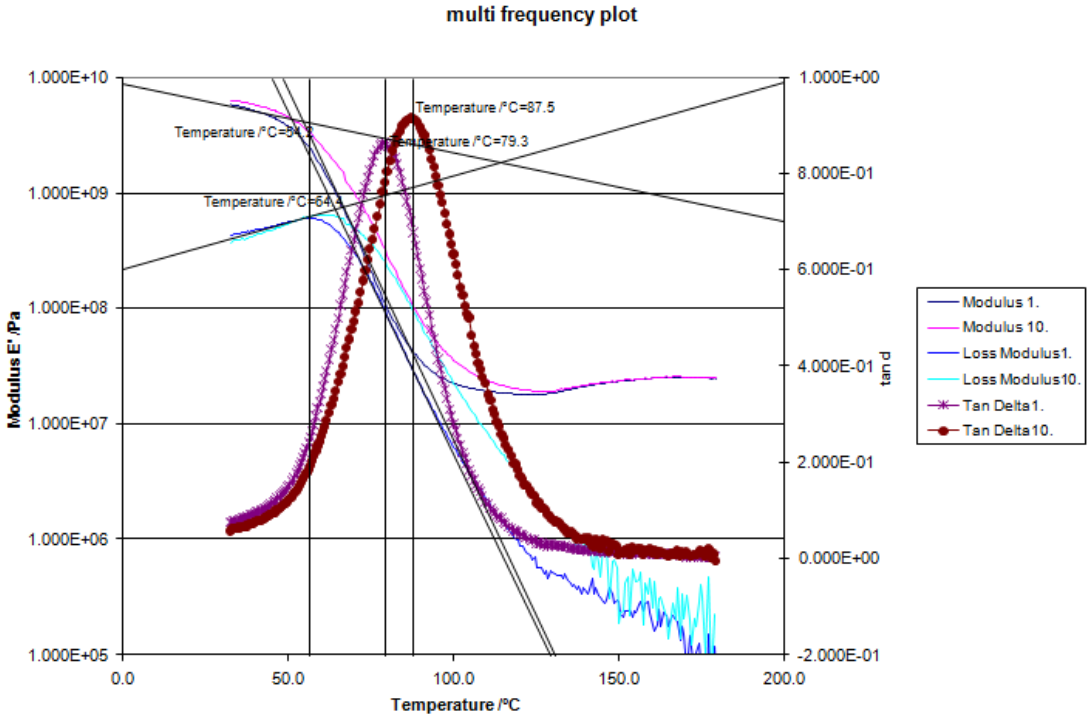

Specimen 23-1-2

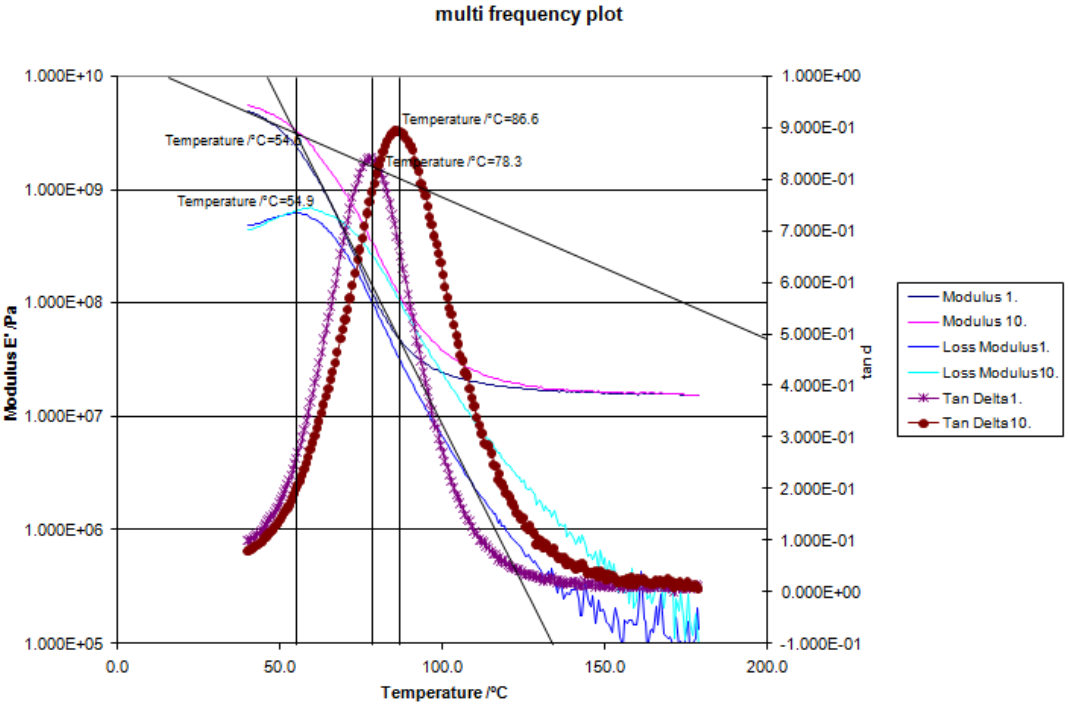

After 1 month of hydrothermal ageing at temperature of 40°C.

Specimen 40-1-1

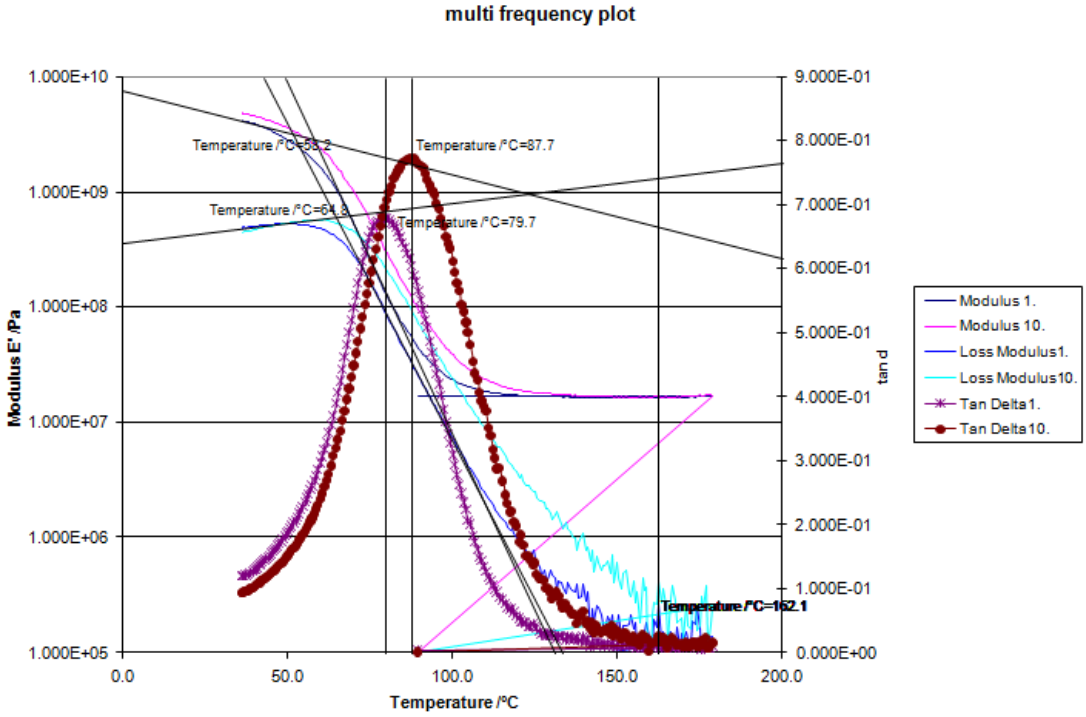

Specimen 40-1-2

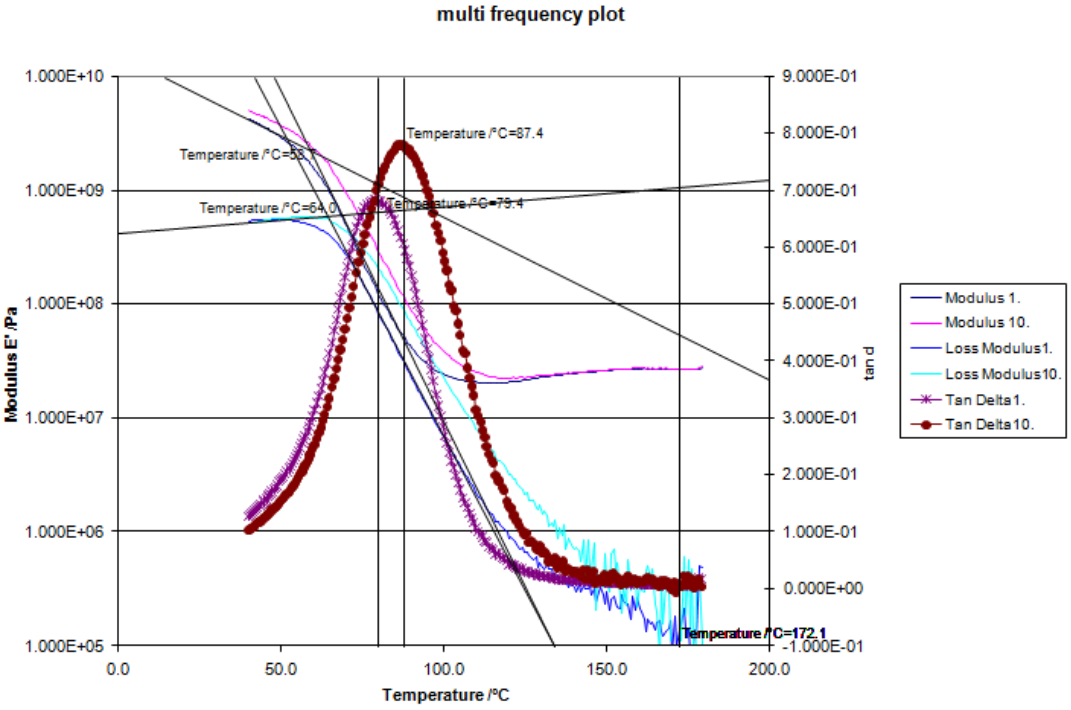

After 1 month of hydrothermal ageing at temperature of 60°C

Specimen 60-1-1

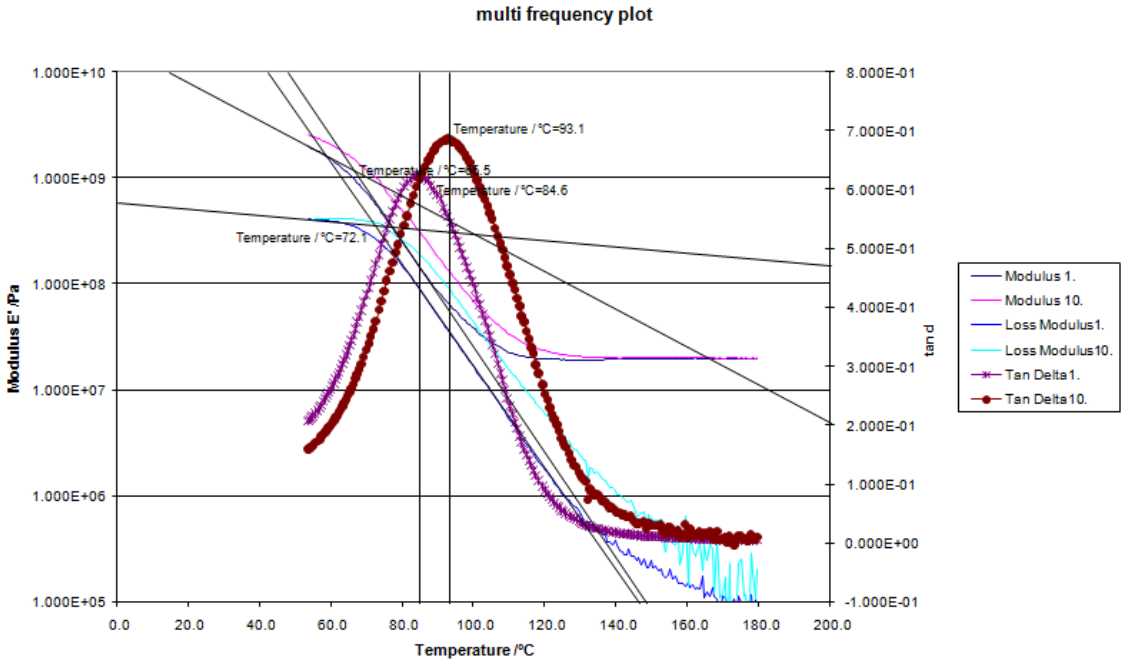

Specimen 60-1-2

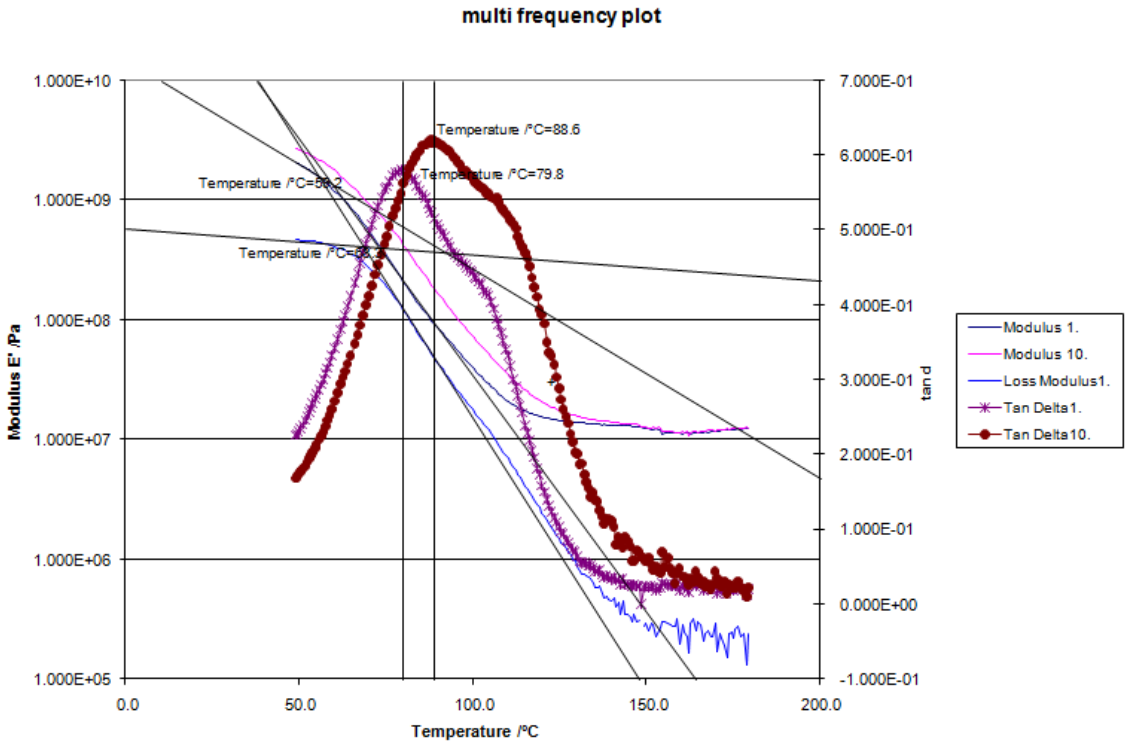

b) After 2 months of hydrothermal ageing at temperature of 23^{o}C

Specimen 23-2-1

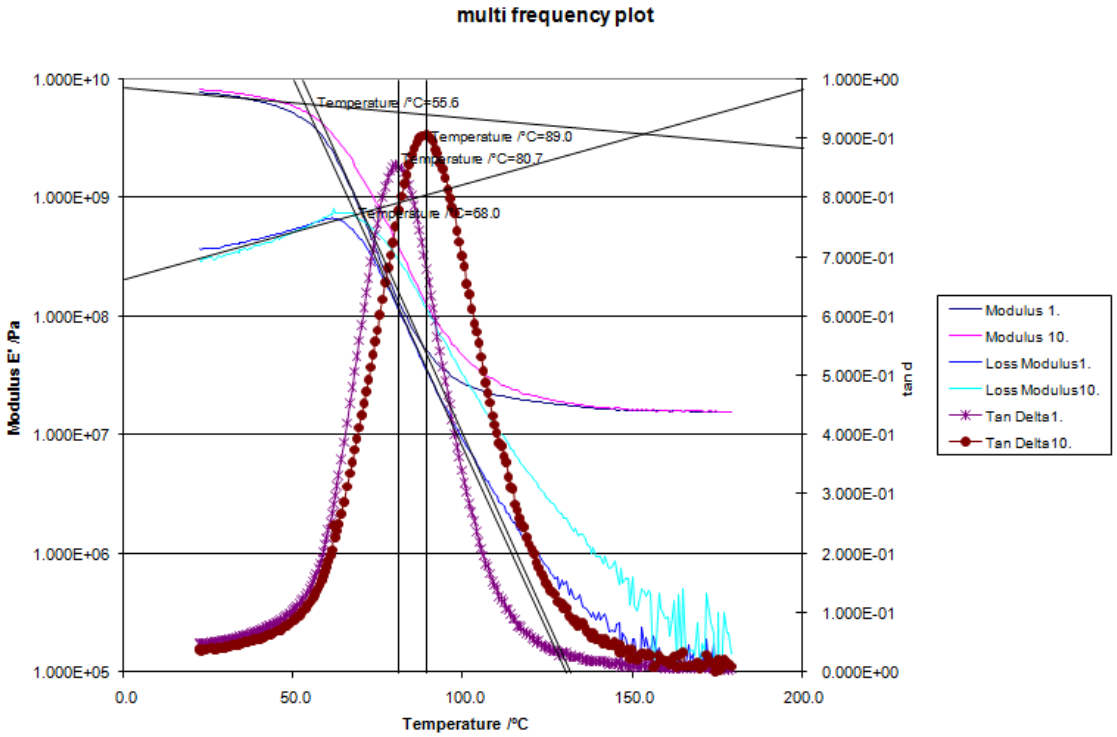

Specimen 23-2-2

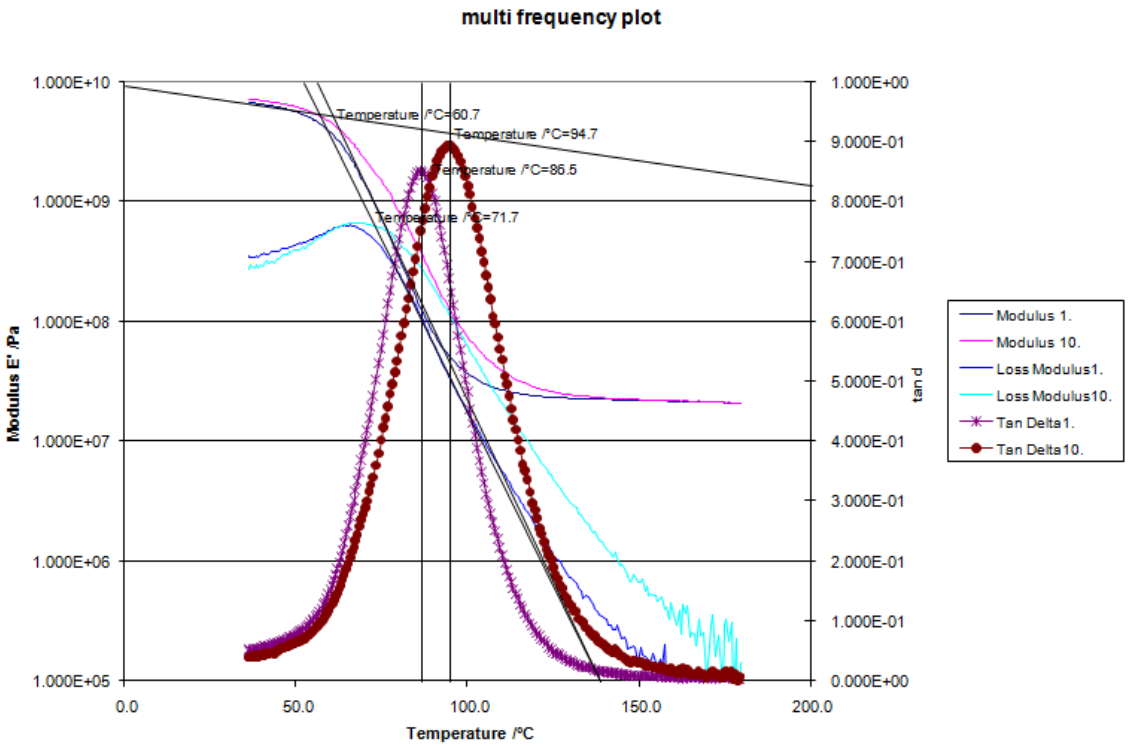

c) After 2 months of hydrothermal ageing at temperature of 40°C

Specimen 40-2-1

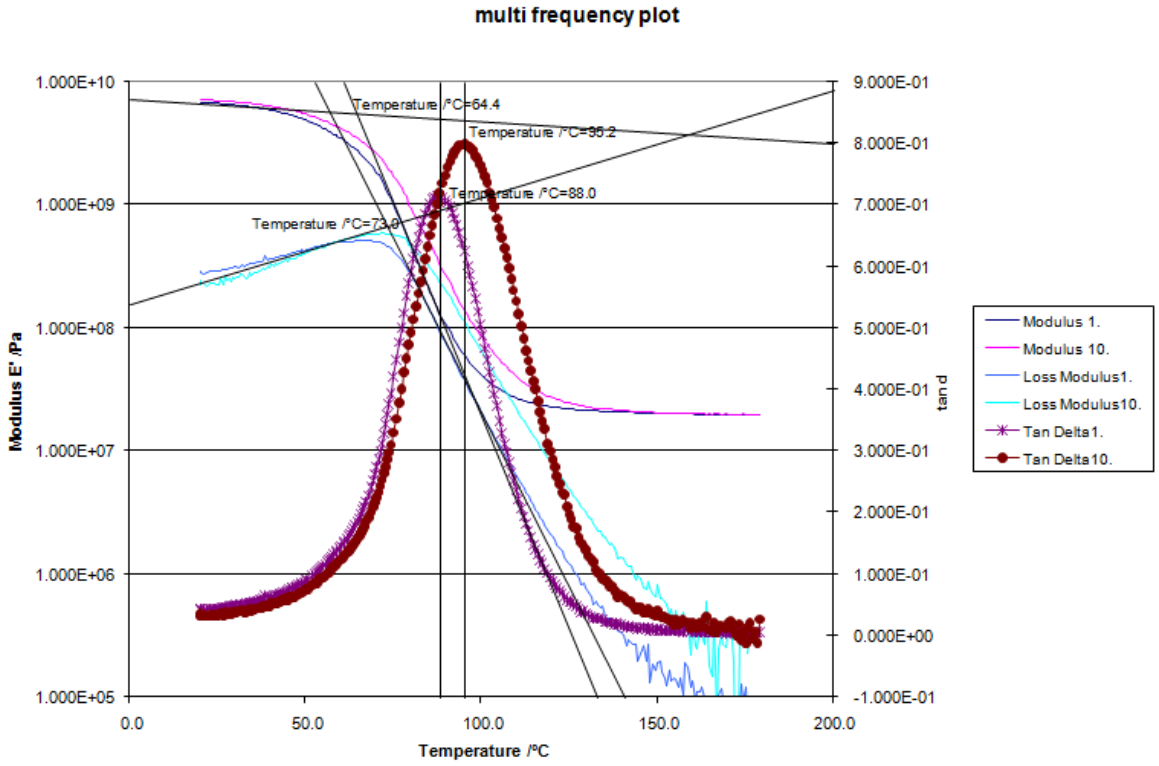

Specimen 40-2-2

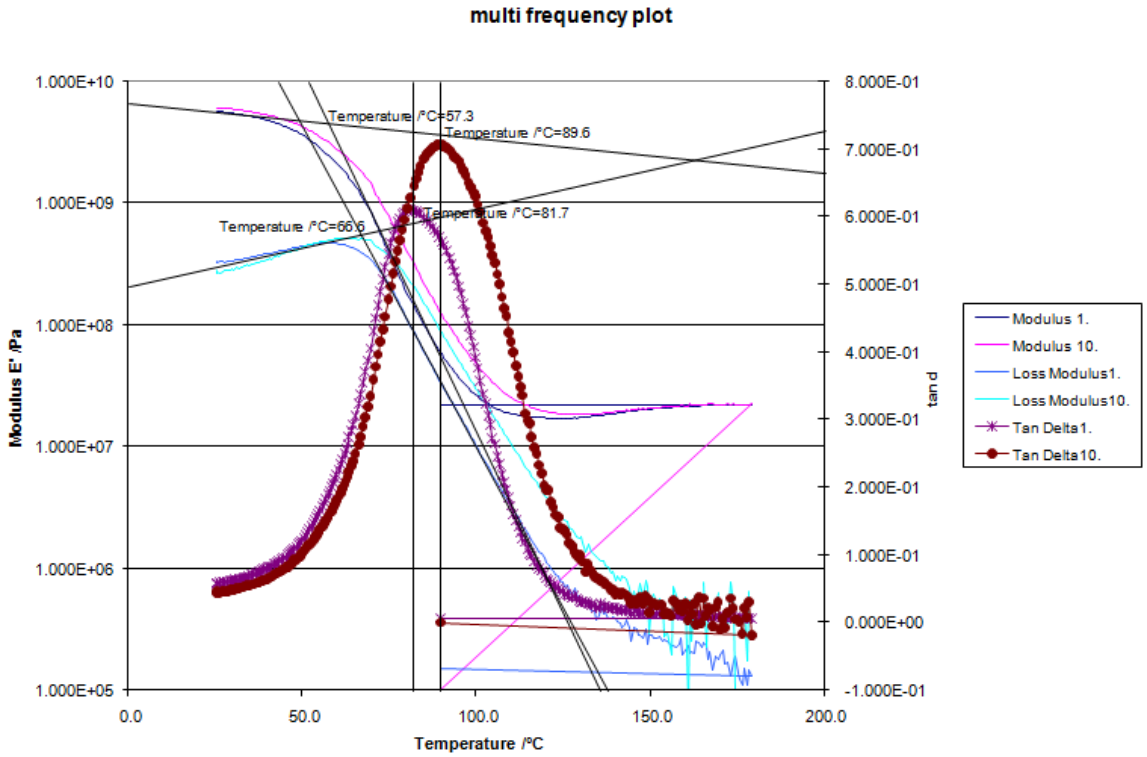

d) After 2 months of hydrothermal ageing at temperature of 60°C

Specimen 60-2-1

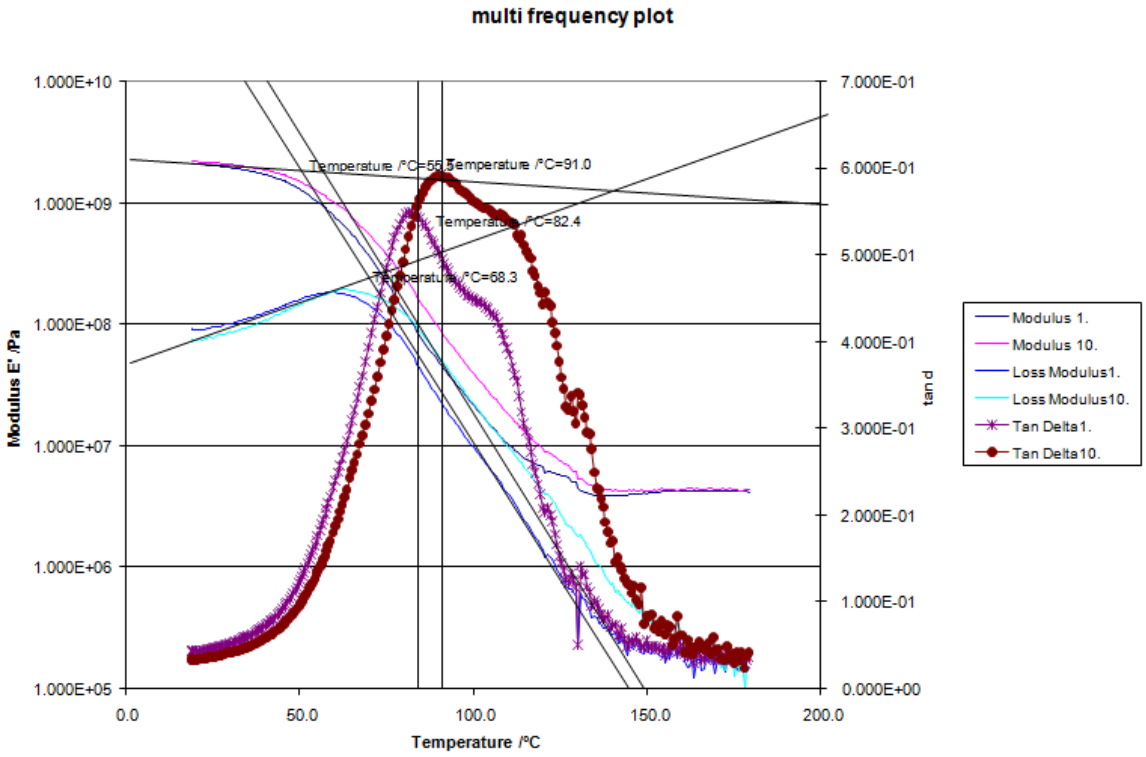

Specimen 60-2-2

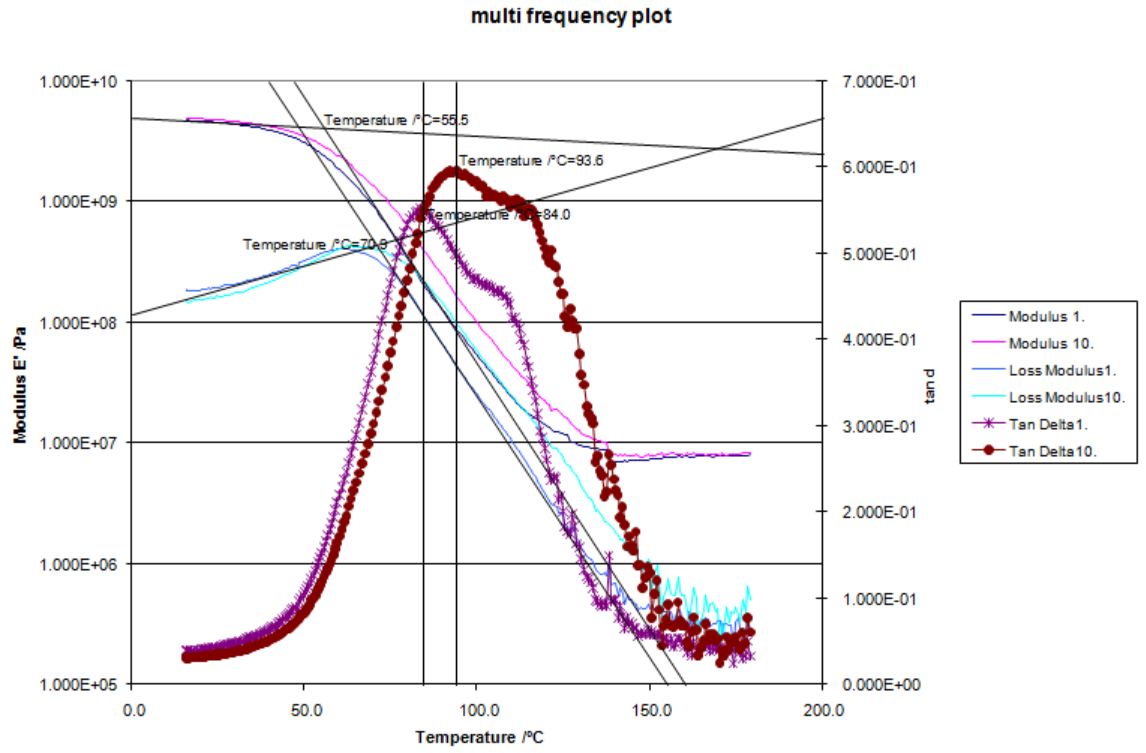

e) After 3 months of hydrothermal ageing at temperature of 23^{o}C

Specimen 23-3-1

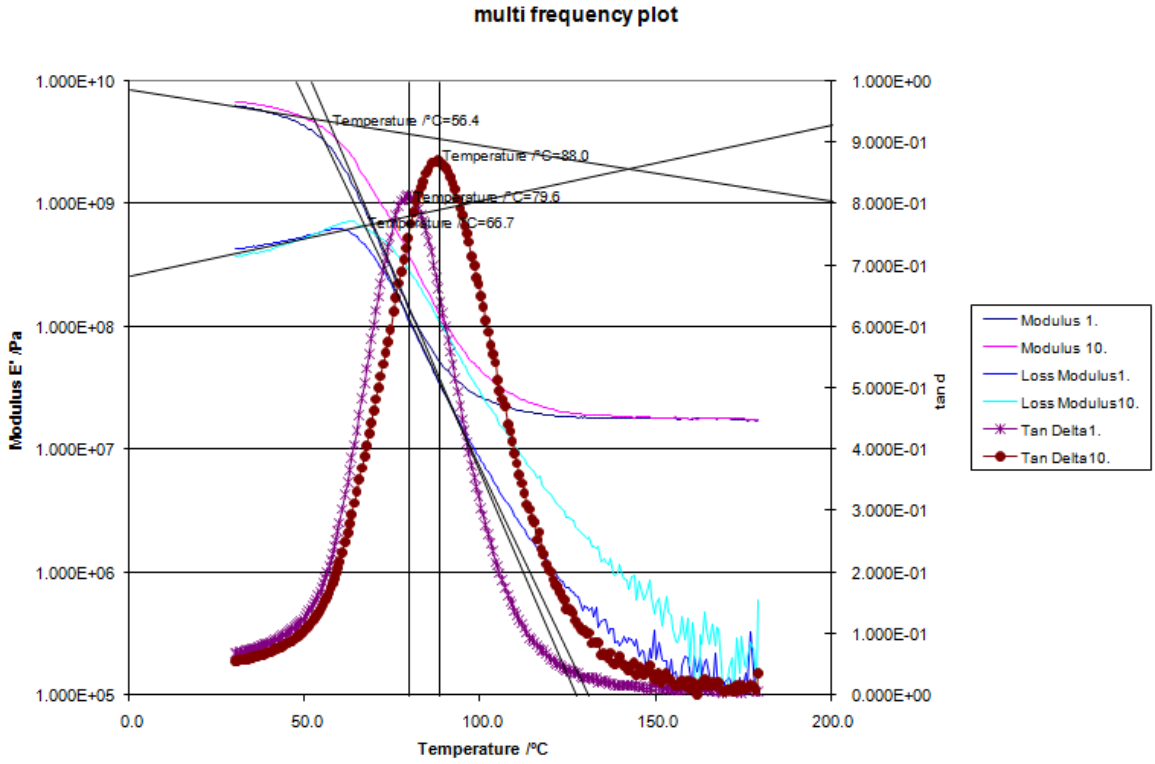

Specimen 23-3-2

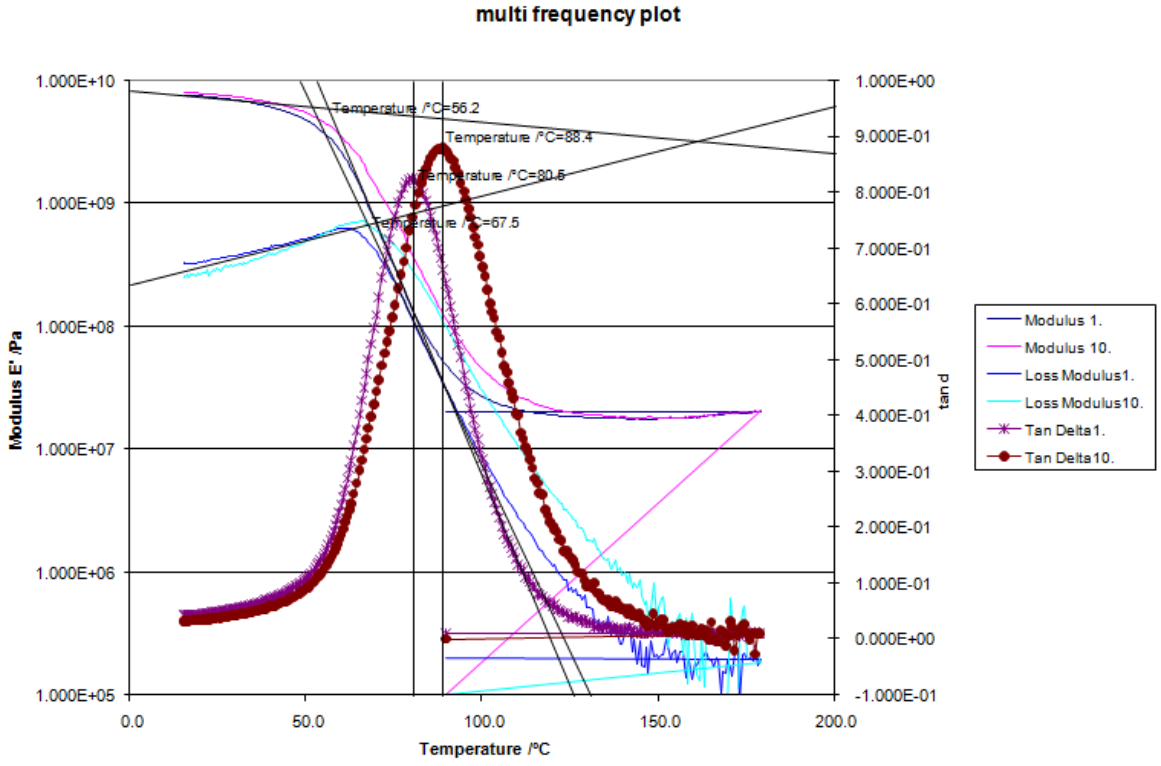

f) After 3 months of hydrothermal ageing at temperature of 40°C

Specimen 40 -3-1

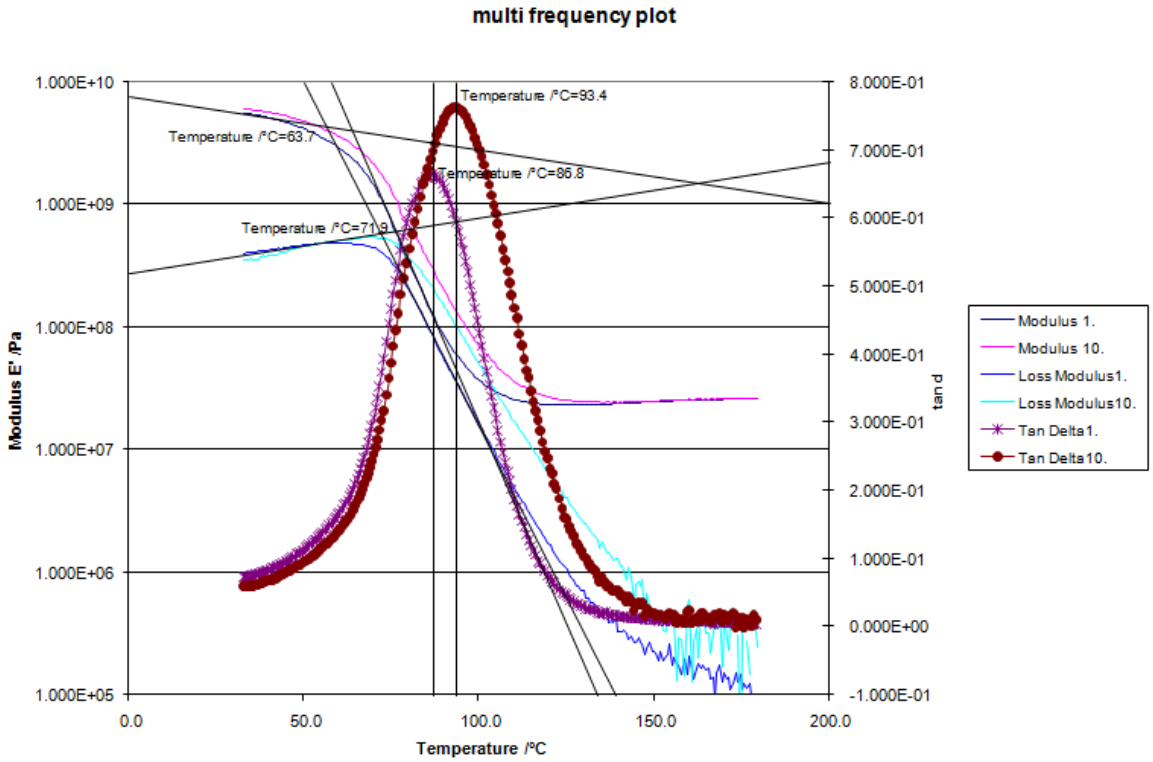

Specimen 40-3-2

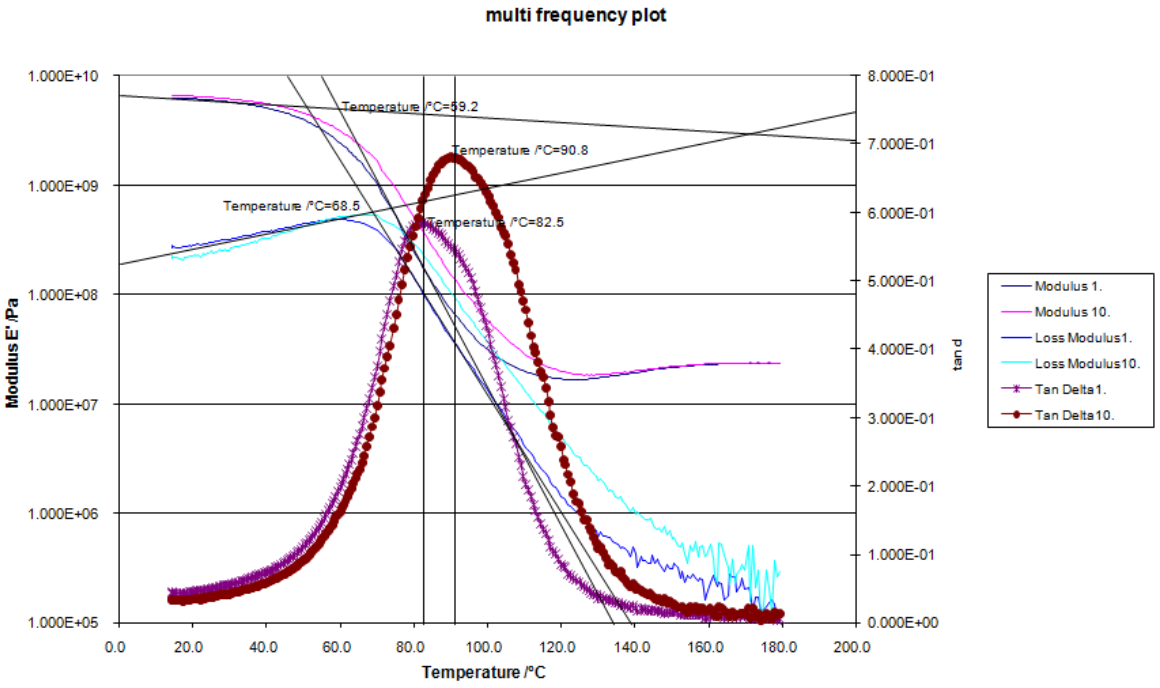

g) After 3 months of hydrothermal ageing at temperature of 60°C

Specimen 60-3-1

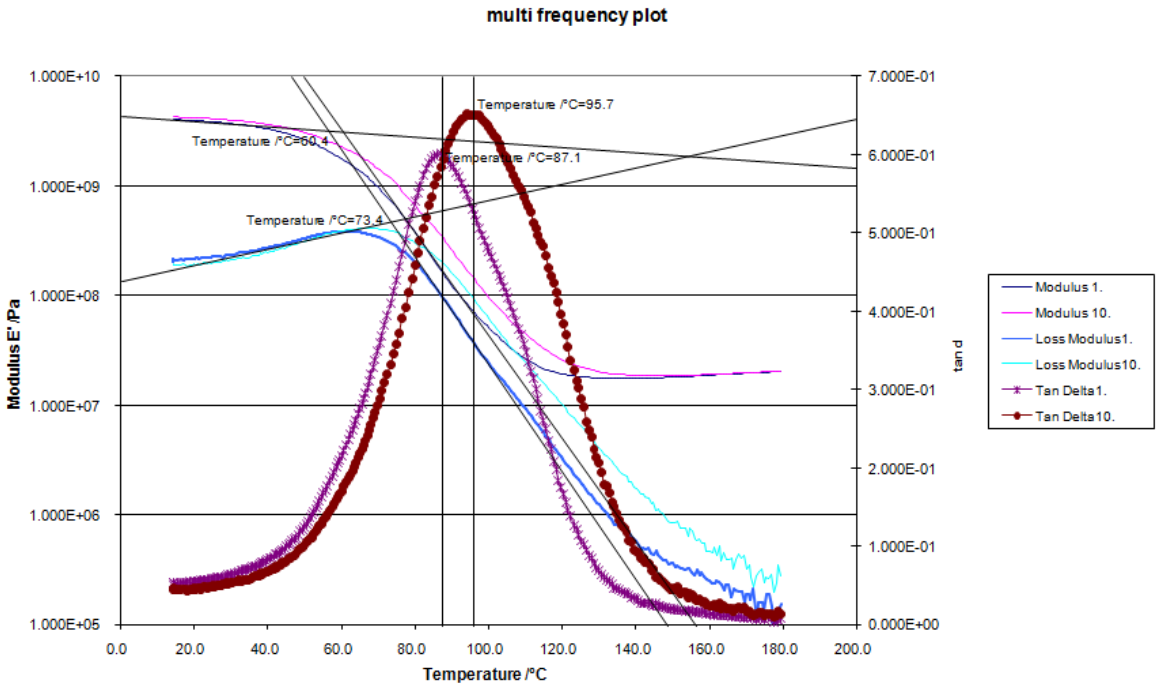

Specimen 60-3-2

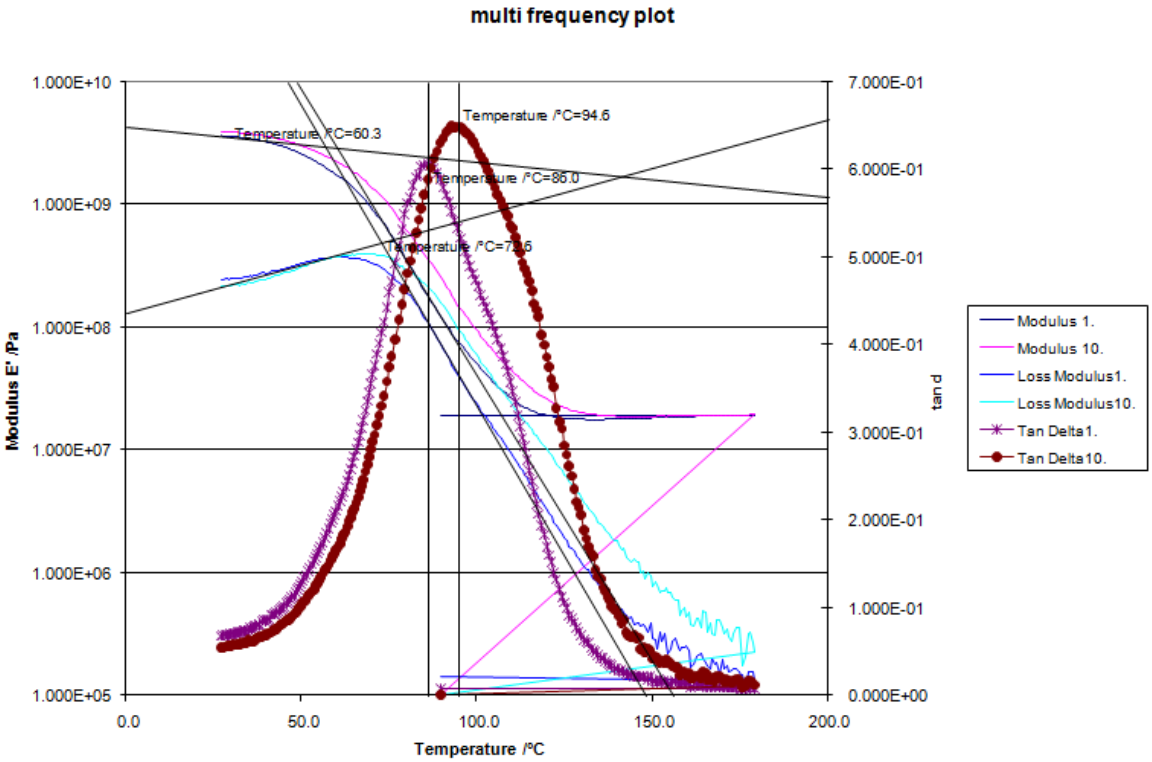

h) After 4 months of hydrothermal ageing at temperature 23^{o}C

Specimen 23-4-1

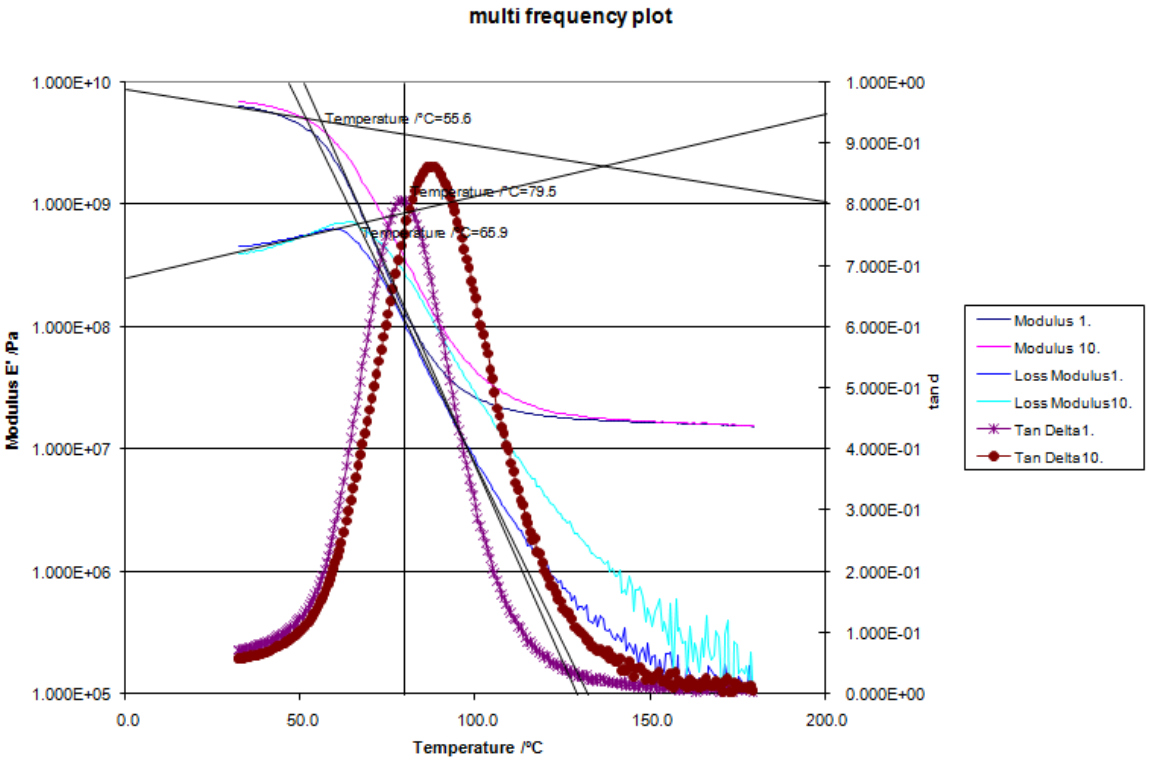

Specimen 23-4-2

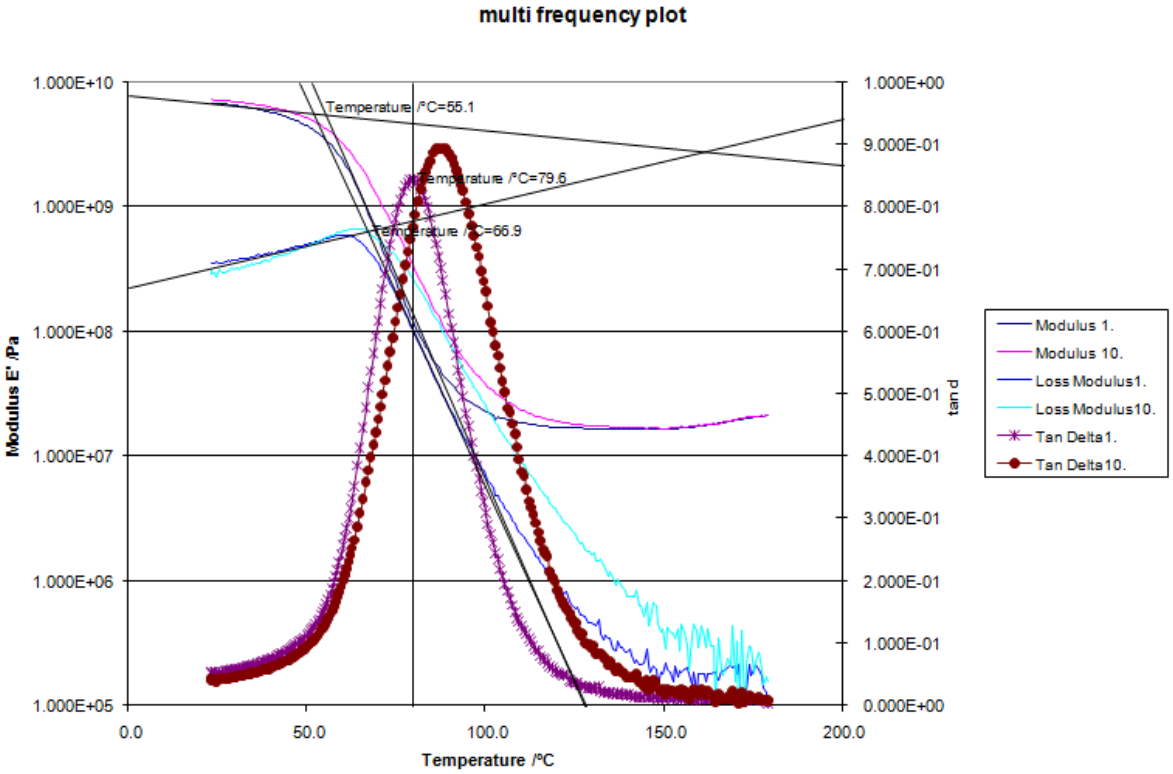

i) After 4 months of hydrothermal ageing at temperature of 40°C

Specimen 40-4-1

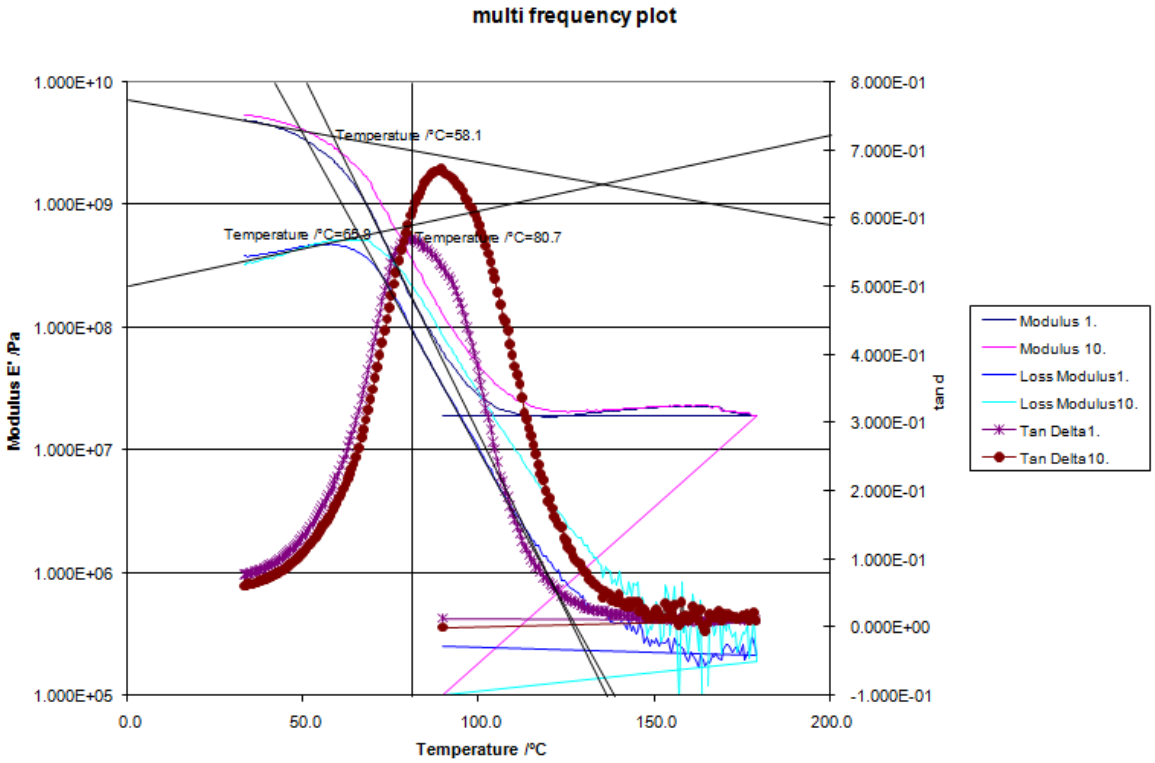

Specimen 40-4-2

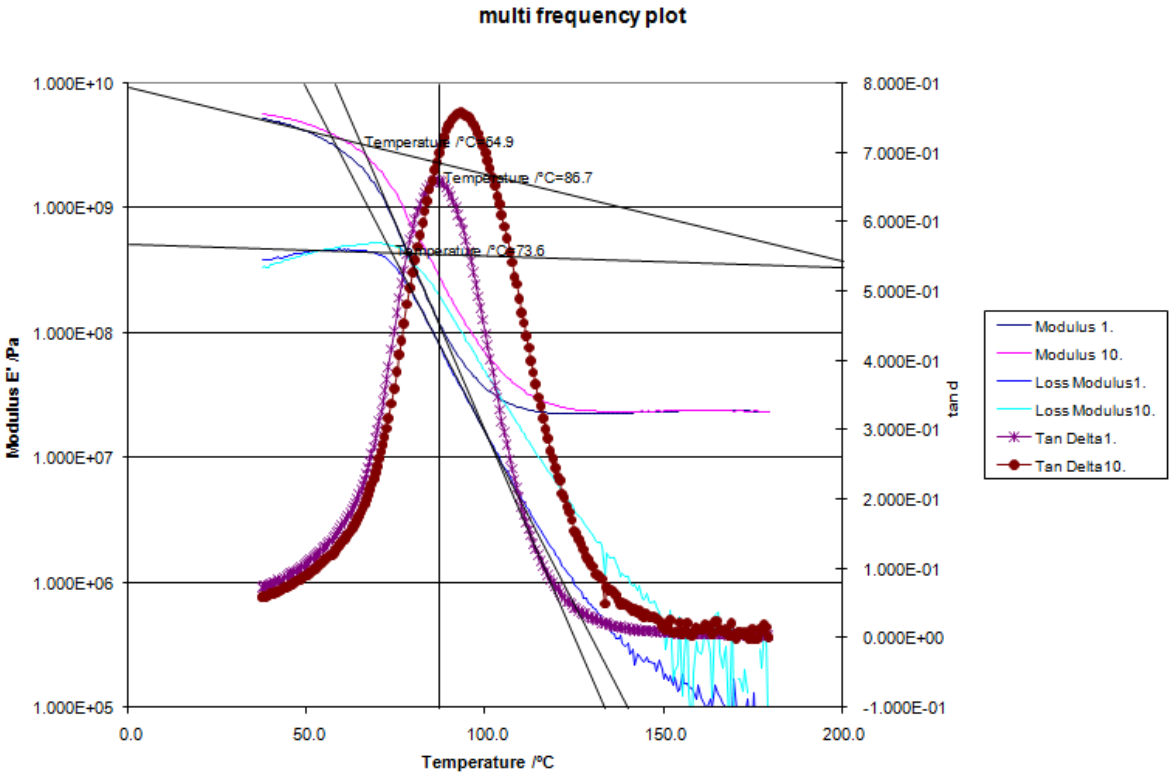

j) After 4 months of hydrothermal ageing at temperature of 60°C

Specimen 60-4-1

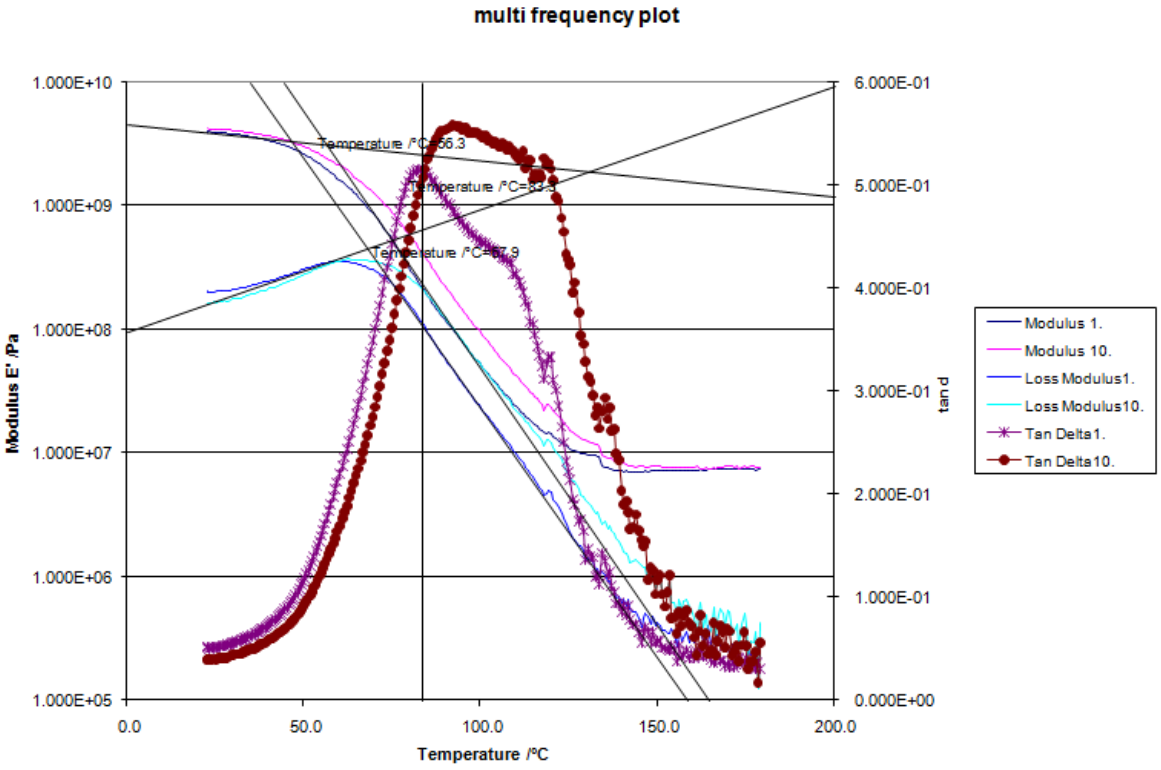

Specimen 60-4-2

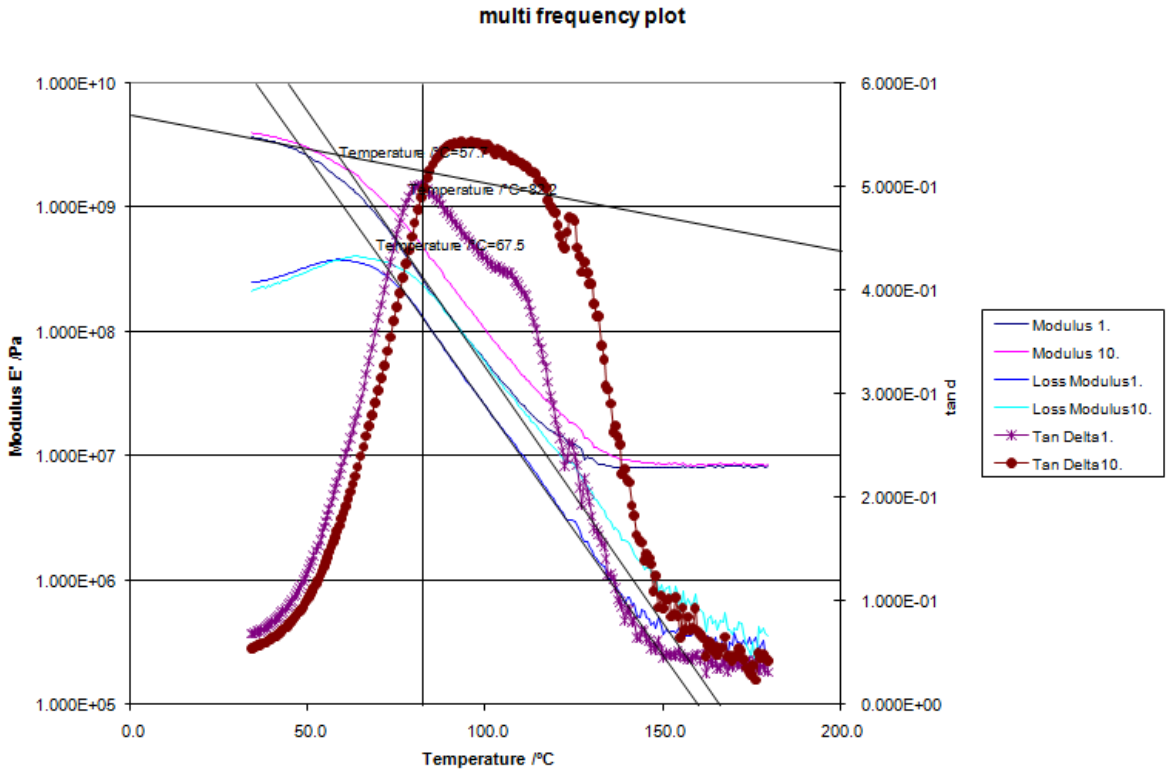

k) After 5 months of hydrothermal ageing at temperature of 23°C

Specimen 23-5-1

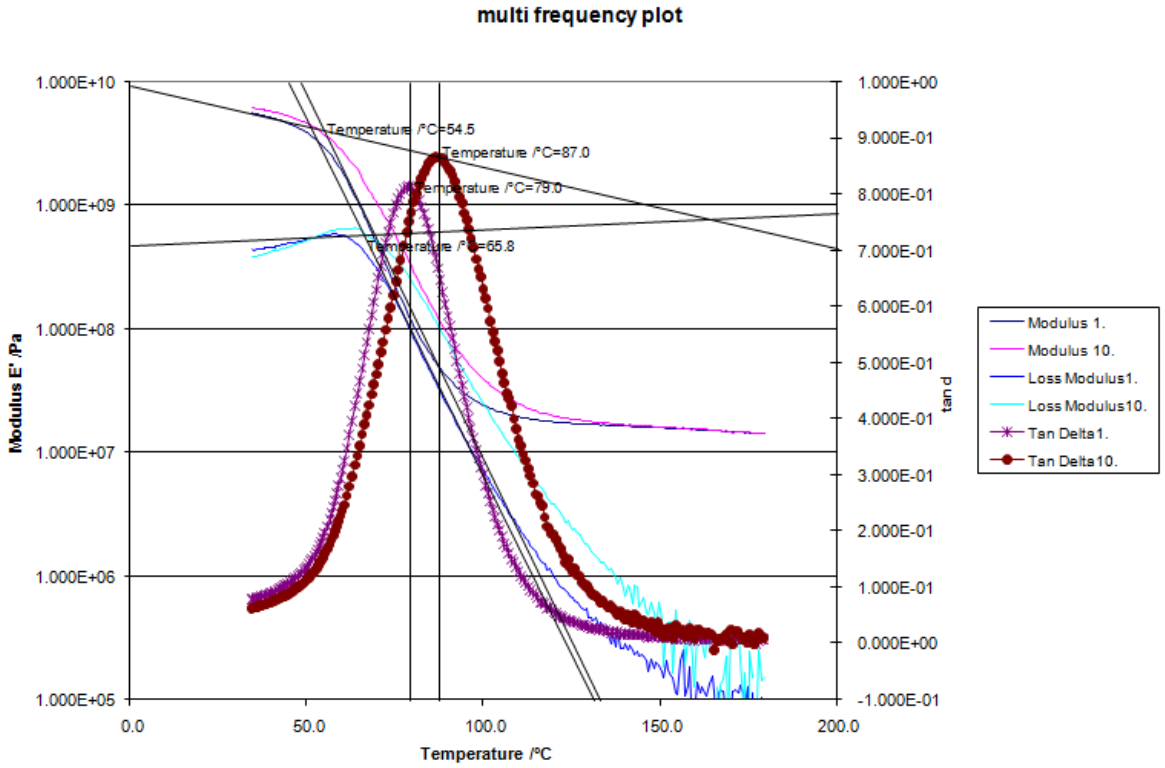

Specimen 23-5-2

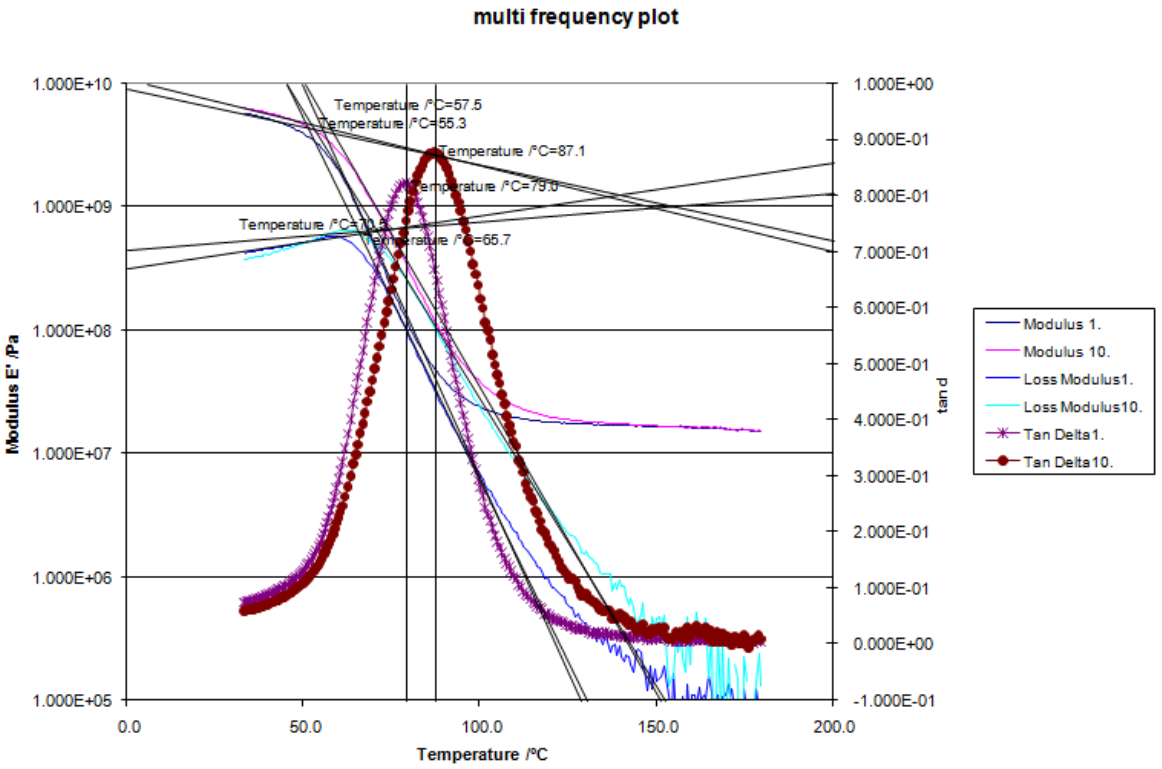

l) After 5 months of hydrothermal ageing at temperature of 40°C

Specimen 40-5-1

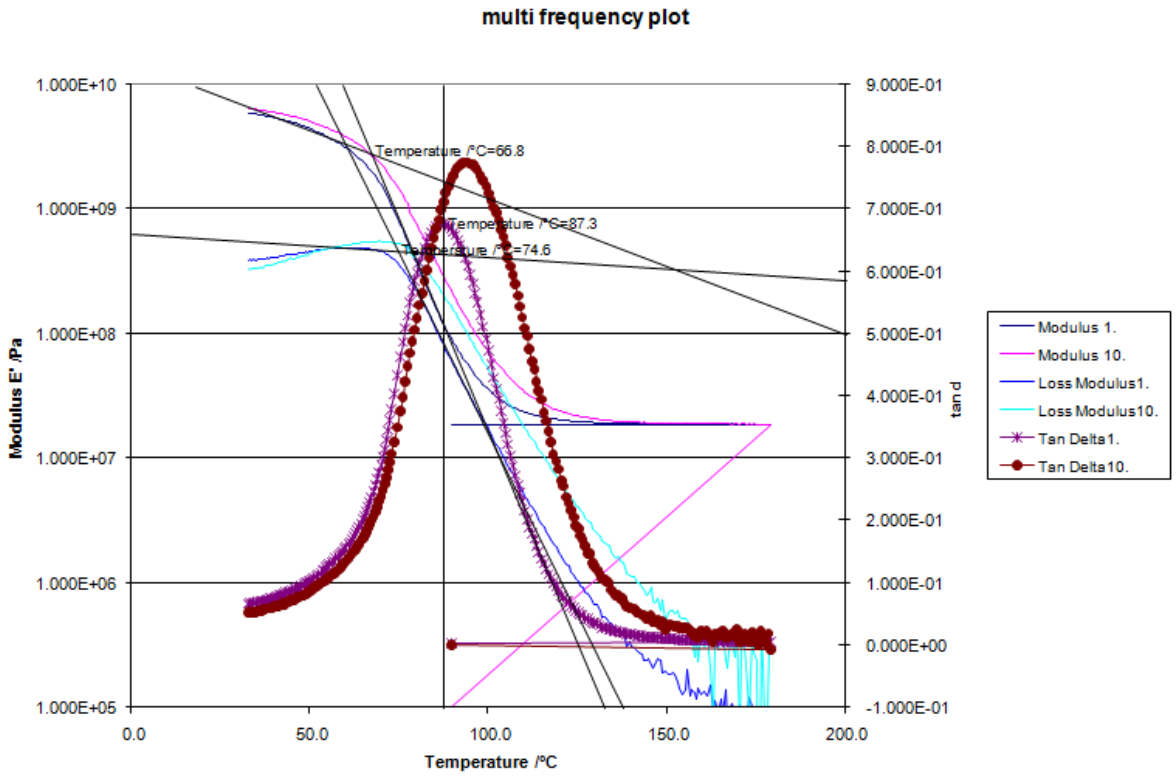

Specimen 40-5-2

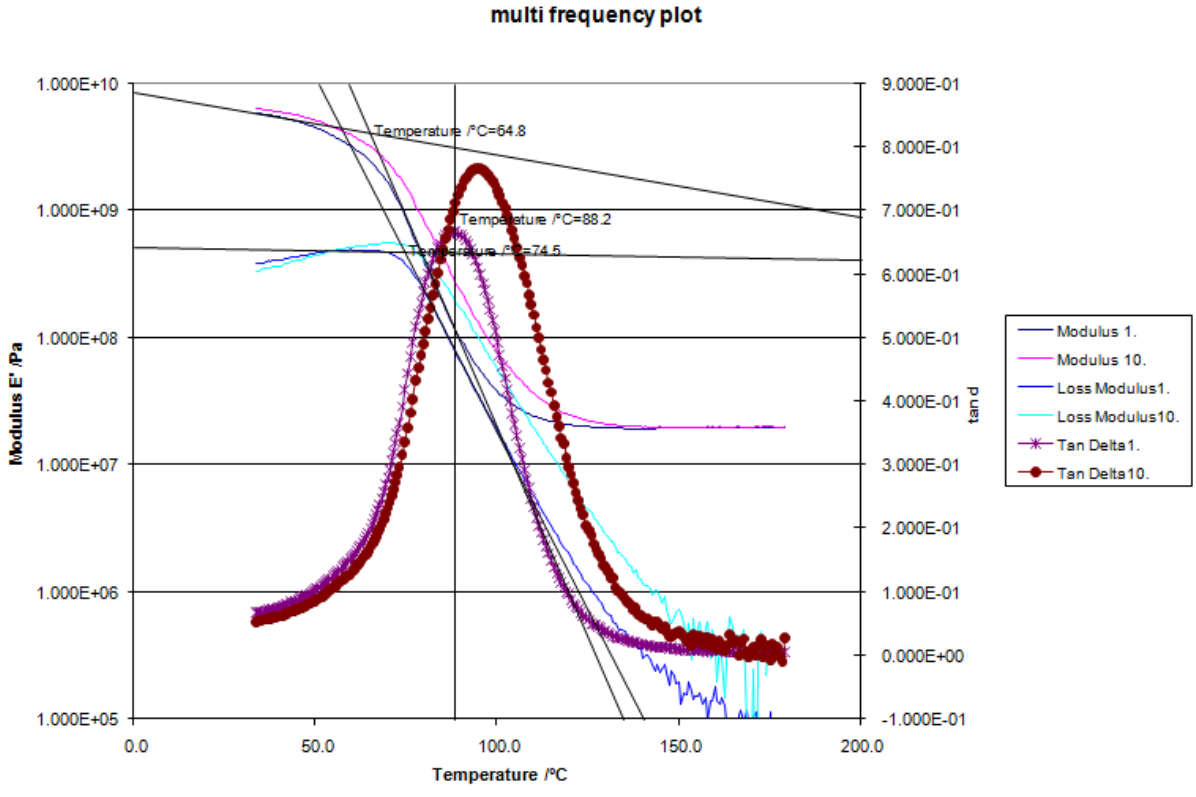

m) After 5 months of hydrothermal ageing at temperature of 60°C

Specimen 60-5-1

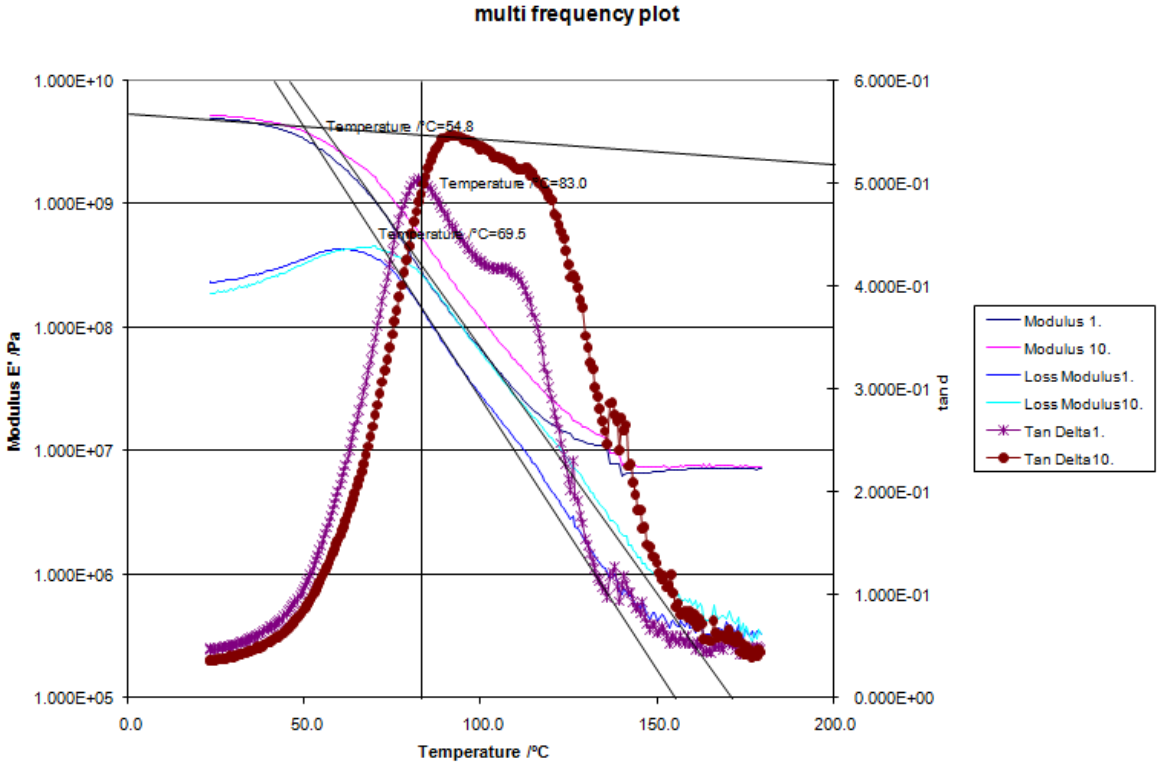

Specimen 60-5-2

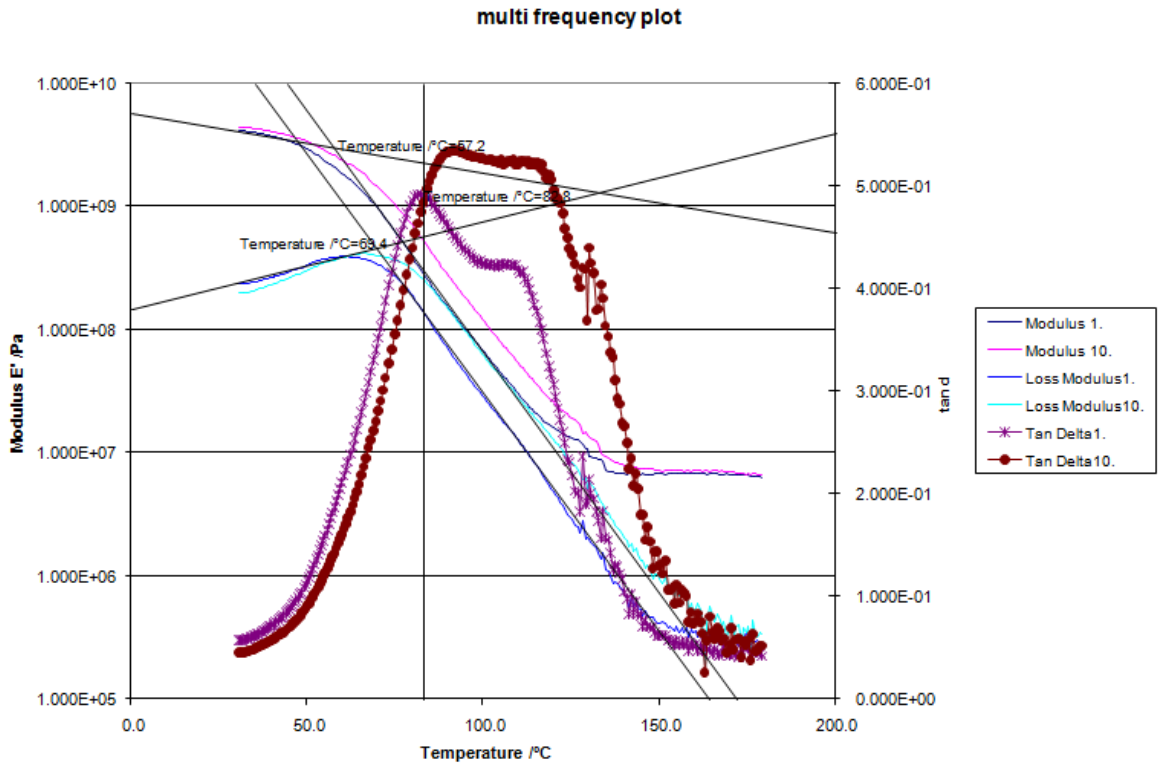

Table 1D: Glass transition temperature results after subjecting specimens to hydrothermal treatment at respective temperatures of 23^{o}C, 40^{o}C and 60^{o}C over a maximum period of 150 days.

Time (days)	Glass Transition Temperature Values (^{o}C)																	
	23°C						40°C						60°C					
	1	2	3	4	Avg	StdDev	1	2	3	4	Avg	StdDev	1	2	3	4	Avg	StdDev
0	90.2	90	89.7	-	89.966	0.251661	90.2	90	89.7	-	89.966	0.251661	90.2	90	89.7	-	89.966	0.25166
30	79.3	78.3	79.3	-	78.966	0.57735	79.7	79.4	87.2	88	83.575	4.66074	84.6	79.8	85.7	79.3	82.35	3.27058
60	80.7	86.5	80.7	81.2	82.275	2.826511	88	81.7	86.9	88.7	86.325	3.171093	82.4	84	83.9	-	83.433	0.89629
90	79.6	80.5	80.2	80.1	80.1	0.458258	86.8	82.5	82.7	88.8	85.2	3.112341	87.1	86	87	81.4	85.375	2.69614
120	79.5	79.6	79.7	-	79.6	0.1	80.7	86.6	82	87.6	84.225	3.386616	83.3	82.3	83.8	89.1	84.625	3.04781
150	79	79	79.5	78.9	79.1	0.270801	87.3	-	88.2	87.1	87.75	0.636396	83	82.8	83.6	82.3	82.925	0.53774

APPENDIX E:

REGRESSION ANALYSIS RESULTS SUMMARY FOR THE GLASS TRANSITION TEMPERATURE.

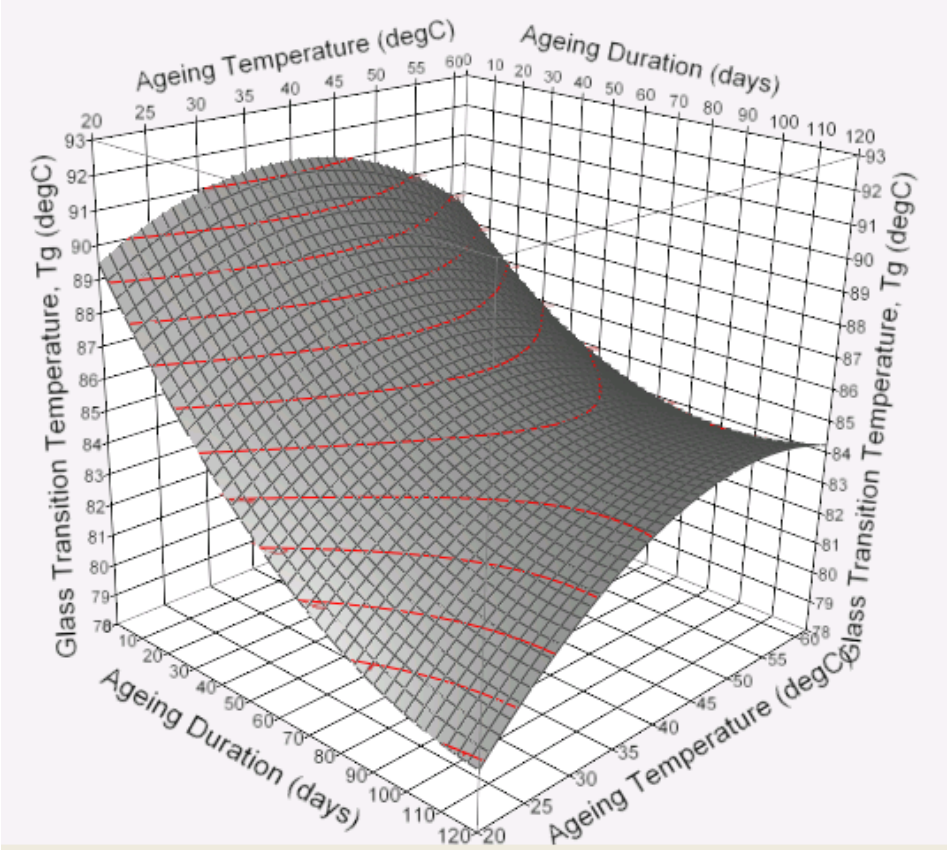

Figure E1: Fitted glass transition temperature surface plot.

The fitted contour plot in Figure E1 can be described by the following regression model prediction expression:

The fitted surface plot in Figure E1 shows the variations in composite's glass transition temperature as a function of hydrothermal ageing temperature and treatment period based on the model. This variation in the property can be described by equation (E.1):

$$T_g = 85.6335 + 1.03416667\alpha - 3.578333\beta + 1.25075\alpha\beta - 2.088\alpha^2 + 2.1534999\beta^2 \quad \text{(E.1)}$$

Where

T_g – The Glass transition Temperature, ^{o}C.

α – is a temperature-based parameter which is equal to:

$$\alpha = \frac{Temp - 40}{20}$$

β – isa ageing duration-based parameter which is equal to:

$$\beta = \frac{Duration - 60}{60}$$

Below is a summary of the regression analysis.

1) Overall Regression model equation Accuracy

According to the analysis data presented in Table E1, the regression equation (E.1) approximates the real data with an accuracy of 95.1%.

Table E1: Summary of Model Fit

RSquare	0.951564
RSquareAdj	0.891018
Root Mean Square Error	1.169596
Mean of Response	85.6728
Observations (or Sum Wgts)	10

2) Probability That This Output Was Not By Chance (ANOVA – Significance of F)

Table E2: ANOVA – Significance of F

Source	**DF**	**Sum of Squares**	**Mean Square**	**F Ratio**
Model	5	107.49765	21.4995	15.7165
Error	4	5.47182	1.3680	**Prob> F**
C. Total	9	112.96947		0.0098*

The significance of F value shows that there is only less that 1% chance that the regression output was merely a chance occurrence. In other words, this means that there is over 99% confidence in the ability of the model to explain the dependent variable (observed response).

3) Individual Regression Model Coefficient and Y-Intercept Accuracy

Table E3: Model Parameter Estimates

Term	**Estimate**	**Std Error**	**t Ratio**	**Prob>|t|**
Intercept	85.6335	0.698967	122.51	<.0001*
Ageing Temperature(20,60)	1.0341667	0.477486	2.17	0.0963
Ageing Period(0,120)	-3.578333	0.477486	-7.49	0.0017*
Ageing Temperature*Ageing Period	1.25075	0.584798	2.14	0.0992
Ageing Temperature*Ageing Temperature	-2.088	0.76568	-2.73	0.0526
Ageing Period*Ageing Period	2.1535	0.76568	2.81	0.0482*

Prediction Model Expression (original)

$$
\begin{aligned}
&85.6335 \\
&\quad 1.03416666666667 \\
&+ * \left[\frac{(\text{Ageing Temperature} - 40)}{20} \right] \\
&+ -3.5783333333333 * \left[\frac{(\text{Ageing Period} - 60)}{60} \right] \\
&+ \left[\frac{(\text{Ageing Temperature} - 40)}{20} \right] \\
&\quad * \left[\left[\frac{(\text{Ageing Period} - 60)}{60} \right] * 1.25075 \right] \\
&+ \left[\frac{(\text{Ageing Temperature} - 40)}{20} \right] \\
&\quad * \left[\left[\frac{(\text{Ageing Temperature} - 40)}{20} \right] * -2.088 \right] \\
&+ \left[\frac{(\text{Ageing Period} - 60)}{60} \right] \\
&\quad * \left[\left[\frac{(\text{Ageing Period} - 60)}{60} \right] * 2.15349999999997 \right]
\end{aligned}
$$

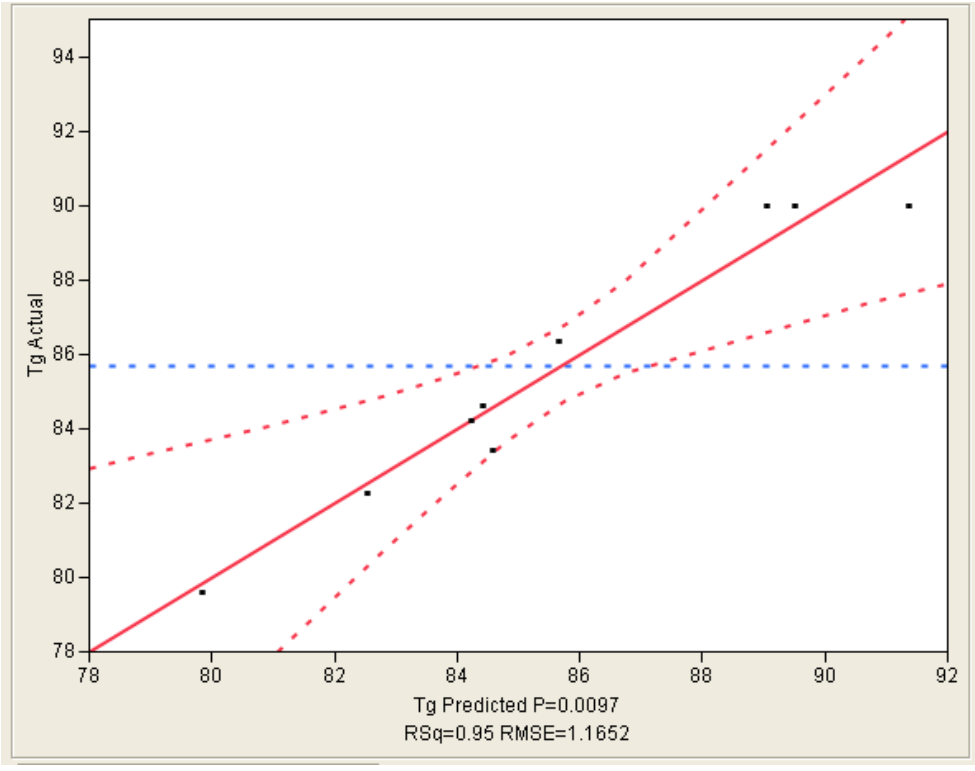

Figure E2: Actual vs predicted glass transition temperature plot.

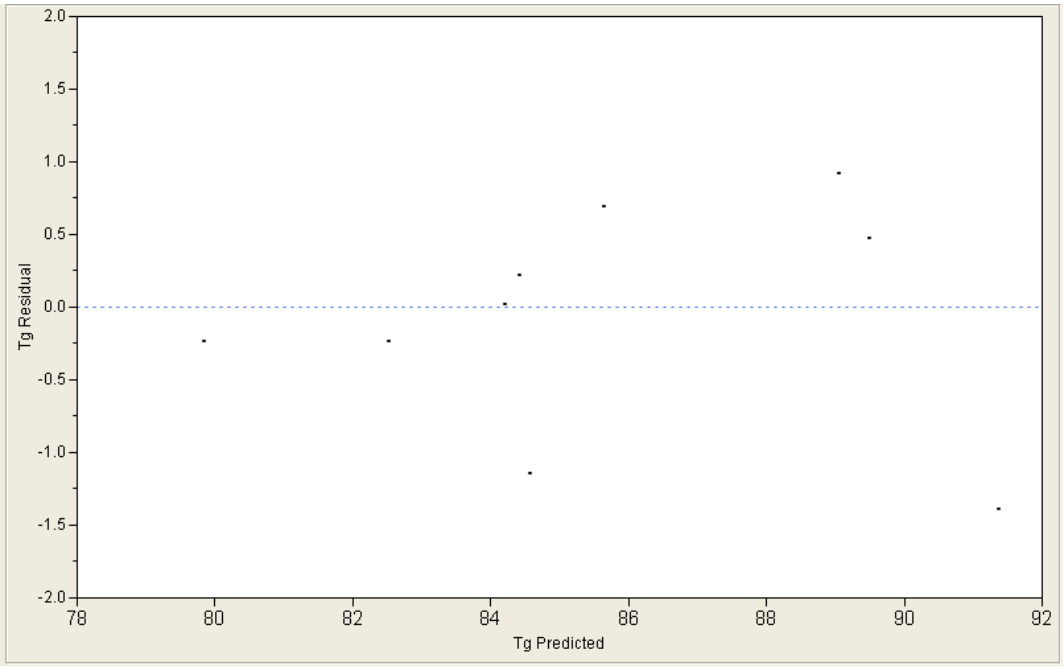

Figure E3: Residual vs Predicted glass transition plot.

APPENDIX F:

REGRESSION ANALYSIS RESULTS SUMMARY FOR THE MICROBOND STRENGTH TESTS.

Response Microbond Strength

Actual by Predicted Plot

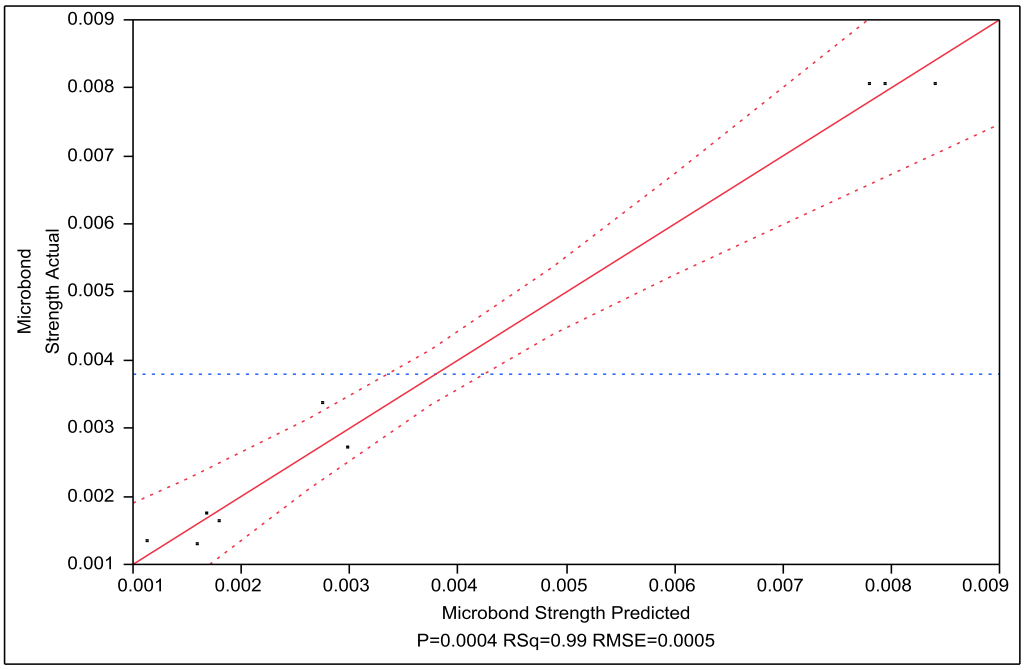

Figure F1: Response Microbond Strength Actual vs Predicted Plot.

Summary of Fit

RSquare	0.989854
RSquareAdj	0.977171
Root Mean Square Error	0.000455
Mean of Response	0.003787
Observations (or Sum Wgts)	10

Analysis of Variance

Source	DF	Sum of Squares	Mean Square	F Ratio
Model	5	0.00008069	0.000016	78.0473
Error	4	0.00000083	2.068e-7	**Prob> F**
C. Total	9	0.00008152		0.0004*

Parameter Estimates

Term	Estimate	Std Error	t Ratio	Prob>|t|
Intercept	0.0017907	0.000272	6.59	0.0027*
Ageing Temperature(23,60)	-0.000575	0.000186	-3.10	0.0363*
Ageing Period(0,8)	-0.003058	0.000186	-16.47	<.0001*
Ageing Temperature*Ageing Period	-0.000348	0.000227	-1.53	0.2011
Ageing Temperature*Ageing Temperature	0.0003786	0.000298	1.27	0.2724
Ageing Period*Ageing Period	0.0029486	0.000298	9.90	0.0006*

Prediction Expression

$$
\begin{aligned}
&0.00179071428571 \\
&+-0.000575*\left(\frac{\left(\text{Ageing Temperature}-40\right)}{20}\right) \\
&+-0.0030583333333*\left(\frac{\left(\text{Ageing Period}-4\right)}{4}\right) \\
&+\left(\frac{\left(\text{Ageing Temperature}-40\right)}{20}\right) \\
&*\left(\left(\frac{\left(\text{Ageing Period}-4\right)}{4}\right)*-0.0003475\right) \\
&\left(\frac{\left(\text{Ageing Temperature}-40\right)}{20}\right) \\
&+\left(*\left(\left(\frac{\left(\text{Ageing Temperature}-40\right)}{20}\right)\right)\right) \\
&*0.00037857142857 \\
&\left(\frac{\left(\text{Ageing Period}-4\right)}{4}\right) \\
&+\left(*\left(\left(\frac{\left(\text{Ageing Period}-4\right)}{4}\right)*0.00294857142857\right)\right)
\end{aligned}
$$

Correlation of Estimates

Corr	**Intercept**	**Ageing Temperature(23,60)**	**Ageing Period(0,192)**	**Ageing Temperature*A geing Period**	**Ageing Temperature*A geing Temperature**	**Ageing Period*Ag eing Period**
Intercept	1.0000	0.0000	0.0000	0.0000	-0.5477	-0.5477
Ageing Temperature (23,60)	0.0000	1.0000	0.0000	0.0000	0.0000	0.0000
Ageing Period(0,8)	0.0000	0.0000	1.0000	0.0000	0.0000	0.0000
Ageing Temperature *Ageing Period	0.0000	0.0000	0.0000	1.0000	0.0000	0.0000
Ageing Temperature *Ageing Temperature	-0.5477	0.0000	0.0000	0.0000	1.0000	-0.1667
Ageing Period*Agei ng Period	-0.5477	0.0000	0.0000	0.0000	-0.1667	1.0000

Microbond Strength Variation as a function of Ageing Temperature and Duration

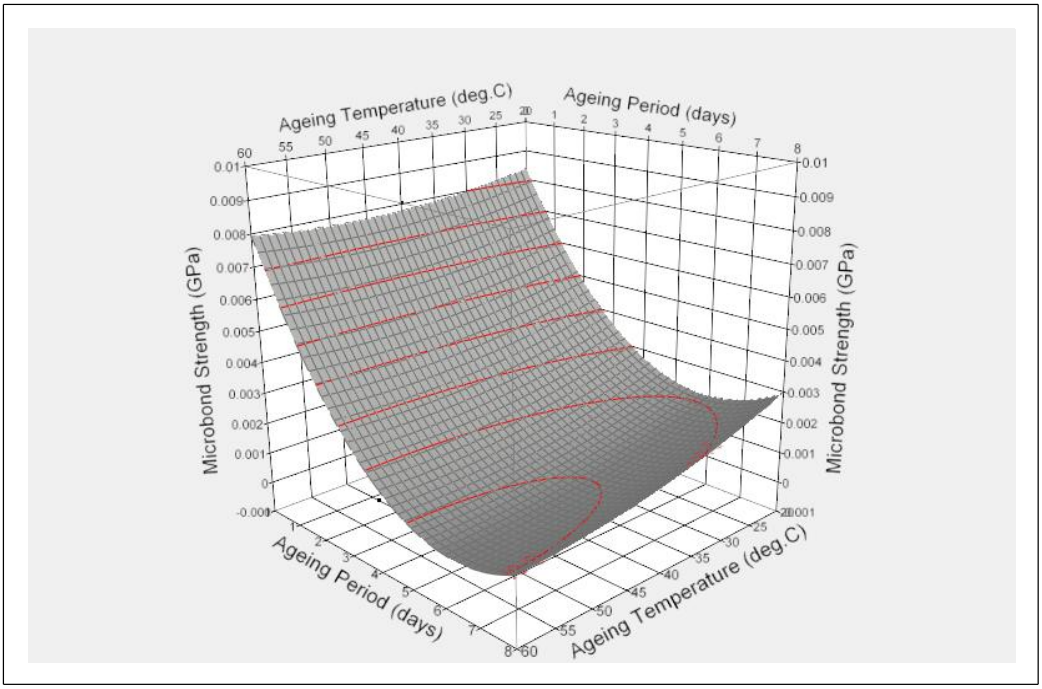

Figure F2: The fitted surface plot describing variations in microbond interfacial strength as a function of hydrothermal ageing temperature and treatment period based on the derived empirical model.

APPENDIX G:

SEM IMAGES

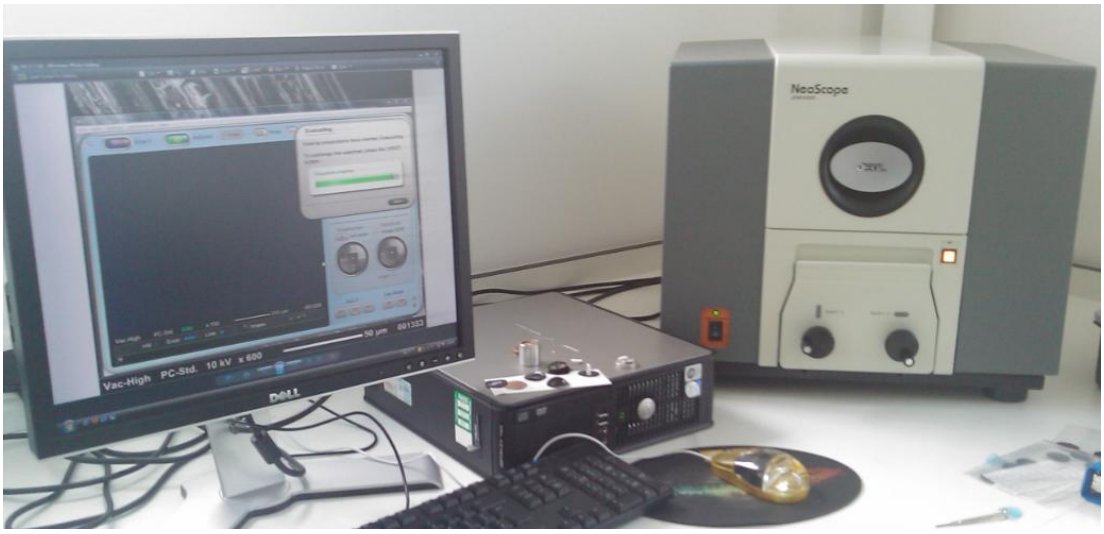

Figure G1: NeoScope JCM 5000 portable scanning electron microscope.

Neat Sisal Fibre

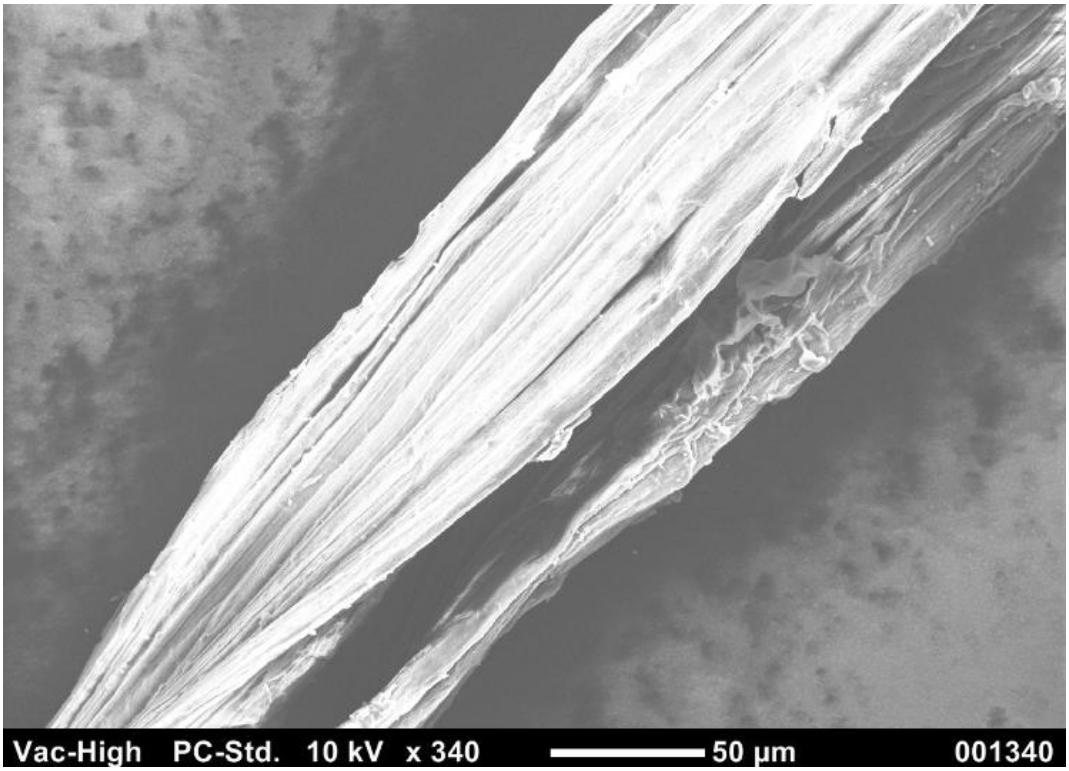

Figure G2: Scanned microscopic image of an unreinforced single sisal fibre.

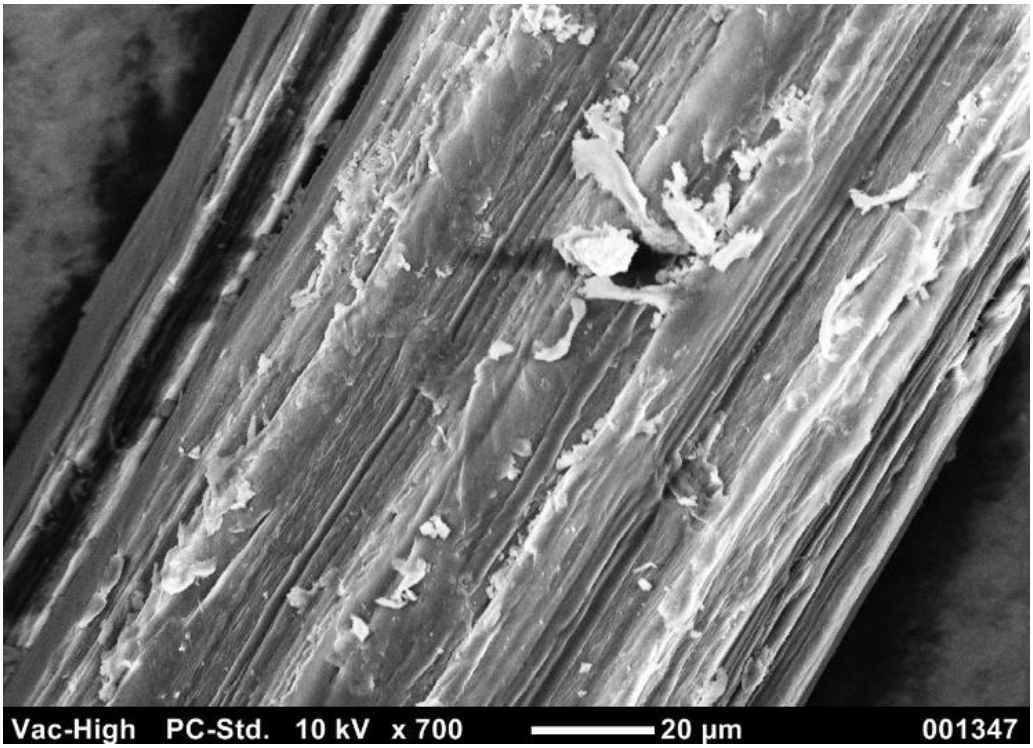

Figure G3: Scanning microscopic image of the surface of a sisal fibre following interfacial debonding of the untreated sisal/polyester microbond composite system.

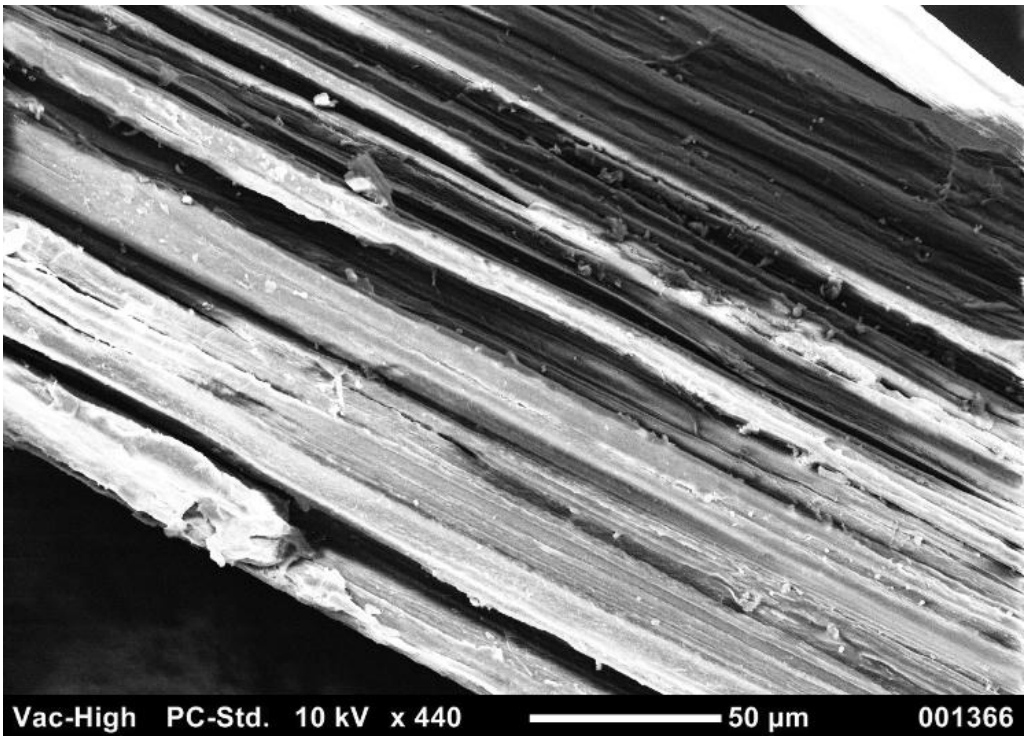

Figure G4: Scanning Microscopic image of the surface of a sisal fibre following interfacial debonding of hydrothermally treated sisal/polyester microbond composite system at temperature of 23^{o}C for a period of two days.

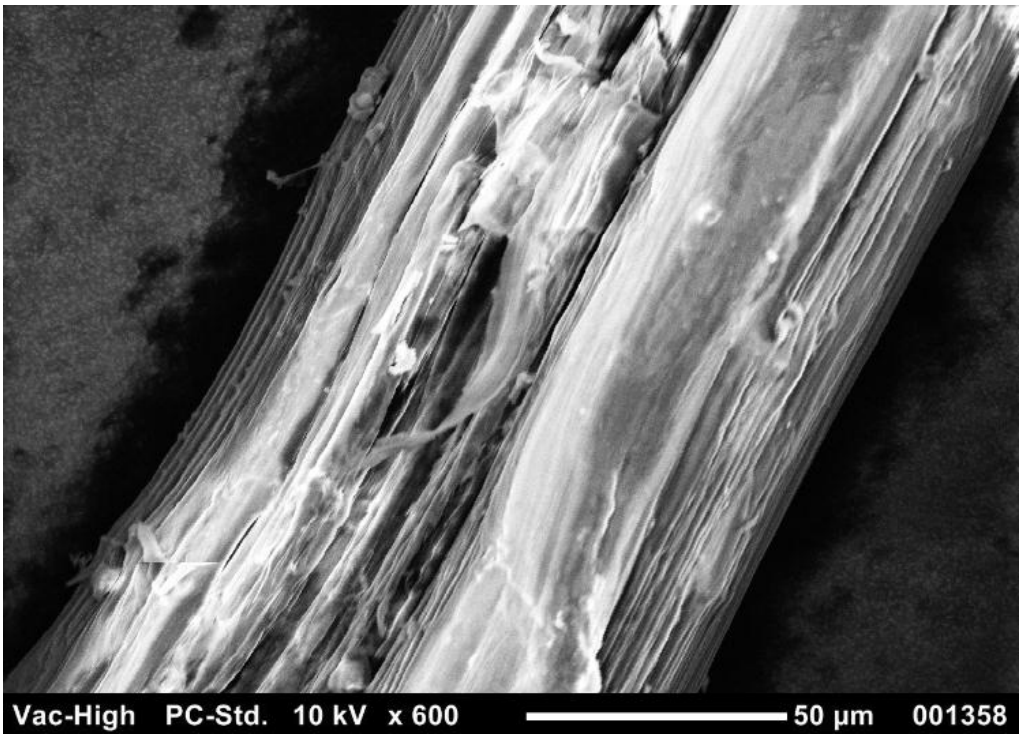

Figure G5: Scanning Microscopic image of the surface of a sisal fibre following interfacial debonding of hydrothermally treated sisal/polyester microbond composite system at temperature of 40^{o}C for a period of two days.

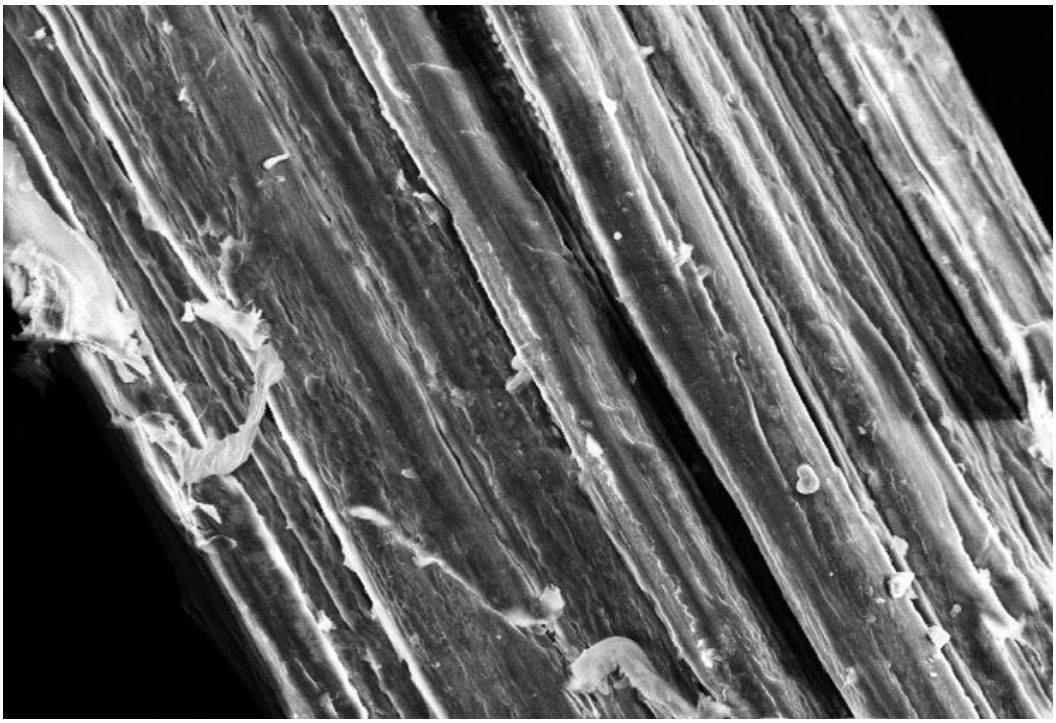

Figure G6: Scanning Microscopic image of the surface of a sisal fibre following interfacial debonding of hydrothermally treated sisal/polyester microbond composite system at temperature of 60^{o}C for a period of two days.

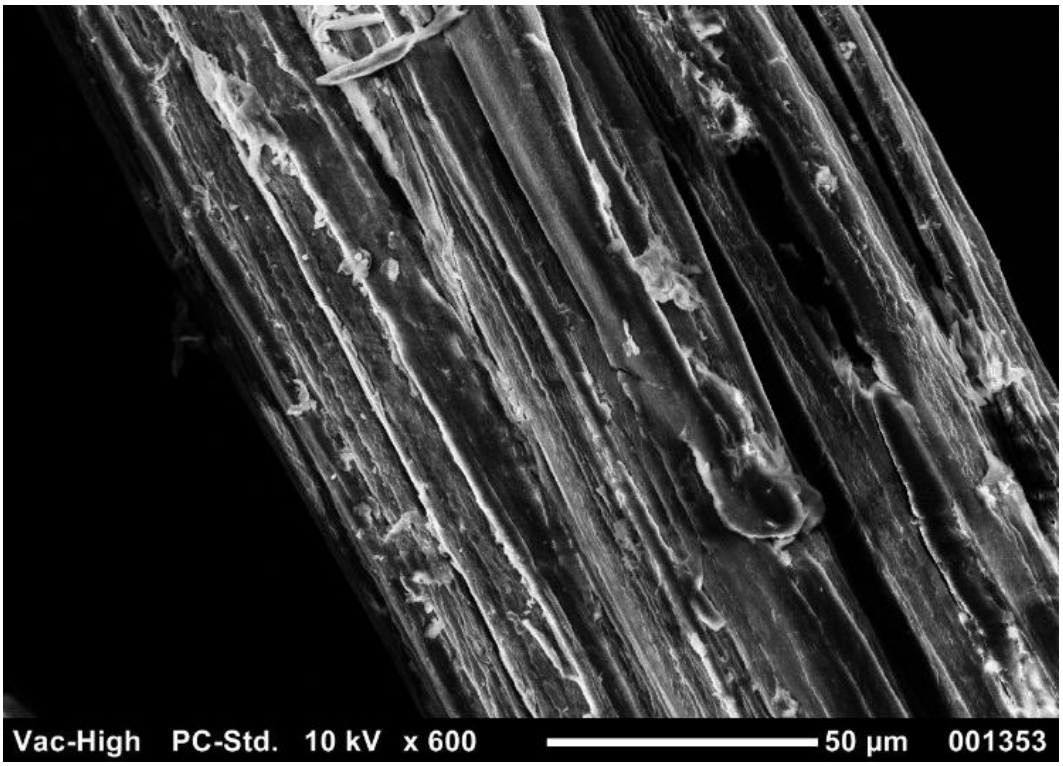

Figure G7: Scanning Microscopic image of the surface of a sisal fibre following interfacial debonding of hydrothermally treated sisal/polyester microbond composite system at temperature of 60^{o}C for a period of four days.

APPENDIX H:

SAMPLE FRACTURE TOUGHNESS TEST RESULT PLOTS.

A) Untreated Specimens

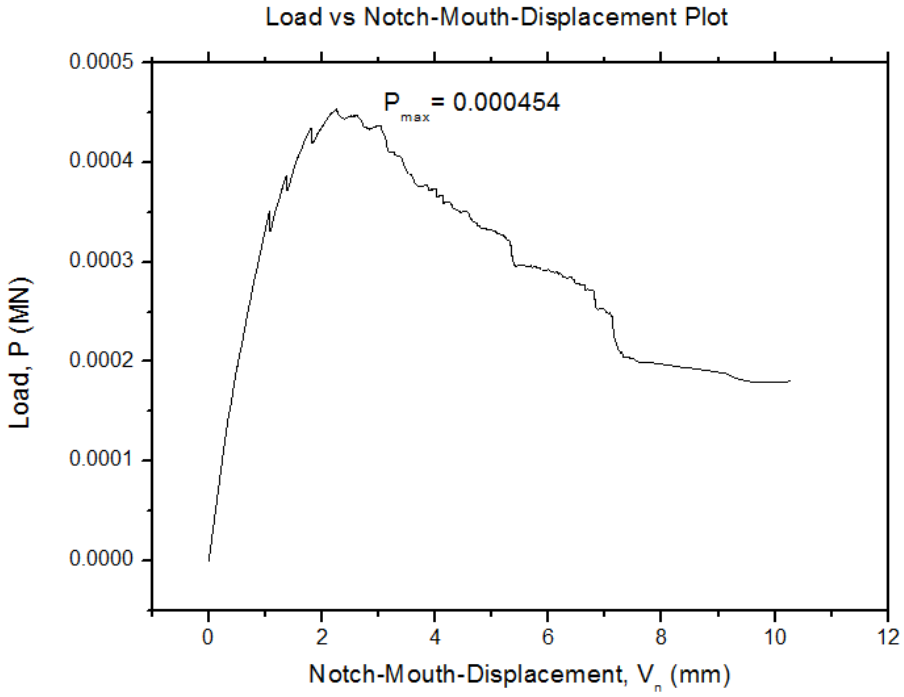

B) After 1 month of hydrothermal treatment of composite specimens.

Specimens hydrothermally treated at 23^{o}C

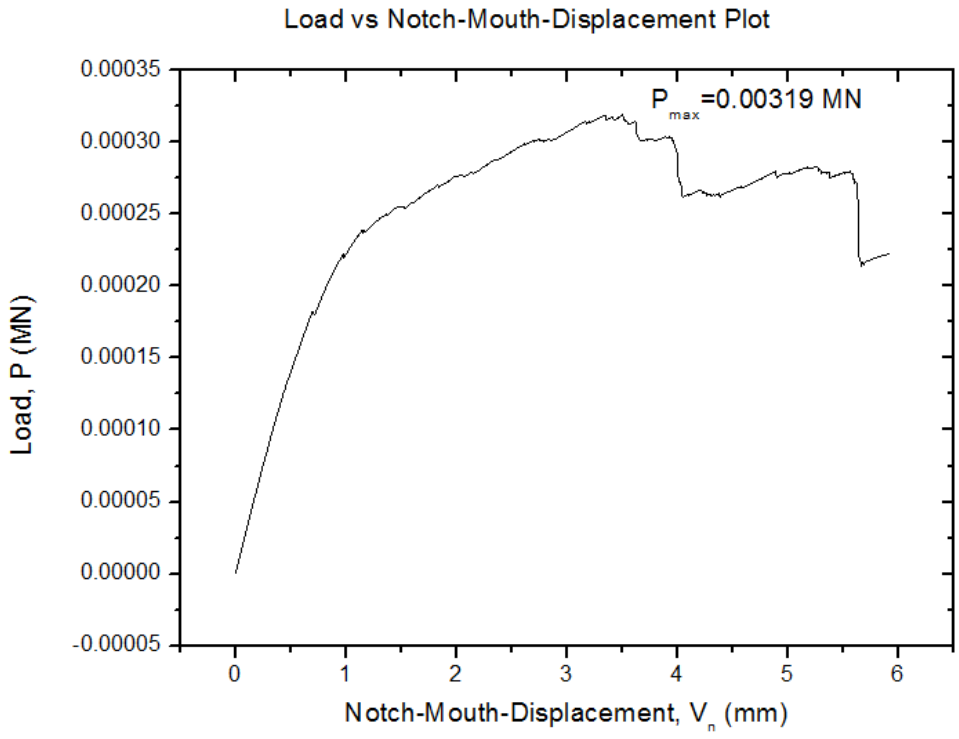

Specimens hydrothermally treated at 40^{o}C

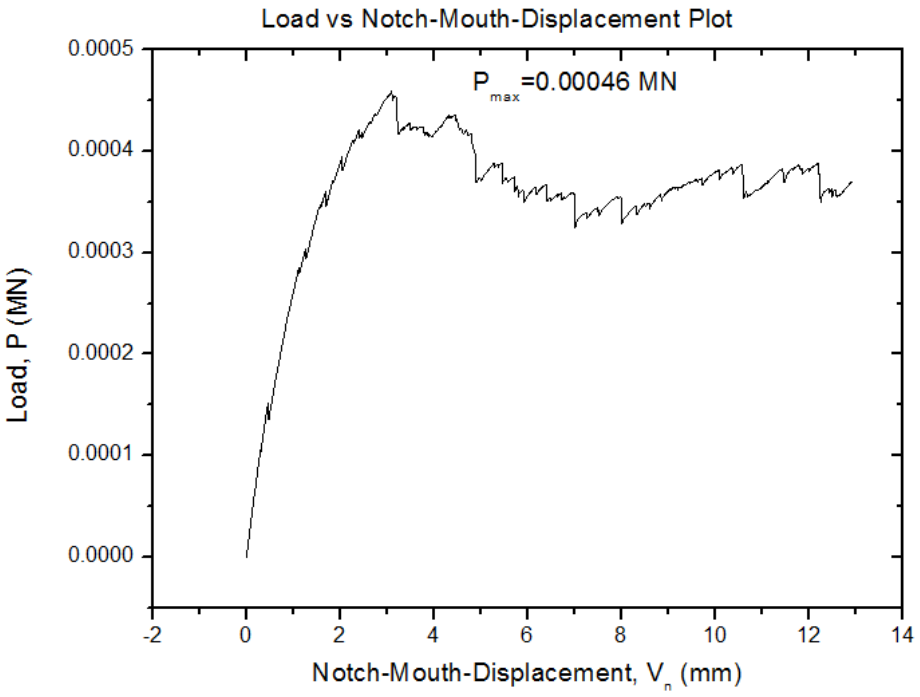

Sample hydrothermally treated at 60^{o}C

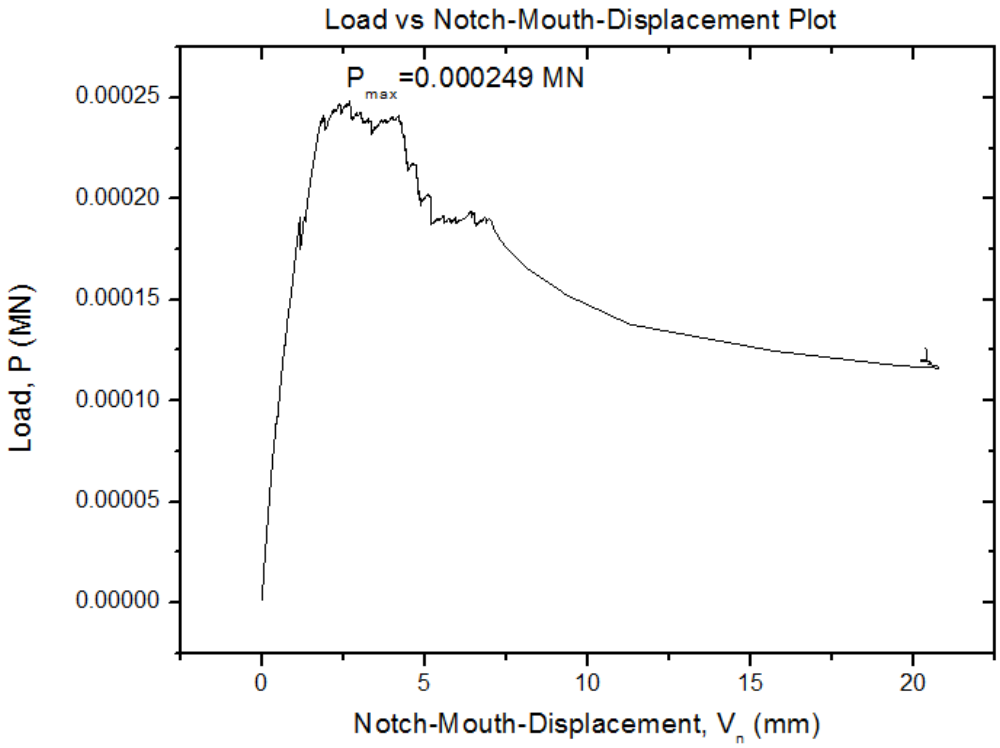

C) After 2 months of hydrothermal treatment of fracture toughness specimens.

Specimens treated at 23^{o}C

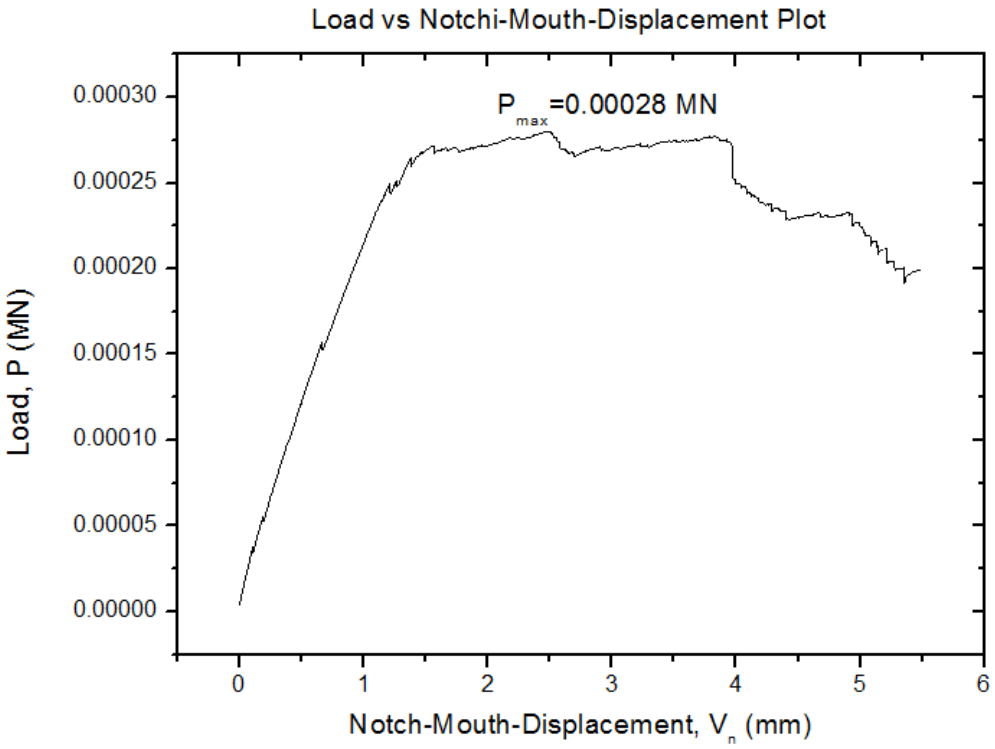

Specimens treated at 40^{o}C

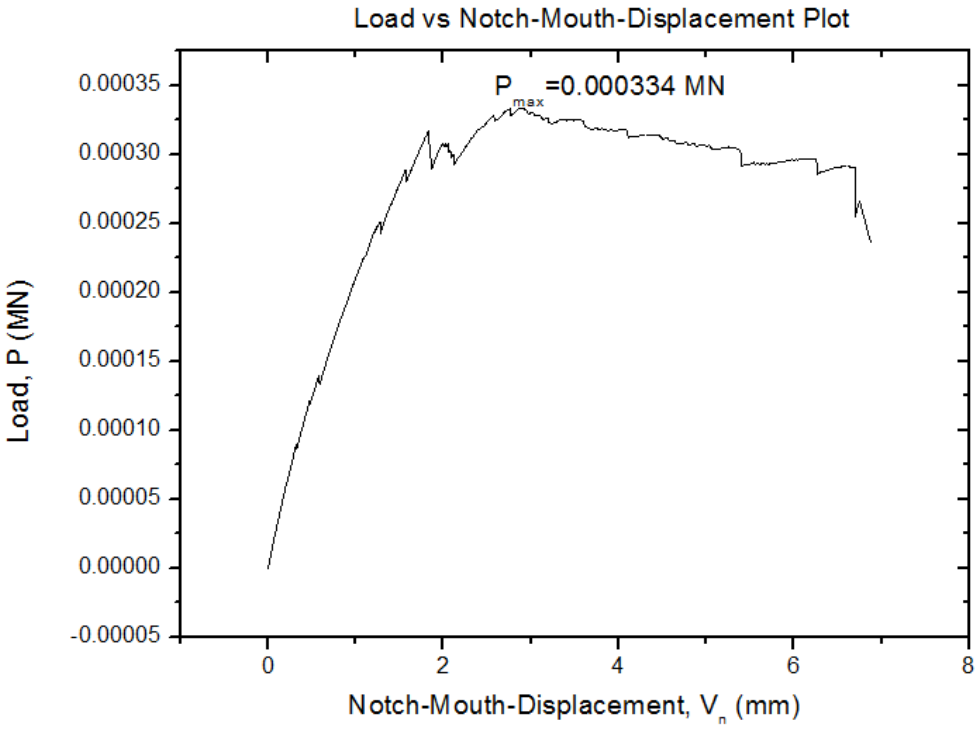

Specimens treated at 60^{o}C

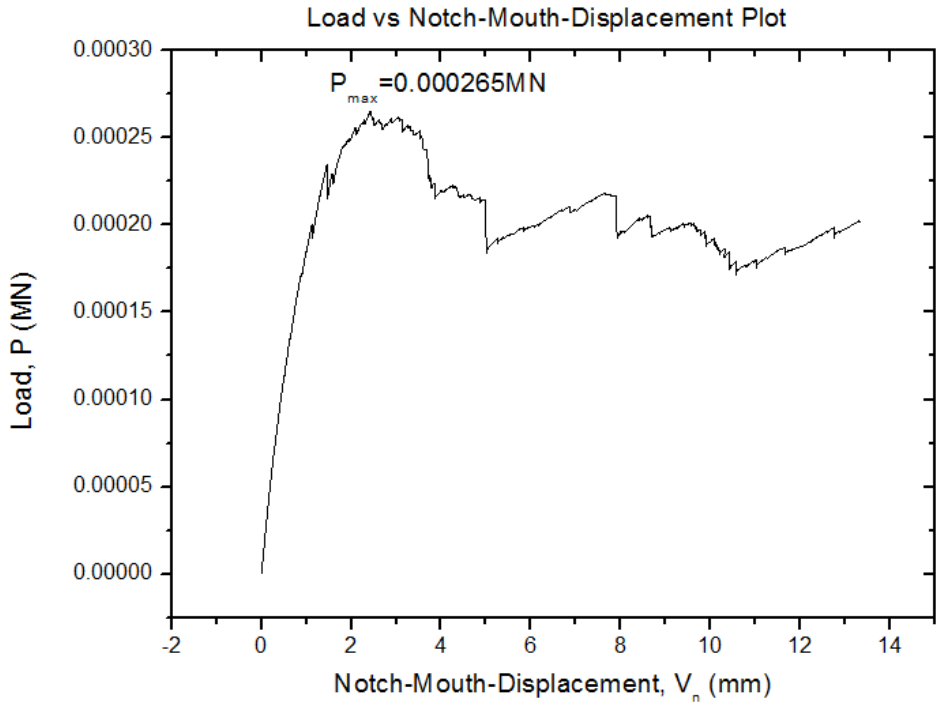

C) After 3 months of hydrothermal treatment of fracture toughness specimens

Specimens treated at 23^{o}C

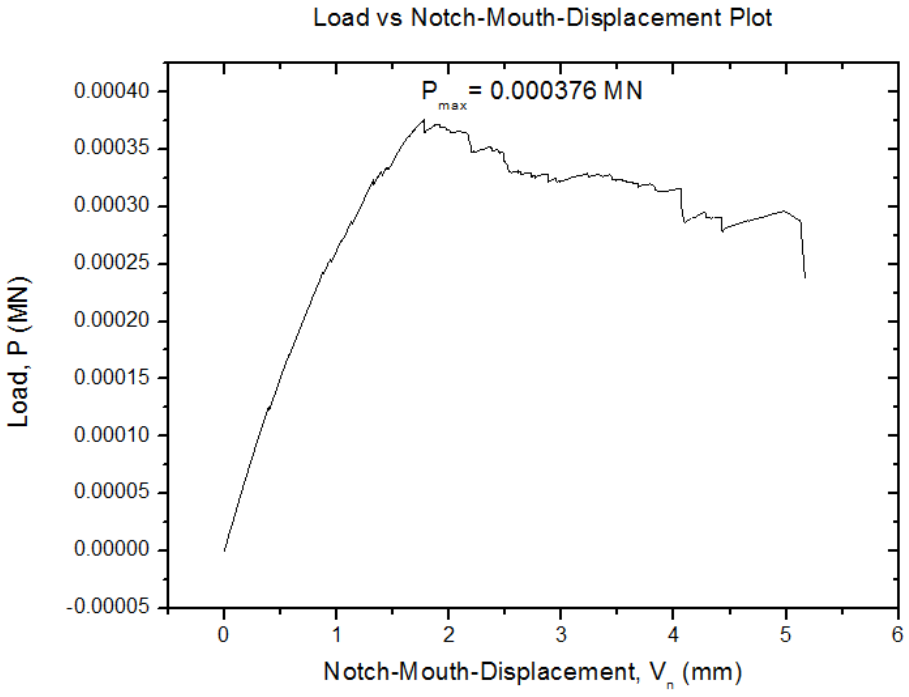

Specimens treated at 40^{o}C

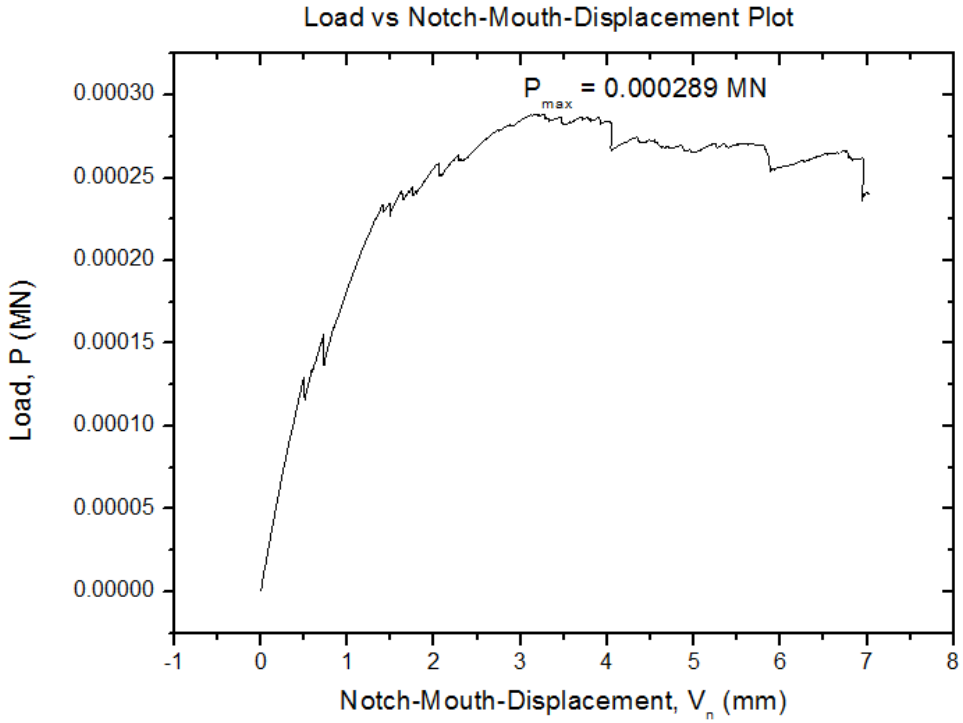

Specimens treated at 60^{o}C

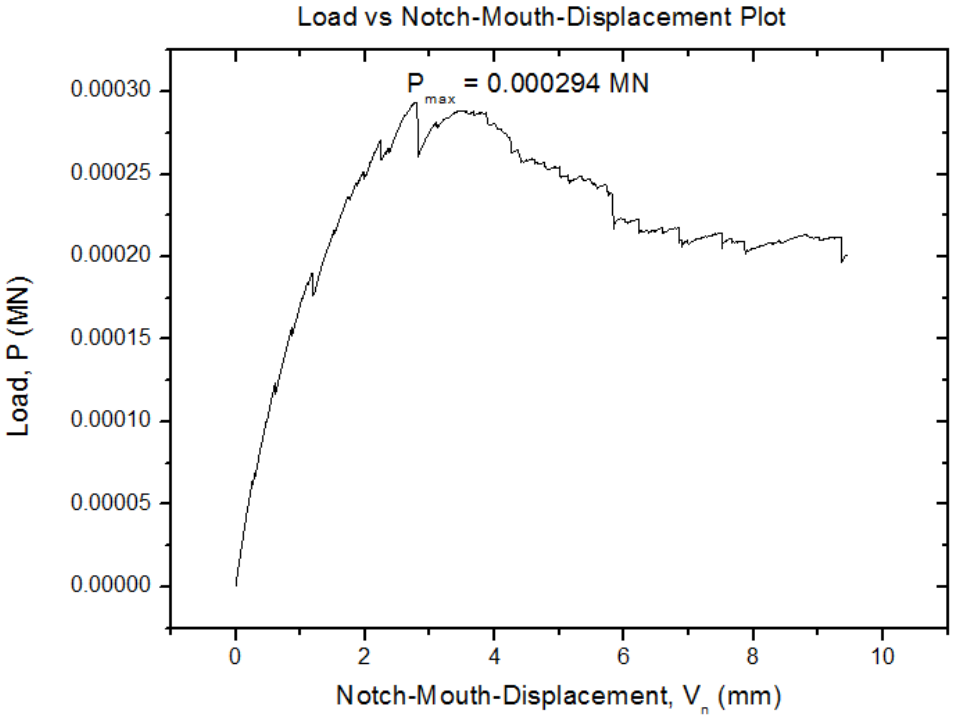

D) After 4 months of hydrothermal treatment of fracture toughness specimens.

Specimens treated at 23^{o}C

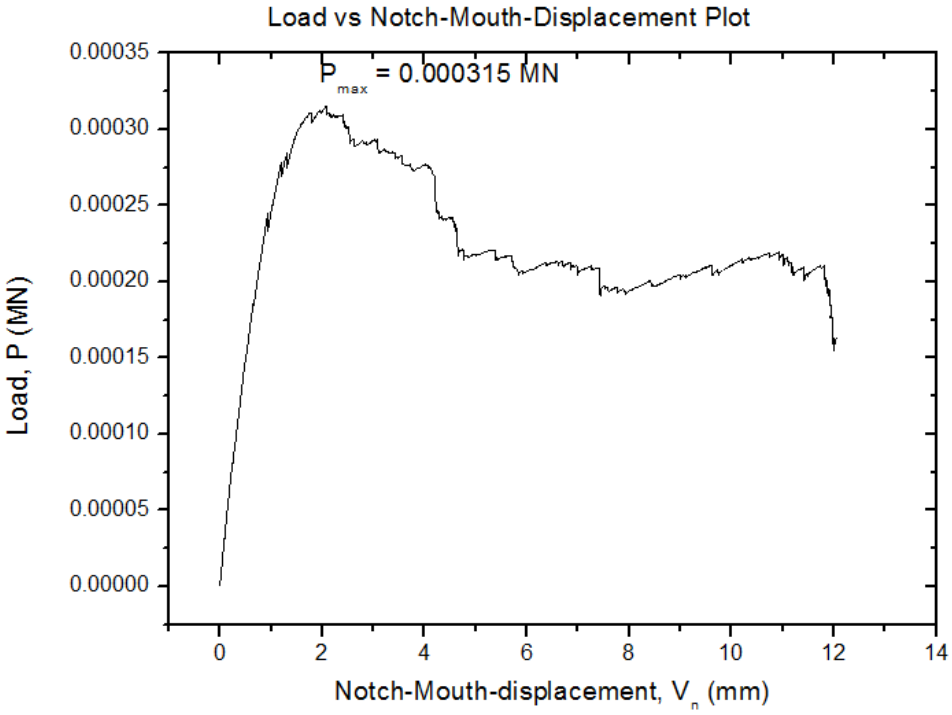

Specimens treated at 40^{o}C

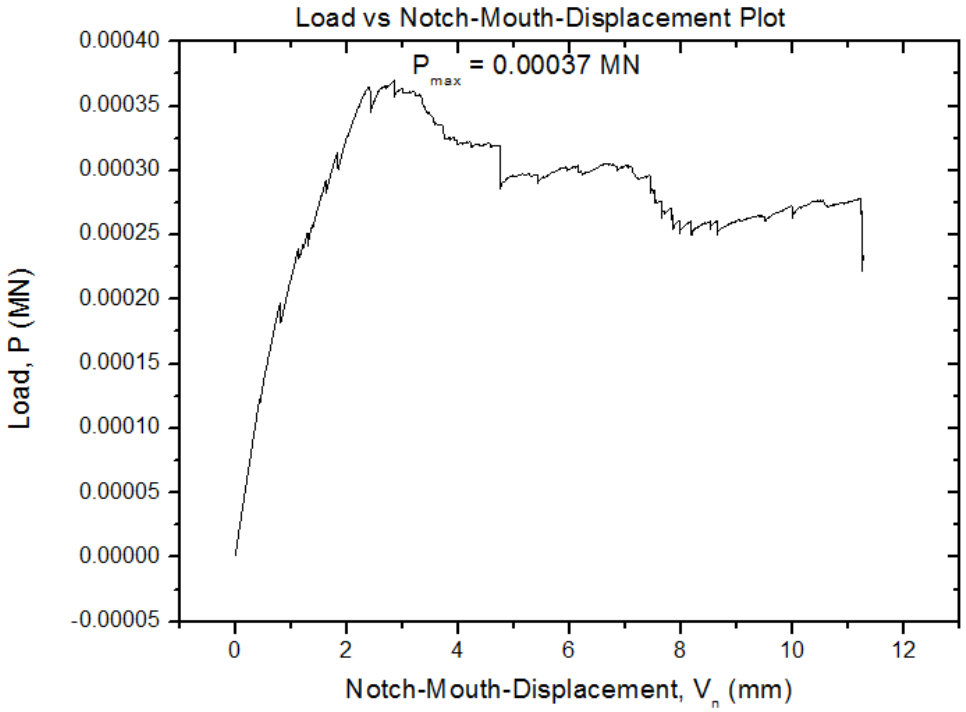

Specimen treated at 60^{o}C

Specimen 60-4-3

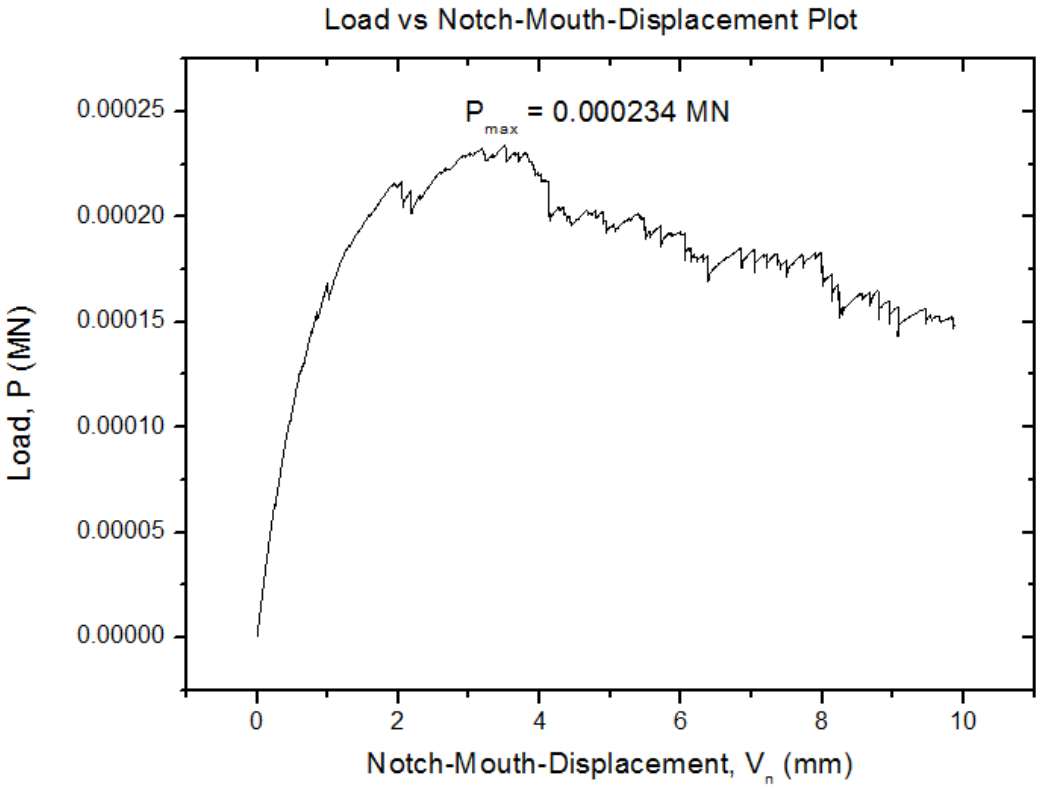

APPENDIX I:

FRACTURE TOUGHNESS TEST SPECIMENS MEASURED DIMENSIONS AND EXPERIMENT TEST RESULTS OF HYDROTHERMALLY TREATED SISAL FIBRE REINFORCED POLYESTER COMPOSITE.

Specimen Code	Dimensions												Experiment Results		
	Notch Length (Nearest 0.1mm)			Thickness, B, around notch (Nearest 0.1mm)					Width, W (Nearest 0.05mm)						Fracture Toughness
	a1	a2	Avg	B1	B2	B3	B4	Avg	W1	W2	W3	Avg	α	P_{max} (MN)	K_{TC} (MPa.m$^{1/2}$)
0-0-1	25.51	27.44	26.5	2.413	2.207	2.36	2.066	2.3	52.74	52.81	52.69	52.75	0.50237	0.000454	6.01
0-0-2	26.19	27.99	27.1	1.988	1.908	2.538	2.234	2.2	53.1	53.2	53.35	53.22	0.509207	0.000543	7.67
0-0-3	25.8	27.01	26.4	2.232	2.356	2.455	2.13	2.3	53.29	53.28	53.18	53.25	0.495775	0.000496	6.38
0-0-4	26.34	27.51	26.9	1.94	2.506	2.187	2.014	2.2	53.12	53.31	53.15	53.19	0.505734	0.000483	6.74
0-0-5	26.03	26.91	26.5	2.539	2.032	2.204	2.566	2.3	53.14	53.31	53.27	53.24	0.497746	0.000381	4.94
0-0-6	25.53	26.93	26.2	1.935	2.301	2.066	1.963	2.1	53.19	53.26	53.22	53.22	0.492296	4.20E-04	5.85
23-1-1	22.55	24.11	23.3	1.733	1.677	1.849	1.516	1.7	50.88	51.3	51.12	51.1	0.455969	0.000333	5.14
23-1-2	25.54	26.06	25.8	2.168	1.891	2.45	2.272	2.2	51.02	51.09	50.92	51.01	0.505783	0.000295	4.2
23-1-3	25.5	26.26	25.9	1.686	1.698	1.86	1.824	1.8	51.26	51.32	51.36	51.31	0.504775	0.000199	3.44
23-1-4	24.11	25.53	24.8	1.68	1.487	1.542	1.559	1.6	49.98	50	50.09	50.02	0.495802	0.000319	6.09
40-1-1	23.81	24.85	24.3	1.982	1.895	2.201	1.987	2	50.72	50.6	50.6	50.64	0.479858	0.000381	5.46
40-1-2	23.49	25.23	24.4	2.54	2.444	2.213	2.377	2.4	50.23	50.29	50.43	50.32	0.484897	0.00046	5.61

Specimen Code	Dimensions												Experiment Results		
	Notch Length (Nearest 0.1mm)			Thickness, B, around notch (Nearest 0.1mm)					Width, W (Nearest 0.05mm)						Fracture Toughness
	a1	a2	Avg	B1	B2	B3	B4	Avg	W1	W2	W3	Avg	α	P_{max} (MN)	K_{TC} (MPa.m$^{1/2}$)
40-1-3	24.94	24.19	24.6	1.737	1.813	1.785	1.773	1.8	50.37	50.55	50.39	50.44	0.487708	0.000323	5.3
40-1-4	24.66	25.42	25	1.952	2.032	2.218	1.874	2	52.13	52.15	52.01	52.1	0.479846	0.000322	4.55
60-1-1	27.86	26.38	27.1	2.057	1.984	2.298	2.263	2.2	51.56	51.77	51.59	51.64	0.524787	0.000249	3.78
60-1-2	25.77	24.44	25.1	2.227	2.226	2.071	2.172	2.2	51.54	51.51	51.36	51.47	0.487663	0.000291	3.86
23-2-1	25.62	24.49	25.1	1.86	1.712	1.933	1.913	1.9	51.16	51.19	51.1	51.15	0.490714	0.000322	5.02
23-2-2	25.68	27.1	26.4	1.731	1.875	1.798	1.86	1.8	51.23	51.27	51.26	51.25	0.515122	0.000262	4.71
23-2-3	23.91	24.07	24	2.663	2.414	2.646	2.834	2.6	50.51	50.59	49.81	50.3	0.477137	0.000319	3.49
23-2-4	25.33	23.97	24.7	2.203	2.325	2.583	2.482	2.4	51.33	51.39	51.42	51.38	0.480732	0.00029	3.45
40-2-1	26.98	25.71	26.3	2.397	2.406	2.214	1.937	2.2	51.61	51.7	51.53	51.61	0.509591	0.000291	4.18
40-2-2	25.3	23.85	24.6	2.432	2.26	2.121	2.263	2.3	50.98	50.7	50.39	50.69	0.485303	0.000253	3.21
40-2-3	26.77	24.56	25.7	2.613	2.302	2.37	2.234	2.4	50.08	50.28	50.44	50.27	0.511239	0.000324	4.35
40-2-4	25.76	23.86	24.8	2.505	2.475	2.405	2.362	2.4	50.55	50.74	51.06	50.78	0.488381	0.000334	4.11
60-2-1	26.73	25.01	25.9	2.44	2.363	2.296	2.296	2.3	51.37	51.61	51.31	51.43	0.503597	0.000265	3.57
60-2-2	25.46	23.94	24.7	2.824	2.558	2.079	2.278	2.4	51.01	51.5	51.18	51.23	0.482139	0.000299	3.58
60-2-3	25.98	24.54	25.3	2.456	2.785	2.279	2.541	2.5	51.4	51.5	51.53	51.48	0.491453	0.000272	3.22
60-2-4			-					-				-	-		-
23-3-1	25.93	24.29	25.1	2.07	1.992	1.958	2.04	2	49.94	50.09	50.06	50.03	0.501699	0.00029	4.52
23-3-2	25.45	26.73	26.1	2.34	2.562	2.311	2.322	2.4	50.9	51.07	51.04	51	0.511765	0.000281	3.75
23-3-3	23.48	25.41	24.4	2.399	2.343	2.155	2.262	2.3	48.28	48.48	48.9	48.55	0.502575	0.000376	5.19
23-3-4	25.48	27.14	26.3	2.628	2.668	2.364	2.517	2.5	50.84	50.89	50.96	50.9	0.516699	0.000316	4.13

Specimen Code	Dimensions												Experiment Results		
	Notch Length (Nearest 0.1mm)			Thickness, B, around notch (Nearest 0.1mm)					Width, W (Nearest 0.05mm)						Fracture Toughness
	a1	a2	Avg	B1	B2	B3	B4	Avg	W1	W2	W3	Avg	α	P_{max} (MN)	K_{TC} (MPa.m$^{1/2}$)
40-3-1	25.11	25.87	25.5	2.39	2.181	2.294	2.238	2.3	51.16	51.02	50.91	51.03	0.499706	0.000289	3.85
40-3-2	25.45	26.45	26	2.287	2.363	2.069	2.099	2.2	41.49	51.46	51.76	48.24	0.538972	0.000321	5.33
40-3-3	24.51	26.6	25.6	2.886	2.724	2.506	2.442	2.6	49.84	50.27	50.37	50.16	0.510367	0.00027	3.34
40-3-4	24.79	26.54	25.7	2.383	2.454	2.37	2.501	2.4	51.67	51.55	51.55	51.59	0.498159	0.000314	3.97
60-3-1	25.38	26.64	26	2.911	2.872	2.486	2.736	2.8	51.47	51.47	51.54	51.49	0.504952	0.000294	3.27
60-3-2	25.61	26.91	26.3	2.179	2.442	2.111	2.215	2.2	51.82	52.01	52.01	51.95	0.506256	0.000196	2.77
60-3-3	26.34	24.77	25.6	2.702	2.473	2.278	2.298	2.4	51.58	51.51	51.59	51.56	0.496509	0.000251	3.15
60-3-4	25.92	24.08	25	2.554	2.618	3.12	2.755	2.8	51.6	51.99	51.72	51.77	0.482905	0.00027	2.76
23-4-1	24.62	26.55	25.6	2.716	2.511	2.892	3.01	2.8	50.6	50.69	50.66	50.65	0.505429	0.000374	4.2
23-4-2	25.04	26.13	25.6	2.384	2.147	2.011	2.202	2.2	51.13	51.04	50.81	50.99	0.502059	0.000315	4.43
23-4-3	25.16	26.52	25.8	2.338	2.396	2.121	1.988	2.2	51.2	51.23	51.01	51.15	0.504399	0.0003	4.25
23-4-4	24.04	25.47	24.8	2.318	2.479	2.481	2.458	2.4	50.93	51.08	51.01	51.01	0.486179	0.000338	4.11
40-4-1	25.38	26.65	26	1.953	2.037	1.889	1.946	2	52.22	51.71	51.91	51.95	0.500481	0.000259	3.95
40-4-2	24.39	25.67	25	2.62	2.565	2.535	2.759	2.6	51.68	51.74	51.52	51.65	0.484027	0.00037	4.1
40-4-3	24.77	25.61	25.2	2.545	2.57	2.563	2.504	2.5	50.3	50.21	50.64	50.38	0.500198	0.000326	4.03
40-4-4	24.44	25.72	25.1	1.886	1.838	1.758	1.893	1.8	51.72	51.72	51.66	51.7	0.485493	0.00019	3.06
60-4-1	25.05	27.14	26.1	2.221	2.244	2.218	2.171	2.2	51.33	50.99	51.06	51.13	0.510464	0.000212	3.07
60-4-2	25.55	26.58	26.1	2.355	2.173	2.156	2.242	2.2	51.78	51.7	51.73	51.74	0.504445	0.000249	3.51
60-4-3	24.73	26.34	25.5	2.422	2.311	2.051	2.236	2.3	50.56	50.8	50.75	50.7	0.502959	0.000234	3.17
60-4-4	24.54	26.36	25.5	2.388	2.306	2.664	2.639	2.5	51.1	50.86	51.55	51.17	0.498339	0.000231	2.82

Specimen Code	Dimensions												Experiment Results		
	Notch Length (Nearest 0.1mm)			Thickness, B, around notch (Nearest 0.1mm)					Width, W (Nearest 0.05mm)						Fracture Toughness
	a1	a2	Avg	B1	B2	B3	B4	Avg	W1	W2	W3	Avg	α	P_{max} (MN)	K_{TC} (MPa.m$^{1/2}$)
60-4-5	23.87	24.67	24.3	2.124	2.24	2.202	2.283	2.2	51.67	51.17	51.01	51.28	0.473869	0.000319	4.04
60-4-6	25.5	26.94	26.2	2.123	2.238	2.462	2.337	2.3	50.34	50.39	50.36	50.36	0.520254	0.000239	3.46
60-4-7	24.46	26.04	25.3	1.972	2.111	2.26	2.121	2.1	51.09	51.33	51.36	51.26	0.493562	0.000233	3.32

APPENDIX J:

REGRESSION ANALYSIS FOR THE FRACTURE TOUGHNESS MODELS.

The following is model function for predicting the translaminar fracture toughness and the resultant predicted plot is shown in Figure J1. This function does take into account all the intermediate temperature and duration values.

$$K_{TL} = 0.087\sigma_{TS_o} - 0.27\alpha - 1.24\beta - 0.23\alpha\beta - 0.061\alpha^2 + 1.15\beta^2, \text{ MPa.m}^{1/2}. \quad \text{(J.1)}$$

Where α – Temperature based parameter which is equal to

$$\alpha = \frac{Ageing\ Temperature - 40}{20}$$

Ageing temperature in ^{o}C.

β – Time based parameter which is equal to

$$\beta = \frac{Ageing\ Time - 60}{60}$$

Ageing time in days.

σ_{TSo} - Composite pre-ageing tensile strength based parameter, in MPa.

Fracture Toughness Variation as a function of Ageing Temperature and Exposure Duration

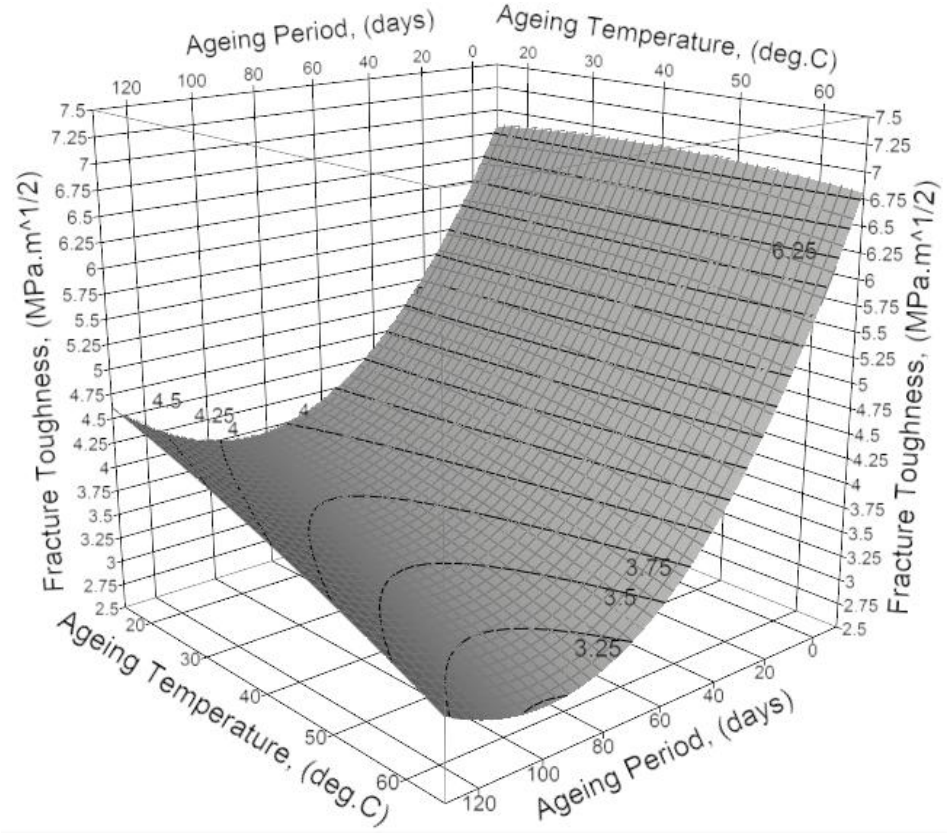

Figure J1: The fitted surface plot describing variations in fracture toughness as a function of hydrothermal ageing temperature and treatment period based on the model.

1) Overall Regression model equation Accuracy

According to the analysis, the regression equation (J.1) approximates the real data with an accuracy of 99.3%.

RSquare	0.997
RSquareAdj	0.993
Root Mean Square Error	0.0947
Mean of Response	4.5715
Observations (or Sum Wgts)	10

2) Probability That This Output Was Not By Chance (ANOVA – Significance of F)

Source	DF	Sum of Squares	Mean Square	F Ratio
Model	5	12.9568	2.59137	288.38
Error	4	0.0359	0.00899	**Prob> F**
C. Total	9	12.9977		<.0001*

The significance of F value shows that there is only less that 1% chance that the regression output was merely a chance occurrence. In other words, this means that there is over 99% confidence in the ability of the model to explain the dependent variable (observed response).

3) Individual Regression Coefficient and Y-Intercept Accuracy

Term		Estimate	Std Error	t Ratio	Prob>|t|
Intercept		3.91771	0.05665	69.16	<.0001*
Temp(20,60)		-0.2695	0.03869	-6.96	<.0001*
Ageing Period (0,120)		-1.237	0.03869	-31.96	<.0001*
Ageing Time*Ageing Temp		-0.2265	0.04739	-4.78	0.0088
Ageing Time*Ageing Time		1.1515	0.06205	18.56	<0.0001
Ageing Temp*Ageing Temp		-0.06192	0.06205	-1.00	0.3748

4) Response Fracture Toughness Actual vs Predicted

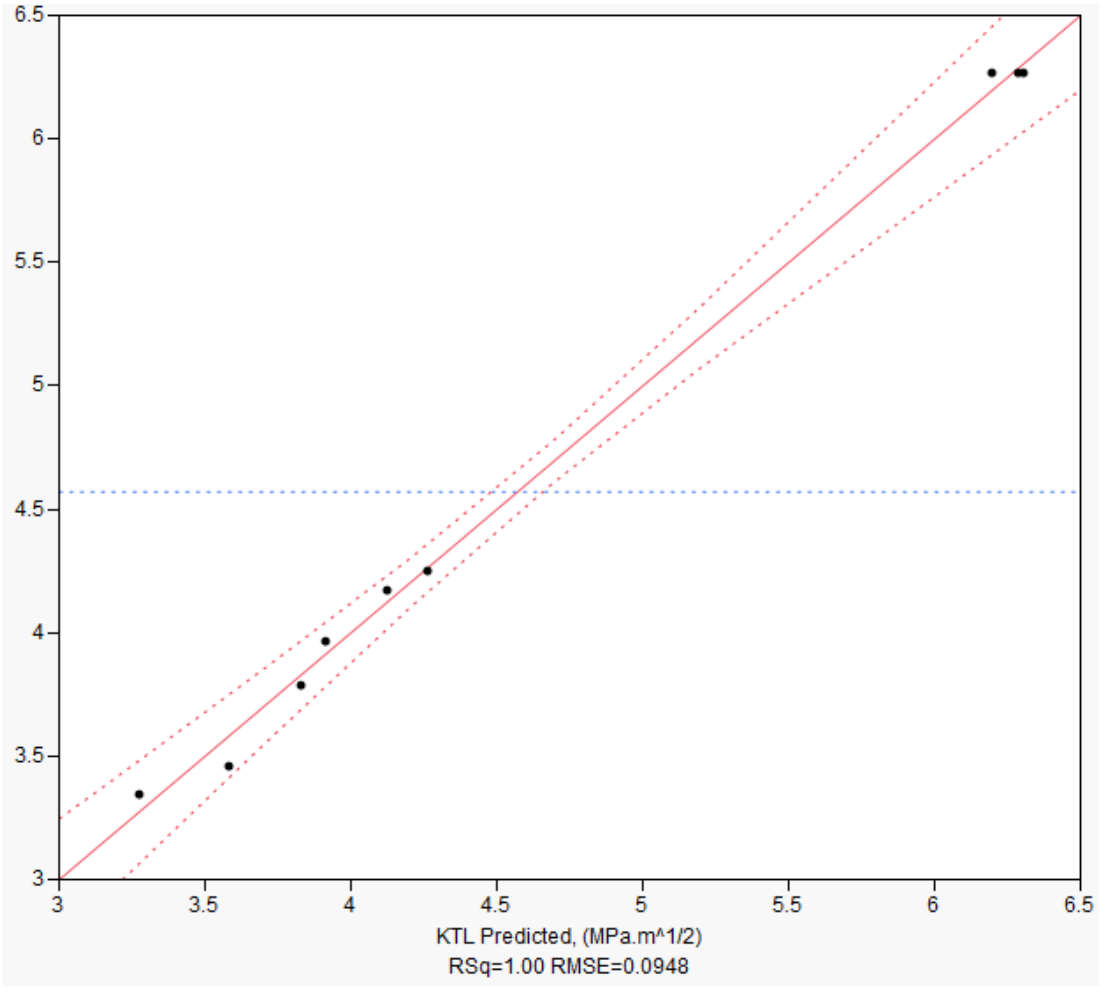

Figure J2: Actual vs predicted fracture toughness plot.

Prediction Profiler

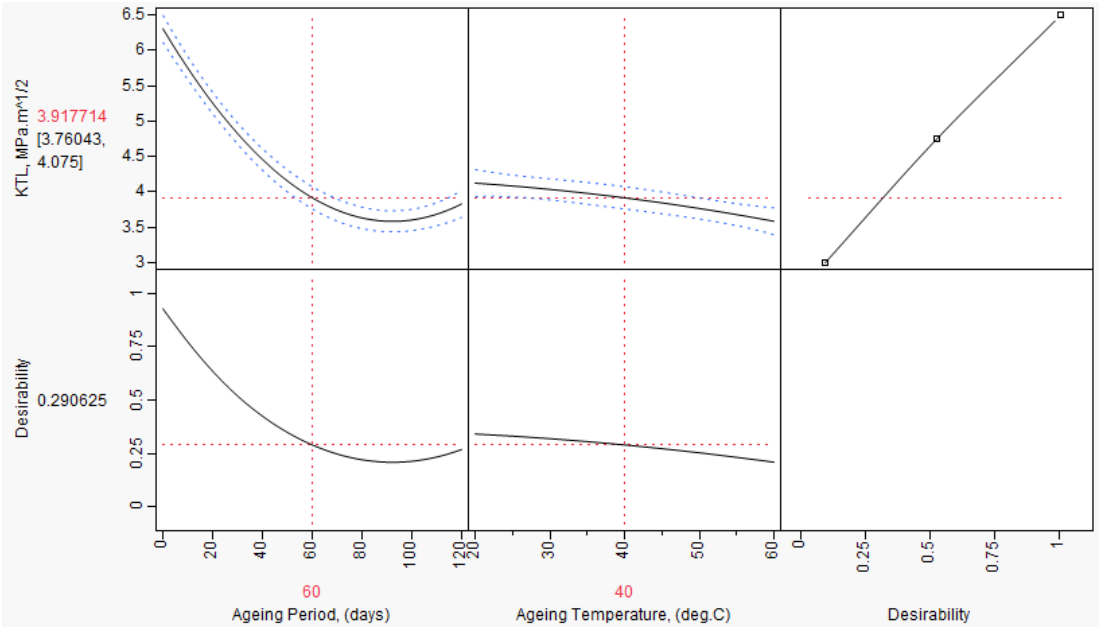

Figure J3: Prediction Profiler

APPENDIX K:

DUMBBELL SHAPED TENSILE TEST SPECIMEN DIE CASTING MOULDS.

Figure K1: Dumbbell shaped die casting mould for neat polyester test specimens.

APPENDIX L:

TEST SPECIMEN END TABBING

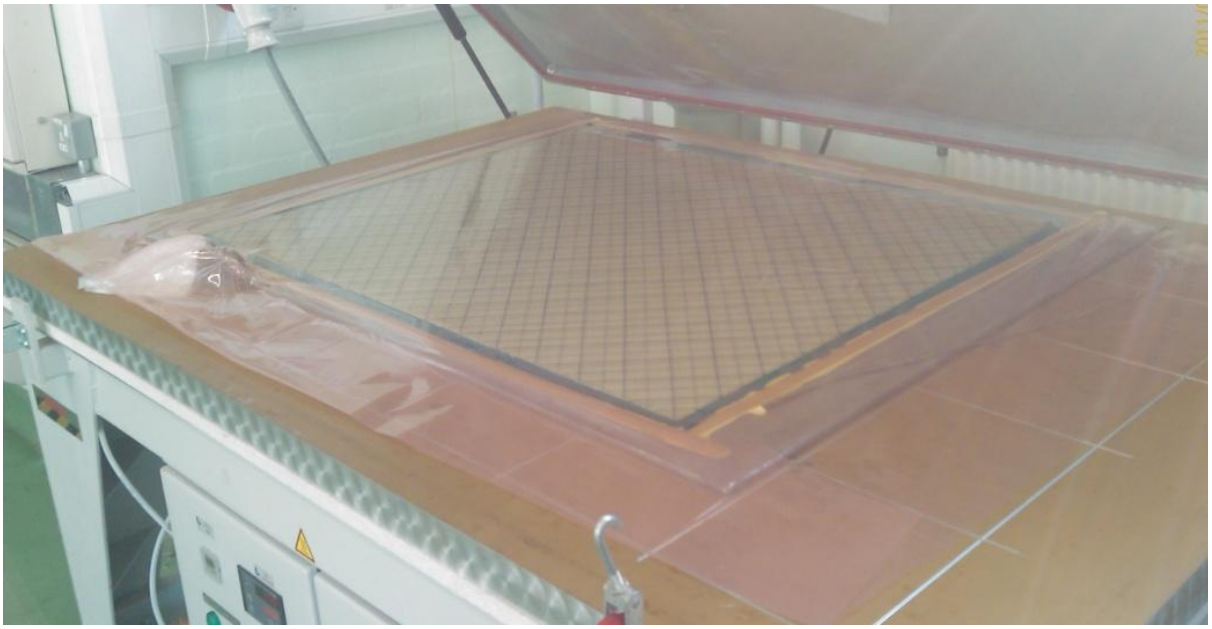

Figure L1: Tabbing prepreg composite material preparation on a vacuum table.

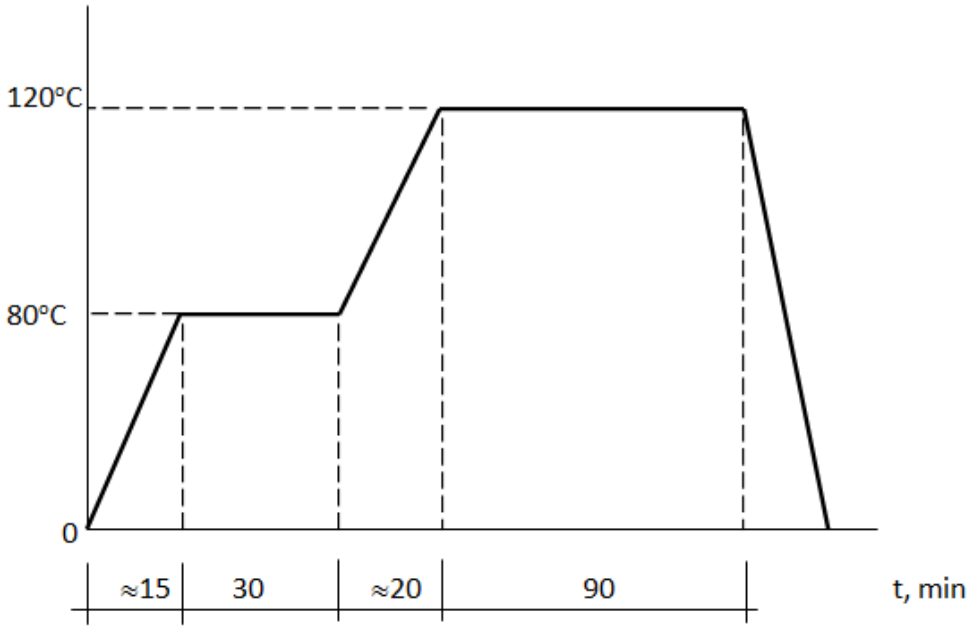

Figure L2: Tabbing glass fibre prepreg composite material curing cycle.

Curing cycles were set on the ELKON vacuum table during the preparation of glass fibre tabbing prepreg material as follows:

1st Cycle: Temperature is ramped up to 80°C and held there for 30 minutes.

2nd Cycle: After the initial 30 minutes, the curing temperature is further ramped up to 120°C and held at that temperature for 90 minutes and then allowed to dropped to down to room temperature. The prepreg is held on the vacuum table under vacuum for a further 24 hours.

Figure L3: End tabbing of test specimens on a vacuum table.

APPENDIX M:

COMPOSITE TEST SPECIMEN TESTING ARRANGEMENT.

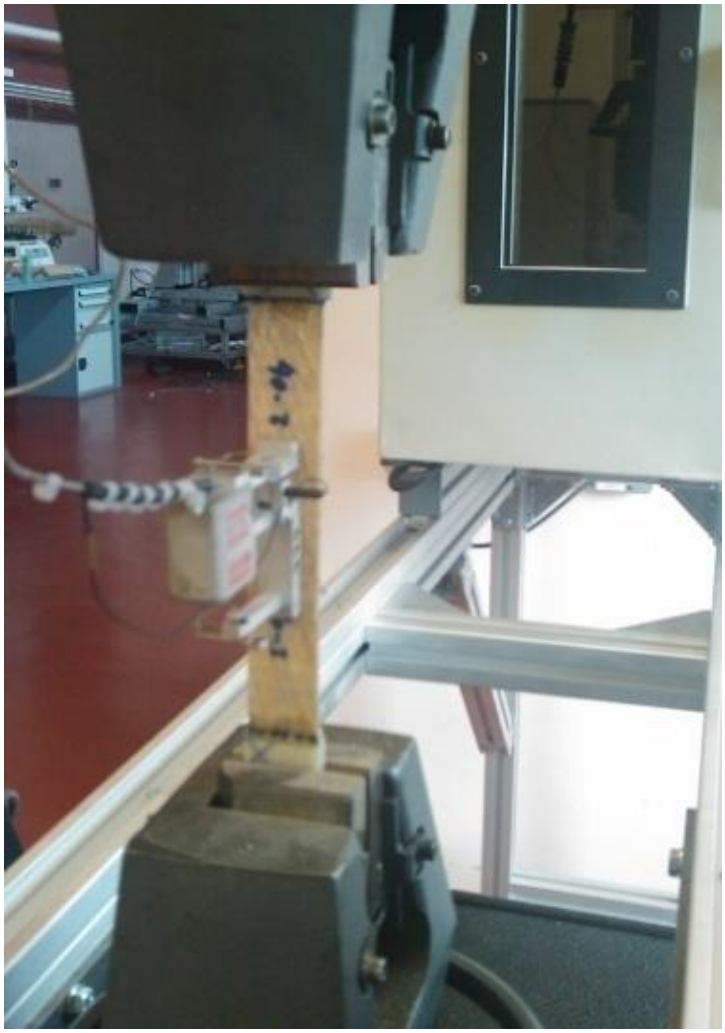

Figure M1: Composite specimen tensile testing arrangement.

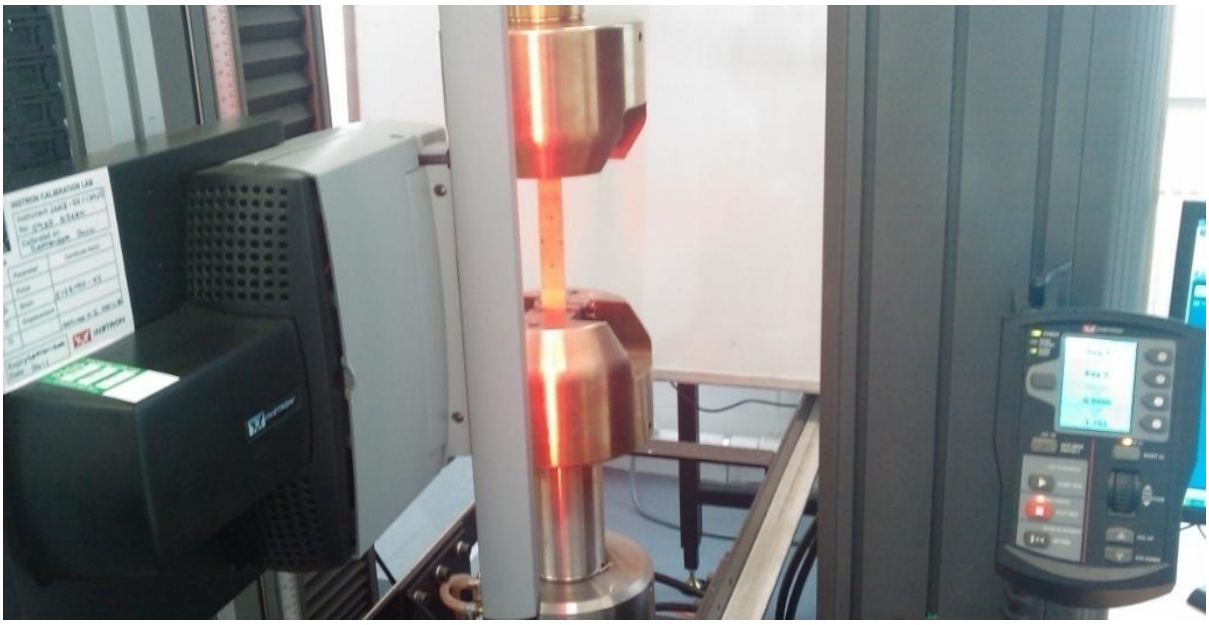

Figure M2: Composite specimen tensile testing arrangement equipped with a laser extensometer.

APPENDIX N:

NEAT POLYESTER SPECIMEN TENSILE TESTING ARRANGEMENT.

APPENDIX O:

Effects of Hydrothermal Ageing on the Fracture Damage of Sisal Fibre Reinforced Polyester Composites.

Chizyuka G Chizyuka, Shamitiba B Kanyanga
University of Zambia
School of Engineering
Department of Mechanical Engineering
P O Box 32379
Lusaka
Corresponding email: chizyukagc@yahoo.com

Abstract

To suitably design structural components, not only do the fundamental mechanical properties of the components' material constituents need to be known, but also the effects of the service environment on the mechanical properties. Moisture is one critical environmental factor that can be destructive to composite properties. Composite components can constantly absorb or desorb moisture due to varying service temperature and relative humidity levels.

This paper, therefore, presents results of a study on the influence of hydrothermal effects on the natural fibre-reinforced composite material fracture damage. Fracture properties of sisal fibre reinforced polyester composites were investigated as a function of ageing period under different thermal loading states. It was observed that the translaminar fracture toughness rapidly reduced with increase in the composite moisture content. Results exhibited a pattern characteristic of the presence of a thermal gradient in the deterioration of the fracture toughness.

Keywords*: Translaminar Fracture toughness, Natural fibre-reinforced Composite, Sisal, Thermal Gradient, Service Environment.*

INTRODUCTION

The development of composite materials and related design and manufacturing technologies is one of the most important advances in the history of materials (Jeyaraj and Arulshri 2012). Fibre composite technology is based on taking advantage of the high strength and high stiffness of fibres, which are combined with matrix materials of similar/dissimilar natures in various ways, creating inevitable interfaces. In fibre composites, although both the fibre and the matrix retain their original physical and chemical identities, when combined they produce great mechanical properties that cannot be achieved with either of the constituents acting alone (Kim and Mai 1998).

Natural Fibre-Reinforced Composites (NFRCs) have received significant attention in many engineering structural applications due to their numerous advantages such as light weight, low cost, increased durability of fibres, low maintenance during service, and ease of fabrication using conventional composite processing practices. The adoption of natural fibre composites in industry is further lead by the motive of marketing ("processing renewable resources) rather than technical demands. The range of products is restricted to interior and non-structural components like door upholstery of rear shelves (Brouwer, 2000). An understanding of the response of these NFRCs under specific environmental conditions is vital for use as engineering structural materials. A lot of attention has in the past been addressed on composites reinforced with traditional reinforcements such as glass and carbon fibres. Buta lot of work remains to be done in the area of natural fibres reinforced composites and how they respond to fracture when subjected to various environment conditions. Aveston, Cooper,*et al*. (1971) have developed a fracture mechanics-based model for the determination of the fracture resistance of composites founded on the assumption that only frictional stress plays a role of holding reinforcing fibres in the surrounding matrix. Then Buduansky, Hutchinson *et al*. (1986) used some of Aveston's results in their study on matrix cracking stress for

composites with unbonded and initially bonded, debonded fibres. Buduansky, Evans,*et al*. (1995)later used the relation existing between crack bridging stress, σ and crack open displacement, u to describe the role fibres play in the overall propagation of a crack, expressed as in Equation (1) (under the assumption that the interfacial sliding stress, τ remains constant),

$$u = \lambda\sigma^2 \quad (1)$$

where $\lambda = \frac{2r(1-V_f)^2E_m^2}{4V_f^2\tau E_f E^2}$

E – Composite's modulus of elasticity

E_m and E_f–Matrix and fibre moduli of elasticity

r – reinforcing fibre radius

V_f– Fibre volume fraction.

τ - Interfacial sliding stress

Marshall, Cox,*et al*. (1985) and Marshall and Cox (1987) used the stress intensity approach to determine the matrix cracking stress in composite with the fibre held by the matrix merely by friction. In this case, the bridging fibre was represented by the traction forces which connect the fibres though the crack. By equating the composite stress intensity factor to the matrix critical stress intensity factor, the matrix cracking stress was determined.

Pagano and Kim (1994) studied damage initiation and propagation in glass fibre reinforced ceramic composites when subjected to flexural loading. Assuming that a crack surrounding a fibre only extends to the neighbouring fibre of the hexagonal array fibre set up, a damage model was developed which was used to further relate the energy release rate as a function of the composite fibre volume fraction.

The behaviour of carbon fibre reinforced epoxy composite under static and fatigue loading was studied by Kanyanga (1988) using centre notched unidirectional and cross-ply laminate specimens. Under static loading conditions, the investigation involved determining the fracture strengths of research specimen type and monitoring damage initiation and growth from notch tips. Static strength results were analysed and compared with existing theories. Fracture stresses generally exhibited a dependence on notch size but showed a limited dependence on notch type. The initiation of splitting under static loads was governed by a parameter H_s in Equation (2) dependent on split initiation stress (σ_s) and notch size (a). The cross-ply laminates were less resistant to splitting than unidirectional ones.

$$H_s = \sigma_s\sqrt{a} \quad (2)$$

Assuming that initially the composite laminate is exposed to hydrothermal environment on two sides, the sides being parallel, the initial temperature and moisture distribution inside the material are uniform, the moisture content and temperature of the environment are constant, Fickian diffusion theory describes the moisture content during absorption and desorption M_t. (Shen and Springer 1976;Surathi and Karbhari 2006)

$$M_t = G(M_m - M_i) + M_i \quad (3)$$

Where

M_t= Percentage moisture gain with time.

M_i= Initial moisture content of the composite specimen.

M_m= Maximum moisture content in the composite specimen at saturation.

G = Time dependent parameter which is described as

$$G = 1 - \frac{8}{\pi^2}\sum_{n=0}^{\infty}\frac{exp\left[(2n+1)^2\pi^2\left(\frac{-Dt}{h^2}\right)\right]}{(2n+1)^2} \quad (4)$$

Where

D= Diffusivity of the composite material normal to the surface, at times referred to as diffusion coefficient.

h= Thickness of the material.

It is assumed that the specimen used in moisture absorption study would be dry and free of moisture; M_i is taken to be equal to zero. The resultant moisture content of the composite specimen after being exposed to the environment for time t, M_t is expressed as

$$M_t = M_m\left[1 - \frac{8}{\pi^2}\sum_{n=0}^{\infty}\frac{exp\left[(2n+1)^2\pi^2\left(\frac{-Dt}{h^2}\right)\right]}{(2n+1)^2}\right] \quad (5)$$

For the approximation of both short and long term moisture contents, Equation (5) can be reduced by defining a non-dimensional time parameter Dt/h^2. For short term exposure, $Dt/h^2<0.04$, Equation (5) can be written as:

$$M_t = M_m\left[\frac{4}{\pi}\sqrt{\frac{Dt}{h^2}}\right] \quad (6)$$

For long term exposure approximation,

$Dt/h^2 > 0.04$ (6(a))

$$M_t = M_m \left[1 - \frac{8}{\pi^2} exp\left(\frac{-Dt}{h^2}\pi^2\right)\right] \quad (6(b))$$

Accelerated Ageing Through Hydrothermal Induction

Moisture absorption for composite materials is for the most part a diffusion process dependent on the prevailing environmental conditions. As a result, time is an important factor in reproducing these effects. Since moisture absorption to saturation under typical field environmental conditions can take years, the ability to reproduce these effects in the laboratory in a more reasonable duration of days or weeks is essential.

The intent is that after accelerated ageing conditioning process for a period of weeks, the state of the test specimens would have closely approximated the conditions that they would be expected after years of service when exposed to moisture at different temperatures. If this is not accomplished, the results would not be credible. This, accelerated aging, could be possible with the help of hydrothermal induced degradation of the composite.

Materials Constituents of the Composite

The following is an overview of the materials used in making Sisal fibre-reinforced composite test specimens:

Sisal Fibres

Sisal, an easily cultivated material, remains one of the most extensively used natural fibres. However, its use over the years has steadily diminished with the introduction polymeric yarns such as polypropylene to be used for the same purpose. Amid the variety of natural fibres being exploited as reinforcement, sisalfibre still remains a worthwhile material in that it forms high impact strength composites despite having moderate flexural and tensile strengths ((Bledzki, Sperber,*et al*. 2002).

The global sisal production of sisal fibre in 2007 amounted to 240 thousand tonnes; Tanzania and Brazil being the two major producers (Sharma, *et al*. 2011).Sisal is a hard fibre extract from sisal leaves (*Agave sisalana*) through a process known as decortication. The length of sisal lies between about 0.5 and 1.5m with diameter of 100 - 300µm (Li, Mai,*et al*. 2000). The interface between the sisal and the matrix plays a major role in the transfer of load within the composite; a good interface is indispensible in taking advantage of both composite components(Kim and Mai 1998); (Geo and Cotterell 1988). As such, it is essential to surface treat the fibres to give them improved surface strength and toughness. The effects of suface treatment on the mechanical properties of natural fibre reinforced composites are extensively studied ((Valadez-Gonzalez, Cervantes,*et al*. 1999); (Sreekala and Thomas 2003); (Thais, Sydenstricker,*et al*. 2003); (Rong, Zhang,*et al*. 2001); (Luyt and Malunka 2005)). However, there have not been many studies focusing on the fracture characteristics and fracture properties of natural fibre-reinforced composites.

Polyester Resin

Polyester is a synthetic polymer made of purified terephthalic acid (PTA) or its dimethyl ester dimethyl terephthalate (DMT) and monoethylene glycol (MEG). With 18% market share of all plastic materials produced, it ranges third after polyethylene (33.5%) and polypropylene (19.5%). Polyester is a category of polymers which contain the ester functional group in their main chain. Although there are many polyesters, the term "polyester" as a specific material most commonly refers to polyethylene terephthalate (PET).(Pai and Chandra 2013)

Depending on the chemical structure, polyester can be a thermoplastic or thermoset. However, the most common polyesters are thermoplastics (Rosato, Rosato,*et al*. 2004). Polyester resins can be formulated with a variety of properties ranging from hard and brittle to soft and flexible. Its advantages are low viscosity, fast cure time, and low cost.

EXPERIMENTAL PROCEDURES

Reinforcing Sisal Fibre Preparation

The sisal yarn used in this research was purchased from James Lever Ltd of Bolton, England. Table 1 lists some of its properties.

Table 1: Properties of Sisal Fibres (Source: James Lever Ltd)

Properties	**Values (SI)**
Specific Gravity	1.35
Young's Modulus (Average)	≈29 GPa
Coefficient of Thermal Expansion	16.8µm/m^{o}C – Longitudinal 70.8µm/m^{o}C – Transverse
Operating Temperature	Up to 135^{o}C

A two-dimensional plain weaved sisal fibre fabrics used as reinforcement in the composite panels were weaved on a hand loom. Prior to the

resin infusion process, the woven fibre fabrics were initially subjected to a 5% diluted sodium hydroxide (NaOH) treatment of one hour in order to improve the fibre surface in readiness for bonding with the polyester matrix.

Polyester Resin Preparation

The matrix material selected for the sisal fibre reinforced composite was a general purpose polyester laminating resin supplied by ABL (Stevens) Resin and Glass Co. of Cheshire, England. Table 2 lists some mechanical properties of cured unreinforced polyester resin material.

A considerable amount of resin was first prepared in an open polypropylene container by mixing the polyester resin with an organic peroxide catalyst (Methyl Ethyl Ketone Peroxide). The amount of the catalyst in the mixture was 2% by weight. The catalyst was acquired from the suppliers of the polyester resin.

Composite Panel Making

The sisal fibre reinforced composite panels from which test specimen were cut were moulded using the Vacuum Assisted Resin Infusion moulding process. This process yields panels with fibre volume fractions of 50 – 55%. The curing process of polyester resin is exothermic and as such, had to be done under ambient temperature as prescribed by the resin suppliers without following any particular curing regime pattern.

The infusion process setup is shown in Figure 1.

The mould assembly was allowed to stay in the film cardboard for 24 hours as prescribed by the resin manufacturer for complete resin curing to take place before de-bagging. Test pieces were cut out from moulded composite panels with the use of a circular diamond cutter to avoid inducing damage to the specimen edges.

Accelerated Ageing Through Hydrothermal Induction

Hydrothermal conditioning was done in three distilled water-filled 36 litre Grant water baths set at ideal operating temperatures of 23^{o}C, 40^{o}C and 60^{o}C.Temperature beyond 60^{o}C may not be ideal as operating temperature for the matrix as it tend to affect the viscoelastic properties of the matrix which would in turn result in misleading observations in the experiments. Exposure to these conditions was for a maximum period of four months, a period during which it was assumed that considerable amount of accelerated aging would have taken place and this was to be confirmed by mechanical property tests throughout the period. Prior to the mechanical testing, test specimens were vacuum dried at room temperature for 24 hours to ensure that no moisture remained trapped inside the composite specimens. Any undesired trapped moisture would further continue the ageing process outside the conditioning environment chamber.

Experiment conditions for hydrothermal ageing are listed in Table 3.

Table 3: Experimental hydrothermal ageing conditions for fracture toughness test specimens.

Solution	Distilled water
Water Temperature *T(°C)*	23°C, 40°C, 60°C
Immersion Time *t(hours)*	0 (unconditioned), 720, 1440, 2160, 2880

Isothermal water uptake studies

Isothermal water uptake studies were conducted alongside the accelerated hydrothermal ageing for the determination of the relative rate of absorption of water by the sisal-polyester composite by immersing standard test specimens into distilled water at different pre-set temperatures of 23^{o}C, 40^{o}C and 60^{o}C. This study was conducted in accordance with ASTM D570-98 testing standard. Water uptake was monitored on three specimen samples, each consisting of three composite specimens (with dimensions of 76.2mm x 25.5mm x 2.5mm), by gravimetric changes in the test specimens throughout the observation period.

Fracture Toughness Testing

The assessment of the fracture toughness properties for fibre reinforced composites made

Table 2: Mechanical properties of clear-cast (unreinforced) polyester resins. (Source: ABL (Stevens) Resin and Glass Co)

Tensile Strength (MPa)	Tensile Modulus (GPa)	Elongation (%)	Flexural Strength (MPa)	Flexural Modulus (GPa)	Compressive Strength (MPa)	Heat Deflection Temperature (°C)
75	3.38	3.3	130	3.59	120	90

from thermosetting matrices is normally conducted through the stress intensity factor approach, as a result of their common brittle tendencies (Zhao and Botsis 1996). For this reason, periodic translaminar fracture toughness tests of hydrothermally aged unidirectional sisal fibre reinforced polyester specimens were conducted in accordance with the ASTM E1922-97 testing standard. Prior to running these tests, test specimens were initially subjected to a hydrothermal ageing process.

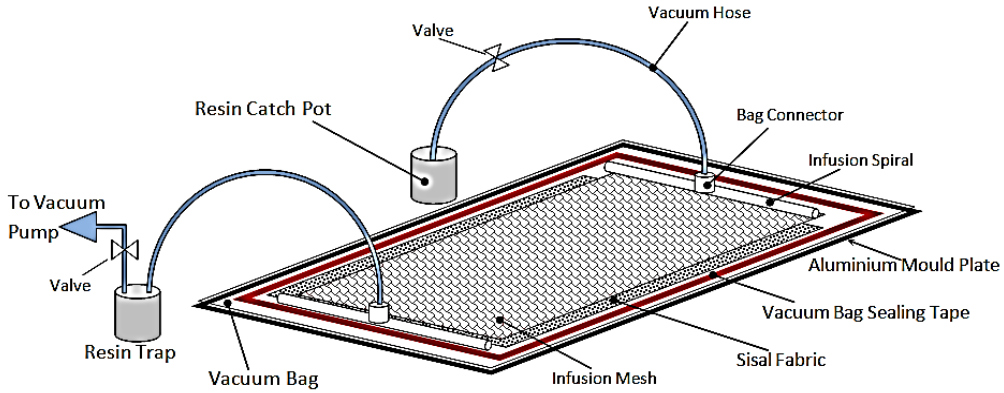

Figure 1: Vacuum assisted resin infusion process mould

Test specimens were prepared in accordance with the dimensions and tolerances prescribed in the ASTM E1922-97 test standard. The notch was cut using a diamond cutter producing the required narrow slit. Specimen specifications are shown in Figure 2.

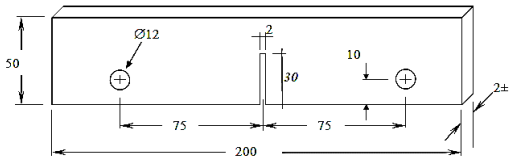

NOTE 1: All dimensions +/– 0.01 *W*, except as noted.
NOTE 2: All surfaces perpendicular and parallel as applicable within 0.01*W*.

Figure 2:Translaminar Fracture Toughness Test Single-Edge-Notch ESE (T) Specimen

In accordance with the Standard, a single-edge-notch, ESE(T), specimen was eccentrically loaded in tension (mode I). The attained load versus resultant displacement across the notch mouth at the specimen edge was recorded. A displacement gauge model type MTS 634.31F-24 was used to simultaneously measure the notch-mouth displacement during loading. Knife edges affixed to test specimens at the notch mouth enabled attachment of the displacement gauge to the specimens.

From the acquired load-displacement data, the load corresponding to the prescribed increase in the normalised notch length was established. From this load, the translaminar fracture toughness, K_{TL}, was further computed using Equation (7) founded on the basis of elastic stress analysis of the modified single-edge notched specimen.

Tests were conducted on an Instron 5569 tensile testing machine that has provision for simultaneous recording of the applied load (using a 10 kN load cell) to the specimen at a constant crosshead speed of 2 mm/min and the resulting notch-mouth displacement with the use of an extensometer (model type MTS 634.31F-24) attached to the notch mouth. A typical arrangement is shown in Figure 3. Typical pin-loading clevises similar to the type used in test method ASTM E 399 were used to apply the load onto the specimen.

Fracture toughness tests of non-hydrothermally treated test specimens were also conducted. This was to establish a baseline for comparison when determining the effect the ageing process had on the fracture toughness of the composite material.

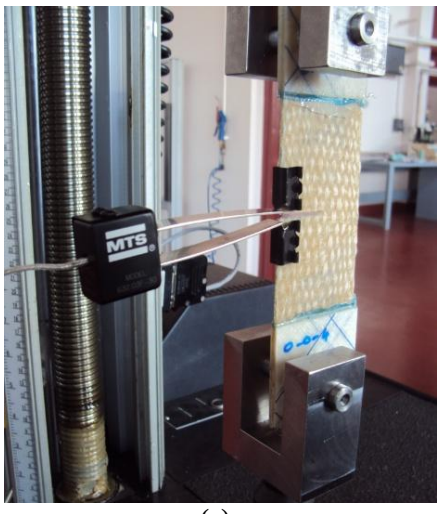

(a)

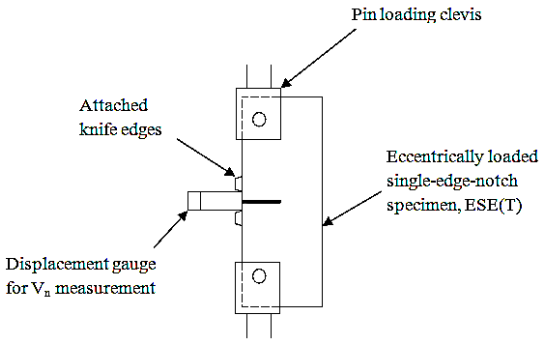

(b)

Figure 3: (a) Actual picture of the test arrangement for translaminar fracture toughness tests. (b) Diagrammatic representation of the setup.

Five test specimens per sample were required due to the fact that material variations were to be expected and also considering the available limited ageing chamber capacities.

$$K_{TL} = \left[P/BW^{1/2}\right]\alpha^{1/2}[1.4+\alpha][3.97 - 10.88\alpha + 26.25\alpha^2 - 38.9\alpha^3 + 30.15\alpha^4 - 9.27\alpha^5]/[1-\alpha]^{3/2} \quad (7)$$

Where:

K_{TL} - Translaminar fracture toughness, MPa.m$^{1/2}$.
P - Applied load, MN.
α - a/W (dimensionless).
a_n - Notch length, m.
B - Specimen thickness, m.
W - Specimen width, m.

JMP8 statistical analysis software was used to further conduct the regression analysis and analysis of variance on the empirical model generated from the test results.

RESULTS

A sample result plot obtained from a single fracture toughness test is shown in Figure 4. From these results, it is observed that sisal fibre reinforced polyester composite exhibits a linear characteristic response during the initial phase of testing up to approximately $0.7P_{max}$ of loading. Internal microcracking, which subsequently develop inside the composite, lead to a nonlinear response which continues up to the pick load, P_{max}. Upon reaching this critical load, fracture propagated consistently and steadily with reduction of the applied load to some lower value of about $0.5P_{max}$ before the test was stopped.

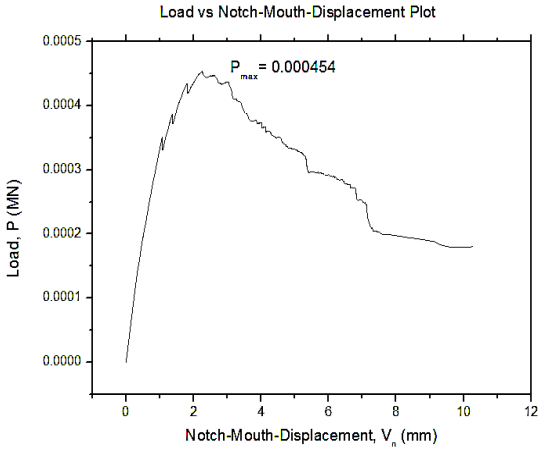

Figure 4: A sample plot of Load vs Notch-mouth displacement in a translaminar fracture toughness test.

Figure 5 shows a combined fracture toughness variation plot of hydrothermally treated sisal fibre reinforced polyester composite specimens. Figures 6 to 8 show composite plots variation of the fracture toughness at temperatures of 23°C, 40°C and 60°C respectively with changes in the amount of absorbed moisture by the same composite. These composite plots point out that as moisture increased, the fracture toughness initially reduced rapidly during the first 50 days of exposure to these ageing environments. This was then followed by a steady levelling of the property until the end of the observation period for specimens treated at 23°C. Specimens treated at 40°C and 60°C experienced gradual reductions in fracture toughness throughout the rest of the conditioning period. In all, the 23°C and 40°C hydrothermally treated specimens registered average reductions in the fracture toughness amounting to 32.2% and 39.5% respectively, while the 60°C treated specimens yielded the most reduction of 46.7%.

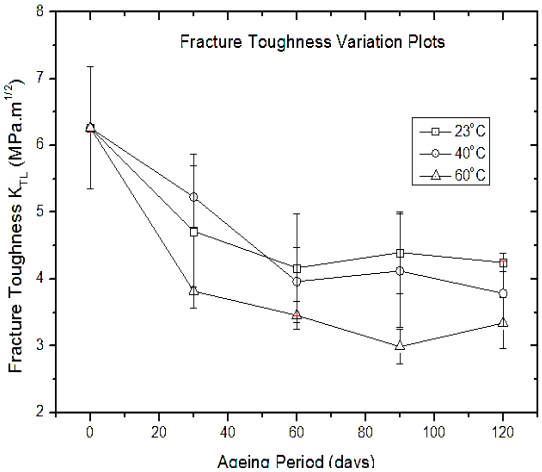

Figure 5: Fracture toughness variation plot of hydrothermally treated sisal fibre reinforced polyester composite test specimens.

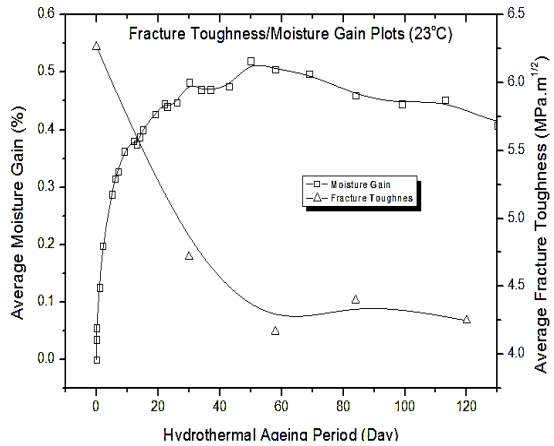

Figure 6: The relationship between water absorption and fracture toughness with increasing exposure times for sisal fibre reinforced polyester composite specimens hydrothermally treated at 23°C.

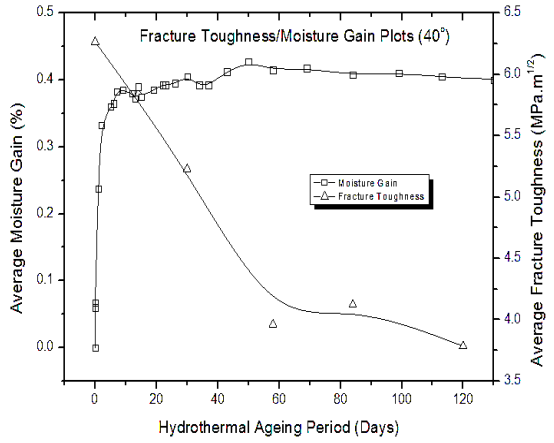

Figure 7: The relationship between water absorption and fracture toughness with increasing exposure times for sisal fibre reinforced polyester composite specimens hydrothermally treated at 40°C.

Isothermal water uptake studies presented in the composite plots were conducted in the same chambers as for isothermal ageing of fracture toughness test specimens in order to determine the relative rate of absorption of water by the sisal-polyester composite. Based on the Fickian diffusion model, the isothermal water uptake study yielded diffusion coefficients of 0.00327 $mm^2.s^{-1}$, 0.01277 $mm^2.s^{-1}$ and 0.0.03695 $mm^2.s^{-1}$ for specimens placed in the respective study environments.

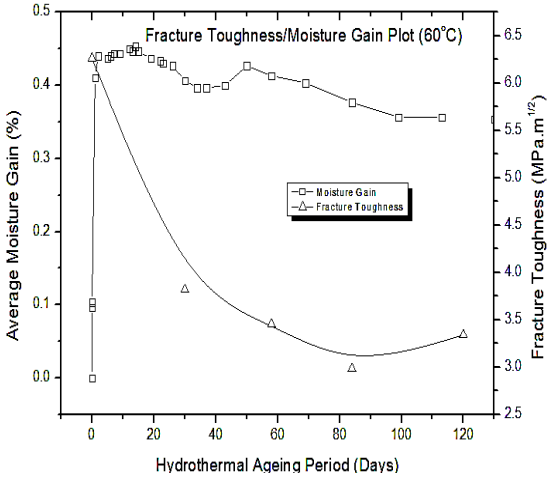

Figure 8: The relationship between water absorption and fracture toughness with increasing exposure times for sisal fibre reinforced polyester composite specimens hydrothermally treated at 60°C.

Following a regression analysis of the fracture toughness test results, a more comprehensive model description of the effects of intermediate temperatures and absorbed water pose on the fracture toughness over time was developed. Figure 9 shows a much clearer picture of the effect hydrothermal treatment poses on the sisal reinforced polyester composite system, depicting a 3-dimensional surface plot of the fracture toughness as a function of ageing period and hydrothermal ageing temperature. This plot was based on a generated regression model of the experimental data. A corresponding model function is shown in Equation (8) which describes the variation with $R^2 = 0.997233$. This suggests that this empirical model fits the experiment data well.

$$K_{TL} = 3.92 - 0.26a - 1.23b - 0.22ab - 0.062a^2 + 1.15b^2 \quad (8)$$

where

K_{TL} = Translaminar fracture toughness, $MPa.m^{1/2}$.

A = Temperature based parameter which is equal to, $a = \frac{t-40}{20}$

T = Ageing temperature, in °C.

b = Duration based parameter which is equal to, $b = \frac{d-60}{60}$

d = Ageing duration, in days.

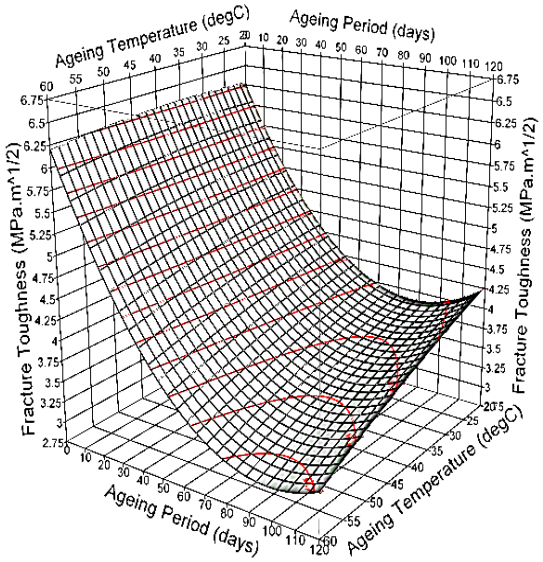

Figure 9: The fitted surface plot describing variations in fracture toughness as a function of hydrothermal ageing temperature and treatment period based on the derived empirical model.

Figures 10 and 11 show scanning electron microscopic (SEM) images of two debonded microbondpullout test sisal fibres. Figure 10 shows the surface of a non-hydrothermally treated sisal fibre following a microbond pullout test, while Figure 11 shows one from a hydrothermally treated microbond sisal-polyester composite system for a period of 14 days at temperature of 23^{o}C. When comparing the SEM images, it can be noted that the hydrothermally treated debonded fibre barely contain residues of fractured matrix on its surface. This is indicative of the dilapidating effect of the absorbed moisture on the fibre-matrix interface when exposed to a moist environment.

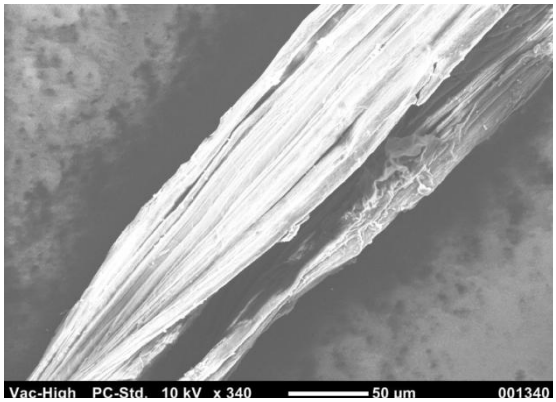

Figure 10: SEM image of a sisal fibre surface following interfacial debonding of a non-hydrothermally treated microbond sisal-polyester composite system.

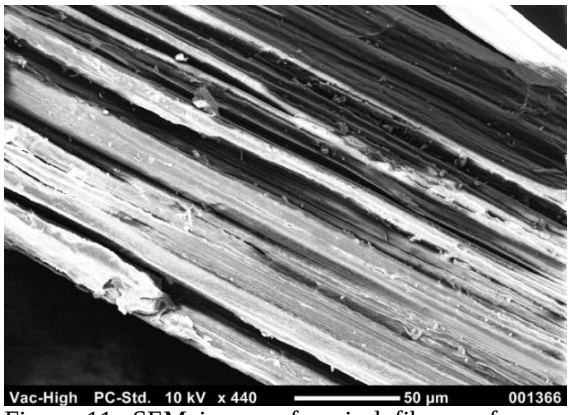

Figure 11: SEM image of a sisal fibre surface following interfacial debonding of a hydrothermally treated microbond sisal-polyester composite system.

DISCUSSION

The first 60 days of hydrothermal treatment yielded steep drops, with increase in the conditioning temperature, in the fracture toughness of the sisal fibre reinforced composite before levelling up. It was found that at the end of observation period, these ageing environments yielded total reductions in the fracture toughness averaging 32.2%, 39.5% and 46.7% for the 23^{o}C, 40^{o}C and 60^{o}C treatment environments respectively. This clearly shows a presence of a thermal gradient which, from these resultant diffusion coefficients amounting to 0.00327 mm^2.s^{-1}, 0.01277 mm^2.s^{-1} and 0.0.03695 mm^2.s^{-1} for the respective environments, enhanced water uptake into the composite material and subsequently lowered the fracture toughness.

This reduction in the fracture toughness after hydrothermal treatment of test specimens is mainly as a result of the reduction in the interfacial bonding between the fibres and the surrounding matrix material. This can be attributed to the volumetric expansion of the matrix in the area surrounding the fibre as a result of the absorbed moisture, which in turn lowered the residual compressive stresses at the sisal fibre–polyester matrix interface which were initially partly brought about by the polyester matrix curing shrinkage. This lowering of the compressive stresses result in the relaxation of the chemical bonding and the mechanical interlocking that exist in bonded fibre-matrix interface leading to its eventual failure during prolonged exposure to this ageing environment. Void content in composites have a tendency to dramatically increase both the equilibrium moisture concentration and also the diffusion coefficient of the composite product and consequently resulting in the further relaxation of the remaining bonded interface.

CONCLUSION

The moisture absorption behaviour and the influence of moisture on the fracture properties of sisal fibre reinforced polyester composites were investigated as a function of ageing period under different thermal loading states.

In addition, SEM images on the surface of the fibre extracted from the fractured specimens (non-aged and the other after the ageing of the test specimens in the hydrothermal ageing environments), revealed the harshness imposed by the infused moisture through microcracks along the fibre-matrix interfacial bonding, signifying a strong influence of water degradation on the fracture toughness of the composite by respective averages of 32.2%, 39.5%, and 46.6% for the 23^{o}C, 40^{o}C and 60^{o}C treatment environments mainly though interfacial failure. This mechanism subsequently leads to interfacial debonding which further causes composite failure by sisal fibre pullout. It can therefore be concluded that this fractographic difference in the SEM images of the fibre surfaces is one indication that debonding is an established fracture mechanism in hydrothermally aged sisal fibre–polyester composite systems. It is worth noting that the influence of moisture on facture toughness of this polymeric composite system is enhanced with the increase of prevailing ambient temperature coupled with the exposure period.

REFERENCES

Aveston, J., G. A. Cooper, and A. Kelly (1971). Single and Multiple Fracture. The Properties of Fibre Composites. Surrey, IPC Science And Technology Press**:** 15 - 26.

Bledzki, A. K., V. E. Sperber and O. Faruk (2002). Natural and Wood Fibre Reinforcement in Polymers. Rapra Review Report, Rapra Technology Ltd. **13:** 144.

Brouwer, W.D. (2000), "Natural Fibre Composites in Structural Components: Alternative Applications for Sisal?",Common Fund for Commodities and FAO, Proceedings from the seminar on alternative applications for Sisal, Rome 13 December 2000

Buduansky, B., A. G. Evans andJ.W. Hutchinson (1995). "Fibre-Matrix Debonding Effectes on Cracking in Alighned Fibre Ceramic Composites." International journal of Solid and Structures**32**(3): 315 - 328.

Buduansky, B., J. W. HutchinsonA.G. Evans (1986). "Matrix Fracture in Fibre-Reinforced Ceramics." Journal of the Mechanics and Physics of Solids**34**(2): 167 - 189.

Chand, N., R. K. Tiwaryand P.K. Rohatgi (1988). "Bibliography Resource Structure Properties of Natural Fibres – An Annotates Bibliography." International Journal of Material Science**23**: 381 – 387.

Geo, Y. C. and B. Cotterell (1988). "Fracture of Fibre-Reinforced Materials." ZAMP(Journal of Applied Mathematics and Physics)**39**: 550 -572.

Jeyaraj, S. and K. P. Arulshri (2012). "Characterisation of Electrdeposited Nickel-Al_2O_3 Composite Coatings by Experimental Method and Neural Networks." Journal of Applied Sciences**12**(10): 911 - 919.

Kanyanga, S. B. (1988). Fatigue and Fracture Behaviour of Carbon Fibre Reinforced Plastics. Department of Mechanical Engineering. Sheffield, University of Sheffield. **PhD:** 175.

Kim, J. K. and Y. W. Mai, Eds. (1998). Engineered Interfaces in Fibre Reinforced Composites. Oxford, Elsevier Science Ltd.

Li, Y., Y. W. Mai and L.Ye (2000). Microstructure and Mechanical Properties of Sisal Fibre and Adhesion to Vinyl Ester Resin. Proceedings of the 9th European Conference on Composite Materials (ECCM-9), Brighton, UK, IOM Communications Ltd, London.

Luyt, A. S. and M. E. Malunka (2005). "Composites of Low-Density Polyethylene and Short Sisal Fibres: The Effect of Wax Addition and Peroxid Treatment on the Thermal Properties." Thermochimica Acta**426**: 101 – 107.

Marshall, D. B. and B. N. Cox (1987). "Tensile Properties of Brittle Matrix Composites: Influence of Fibre Strength." Acta Metallurgica et Materialia**35**: 2607 - 2619.

Marshall, D. B., B. N. Cox and A.G. Evans (1985). "The Mechanics of Matrix Cracking in Brittle-Matrix Fibre composites." Acta Metallurgica et Materialia**33**: 2013 - 2021.

Pagano, N. J. and R. Y. Kim (1994). "Progressive Microcracking in Unidirectional Brittle Matrix Composite." Mechanics of Composite Materials and Structures**30**(4): 3 - 29.

Pai, S. and K. L. Chandra (2013). "Analysis of Polyester Fibre-Reinforced Concrete Subjected

to Elevated Temperatures." International Journal of Civil, Structural, Environmental and Infrastructure Engineering Research and Development**3**(1): 1-10.

Rong, M. Z., M. Q. Zhang, G.C. Yang and H.M. Zeng(2001). "Treatment on the Mechanical Propertie of Unidirectional Sisal Reinforced Epoxy Composites." Composite Science Technology**61**: 1437 – 1447.

Rosato, D. V., D. V. Rosato and M.V. Rosato (2004). Plastic Product Material and Process Selection Handbook. Oxford, Elsevier Science & Technology Books.

Sharma,S. and K. Varshney (2011). "Chemical Analysis of Agrava Sisalana Juice for its Possible Ultilization."ActaChim. Pharm. Indica 2(1): 60-66.

Shen, C. H. and G. S. Springer (1976). "Moisture absorption and desorption of composite Materials." Journal of Composite Materials**10**(2): 2-20.

Sreekala, M. S. and S. Thomas (2003). "Effects of Fibre Surface Modification on Water-Sorption Characteristics of Oil Palm Fibres." Composite Science Technology **63**: 861 – 869.

Surathi, P. and V. M. Karbhari (2006). Hygrothermal Effects on Durability and moisture Kinetics of Fiber-Reinforced Polymer Composites.Report, University of California**. SSRP-06/15:**1-294.

Thais, H. D., S. M. Sydenstricker and C.A. Sandro (2003). "Pull-out and other Evaluations in Sisal Reinforced Polyester Biocomposites." Polymer Testing**22**: 375 – 380.

Valadez-Gonzalez, A., J. M. Cervantes, R. Olayoand P.J.Herrera-Franco (1999). "Effects of Fibre Surface Treatment on Fibre-Matrix Bond Strength of Natural Fibre Reinforced Composites." Composites **30**: 300 – 320.

Zhao, D. and J. Botsis (1996). "Experimental and Numerical Studies in Model Composites, Part I: Experimental Results." International Journal of Fracture**86**: 153–174.